*Valorization of low
concentration sugar side-stream
from dissolving pulp production*

Gerardo Gómez Millán

Valorization of Low Concentration Sugar Side-Stream from Dissolving Pulp Production

Gerardo Gómez Millán

Supervisors
Prof. Dr. Herbert Sixta
Prof. Dr. Jordi Llorca

SELECT+
(Environomical pathways for sustainable energy services)

Thesis by compendium of publications

Universitat Politècnica de Catalunya – BarcelonaTech

Aalto University – School of Chemical Engineering

Abstract

Among the platform chemicals that can be produced from lignocellulosic biomass, furfural (FUR) constitutes a promising intermediate that can be processed into a variety of advanced end products.

In this thesis, the catalytic dehydration of C5-sugars was first developed and optimized using aqueous xylose solutions before the prehydrolysate of birch wood was used as a real substrate. Initially, the use of various metal oxides, such as sulphated zirconium dioxide (SZ) on cordierite and aluminium oxide on cordierite, as catalysts for the conversion of xylose to FUR was investigated and optimized, as they were considered relatively stable under hydrothermal conditions and also exhibit a relatively high proton activity. The maximum FUR yields from xylose were 41 mol% when using SZ on cordierite after 2 min at 210 °C, 43 mol% when using alumina on cordierite for 30 min at 210 °C and 48 mol% using autocatalysis for 60 min at 210 °C. After five reusability cycles with SZ on cordierite, this catalyst can be regenerated with similar performance and FUR yield in the 6th cycle. In addition to heterogeneously catalyzed xylose dehydration into FUR in a monophasic, aqueous system, FUR formation in a biphasic system under auto-catalyzed conditions was also investigated. With water-immiscible organic solvents such as isophorone, cyclopentyl methyl ether (CPME), 2-methyltetrahydrofuran and 2-sec-butylphenol (SBP) FUR was immediately extracted from the aqueous phase to avoid degradation as far as possible. The maximum FUR yields reached from xylose were 48 mol% when using isophorone, 78 mol% when using CPME and 59% when employing SBP. The use of birch prehydrolysate as a source of C5-sugars led to a yield of 68% furfural and 0.01 mmol of 5-hydroxymethylfurfural at 190 °C when using CPME. When using SBP as organic solvent, a furfural yield of 54% was reached at 190 °C under optimized conditions.

In the second phase of the dissertation, Starbon®, a carbonaceous sulfonated acid catalyst, was used in a two-phase system to produce furfural from xylose. A maximum furfural yield and selectivity of 70 mol% was achieved at complete xylose conversion under optimum experimental conditions. This work suggests that functionalized Starbon® can be used as solid acid catalyst for the conversion of C5-sugars into FUR that has significant hydrothermal stability and can be reused for several cycles.

Finally, a techno-economic analysis was completed for a furfural plant with a production capacity of 5 kt/a with a minimum selling price to be 1.33 EUR/kg. This value is comparable to similar studies in the field.

Summary in Spanish

Entre los productos químicos que pueden ser producidos a partir de estos materiales de origen biológico, el furfural (FUR) constituye un producto de interés que puede ser transformado en una gran variedad de productos finales avanzados.

En esta tésis doctoral, la deshidratación catalítica de pentosas se desarrolló y optimizó utilizando disoluciones acuosas de xilosa antes que el prehidrolizado de madera de abedul fuera utilizado como sustrato real. Inicialmente, se utilizaron varios óxidos metálicos, como dióxido de zirconio sulfatado (SZ) sobre cordierita y óxido de aluminio sobre cordierita, como catalizadores para la conversión de xilosa a FUR, los cuales fueron relativamente estables bajo condiciones hidrotermales. Las producciones de FUR a partir de xilosa fueron 41 mol% cuando se utilizó SZ sobre cordierita después de 2 min a 210 °C y 43 mol% cuando se utilizó alumina sobre cordierita por 30 min a 210 °C, mientras que el sistema autocatalizado produjo 48 mol% después de 60 min a 210 °C. El catalizador SZ sobre cordierita puede ser regenerado con rendimiento y producción de FUR similares. Adicionalmente a la deshidratación catalítica heterogénea de xilosa a FUR en un sistema monofásico acuoso, la formación de FUR en un sistema bifásico bajo condiciones autocatalizadas también fue investigado. Con la adición de disolventes inmiscibles en agua como isoforona, ciclopentil metil eter (CPME), 2-metiltetrahidrofurano (2-MTHF) y 2-sec-butil-fenol (SBP), el FUR extrae desde la fase acuosa y así se evita su degradación. La producción máxima de FUR alcanzada de xilosa fue 48 mol% cuando se utilizó isoforona, 78 mol% cuando se utilizó CPME y 59% con SBP. El uso de prehidrolizado de abedul como fuente de pentosas condujo a una producción de 68% de FUR y 0.01 mmol de 5-hidroximetilfurfural a 190 °C cuando se empleó CPME. Cuando se utilizó SBP como disolvente orgánico, se alcanzó una producción de furfural del 54% a 190 °C.

En la segunda parte de esta tésis doctoral, se utilizó Starbon®, un catalizador ácido sulfonado de naturaleza carbonosa, en un sistema bifásico para producir furfural a partir de xilosa. Se alcanzó una producción máxima de furfural y una selectividad de 70 mol% con una conversión completa de xilosa. Se concluye, por tanto, que el Starbon® funcionalizado puede ser utilizado como catalizador ácido sólido para la conversión de pentosas a furfural puesto que, además, tiene una estabilidad hidrotermal elevada y puede ser reutilizado por varios ciclos.

Finalmente, un análisis tecno-económico se realizó para una planta de furfural con una capacidad de producción de 5 kt/a con un precio minimo a la venta de 1.33 EUR/kg. Este valor es comparable con estudios similares en el campo de investigación.

Acknowledgements

The contents of this work are based on more than four years of full-time research. During this time, I have been part of the staff of Aalto University, Finland and Universitat Politècnica de Catalunya (UPC), Spain under the SELECT+ PhD Programme. While finishing my bachelor studies in Mexico City, I became more aware of the world changing around me as murmurs of climate change began. I went to Germany, Denmark and Portugal during my Master studies on a quest to understand various topics about environmental concerns and how to tackle them from the engineering, chemical and managerial perspectives. I then realized that in order to decrease consumption of fossil derivatives, valorization of waste into chemicals and fuels could be the answer. Fortunately, I found a project that met my expectations converting side-streams from the pulp and paper industry into value-added chemicals. During my doctoral studies I had the opportunity to read *This Changes Everything* (Naomi Klein 2014), which is an eye-opening text on the climate crisis, and still grants reasons to hope. In order to complete this, we need to act now. My hope is that research in this field will point toward a greener approach in the production of chemicals and fuels.

Firstly, I would like to thank my supervisors. To Herbert Sixta for welcoming me into the Biorefineries research group; your encouragement to work independently has made me become a better and stronger chemical engineer. Also to Jordi Llorca for welcoming me to the NEMEN group, motivating and supporting my research ideas while guiding me through the challenging paths of catalysis. It has been an honor working with you.

Secondly, I would like to thank all my co-authors. With additional thanks to Dr. Sanna Hellsten, for being my instructor during the first years of my PhD, which were the toughest. Thank you for hanging in there with me.

I would like to take this opportunity to offer particular thanks to my external pre-examiners, Univ.-Prof.Dipl.-Ing.Dr. Matthäus Siebenhofer from the TU Graz, Austria; and Dr. MBA

*Feet, what do I need you for
when I have wings to fly?*

Frida Kahlo

x

List of publications

This thesis consists of an overview of the following four publications, which from hereafter are referred to as Roman numerals in the text:

I   Gerardo Gómez Millán, Zouhair El Assal, Kaarlo Nieminen, Sanna Hellsten, Jordi Llorca, Herbert Sixta. **2018**. Fast furfural formation from xylose using solid acid catalysts assisted by a microwave reactor. *Fuel Processing Technology*, Volume 182, Pages 56-67. DOI:10.1016/j.fuproc.2018.10.013

II   Gerardo Gómez Millán, Sanna Hellsten, Alistair W. T. King, Juha-Pekka Pokki, Jordi Llorca, Herbert Sixta. **2019**. A comparative study of water-immiscible organic solvents in the production of furfural from xylose and birch hydrolysate. *Journal of Industrial and Engineering Chemistry,* Volume 72, Pages 354-363. DOI:10.1016/j.jiec.2018.12.037

III Gerardo Gómez Millán, Josphat Phiri, Mikko Mäkelä, Thad Maloney, Alina M. Balu, Antonio Pineda, Jordi Llorca, Herbert Sixta. **2019**. Furfural production in a biphasic system using a carbonaceous solid acid catalyst. *Applied Catalalysis A: General,* Volume 585, Pages. DOI: 10.1016/j.apcata.2019.117180

IV   Gerardo Gómez Millán, Rahul Prasad Bangalore Ashok, Pekka Oinas, Jordi Llorca, Herbert Sixta. **2019**. Furfural production from xylose and birch hydrolysate liquor in a biphasic system and techno-economic analysis. Submitted to *Biomass Conversion and Biorefinery*.

Author's contribution

I   GGM was responsible for the experimental design together with SH. GGM analyzed the results and wrote the manuscript under supervision of SH, JL and HS. GGM was responsible of the synthesis and characterization of solid catalysts used in the experiment sets and interpreting the results. He also performed all lab experiments and interpreted the results. ZEA contributed with the analysis of temperature-programmed desorption of ammonia (NH_3-TPD). KN carried out the kinetic model based on experimental data.

II   The conceptual approach of the study was designed by GGM. He ran the laboratory experiments and analyzed the samples. AWTK contributed with the analysis of furfural degradation samples with NMR and interpreted the results. JPP contributed with the binary liquid-liquid equilibrium model. GGM interpreted the results and wrote the manuscript under the supervision of SH, JL and HS.

III GGM and MM were responsible for the experimental design. GGM performed the experimental work, analyzed the results and wrote the manuscript under supervision of JL and HS. JP carried out Raman studies and interpreted the results. TM critically reviewed the manuscript. AMB contributed with the synthesis of the catalyst. AP carried out infrared and thermogravimetric analysis of the solid catalyst.

IV   GGM designed the study. He was responsible for planning and running the experimental plan, interpreting the results and wrote the manuscript under the supervision of PO, JL and HS. RPBA contributed with the techno-economic assessment and interpreted the results.

Other featured publications

List of Abbreviations

DRIFT	Diffuse Reflectance Infrared Fourier Transform Spectroscopy
EDX	Energy-Dispersive X-ray Spectroscopy
EU	European Union
FID	Flame Ionization Detector
GBHS	Gentle Beam Super High Resolution
GC	Gas Chromatography
HPLC	High-Performance Liquid Chromatography
HPAEC	High-Performance Anion-Exchange Chromatography
HSP	Hansen Solubility Parameters
IC	Ion Chromatography
ICP-OES	Inductively Coupled Plasma–Optical Emission Spectrometry
IEC	Ion-exchange Capacity
IR	Infrared Radiation
IS	Internal Standard
NH_3-TPD	Temperature-Programmed Desorption of Ammonia
NMR	Nuclear Magnetic Resonance
PAD	Pulse Amperometric Detection
RI	Refractive Index
RT	Room Temperature
SEM	Scanning Electron Microscopy
TCD	Thermal Conductivity Detector
TGA	Thermogravimetric Analysis

USDOE	United States Department of Energy
UV/VIS	Ultraviolet/Visible Spectroscopy
XPS	X-ray Photoelectron Spectroscopy
XRD	X-ray Diffraction

Chemical compounds and minerals

2-BuOH	2-buthanol
Al_2O_3	alumina
CPME	cyclopentyl methyl ether
DMF	dimethylfuran
DMI	1,3-dimethyl-2-imidazolidinone
DMSO	dimethyl sulfoxide
GBL	gamma-butyrolactone
GHL	gamma-hexalactone
GVL	gamma-valerolactone
FuOH	furfuryl alcohol
FUR	furfural
H_2SO_4	sulfuric acid
HMF	5-(Hydroxymethyl)furfural, 5-Hydroxymethyl-2-furaldehyde
KBr	potassium bromide
MF	2-methylfuran
MIBK	methyl isobutyl ketone
MTHF	2-methyltetrahydrofuran

NaOH	sodium hydroxide
Py	pyridine
SBP	2-*sec*-butylphenol
SZ/ ZrO$_2$(SO$_4^{2-}$)	sulfated zirconia
THF	tetrahydrofuran

Symbols

atm	atmosphere	[atm]
°C	Celsius degree	
€	Euro	
M	molarity	[mol dm^{-3}]

Contents

1. Introduction

Continuous global concern about the high reliability of fossil-derived materials (i.e. coal, natural gas and petroleum), which currently supply most of the energy, fuels and chemicals consumed on the planet, and the dependency of the global economy on them, serve as the motivation to search for alternative renewable resources. Among the abundant and non-contaminant renewable resources across the globe, biomass has stood out as the only renewable source of organic carbon currently available on Earth. Therefore, biomass can be used to substitute petroleum in the production of chemicals and fuels in gas, liquid and solid form (Serrano-Ruiz et al. 2012). Waste material from forest biomass emerges as an especially promising feedstock, since it is not involved in the food vs. fuel debate.

The particular composition of biomass (highly oxygenated compounds) makes its conversion into chemicals and fuels energy-intensive and involves deep chemical changes. One alternative to overcome biomass feedstock's complexity involves its conversion into simpler fractions, which could be processed downstream (Figure 1). Attractive biomass-derived molecules have recently been identified, the so-called platform molecules (Werpy and Petersen 2004), that contain multiple functionalities in their structures, which can be further transformed to a wide range of valuable chemical compounds.
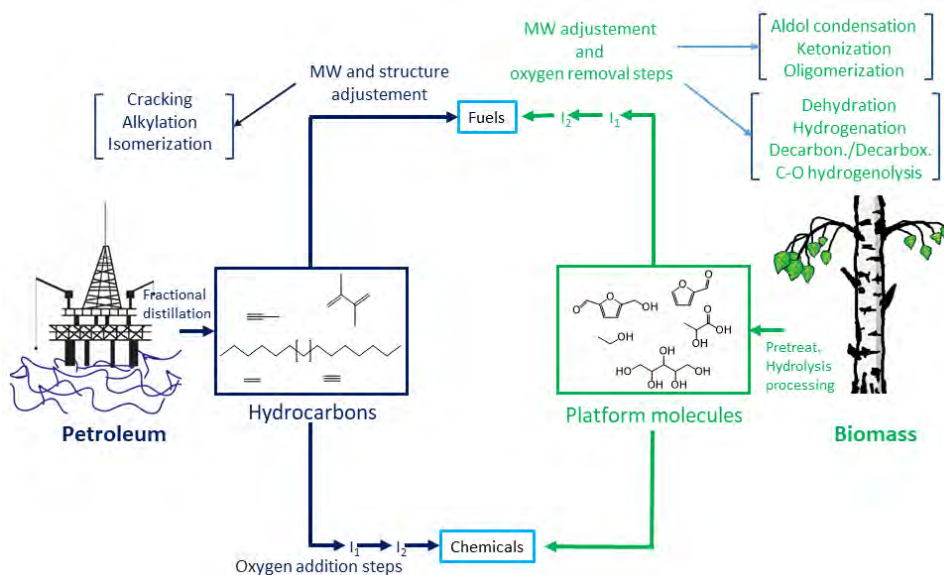
Figure 1. Comparative processing approaches of petroleum and biomass to chemicals and fuels. Adapted with permission of the Royal Society of Chemistry (Serrano-Ruiz et al. 2011).

Waste utilisation is an attractive alternative to disposal, as it can reduce reliance on land-fill practices, the extraction of virgin raw materials, and possibly enable savings in valuable materials and energy resources otherwise consumed in the process of converting raw materials into products. So far, the competitiveness of pulp and paper mills is struggling as a result of the digitalisation of literature, climate change and globally increasing capacities, especially in equatorial and sub-equatorial countries with larger tree-growing quotas and low-cost labour, which imposes severe economic strain on producers in temperate latitudes like the Nordic region (Lê 2018). This ongoing trend can provide new potential to existing forest companies to also develop significant biobased chemical and biofuel products, in addition to cellulose-based products. This position urges the transformation of their mass production of paper-grade pulp en route to other products with smaller production quantities but larger gross margins, such as methane gas from wastewater (Rodriguez-Chiang et al. 2017), bio-oil from lignin (Hashmi et al. 2017), and value-added chemicals like furfural (FUR), 5-hydroxymethylfurfural (HMF) and acetic acid from hydrolysate liquor from dissolving pulp (Gómez Millán, Hellsten et al. 2019).

Catalysts play a key role in the efficient conversion of biomass in the chemical industry. They are defined as 'a substance that changes the velocity of a reaction without itself being changed in the process' (Sheldon et al. 2007). It lowers the activation energy of the reaction but, in so doing, it is not consumed. Every year there are worldwide sales values of solid catalysts of approximately 13 billion €/ year, which in turn create an added value about 100 to 1,000 times higher. Solid catalysts are preferred in a wide range of industrial applications due to their reusability potential and lower toxicity, among other advantages. From 80% to 85% of current industrial processes use solid catalysts of some kind (Rinaldi and Schuth 2009).

The key focus of this research work was to develop a process to produce value-added chemicals, especially FUR, from a side-stream of the dissolving pulp production in the pulp and paper industry. Firstly, solid acid catalysts were developed to efficiently form FUR from a model compound (xylose) in the monophasic (aqueous) phase, in order to substitute state-of-the-art corrosive, toxic, mineral acids. Secondly, an organic solvent was introduced that could immediately extract formed FUR and avoid degradation reactions. Thirdly, the benefits of a solid acid catalyst in a biphasic system were addressed. Lastly, a techno-economic assessment was completed using a water-immiscible organic solvent to extract FUR. As the competitiveness of the pulp and paper industry declines and changing markets affect it significantly, investigating possible market diversification from traditional pulp and paper production to a chemical biorefinery can help increase the market portfolio of pulp and paper mills.

2. Background

Originally, the United States Department of Energy (USDOE) stressed the 12 most-relevant platform molecules as the key starting materials on which to focus future research endeavours. These compounds have gained a valuable niche among industry and academia within the past decade due to their effective development, environmentally benign technology and potential solution to agricultural and forestry waste (Yan et al. 2015). Years later, Bozell and Petersen revisited this list and included platform molecules, e.g. ethanol, furfural (FUR) and succinic acid (Holladay et al. 2007).

Pursuing the same philosophy, an industry that is able to conceive efficient catalytic biomass conversion would accomplish the complete employment of plant matter feedstock into useful chemicals, fuels and energy. To achieve these goals, biorefineries play a dominant role by carefully selecting biomass derivates, the so-called platform molecules or building blocks (Gómez Millán, Hellsten et al. 2019).

Lignocellulosic matter is primarily constituted by cellulose, hemicellulose and lignin (Besson et al. 2014; Centi et al. 2011; De Oliveira Vigier and Jerome 2010). Holocellulose considers cellulose and hemicellulose (the carbohydrate fraction of lignocellulose). Hemicellulose is formed by pentoses (xylose, arabinose and ribose) and hexoses (glucose, fructose, galactose and mannose), of which xylose, a monomer of xylan, is the most common component (Mäki-Arvela et al. 2011; Martel et al. 2010). Hemicellulose is linked to cellulose by hydrogen bonds, and it is more easily hydrolysed than cellulose. Moreover, hemicellulose-derived compounds (xylan and xylose) have not yet been completely valorised. At present, the pulp and paper industry combines a significant part of C_5-sugar-rich streams with lignin derivates, which are burned to obtain energy, used as process heat (Hinman et al. 1989). Nevertheless, the valorisation of this stream is of major interest for academia and industry.

An attractive route, namely the dehydration of sugars to furans, is considered as one of the most promising paths to form platform molecules. Among these furanic compounds, FUR, HMF and 2,5-furandicarboxylic acid (FDCA) have gained momentum in both academia and industry. Interest in using FUR as a feedstock for chemicals and fuels is dramatically increasing, as evidenced by the number of publications on catalytic technologies for FUR production and/or further synthesis into value-added chemicals, particularly in the past 10 years (Figure 2).
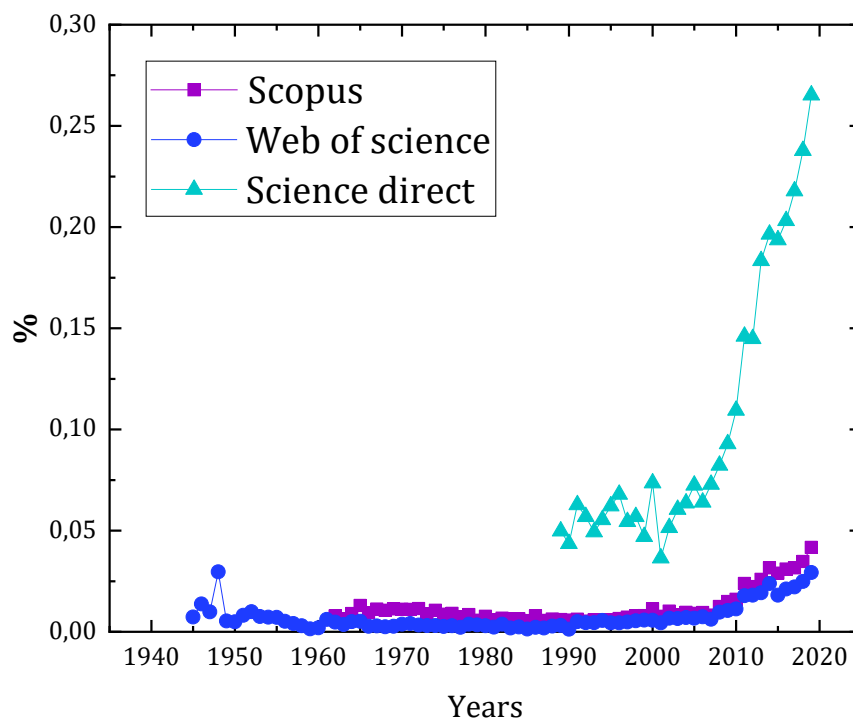
Figure 2. *Percentage of publications on furfural (FUR) related to total number of publications per year (Jan 1945 – Sep 2018). Sources: Scopus, Web of science and Science direct (keyword: furfural).*

2.1 Furfural production

FUR (OC$_4$H$_3$CHO, furan-2-carbaldehyde, FUR) is the dehydration product of C$_5$-sugars (i.e. xylose and arabinose) found typically in the hemicellulose fraction of lignocellulosic biomass. The production of FUR from lignocellulosic biomass occurs via hydrolysis of hemicellulose into monomeric sugars and the dehydration of sugars into FUR, as shown in Figure 3.

FUR can be produced from xylose-rich lignocellulosic residues, such as corncobs, oat hulls, almond husks, birch wood, bagasse and switchgrass (Zeitsch, Karl J. 2000c).
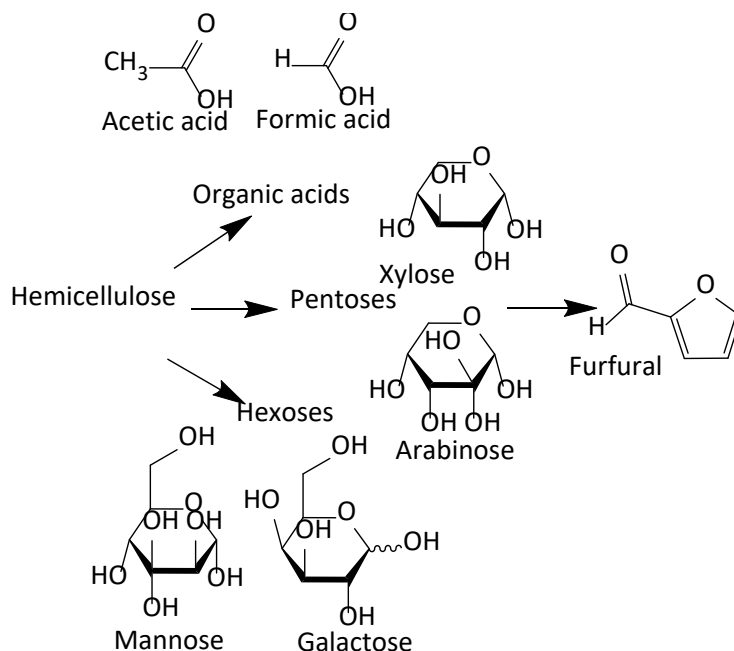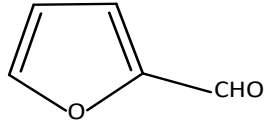
Figure 3. *Furfural formation from hemicellulose (Adapted from (Lamminpää, K. 2015)).*

2.2 Furfural derivatives and industrial applications

FUR is a clear, viscous liquid with a light-brown colour. It is also a water-miscible solvent (Table 1).

Table 1. *Furfural properties (Domalski and Hearing 1996; Sigma-Aldrich 2019; Stephenson and Malanowski 1987; Zeitsch, Karl J. 2000a)*

Property	Value
Structure	
Formula	$C_5H_4O_2$
CAS	98-01-1
Molar mass [g mol^{-1}]	96.082
Relative density [g ml^{-1}] at 25 °C	1.16
Refractive index [n_{20}/D]	1.53
Melting point [°C]	-36
Flash point [°C]	61.7
Boiling point [°C]	162
Ignition temperature (°C)	315
Enthalpy of vaporization (ΔH_{vap})[kJ mol^{-1}]	44.7
Enthalpy of fusion (ΔH_{fus})[kJ mol^{-1}]	14.4
Solubility in water at 20 °C (g 100 ml^{-1} water)	8.3
Dielectric constant (ε) at 25 °C	41.799
LD$_{50}$ (Rat/Oral) [mg kg^{-1}]	127
LD$_{50}$ (Rabbit/Dermal) [mg kg^{-1}]	>2.000
Vapor pressure	18 hPa at 55° C
	2.3 hPa at 20 °C

In addition, more than 80 chemicals have been identified as direct or indirect derivatives of FUR, as shown in Figure 4 (Mariscal et al. 2016; Zeitsch, Karl J. 2000d).

The most important application of FUR is to synthesise furfuryl alcohol (FuOH), reduction at 120 °C at atmospheric pressure (Heng and Grinstaff 2014), which represents approximately 60% of the FUR market. FuOH has applications in the manufacture of foundry resins, the component production of P-series fuels, in liquid alkanes and in the food industry (Carlos Serrano-Ruiz and Dumesic 2009; Chheda et al. 2007; Weingarten et al. 2010). Tetrahydrofuran (THF) and tetrahydrofurfuryl alcohol are two very appealing chemicals also formed from FUR that have wide applications in the chemical industry. FUR can also be derived into levulinic acid, a promising value-added chemical from biomass via hydrolysis of FuOH (Timokhin et al. 1999). Other interesting compounds are 2-methylfuran (MF), dimethylfuran (DMF) and 2-methyltetrahydrofuran (MTHF), which are formed via hydrogenation and can be used as biofuels (Gürbüz et al. 2013; Mukherjee et al. 2015). Furthermore, MTHF is a promising substitute for dichloromethane, a common solvent used in pharmaceuticals and agricultural products, and a probable carcinogen (Schlosser et al. 2015). Carboxylic acids can also be produced via oxidation from FUR. Furoic acid (employed in the pharmaceutical, agrochemical and cosmetic industries) (Escobar et al. 2015) and maleic acid (Wojcieszak et al. 2015) can be formed from FUR by adding O_2 as an oxidant.
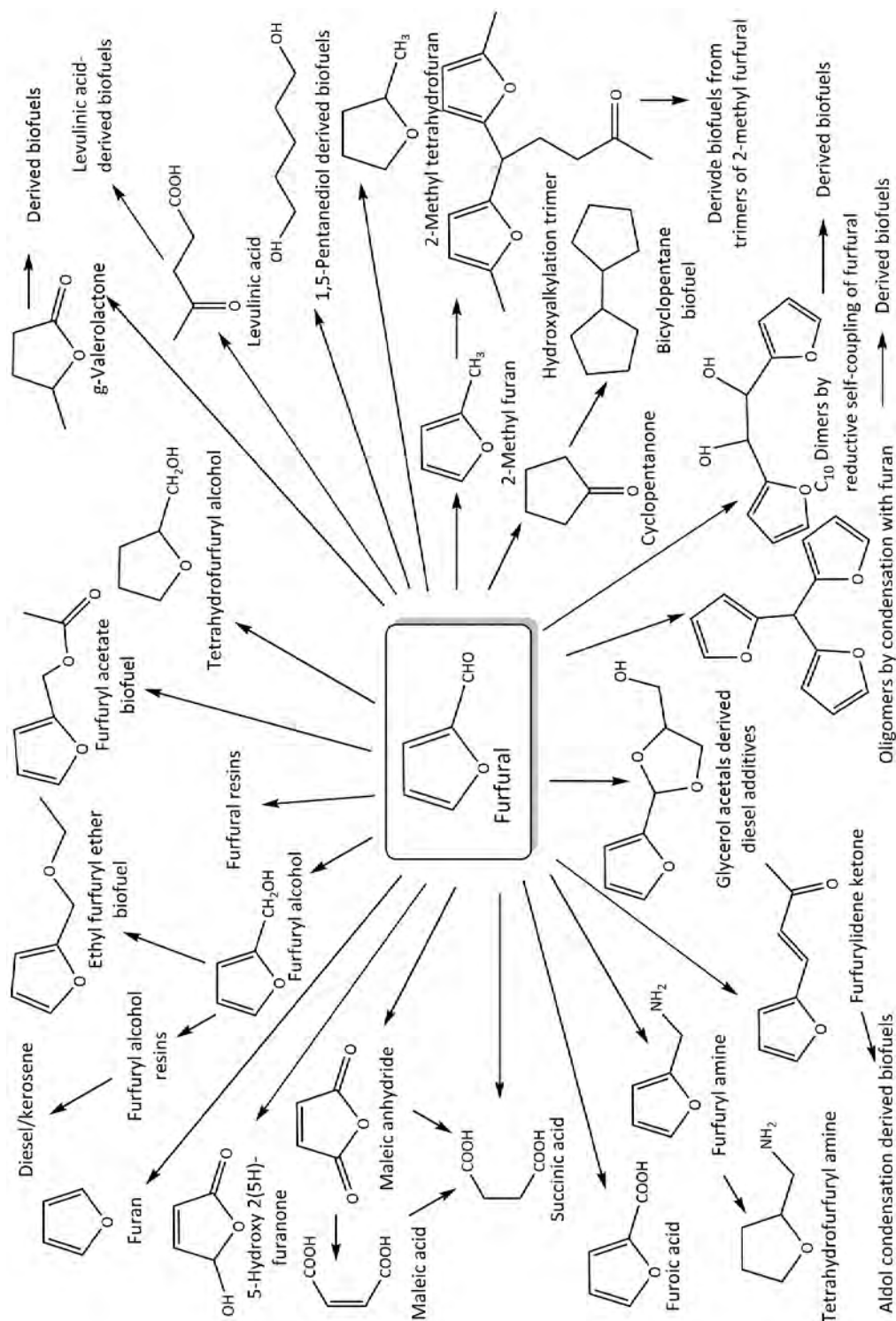
Figure 4. *Furfural derivatives: chemicals and biofuels (Reproduced and adapted from (Mariscal et al. 2016)).*

2.3 Established commercial processes

In the commercial process, FUR yield production still relies on sulfuric or hydrochloric acid and yields that do not exceed 50 mol%. Furthermore, FUR is produced industrially and is associated with a variety of environmental concerns – for instance, toxic effluents origi-

nating from mineral acids at temperatures <200 °C. Another issue is the high energy consumption related to the steam stripping process, to avoid further FUR degradation and fuel employment to generate steam.

The QUAKER OATS process dates back to 1921. The feedstock is mixed with sulfuric acid and cooked for 5 h at 153 °C. In China, which still continues to produce over 70% of the total FUR market volume, followed by the Dominican Republic and South Africa, the feedstock is sprayed with 4% aqueous sulfuric acid to give 1.5 kg of acid per 100 kg of liquid phase. The reactor is charged to 75% filling, and then closed. The batch reactor is operated for a period of 4 to 5 h at $6-7$ atm with 1-1.5 t/h of steam. This process passes the reactor vapor directly through the reboiler of the azeotropic distillation column. In this process, similar to the QUAKER OATS process, the FUR yield in the distillate is in the order of 50%. These processes are accompanied by environmental concerns, including toxic effluents and high energy consumption.

Other processes, such as Agrifurane, Rosenlew and Escher Wyss, differ mainly by the operational mode, batch or continuous process, and reaction temperature. Among these processes, the Rosenlew process can be highlighted, due to the absence of the acid addition. The feedstock enters the reactor at the top after being screened and moves in a downward direction following gravity. The residence time in the reactor is 2 h, and superheated steam of 10 bar is fed into the bottom part of the reactor. The catalysts are mainly acetic and formic acids formed from the raw material fragmentation (Kamm et al. 2013; Zeitsch, Karl J. 2000e).

Currently, the Nordic oil company St1 Oy produces FUR, lignin and turpentine as by-products in their Cellulonix® process, which aims to form ethanol from saw dust (Talvitie and Pitkänen 2014).

2.4   Homogeneous catalysis

Besides mineral acids (H_2SO_4, HCl, H_3PO_4), organic acids (formic, maleic, levulinic, succinic acid) have been shown to provide catalytic properties in FUR formation (Delbecq et al. 2018; Lamminpää, K. et al. 2014; Xing et al. 2011). In fact, studies have shown that some organic acids are formed as secondary products from xylose dehydration as fragmentation products, i.e. acetic and formic acid, and that they have catalytic effects in the formation of FUR (Oefner et al. 1992; Sairanen et al. 2013).

2.5   Heterogeneous catalysis

As a counterpart, there are new methodologies that address challenges mainly associated with the development of heterogeneously catalysed systems in the pursuance of reutilisation and ease of separating solid catalysts from the reaction medium to avoid corrosive and toxic effluents, and these can be synthesised with broad surface acidities and porosity properties to improve selectivities (Table 2). Easily separable solid catalysts include:

- zeolites (Lessard et al. 2010; Lima et al. 2008; Lima, Antunes et al. 2010; Lima, Fernandes et al. 2010; Moreau et al. 1998; O'Neill et al. 2009; Sahu and Dhepe 2012),
- aluminosilicates supported with metals (Yepez et al. 2014),
- modified silicas (Agirrezabal-Telleria, Iker et al. 2012; Agirrezabal-Telleria, I. et al. 2013; Agirrezabal-Telleria, I. et al. 2014; Bhaumik et al. 2014; Dias et al. 2005b; Jeong et al. 2011; Kaiprommarat et al. 2016; Molina et al. 2015);
- metal oxides like alumina (Weingarten et al. 2011) and zirconia (Li et al. 2014a; Weingarten et al. 2011);
- heteropolyacids (Dias et al. 2005a; Dias et al. 2005b; Dias et al. 2007);
- resins (Agirrezabal-Telleria, I. et al. 2011; Agirrezabal-Telleria, Iker et al. 2013; Lam et al. 2011);
- carbon-based materials, such as sulfonated graphenes (Lam et al. 2012) and coated activated carbon (Sairanen et al. 2013);

these catalysts yield furfural in a much more environmentally conscious and efficient process.

Since the present work shows results when working with metal oxides, carbon-based materials and polymeric resins, a review of these catalysts is presented below.

2.5.1 Zeolites

The addition of zeolites for xylose conversion into FUR was first reported by Moreau et al. (Moreau et al. 1998). They studied H-Y faujasites and H-mordenites with different Si/Al ratios in water/MIBK and a water/toluene (1:3 by volume) biphasic system. The highest FUR yields (42%) were obtained using HY Faujasites with Si/Al ratios of 10 and 15 with a xylose conversion of 66% and 51%, respectively, at 170 °C in 50 min. These zeolites present cavities of about 1.3 nm, which allow the rearrangement of the xylose in the pores. They claim that mordenites with a low mesoporous volume were found to be more selective to FUR. However the FUR yields were not as high as when employing HY faujasites. Furthermore, in their article, they do not report acid site density or reusability potential under the presented conditions.

Lessard et al. studied the formation of 2-methylfuran through consecutive xylose dehydration and FUR hydrogenation with zeolites and a Cu/Fe catalyst, respectively (Lessard et al. 2010). The authors investigated the dehydration reaction of xylose in an aqueous-toluene system in a plug-flow reactor at 260 °C and 55 atm. They achieved a FUR yield of 98% and almost complete xylose conversion (99%) in 3 min employing mordenite 13 acidified with H_3PO_4. After two reusability cycles, the FUR yield decreased from 98% to 90%; a similar effect occurred to the selectivity, which decreased from 98% to 89%. After regeneration of the mordenite, it did not fully restore its original activity. In this paper, the authors do not reported textural properties such as the surface area and pore width of the catalyst. Other characteristics of the catalyst, like acid site density, were not studied.

Various zeolites were tested by Kim et al. in water, DMSO and water/toluene (Kim et al. 2011). When increasing the SiO_2/Al_2O_3 molar ratio over the zeolites, the xylose conversion and FUR yield decreased independently of the solvent employed. When comparing the three solvent systems they used, xylose conversion and FUR yield decreased in the following order: water/toluene>DMSO>water. Nevertheless, the authors did not perform reusability tests to test their hydrothermal stability. The surface area of the zeolites is also missing, which could have been interesting to study.

Sn-beta zeolite (Lewis acid) was investigated by Choudhary et al. (Choudhary et al. 2011) for xylose isomerisation in an aqueous medium with Amberlyst 15 (Brønsted acid). The Sn-Beta displays a specific surface area of $100 \ m^2 \ g^{-1}$ and a pore volume of $0.16 \ m^3 \ g^{-1}$. The presence of Lewis acid sites altered the reaction mechanism to give xylulose intermediates. The use of Sn-beta zeolite at 110 °C allowed a similar xylose conversion as at 150 °C under hydrothermal conditions. For the purpose of increasing the FUR yield, Amberlyst 15 was employed. Nevertheless, the combination of catalysts did not reach a FUR yield over 10%. Even though the reusability studies of the catalyst to isomerise xylose have been presented, the acid site density analysis is not included in the paper.

O'Neill et al. investigated a H-ZSM zeolite in its proton form during xylose dehydration employing a batch reactor (O'Neill et al. 2009). H^+-ZSM-5 presents a mean pore size diameter larger than the average ZSM catalysts (1.2 nm). The catalytic tests were designed to study the dehydration of xylose from 140 °C to 220 °C in water. The highest FUR yield, 46%, was obtained at 200 °C in 16 min. It was assumed that the pore size was large enough to allow FUR molecules enough time to congregate and react with each other. Hence, a smaller pore size was suggested (around 0.8 nm) due to the approximate molecular diameters of xylose (0.68 nm) and FUR (0.57 nm). The authors also investigated the acid site of the catalyst, which shows a total acid site density of $1.6 \ mmol \ H^+ \ equiv \ g^{-1}$, but no studies on its hydrothermal stability or reusability potential were performed.

An interesting study was completed by Dhepe and Sahu using softwood- and hardwood-derived hemicellulose to form FUR, testing various solid acid catalysts (zeolites, clays and metal oxides) in aqueous media (Dhepe and Sahu 2010). Among the different tested catalysts, H-USY (Si/Al = 15) stood out, reaching the highest FUR yield (12 %) and a xylose+arabinose yield of 41% at 170 °C in 3 h. Since the pore width of H-USY (Si/Al = 15) is 0.74 nm, the authors assumed that hemicellulose hydrolyses on the external acid sites, and that once dimers and trimers are produced, these can access the zeolite pores and interact with internal acid sites (present inside the pores of zeolites) to yield monomer sugars, xylose and arabinose. Furthermore, NH_3-TPD revealed that the fresh catalyst total acid site density ($0.55 \ mmol \ g^{-1}$) decreased after reaction as a result of Na and K presence in the feedstock, which replaced H^+ on the catalyst.

Table 2 summarizes the reported FUR yield values testing different zeolites during pentose dehydration.

Table 2. *Zeolites employed in the conversion of pentoses into furfural.*

Catalyst	Substrate	Pore width (nm)	Surface area (m² g⁻¹)	Total acidity (µmol g⁻¹)	Temperature (°C)	Time (min)	Solvent	Xylose conversion (%)	FUR yield (%)	Reference
Amberlyst 15	Xylulose	N/R[a]	N/R[a]	N/R[a]	110	60	Water	66	24	(Choudhary et al. 2011)
Sn-Beta + HCl	Xylose	N/R[a]	100	N/R[a]	110	180	Water	84	14	(Choudhary et al. 2011)
Sn-Beta + Amberlyst 15	Xylose	N/R[a]	N/R[a]	N/R[a]	110	180	Water	92	10	(Choudhary et al. 2011)
H-Beta Si/Al = 25	Xylose	0.66×0.67 ↔ 0.51×0.56	N/R[a]	N/R[a]	140	240	Water/toluene	90	40	(Kim et al. 2011)
H-mordenite Si/Al = 20	Xylose	N/R[a]	N/R[a]	N/R[a]	140	240	Water/toluene	43	35	(Kim et al. 2011)
H-ZSM-5 Si/Al = 23	Xylose	0.51×0.55 ↔ 0.53×0.56	N/R[a]	N/R[a]	140	240	Water/toluene	90	43	(Kim et al. 2011)
H-Faujasite Si/Al = 15	Xylose	1.3	N/R[a]	N/R[a]	170	50	Water/toluene	51	42	(Moreau et al. 1998)
HSUY, Si/Al = 15	Softwood-hemicellulose	0.74	N/R[a]	550	170	180	Water	30-40[b]	12	(Dhepe and Sahu 2010)
H-ZSM-5	Xylose	1.2	N/R[a]	1.6×10^3	200	16	Water	100	46	(O'Neill et al. 2009)
H_3PO_4-Mordenite 13	Xylose	N/R[a]	N/R[a]	N/R[a]	260	3	Water/toluene	99	98	(Lessard et al. 2010)

[a] Not reported
[b] xylose+arabinose yield

2.5.2 Metal oxides and polymeric resins

Besides zeolites, polymeric resins and metal oxides have also been reported to produce furans. Table 3 summarises the reported FUR yield values testing different metal oxides during pentose dehydration into FUR. In some cases, metal oxide catalysts have been used with phase modifiers to increase FUR yields in biphasic systems.

2.5.3 Metal oxides and polymeric resins

Besides zeolites, polymeric resins and metal oxides have also been reported to produce furans. Table 3 summarises the reported FUR yield values testing different metal oxides during pentose dehydration into FUR. In some cases, metal oxide catalysts have been used with phase modifiers to increase FUR yields in biphasic systems.

Solid acid SO_4^{2-}/TiO_2-ZrO_2/La^{3+} was used as the catalyst by Li et al. in a modified biphasic system to form FUR from xylose (Li et al. 2014a) . Different aprotic organic solvents (DMSO, dimethyl formamide and DMI) were added to the aqueous phase, while the MIBK organic phase was modified with 2-BuOH. The highest FUR yield reported (3563 µmol of FUR/g of xylose) was reached in 12 h at 180 °C. However, the article lacks hydrothermal stability studies and the reusability potential of the metal oxide catalyst. Furthermore, the textural properties of the catalysts, such as pore width and surface area were not investigated.

Dias et al. investigated different sulfated zirconias in the conversion of xylose into FUR in an aqueous-toluene system in 4 h at 160 °C (Dias et al. 2007). They were capable to identify a correlation of the catalytic activity with the sulphur content of the sulfated zirconia. The highest FUR yield (43%) was achieved using a persulfated zirconia supported on an ordered mesoporous silica (PSZ-MCM-41), which offered a high surface area (382 m^2 g^{-1}) and a characteristic pore width (2–50 nm), although exact values were not reported by the authors. In comparison to the other catalysts tested, PSZ-MCM-41 did not leach Zr during the reaction, but a significant amount of sulphur leaching is observed in the reusability tests.

Zhang et al. used a SO_4^{2-}/ZrO_2-TiO_2 catalyst in a sugar mixture employing an aqueous-n-butanol biphasic system (Zhang, J. et al. 2014). The maximum FUR yield (48 %) was reached at 170 °C in 2 h. Even though the authors performed a reusability test and the FUR yield and xylose conversion remained consistent for two cycles, it might not be enough to observe hydrothermal stability of the catalyst. Furthermore, studies of the catalyst surface area and pore width were excluded of the research.

14

Table 3. *Metal oxides and polymer-based catalysts utilized in the conversion of pentoses into furfural.*

Catalyst	Substrate	Pore width (nm)	Surface area ($m^2 g^{-1}$)	Total acidity ($\mu mol\ g^{-1}$)	Temperature (°C)	Time (min)	Solvent	Xylose conversion (%)	FUR yield (%)	Reference
Amberlyst 15	Xylulose	N/R[a]	N/R[a]	N/R[a]	110	60	Water	66	24	(Choudhary et al. 2011)
Persulfated zirconia-MCM-41	Xylose	2-50	382	N/R[a]	160	240	Water/toluene	95	43	(Dias et al. 2007)
SO_4^{2-}/ZrO_2-TiO_2 Zr-Al = 7:3	Xylose	N/R[a]	N/R[a]	210	170	120	Water/n-BuOH	98	48	(Zhang, J. et al. 2014)
SO_4^{2-}/TiO_2 ZrO_2/La^{3+}	Xylose	N/R[a]	N/R[a]	N/R[a]	180	720	Water:DMI / MIBK-2-BuOH	98	3563.3[b]	(Li et al. 2014a)

[a] Not reported
[b] mol of furfural/g of xylose

15

2.5.4 Carbon-based catalysts

Among the current solid acid catalysts used for biomass conversion, carbon-based heterogeneous catalysts are attractive since they have a high BET surface area, good hydrothermal stability and controllable acid site density with modified functionalities (Delbecq et al. 2018; Romo, Joelle E. et al. 2018; Xiong et al. 2014) (Figure 5).
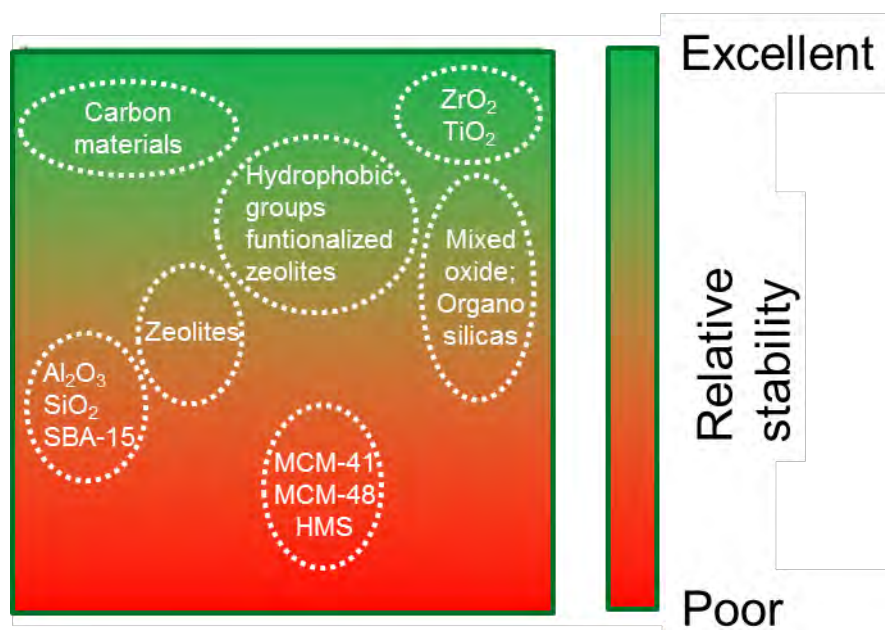
Figure 5. Illustration of hydrothermal stability of heterogeneous catalysts and catalyst supports in sub-critical liquid water (T<374 °C) (Adapted and reproduced with permission from (Xiong et al. 2014) Copyright: 2019 Royal Society of Chemistry).

Sairanen et al. impregnated activated carbon with H_2SO_4, HNO_3 and a combination of both in order to convert xylose to FUR in aqueous media (Sairanen et al. 2013). Even though xylose conversion is complete under the reported experimental conditions (200 °C), FUR yield is not shown in the paper, and the reusability of the catalyst is not mentioned. However, the FUR yield (18%) was calculated from their reported selectivity to FUR and xylose conversion. They tested the catalyst stability with two cycles in water under analogous experimental conditions, which displayed identical conversions. Around 40% of the total pore volume showed a pore radius of 1-2 nm, which indicates that micropores yielded the best FUR selectivities. The rest varied from 2 to 30 nm.

In a similar way, Termvidchakorn et al. functionalised multi-wall carbon nanotubes (MWCNTs) with H_2SO_4, H_3PO_4, HCl and HNO_3 (Termvidchakorn et al. 2017). They employed the functionalised catalysts to form FUR from xylose and achieved the highest xylose conversion (95%) when adding Co ($Co(NO_3)_2 \cdot 6H_2O$ was used as precursor) in 3 h at 170 °C. Nevertheless, the highest selectivity to FUR was obtained when the MWCNTs were functionalised with H_2SO_4. This could be due to the high total acid site density determined by NaOH titration. Moreover, the carbon-based catalysts employed were not investigated for their hydrothermal stability or reusability potential.

Unlike previous carbon-based catalysts, Lam et al. developed a sulfonated graphene oxide that yielded 62% FUR in 35 min at 200 °C in water (Lam et al. 2012). Moreover, after 12

reusability cycles under optimum conditions, the FUR yield remained at 61%. The authors associate the high catalytic activity of the catalyst to the excellent thermal and mechanical properties associated with carbon materials, and to the strongly acidic aryl SO_3H groups. However, the production of graphene oxide includes several steps and various toxic chemicals. Jalili et al. reported in their recent paper that graphene derivatives contain silicon, which has a significant impact on their performance (Jalili et al. 2018).

Antonyraj and Haridas sulfated a lignin-derived carbon catalyst to produce FUR and HMF from xylose and fructose, respectively. They employed a MIBK/H_2O (7:3) biphasic system yielding up to 65% FUR with a xylose conversion of 97% in 3 h at 175 C. After a 4th reusability cycle, its catalytic activity declined – but after regeneration, the catalyst showed minimal loss in activity (Antonyraj and Haridas 2018).

Wang et al. used Miscanthus *x giganteus* as the source of biomass to produce char by carbonisation in the process of slow pyrolysis. After producing the char, they used concentrated sulfuric acid to sulfonate the material. Under optimised conditions (xylose: 1 mmol, catalyst: 15 mg, water-CPME (1:3, v/v), 190 °C) they yielded 60% FUR. They reused the catalyst for 10 cycles at 190 °C and 60 min, which showed good hydrothermal stability and catalytic activity in every cycle (Wang et al. 2017). Xylan from benchwood was also used to produce FUR. The highest FUR yield (42%) was achieved at 190 °C in 80 min in the presence of 20 wt% of catalyst in a water-CPME (1:3, v/v) biphasic system.

A carbon-based catalyst with Lewis and Brønsted acid sites was developed by Mazzotta et al. in a biphasic water/MTHF (1:2, v/v) system (Mazzotta et al. 2014) to produce HMF and FUR. They sulfonated a carbonaceous TiO_2 catalyst with the aim that the Lewis acidity of the TiO2 would isomerise the sugar (glucose or xylose), allowing for increased activity. The highest FUR yield (51%) was obtained over 30 min at 180 °C. In comparison to the reaction without catalyst under similar conditions, the yield of FUR was three times lower (17%). The reusability of the catalyst was tested at 180 °C for 60 min using fructose to produce HMF in the biphasic system. After four reusability cycles, the loss of activity of the catalyst in terms of HMF yield was negligible.

A sulfonated biochar was used to produce FUR from the pre-hydrolysis liquor of corncob in a biphasic system (Deng et al. 2016). It was found that 81% FUR yield was obtained from the concentrated pre-hydrolysis liquor at 170 °C for 60 min using dichloromethane as an organic solvent. The use of sodium chloride was reported as a phase modifier. In the reusability tests, a considerable decrease in FUR yield (from 81% to 25%) was observed after five runs. The concentration of total acid site density and the density of –SO_3H decreased after each reuse experiment. Nevertheless, the catalyst can be regenerated employing H_2SO_4 with similar catalytic activity after each run.

Carbon-based catalysts displayed high FUR yield and high hydrothermal stability. When these catalysts were added to a biphasic system, they benefited from higher organic to aqueous phase ratios.

Table 4 summarises the reported FUR yield values testing different carbon-based catalysts during formation of FUR from different feedstocks.

Table 4. *Carbon-based catalysts employed in the conversion of pentoses into furfural.*

Catalyst	Substrate	Pore width (nm)	Surface area ($m^2\,g^{-1}$)	Total acidity ($\mu mol\,g^{-1}$)	Temperature (°C)	Time (min)	Solvent	Xylose conversion (%)	FUR yield (%)	Reference
Sulfonated bio-char	Corncob pre-hydrolysis liquor	N/R[a]	9.6	2970	170	60	Water/dichloromethane	98	81	(Deng et al. 2016)
H_2SO_4-MWCNTs	Xylose	3.3	131	309.1 ± 34.2	170	180	Water	63	36	(Termvidchakorn et al. 2017)
Sulfated lignin-derived carbon	Xylose	N/R[a]	37	0.85[d]	175	180	Water/MIBK	97	65	(Antonyraj and Haridas 2018)
TiO_2-containing carbon catalyst	Xylose	4.5	42.5	1030	180	60	Water/MTHF	N/R[a]	51	(Mazzotta et al. 2014)
Sulfonated Char	Xylose	N/R[a]	317	N/R[a]	190	60	Water/CPME	90-100	60	(Wang et al. 2017)
Sulfonated Char	Xylan	N/R[a]	317	N/R[a]	190	80	Water/CPME	5[e]	42	(Wang et al. 2017)
SGO	Xylose	N/R[a]	680	1700	200	35	Water	83	62	(Lam et al. 2012)
C ($HNO_3 + H_2SO_4$)	Xylose	1-2	1090	1720	200	120	Water	70[b]	18[c]	(Sairanen et al. 2013)

[a] Not reported
[b] Observed from figure reported by Sairanen et al. (Sairanen et al. 2013)
[c] Calculated from figures reported by Sairanen et al. (Sairanen et al. 2013)
[d] $MeqH^+\,g^{-1}$
[e] Xylose yield from xylan

2.6   Reaction mechanism of furfural production

The ongoing discussion of the proper reaction mechanisms of FUR formation has generated proposals for different formation pathways under homogeneous and heterogeneous catalysis. O'Neill and co-workers claimed that xylose could be isomerised to lyxose via adsorption onto the acidic active sites of ZSM-5 zeolite (O'Neill et al. 2009). These steps would occur through the formation of the linear open chain of xylose molecules caused by the acid-catalysed hydrolysis. On the other hand, Verma et al. proposed a mechanism via the formation of 2,5-an-hydoxylose furanose cyclic intermediate using a sulfonated graphitic carbon nitride (Verma et al. 2017). Xylulose, a xylose isomer, has been under discussion as a possible intermediate in FUR formation (Choudhary et al. 2012; Ershova, O. et al. 2015). However, there is no conclusive information on either pathway. The reaction mechanisms presented in this thesis (vide infra) consider a pathway of FUR formation via an intermediate or xylose itself; a pathway solely via an intermediate was not considered. These reaction mechanisms are as follows: xylose can be converted to FUR directly (k_1) (Scheme 1). In Scheme 2, FUR can be formed from xylose either stepwise with an intermediate product ($k_4 + k_5$), or via a direct or pseudo-direct reaction pathway (k_1). In the reaction model presented in Scheme 3, FUR is formed stepwise via an intermediate ($k_4 + k_5$) (Ershova, Olga et al. 2017) or via a direct or pseudo-direct reaction pathway (k_1). The latter scheme proposes a parallel reaction model from the intermediate. The produced FUR further forms degradation products (DP). Simultaneously, some fraction of xylose and intermediates also form degradation products. Previous kinetic studies have used either Scheme 1 (Mellmer et al. 2014) or Scheme 2 (Danon, Bart et al. 2014; Ershova, Olga et al. 2017; Lamminpää, Kaisa et al. 2015) using homogeneous catalysts. Different formation pathways include isomerisation of xylose to other pentoses, such as lyxose and xylulose. Dias et al. proposed a similar reaction mechanism for sulfated zirconia as Scheme 2 shown in the present study; however, there were no kinetic studies reported on the pathway of FUR formation from the intermediate (Dias et al. 2007).
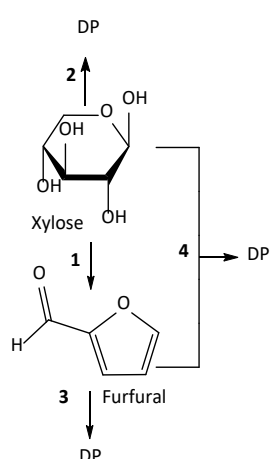
Scheme 1. FUR formation with Direct Xylose Decomposition
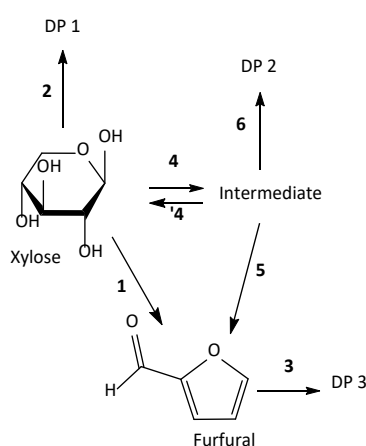
Scheme 2. FUR Formation with Side Reaction between Intermediate and FUR
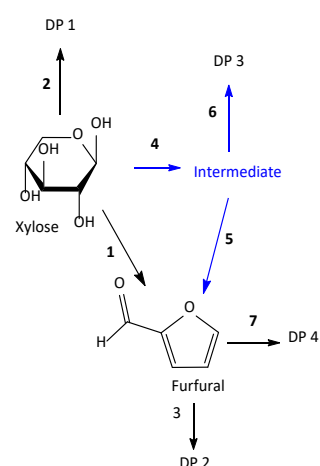
Scheme 3. FUR Formation with Side Reaction Decomposition

Choudhary et al. studied the pentose conversion into FUR employing HCl as a Brønsted acid catalyst (Choudhary et al. 2012). It seems that the dehydration of xylose in the presence of Brønsted acid follows a direct path; whereas when Lewis acid is present, xylose could isomerise to xylulose and lyxose by and subsequently dehydrate to FUR.

2.7 Degradation of furfural

Chemocatalytic conversion of sugars often leads to numerous side-products that limit aimed product yields. Figure 6 shows the types of degradation reactions occurring when forming FUR from xylose. Besides, not all of the pentoses will necessarily convert to FUR, due to the occurrence of parallel reactions (Sairanen et al. 2013; Zeitsch, Karl J. 2000b):

- resinification reactions: reactions of FUR with itself;
- condensation reactions: reactions of FUR with an intermediate of the pentose-to-FUR conversion;
- fragmentation reactions: reactions of pentoses leading to compounds with lower molecular mass, such as carboxylic acids.
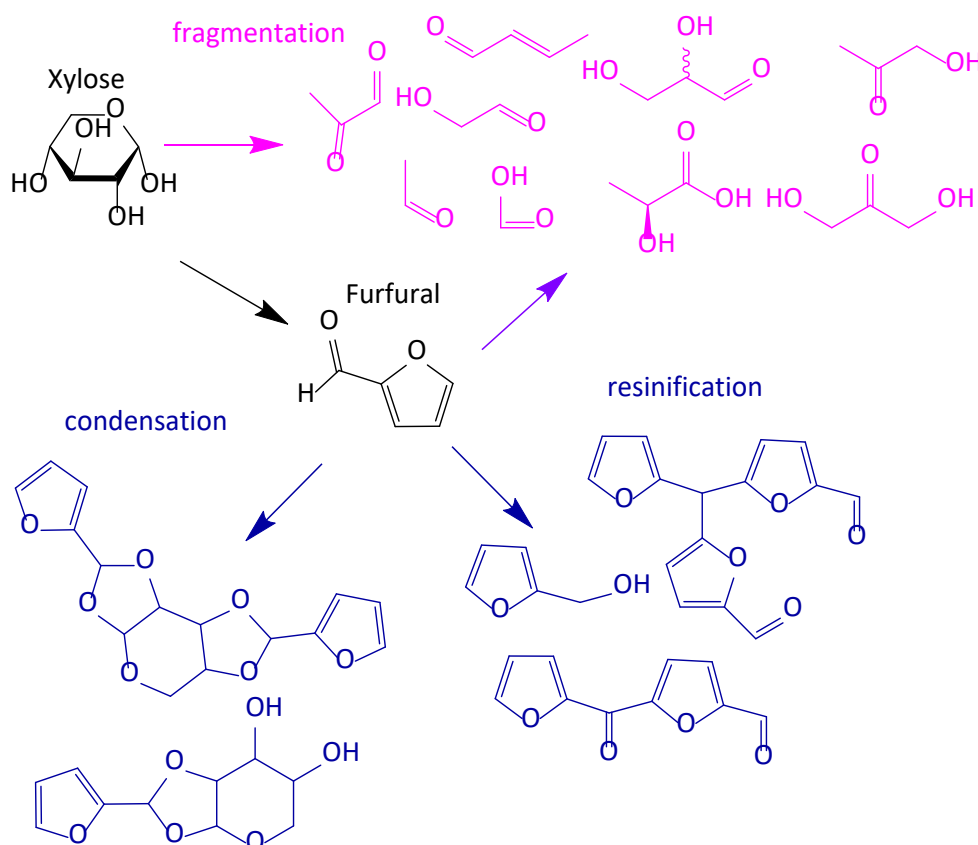
Figure 6. *Formation of furfural from xylose and subsequent degradation of furfural and xylose. Adapted from (Karinen et al. 2011).*

2.8 Biphasic systems

Biomass conversion typically occurs in aqueous systems. Hence, the dehydration of xylose into FUR is associated with a significant challenge that promotes the formation of by-products. An efficient approach to avoid this issue is the addition of an organic co-solvent, which would continuously extract FUR from the aqueous phase into the organic phase. Therefore, FUR would be protected in the organic solvent and hence avoid losses by humin formation, and the FUR yield would be improved (Weingarten et al. 2010).

Amongst various properties to consider when selecting a solvent for biphasic systems, the properties that stand out and need to be balanced are the following (Romo, Joelle E. et al. 2018):

- toxicity
- cost
- viscosity
- solubility of solute and carrier
- the partition coefficient of the solute
- requirement of phase modifiers

Several publications have reported the addition of the following organic solvents as efficient co-solvents for the formation of FUR):

- MIBK (Weingarten et al. 2010),
- MTHF (vom Stein et al. 2011),
- cyclohexanol (Mittal et al. 2017),
- THF (Yang et al. 2012),
- DMSO (Dias et al. 2005a; Dias et al. 2005b; Dias, Lima et al. 2006),
- CPME (Campos Molina et al. 2012; Guenic et al. 2015),

and the widely used toluene (Agirrezabal-Telleria, I., Requies et al. 2014; Agirrezabal-Telleria, I. et al. 2014; García-Sancho et al. 2014).

Figure 7 shows the formation of furfural in a biphasic system using a solid acid catalyst (Starbon®450-SO$_3$H) (Gómez Millán et al. 2019).
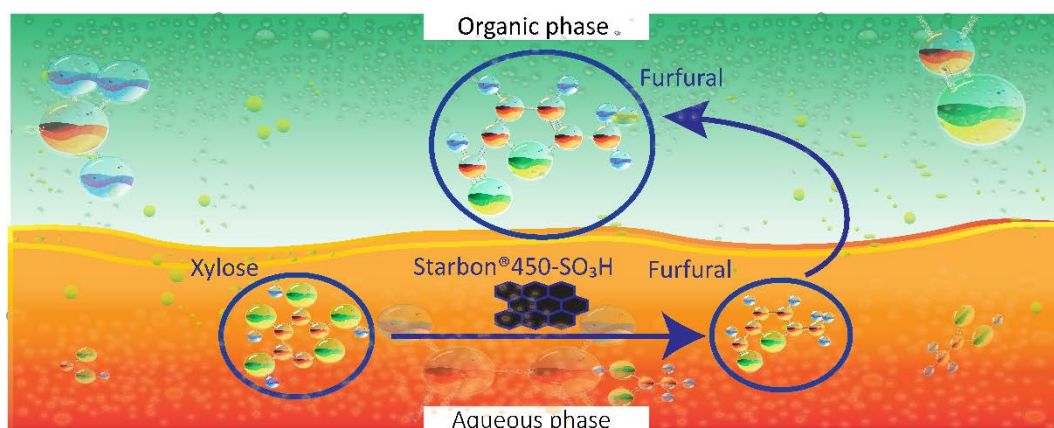
Figure 7. *Furfural formation using Starbon®450-SO$_3$H and further extraction in a biphasic system (Paper III).*

The solvents explored for extracting and synthesising FUR have a wide range of properties, yet Table 5 covers only a small fraction of considerations.

For biphasic systems in the furanic research field, toluene is widely used due to its low solubility in water and a low boiling point (110 °C) compared to FUR (162 °C).

Green solvents, such as MTHF and CPME, are commercially available, offering sustainable alternatives to extract FUR without the addition of salts due to their aqueous-immiscible nature and to provide a superior phase separation at the organic–water interface without forming emulsions (Tenne et al. 2013).

Table 5. *The properties of organic solvents used in the extraction of furfural from the aqueous phase. (Domalski and Hearing 1996; Sigma-Aldrich 2019; Stephenson and Malanowski 1987; Zeitsch, Karl J. 2000a).*

Solvent	Solubility in water (g/100 g) (25 °C)	Density (at 25 °C)	Partition coefficient	Melting point (°C)	Boiling point (°C)	Vapor pressure [mm Hg]	Azeotrope with FUR	Reference
MIBK	19	0.7965	--	-85	116.5	19.9[e]	--	(Weingarten et al. 2010)
MTHF	14[a]	0.853	10	-136	78	97.3[d]	--	(vom Stein et al. 2011)
Cyclohexanol	3.6[a]	0.9624[a]	--	25.4	160.8	0.657[f]	--	Mittal et al. 2017
THF	Miscible	0.8833	--	-108.5	65	162.2[g]	--	Yang et al. 2012
DMSO	Miscible	1.1[a]	--	18.5	189	0.6[h]	--	Dias et al. 2005a; Dias et al. 2005b; Dias et al. 2006
Cyclopentyl methyl ether	1.1[b]	0.8601[a]	12	-140	106	44.9[i]	--	Campos Molina et al. 2012; Guenic et al. 2015; R(Watanabe et al. 2007; Zhang, H. 2015)
2-sec-butylphenol		0.9820[a]	19.8	12	227	0.08[j]	none	(Lin et al. 2015)
Isophorone	1.2[a]	0.9255	13	-8.1	215.2	0.44[c]	--	(Ershova, Olga et al. 2018)
Toluene	0.526	0.8623[a]	--	-95	110.6	28.5[k]	--	Agirrezabal-Telleria, I., Requies et al. 2014; Agirrezabal-Telleria, I. et al. 2014; García-Sancho et al. 2014

[a] Measured at 20 °C. [b] Measured at 23 °C.

[c] (U.S. Environmental Protection Agency. Chemistry Dashboard. a), [d] (U.S. Environmental Protection Agency. Chemistry Dashboard. b), [e] (U.S. Environmental Protection Agency. Chemistry Dashboard. c), [f] (National Center for Biotechnology Information. PubChem Database. a), [g] (National Center for Biotechnology Information. PubChem Database. b), [h] (National Center for Biotechnology Information. PubChem Database. c), [i] (Chemical Book 2017), [j] Measured at 20 °C. (International Labour Organization and World Health Organization 2002a), [k] (International Labour Organization and World Health Organization 2002b).

2.9   Economic aspects

FUR has an estimated global production of 400 kt per year worldwide. China is leading the production of FUR from corncobs, accounting for 70% of the FUR in the global market. The Dominican Republic and South Africa are the other two countries producing FUR from bagasse. In contrast, FUR commercialisation in Europe has been limited and penalised with antidumping taxes (Zeitsch, K. J. 2000).

By 2002, the market price of FUR was around 1500 €/t (Toor et al. 2011). This value sunk to 1200 – 1300 €/t (DalinYebo 2014), which is highly dependent on oil prices. The market price of FUR started to decrease in early 2015 from 1230 EUR/t to 880 EUR/t one year later (CCM 2016). It is expected that the global FUR market will reach around EUR 1,050 million by 2020 (650 kt). In a recent article from Huber's group, they reported a market price in December 2015 of 1660 €/t and an estimated minimum selling price of 1540 €/t (Olcay et al. 2018). Bbosa and Brown recently completed a techno-economic analysis of a corn stover-ethanol biorefinery concept, whereby they set a market price of FUR of 933 €/t (Bbosa et al. 2018). Currently, the prices available in Alibaba are in a range from 910 to 1630 €/t (Alibaba 2019).[1]

---

[1] Original prices reported in USD were converted to EU with a conversion rate of 1 USD = 0.90612 € on September 10th 2019.

3. Research questions

The central objective of this thesis was to develop assessments to produce high FUR yields from a side-stream of dissolving pulp production. Inspired by this aim, we started this project to develop solid acid catalysts in order to offer alternatives to current industrial practices, which are related to environmental concerns and low FUR yields. Furthermore, once FUR is formed in the aqueous phase, it undergoes degradation. In order to prevent FUR degradation, organic solvents in biphasic systems extract immediately formed FUR, while the sugar and carboxylic acids, formed as by-products from the reaction, remain in the aqueous phase.

The feasibility of such a process was investigated by the following research questions:

1. What is the reaction mechanism of FUR formation from xylose when using solid acid catalysts? (Paper I)
2. What is the effect of solid acid catalysts on FUR formation? (Papers I and III)
3. What characteristics of solid acid catalysts play a key role in the efficient production of FUR? (Papers I and III)
4. What properties of organic solvents affect the extraction of FUR in biphasic systems? (Paper II and Paper IV)
5. What is the highest FUR yield reached when adding organic solvents into the system (Paper II, Paper III and Paper IV)
6. Is it feasible to produce FUR from a birch hydrolysate liquor? (Paper IV)

The relationship between the papers is illustrated in Figure 8.

Paper I was directed towards heterogeneous catalysis in aqueous phase. Two catalysts (metal oxides) were developed for this purpose and compared with two commercially available polymeric resins (Nafion NR40 and Amberlyst DT). A kinetic model was proposed to address FUR formation from xylose when using solid acid catalysts.

The second approach, **Paper II**, studied the formation of FUR under auto-catalysed conditions in a biphasic system comparing different organic solvents. Furthermore, it addressed FUR degradation and the role that organic solvents play in the process.

The third approach, **Paper III,** discusses the formation of FUR in combination with heterogeneous catalysis in a biphasic system (vide infra). This approach considers a hydrothermally stable solid acid catalyst that can be reused in various cycles without losing its catalytic activity.

Paper IV focused on the formation of FUR in a biphasic system under auto-catalysed conditions and the recovery of value-added chemicals produced in the process. A techno-economic study was performed to evaluate the feasibility of the process.
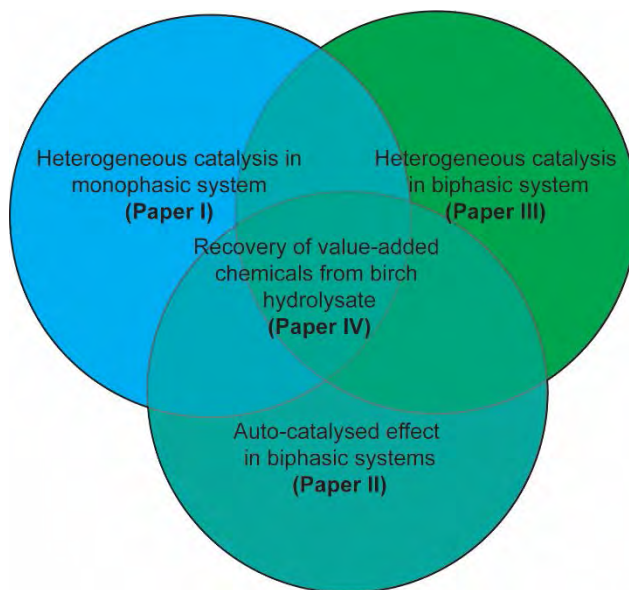
Figure 8. *Fields of research work described in this thesis.*

4. Materials and methods

This chapter briefly describes the materials and the most essential methods used throughout this study. A more detailed description can be found in **Papers I – IV**.

4.1   Materials

Xylose was obtained from Sigma-Aldrich at ≥99 wt% purity. FUR was obtained from Sigma-Aldrich at 99% wt% purity. For experiments requiring higher purity, vacuum-distilled FUR with 99.8 wt% purity was used. Water was produced by the Millipore Synergy® UV purification system (water resistivity of 18.2 MΩ).

Birch hydrolysate liquor was supplied by Stora Enso (Stora Enso, Imatra, Finland), which was used for the dehydration reaction experiments.

Cordierite was obtained from Corning (Germany) and $ZrOCl_2 \cdot 8H_2O$ from Sigma Aldrich.

Potato starch was obtained from Sigma-Aldrich.

Iso-butanol (99.9%) and acetone (99.9%) were obtained from Sigma-Aldrich and were used as internal standards (IS) in **Paper II** and **Paper III**; and **Paper IV**, respectively.

4.2 Microwave-assisted reactor

Experimental tests were conducted in 10-ml vials in a microwave reactor (Anton Paar Monowave 300), with holding times ranging from 2 to 180 min (Figure 9). The samples were stirred with a speed of 600 rpm.

In the solid acid-catalysed reaction, 50 mg of SZ on cordierite was added to 3 ml of a xylose solution (186 mmol l^{-1}). The resulting solutions were analysed for xylose, furanic compounds and carboxylic acids by the same analytical procedure (**Paper I, II and IV**).

Figure 9. Valorisation of hemicelluloses using a microwave reactor (Monowave 300, Anton Paar GmbH, Graz, Austria) in papers I, II and IV.

4.3 Oil bath reactor

Due to incompatible operational limits of the microwave reactor described above and the experimental design, an oil bath with conventional heating was used. The microwave reactor can only be operated for 3 h at 200 °C. Experimental tests were conducted in 5-ml vials with holding times ranging from 1 to 24 h and reaction temperatures from 150 to 200 °C (**Paper III**).

4.4 Catalyst preparation

Catalysts used in **Paper I** were prepared following the method of Ledesma and Llorca with few modifications (Ledesma and Llorca 2009). Pieces of cordierite (1–4 mm) were used as support. Sulfated zirconia (SZ, $ZrO_2(SO_4^{2-})$) and Al_2O_3 were prepared by impregnation of $ZrOCl_2 \cdot 8H_2O$ and boehmite suspensions as precursors over cordierite. The notation for SZ over cordierite is SZ_{cord}; while for Al_2O_3 over cordierite, the notation is Al_2O_{3cord}. The resulting samples were dried at 105 °C and then calcined in air for 2–5 h to obtain the corresponding active oxides (SZ_{cord} at 500 °C; Al_2O_{3cord} at 450 °C). The inclusion of cordierite in the catalyst preparation was aimed at providing the catalyst a physical support for practical application.

Commercially available polymeric resins, such as Nafion NR40 and Amberlyst DT, were purchased. Reaction tests were conducted with these polymeric resins for the sake of comparison. Nafion NR40 was purified by treatment with hot hydrogen peroxide (5%) to remove organic impurities and soaked in 5 wt% hot hydrochloric acid to remove cations and exchange them by protons. It was dried overnight at 105 °C. Amberlyst DT was also dried overnight at 105 °C prior to experimental tests.

A carbonaceous-based catalyst (Starbon®) was used in **Paper III**. Starbon refers to STARch carBONised at different temperatures. The catalyst was synthesised according to published literature procedures with minor modifications (Ojeda et al. 2014). First, the starting material, potato starch, was heated in water to 140 °C for 2 h (150 g starch in 3 litres of deionised water). Upon cooling, the warm solution was poured into a vial at room temperature, and it was further cooled down to 5 °C for 48 h until the formation of a porous gel in water. To avoid the structure collapsing while drying, several solvent exchange steps were conducted until the water was fully replaced by ethanol (5 times), and finally by acetone (2 times) to stabilise the porous network. The resulting materials were then filtered off and dried overnight at 50 °C under a vacuum, rendering the mesoporous starch structure, and subsequently calcined at 450 °C under inert atmosphere (N_2, 50 mL min^{-1}) by using the following heating conditions: from RT to 450 °C, heating rate 1 °C min^{-1}; temperature maintained for 1 h. A purge with nitrogen prior to carbonisation was conducted to ensure the absence of oxygen in the first steps of carbonisation. For sulfonation, the calcined Starbon®450 material was suspended in H_2SO_4 of 95-97% purity (10-mL acid per gram of material and 4 h at 80 °C). After sulfonation, samples were thoroughly washed with distilled water until achieving a neutral pH value, and finally oven-dried at 100 °C overnight. The resulting functionalised mesoporous acid material was denoted as Starbon®450-SO_3H.

4.5 Catalyst characterization methods

Characterisation methods for the solid acid catalysts and liquid samples are summarised in Table 6. Detailed descriptions of the individual analyses can be found in the corresponding papers.

4.5.1 Scanning electron microscopy (SEM)

Scanning electron microscopy (SEM) is currently employed to understand nano-materials. This technique was used to observe the morphology and composition of samples for imaging, diffraction and elemental analysis.

SEM images were recorded at 2 kV (for Amberlyst DT and Nafion NR40) and at 5 kV (for Al_2O_{3cord} and SZ_{cord} on cordierite) in **Paper I** using a Zeiss Neon40Crossbeam Station instrument equipped with a field emission source (Soler et al. 2016). Samples were deposited on conductive carbon tabs. SEM images in **Paper III** were recorded at 5 kV using a JEOL JSM-7800F PRIME Schottky Field Emission Scanning Electron Microscope equipped with a high-resolution Gentle Beam (GBSH). Samples were deposited on conductive carbon tabs. The instrument has a field emission gun and is also equipped with an EDX detector for chemical analysis.

4.5.2 Thermogravimetric analysis (TGA)

Thermogravimetric analysis (TGA) was employed as a technique to monitor the weight of the sample as a function of temperature or time in a controlled atmosphere. Hence, upon heating the sample, its weight increased or decreased.

TGA was carried out in a Setaram Setsys 12 using air as the carrier gas (50 mL min^{-1}). The sample was loaded in ceramic crucibles with α-Al$_2$O$_3$ used as the reference compound, and a Pt/Pt-Rh (10%) thermocouple. The heating rate employed was 10 K min^{-1} in all cases (**Paper III**).

4.5.3 IR spectroscopy

Infrared (IR) spectroscopy is a convenient technique that was used to study surfaces or interfaces of the solid acid catalysts. IR uses the absorption of IR photons at characteristic energies, which are associated with the excitation of the molecules' specific vibrating modes.

IR studies were conducted using Diffuse Reflectance Infrared Fourier Transform (DRIFT). Spectra were recorded on an ABB BOMEM MB 3000 Instrument equipped with an environmental chamber (Spectra Tech, P/N, 0030-100) placed in the diffuse reflectance attachment. The resolution was 8 cm^{-1}, and 256 scans were averaged to obtain the spectra in the 4000-400 cm^{-1} range. Spectra were recorded by using KBr as a reference. The samples for DRIFTS studies were prepared by mechanically grinding all reactants to a fine powder (sample/KBr 1:5.7 ratio).

4.5.4 N$_2$-physisorption

Nitrogen (N$_2$) physisorption is used as a method for probing the molecular interactions occurring at a solid surface. This technique was used to evaluate the specific areas of the samples, the volumes of their pores and their mean pore diameters.

In this study, a Micromeritics Tristar II-Physisorption Analyzer was utilised to record the nitrogen sorption isotherms for fresh and spent catalysts. All samples were dried at 105 °C and exposed to nitrogen gas for 12 h before measurement, and the isotherms were taken at 196.15 °C. The samples were exposed to ~20% humidity room air for about 1 min during the transfer to the holders. The specific surface area (A$_{BET}$) was determined by the Brunauer-Emmett-Teller (BET) model (Brunauer et al. 1938) at relative pressures between 5% and 35%, where the data points were observed to arrange linearly. Five types of isotherms can occur depending on the adsorption scenario. The BET equation is applicable on isotherms type II and IV only, where there is a formation of a monolayer followed by multi-layers and further capillary condensation (Legras et al. 2015). The BET equation is given by Equation 1. The specific pore volume (V$_p$) was estimated from N$_2$ uptake at a p/p$_0$ value of 0.99, while recording approximately 150 equilibrium data points.

$$\frac{P}{n(P_0 - P)} = \frac{C-1}{n_m C}\left(\frac{P}{P_0}\right) + \frac{1}{n_m C} \qquad \text{(Eq. 1)}$$

where P is the solvent partial pressure in the gas phase (Torr), P_0 the saturated solvent vapor pressure (Torr), n the amount of gas adsorbed (mol g^{-1}), n_m the monolayer capacity (mol g^{-1}) and C the BET constant.

The pore width distribution (d_p) was deduced from the desorption branch using the Barrett-Joyner-Halenda (BJH) method (Barrett et al. 1951). The BJH method is a procedure to calculate pore size distributions from experimental isotherms using the Kelvin model of pore filling, where a cylindrical pore geometry is assumed and the desorption branch data of the isotherm are used. It applies only to the mesopore and small macropore size range.

4.5.5 Xylose adsorption tests

Xylose adsorption experiments were carried out to study the adsorption of xylose on the catalyst surface. This was completed in order to determine the availability of reaction-starting material on the surface.

Xylose adsorption tests were completed by stirring 3 mL of an aqueous solution of 186 mmol l^{-1} xylose using a borosilicate glass reactor (V = 10 cm^3) with magnetic stirring (600 min^{-1}) and 50 mg of Starbon®450-SO$_3$H. Agitation of the suspension took place for 24 h at room temperature (25 °C). The determination of xylose adsorption was performed by HPLC analysis.

4.5.6 Pyridine titration

Pyridine (PY) titration experiments were conducted in order to measure the acid properties of the materials. This technique was completed similarly to the method found in the literature, with few modifications (Pineda et al. 2012). The experiments were performed at 200 °C via gas phase adsorption of the basic probe molecules, utilising a pulse chromatographic titration methodology. Briefly, probe molecules (typically 2-5 µL) were injected into a gas chromatograph (GC) through a microreactor in which the solid acid catalyst was previously placed. Basic compounds were adsorbed to full saturation, from which the peaks of the probe molecules in the gas phase were detected in the GC. The quantity of probe molecules adsorbed by the solid acid catalyst could subsequently be easily quantified.

4.5.7 Raman spectroscopy

Raman spectroscopy is a form of vibrational spectroscopy technique, which was employed in this study to determine the chemical makeup of materials. This tool offered information about interactions among functional groups, chain orientation, structural changes upon treatment/modification, and interfacial properties of the sample.

Raman spectra were measured using a WITec alpha300 R Raman microscope (alpha 300, WITec, Ulm, Germany) equipped with a piezoelectric scanner using a 532-nm linear polarised excitation laser. The measurement was conducted directly on the powder catalyst, after washing and drying.

4.5.8 X-ray photoelectron spectroscopy (XPS)

X-ray photoelectron spectroscopy (XPS) revealed the elemental distribution and therefore chemical state of the sample's surface.

The surface characterisation was completed with XPS on a SPECS system equipped with an Al anode XR50 source operating at 150 W and a Phoibos 150 MCD-9 detector. The pressure in the analysis chamber was maintained below 10^{-7} Pa. The area analysed was about 2 mm × 2 mm. The pass energy of the hemispherical analyser was set at 25 eV, and the energy step was set at 0.1 eV. Peak fitting and quantification analysis were performed using the software package CasaXPS (Casa Software Ltd., UK). Binding energy (BE) values were referred to the adventitious C 1s signal at 284.8 eV. Atomic surface ratios were obtained by using the peak areas, normalised on the basis of acquisition parameters after background subtraction, experimental sensitivity factors and transmission factors provided by the manufacturer.

4.5.9 Ion-exchange capacity (IEC)

The ion-exchange capacity (IEC) represents the total of active sites or functional groups responsible for ion exchange in polymer electrolyte materials. It is defined as the milliequivalent of the ion-exchange groups included in a 1-g dry membrane (meq (g dry membrane)$^{-1}$). The concentration of ion-exchange groups was obtained by dividing the IEC with the water content in a 1-g dry membrane (meq (g H_2O)$^{-1}$). Generally, a conventional acid-base titration method is performed to determine the ion-exchange capacity.

For the polymeric resins, the general titration procedure was carried out based on Boehm's method (Boehm 2008; Goertzen et al. 2010). A known mass of the catalyst was added to 50 ml of one of 0.02 M concentration: NaOH (Sigma-Aldrich, 99.998%). The samples were agitated by shaking for 24 h and then filtered to remove the solid, and 10-ml aliquots were taken by pipette from the sample into three different flasks. Each of the three aliquots of the reaction base NaOH were then acidified by the addition of 10 ml of 0.02 M HCl (Sigma–Aldrich, 99.999%). The acidified solutions were then back-titrated with 0.02 M NaOH, the titrator base.

4.5.10 NH$_3$-TPD

Temperature-programmed desorption of ammonia (NH$_3$-TPD) was used to characterise solid catalysts, revealing information on acid site density and adsorption sites. The method is based on the measurement of the desorption profile of a pre-adsorbed probe molecule during controlled heating (Chen, L. et al. 2019).

In this study, NH$_3$-TPD was achieved with an AutoChem II 2920 chemisorption analyser equipped with a TCD detector to measure the total acidity of the samples before and after hydrothermal reaction. Prior to the analysis, the sample (about 100 mg) was pre-treated from RT to 110 °C under flowing He with a heating rate of 10 K min^{-1} for 0.5 h to remove undesirable physisorbed species, followed by heating under an He environment at 600 °C for 1 h, then cooled down to RT. Consequently, the sample was exposed to a flowing NH$_3$ gas mixture (15% NH$_3$ in He with a flow of 50 ml min^{-1}) for 1 h, then purged by He gas for

30 min to remove excessive physisorbed NH_3. The NH_3-TPD of the samples was carried out by increasing the reactor temperature linearly to 600 °C with a heating rate of 10 K min^{-1}.

4.6 Determination of xylose conversion, FUR yield and selectivity to FUR

In this research work, conversion is defined in terms of moles of reactant converted per unit volume of reactor (Eq. 2). Selectivity, at an instant, is the generated amount of moles of desired product relative to the moles of reactant converted (Eq. 3). Yield is the amount in moles of desired product, FUR, produced relative to the amount of the key reactant, xylose (Eq. 4) (Pirola et al. 2013). The following equations have been used for the mathematical evaluation of the obtained results:

$$X_{xyl} = \frac{c_{xyl}^{in} - c_{xyl}^{f}}{c_{xyl}^{in}} \times 100 \ [\%] \qquad \text{(Eq. 2)},$$

$$S_{xyl}^{fur} = \frac{c_{fur}}{c_{xyl}^{in} - c_{xyl}^{f}} \times 100 \ [\%] \qquad \text{(Eq. 3)},$$

$$Y_{fur} = \frac{c_{fur}}{c_{xyl}^{in}} \times 100 \ [\%] \qquad \text{(Eq. 4)},$$

where X, S, Y are the – conversion of xylose, selectivity to FUR and FUR yield, respectively; c is the – concentration in mmol (the subscripts to be read as follows: *xyl*, *fur*, *in*, *f* are the– xylose, FUR, initial, final).

When hydrolysate liquor was used, pentose conversion, selectivity to FUR and FUR yield were calculated equations 4, 5 and 6, respectively.

Conversion of pentoses (namely arabinose and xylose), selectivity to FUR and FUR yield were determined in accordance with the previous section, employing hydrolysate liquor as reactant.

$$X_{xyl} = \frac{c_{Pentoses}^{0} - c_{Pentoses}^{e}}{c_{Pentoses}^{0}} \times 100 \ [\%] \qquad \text{(Eq. 5)},$$

$$Y_{fur} = \frac{(C_{FUR\_ut}^{e} - C_{FUR\_ut}^{0}) + C_{FUR}^{Org}}{C_{Pentoses\_t}^{0} + C_{FUR\_ut}^{0}} \times 100 \ [\%] \qquad \text{(Eq. 6)},$$

$$S_{Pentoses}^{fur} = \frac{\left((C_{FUR\_ut}^{e} - C_{FUR\_ut}^{0}) + C_{FUR}^{Org}\right) \times C_{Pentoses}^{0}}{(C_{Pentoses}^{0} - C_{Pentoses}^{e}) \times (C_{Pentoses\_t}^{0} + C_{FUR\_ut}^{0})} \times 100 \ [\%] \qquad \text{(Eq. 7)},$$

where X, S, Y are the – conversion of xylose, selectivity to FUR and FUR yield, respectively; c is the – concentration in mmol (the subscripts and superscripts to be read as follows: *pentoses*, *fur*, *ut*, *t*, *0*, *e*, *Org*, are the – pentoses (arabinose and xylose), FUR, hydrolysate liquor untreated, hydrolysate liquor treated according to the National renewable Energy Laboratory, before, after reaction and FUR in the organic phase, respectively).

4.7   Analytical methods

Xylose, furanic compounds (FUR and HMF) and carboxylic acids (acetic, formic and levulinic acid) were determined by HPLC from an aqueous phase operating a Dionex Ultimate 3000 HPLC (Dionex, Sunnyvale, CA, USA) device equipped with a refractive index (RI) and ultraviolet (UV) diode array detectors. For **Paper I** and **Paper II**, product separation was achieved on a HyperRez XP Carbohydrate Ca$^+$ column (Thermo Scientific, Waltham, MA, USA). For **Paper III** and **Paper IV**, product separation was achieved on a Rezex ROA-Organic Acid H$^+$ (8%) LC column (7.8 mm × 300 mm, PHenomenex, USA). The FUR concentration was determined by the UV detector at a wavelength of 280 nm. Xylose concentration was simultaneously analysed by the RI detector and the UV detector at 210 nm.

The concentration of monomeric sugars was measured by high-performance anion exchange chromatography with pulse amperometric detection (HPAEC-PAD) by using a Dionex ICS-3000 column.

FUR and HMF from the organic phase were analysed by gas chromatography with a flame ionisation detector (GC-FID). The column used was a DB-WAXetr (30 m, 0.32 mm i.d., 1 μm film thickness) from Agilent Technologies Inc.

Table 6. *Principal analytical methods for solid acid catalysts and liquid characterization.*

Analyses	Methods / Standards	Papers
Catalyst characterization		
Morphology	SEM	I, III
Texture	N$_2$-physisorption	I, III
	NH$_3$-TPD	I
Acid site density	Ion exchange capacity	I
	Py-titration	III
Surface chemistry	XPS	I, III
Weight dependence on temperature	TGA	III
Surface functionalities	IR	III
Molecular vibration	Raman	III
Liquid samples		
Furanics, xylose and acids	Liquid chromatography	I-IV
Furanics and acids	Gas chromatography	II-IV
Carbohydrates	NREL/TP-510-42623	II, IV

5. Results and discussion

The experimental results of this thesis can be divided into five sections, in which FUR formation and its degradation are studied from different perspectives. The first part deals with a study of FUR formation in aqueous phase (monophasic system), where the feasibility of solid acid catalysts to form FUR from xylose is determined. The second part focuses on FUR formation in biphasic systems adding organic solvents to immediately extract formed FUR. In the third part, FUR degradation reactions are studied. In the fourth part, hydrothermal stability, reusability and deactivation of the solid acid catalysts used in the present work are addressed. In the last part, a techno-economic study was completed for FUR formation in a biphasic system from hydrolysate liquor included in a biorefinery concept.

5.1 Monophasic system (Aqueous phase)

5.1.1 Auto-catalyzed dehydration of xylose into furfural (aqueous) phase

Furans can be produced via an auto-catalytic process, with the mechanism initiated by the formation of H^+ and OH^- ions in high temperature water (Akiya and Savage 2002). Later on, carboxylic acids, such as formic acid and acetic acid, and fragmentation products have been shown to contribute to the reaction activity (Chen, Z. et al. 2015).

Auto-catalysed xylose dehydration experiments were performed at various reaction times at temperatures of 170, 190 and 210 °C. Figure 10 shows the FUR yield, xylose conversion and selectivity to FUR under these reaction conditions. The influence of the reaction temperature on the FUR yield and xylose conversion has been observed previously in similar work (Danon, B. et al. 2014; Ershova, O. et al. 2015). Under the present experimental conditions, the maximum FUR yield (48–49%) (Figure 10a) was reached after the first 60 min at 210 °C, which corresponds to a xylose conversion of 94% (Figure 10b) and a FUR selectivity of 52% (Figure 10c). A comparable FUR yield (45-48%) was obtained in 35 min at 220 °C, corresponding to a xylose conversion of 96% when using a xylose solution of 196 mmol l^{-1}. Furthermore, a similar xylose conversion and FUR yield was reached at 200 °C after 115-125 min (Ershova, O. et al. 2015). The decrease of FUR yield in prolonged reaction times occurs due to the degradation and polymerisation associated with humin production (Sievers et al. 2009; van Zandvoort et al. 2013).
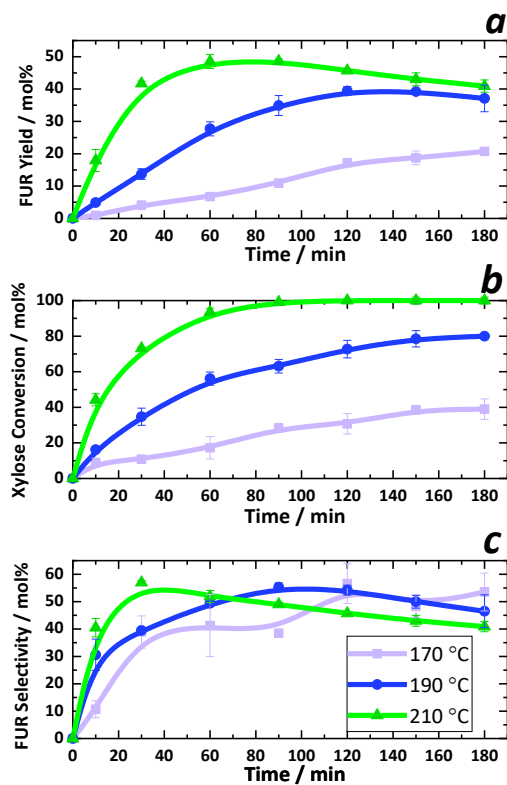
Figure 10. *Furfural yield (a), xylose conversion (b) and selectivity to furfural (c) at various reaction times during auto-catalyzed conversion of xylose 186 mmol l^{-1} (purple square – 170 °C, blue circle – 190 °C, green triangle – 210 °C, lines are to guide the eye).*

At reaction temperatures of 170 and 190 °C, no distinct FUR yield culmination point, with subsequent rapid decrease, was perceived during the reaction time range investigated. However, a yield decrease similar to that observed at 210 °C could be possibly observed at lower reaction temperatures (170 and 190 °C) during prolonged reaction times. Nevertheless, the maximum yield unmistakably shifts to a longer reaction time with a decline of the reaction temperature. Furthermore, the FUR yield (and thus also the selectivity) decreases with decreasing reaction temperature, which is in agreement with the literature [50]. It is worth noting that the maximum selectivity to FUR observed in the auto-catalysed conversion of xylose was 56–58% in the present studied range of reaction temperatures. These results agree with previously published papers (Ershova, O. et al. 2015).

The high reactivity of FUR challenges the production process due to its aldehyde and aromatic ring. These chemical structures tend to react easily with other chemical compounds present in the medium. Besides humins, other compounds were observed and identified in the dehydration reaction, such as formic, levulinic and acetic acid, as well as HMF, when hydrolysate liquor was employed. These by-products affected the selectivity to FUR.

5.1.2   Solid acid-catalyzed dehydration of xylose into furfural

Previous published literature has described the high catalytic activity of metal oxides in the dehydration of xylose into FUR. However, the hydrothermal stability of these materials has not been properly addressed. Furthermore, the reaction times to reach the highest FUR yields usually require from 2 (Weingarten et al. 2011) up to 20 h (Agirrezabal-Telleria,

I., Requies et al. 2014; Dias et al. 2005a; Dias et al. 2005b; Dias, Pillinger et al. 2006; Dias, Lima et al. 2006; Dias et al. 2007).

SZ on cordierite (SZ_{cord}), Al_2O_3 on cordierite (Al_2O_{3cord}), Nafion NR40 and Amberlyst DT were studied in monophasic aqueous systems. Results obtained using SZ_{cord} are discussed in the present work. Al_2O_{3cord}, Nafion NR40 and Amberlyst DT are studied in more detail in **Paper I**.

During the SZ_{cord} -catalysed reaction, the maximum FUR yield was 41% (at 210 °C in 2 min, Figure 11a), corresponding to a xylose conversion of 96% (Figure 11b) and a FUR selectivity of 43% (Figure 11c). In comparison to the auto-catalysed conditions, the highest FUR yield (48%) was reached after the first 60 min at 210 °C. When comparing the present results with the catalysed system using H_2SO_4 (Ershova, O. et al. 2015) and a xylose concentration of 196 mmol l^{-1}, the highest selectivity to FUR is 68% (at 180 °C in 5 min) and 65% (at 200 °C in 1 min, and at 220 °C in 2 min). The maximum yield unmistakably shifts to a longer reaction time with a decline of the reaction temperature.
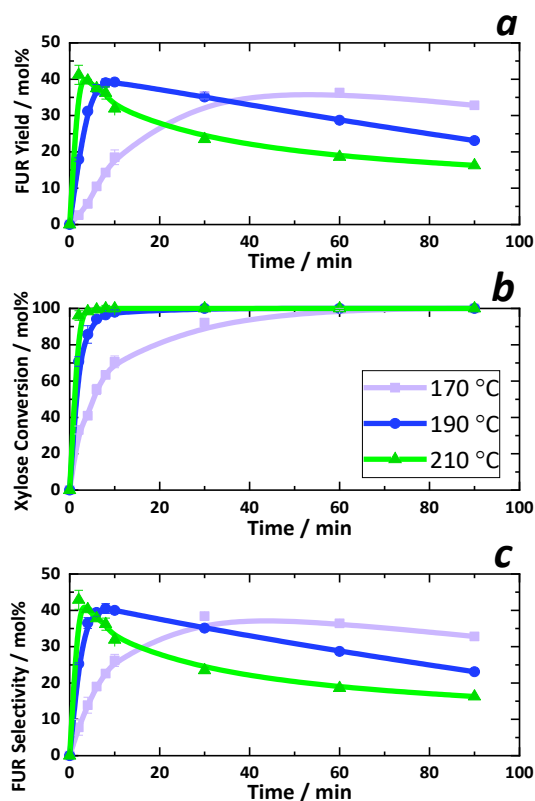
Figure 11. Furfural yield (a), xylose conversion (b) and selectivity to furfural at various reaction times during conversion of xylose 186 mmol l^{-1} using 50 mg of SZ_{cord}. (purple square – 170 °C, blue circle - 190 °C, green triangle – 210 °C, lines are to guide the eye).

Dias et al. (Dias et al. 2007) studied various sulfated zirconias in the formation of FUR from xylose in an aqueous-toluene system at 160 °C in 4 h. They were able to identify a correlation of the catalytic activity with the sulphur content of the sulfated zirconia. Nevertheless, a significant amount of sulphur leaching was observed in the reusability tests. Zhang J. et al. (Zhang, J. et al. 2014) used a SO_4^{2-}/ZrO_2-TiO_2 catalyst in a sugar mixture employing an aqueous-n-butanol biphasic system. The maximum FUR yield (48 mol%) was reached at 170 °C in 2 h. Even though the authors performed a reusability test, two cycles might

not be enough to observe hydrothermal stability of the catalyst. Li et al. (Li et al. 2014b) employed a $SO_4^{2-}/TiO^{2-}ZrO_2/La^{3+}$ catalyst in a biphasic system to form FUR from xylose. The highest FUR yield reported (3563 µmol of FUR/g of xylose) was reached in 12 h at 180 °C. However, the article lacks hydrothermal stability studies and the reusability potential of the metal oxide catalyst.

When Starbon®450-SO_3H (50 mg) was added to the aqueous xylose solution (3 ml of 186 mmol l^{-1}) at 170 °C at various reaction times, the highest FUR yield reached was 42% (**Figure 12**a) at a xylose conversion of 73% (**Figure 12**b) and a selectivity to FUR of 58% (**Figure 12**c) in 6 h.
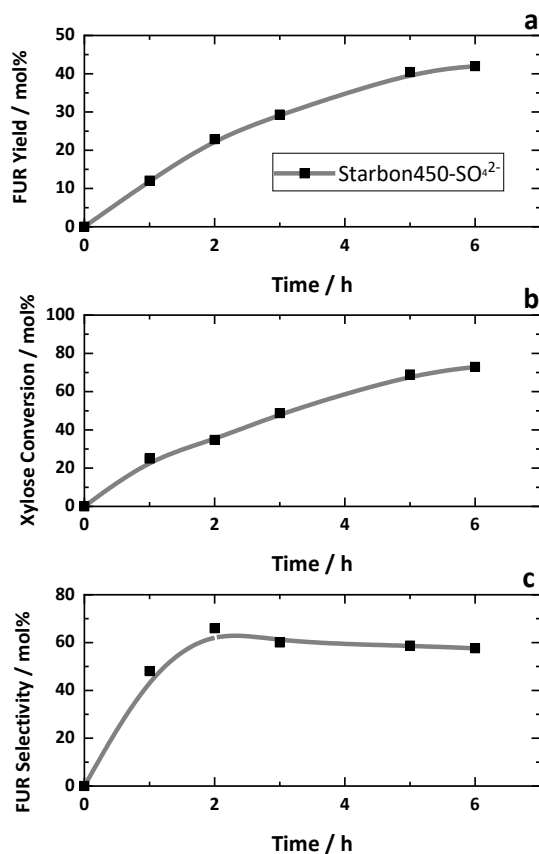
Figure 12. Furfural yield (a), xylose conversion (b) and selectivity to furfural at 170 °C during conversion of xylose 186 mmol l^{-1} using 50 mg of Starbon®450-SO_3H. Lines are to guide the eye.

When using Al_2O_{3cord}, the maximum FUR yield is clearly influenced by the reaction temperature: at 170 °C, it starts from 26%, increasing furthermore up to 43% at 210 °C.

In comparison to the system where SZ on cordierite is used at 170 °C, the highest FUR yield (36%) is reached in 1 h (Figure 11a) with complete xylose conversion. Degradation of FUR when increasing reaction time is visible after this point.

When comparing the present results with the catalysed system using H_2SO_4 (Ershova, O. et al. 2015) and a xylose concentration of 196 mmol l^{-1}, the highest selectivity to FUR is 68% (at 180 °C in 5 min) and 65% (at 200 °C in 1 min, and at 220 °C in 2 min).

Amberlyst DT was only tested at 170 °C (maximum operational temperature) due to its limited hydrothermal stability as stated by the manufacturer. The maximum FUR yield (30%) was reached in 60 min at 170 °C with a xylose conversion of 70% (**Paper I**).

In the same way that reaction temperature strongly influences FUR yield and xylose conversion in the auto-catalysed process, the effect can also be observed when adding Nafion NR40. When adding Nafion NR40 pellets to the aqueous system, the maximum FUR yield is determined by the reaction temperature: at 170 °C, it starts from 33%, furthermore increasing up to 41% at 210 °C (**Paper I**). Due to the nature of the catalysts, the standard deviation increased at high reaction times and at high temperatures (> 190 °C), even though the manufacturer guarantees its stability from 220 to 240 °C in aqueous systems. The catalysts clogged into each other, making a barrier in the middle of the reactor. Therefore, the FUR and xylose concentrations do not follow a smooth tendency. Nevertheless, xylose conversion behaves similarly to the auto-catalysed system, since it requires longer reaction times to convert the same amount of xylose at a lower reaction temperature. In the case of Nafion NR40, the maximum FUR yield (41%) was reached in 8 min at 210 °C, resulting in a xylose conversion of 70% and a FUR selectivity of 60%. During the Nafion NR40-catalysed reaction, the maximum selectivity to FUR was 67% (at 210 °C in 2 min) in contrast to 43% (at 210 °C in 2 min) obtained in the SZ_{cord}-catalysed reaction system, and 52% (at 210 °C in 60 min) in the auto-catalysed reaction system.

5.1.3 Catalyst characterization

Metal oxides and polymeric resins from **Paper I** were characterised using SEM, N_2-physisorption, XPS, ion exchange capacities and NH_3-TPD. Starbon®450-SO$_3$H from **Paper III** was characterised, employing TGA, IR, SEM-EDX, N_2-physisorption, Raman, XPS, Py-titration and xylose adsorption tests. In the present work, results of SEM and XPS will be shown and discussed. For details on other characterisation methods regarding metal oxides and Starbon®450-SO$_3$H, the author refers to **Paper I** and **Paper III**, respectively.

Figure 13 shows, as an example, the scanning electron micrographs of SZ_{cord} before hydrothermal reaction. The SEM images show the similitude of the SZ_{cord} characteristically cylindrical-like structure as reported by (Al-Hazmi and Apblett 2011).
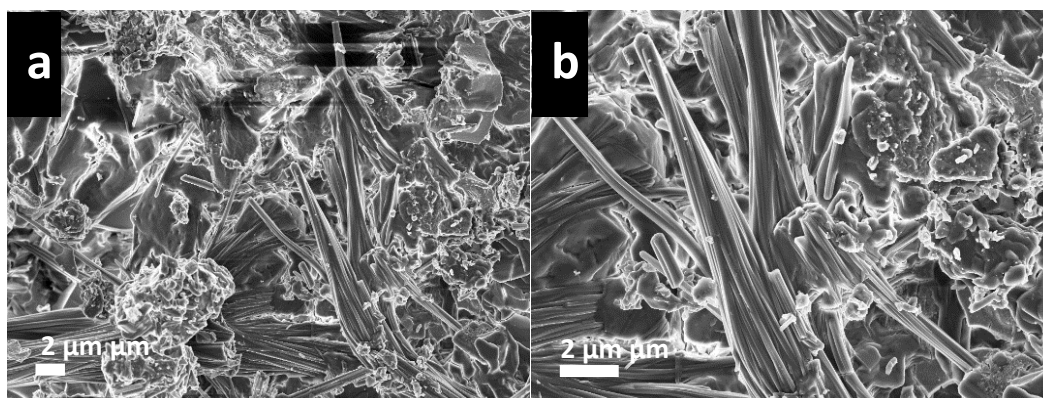
Figure 13. SEM images of SZ on cordierite obtained (Paper I).

In addition to the thorough microscopic analysis, a detailed XPS analysis was performed to gain a deeper insight into the surface composition of the materials. Figure 14 shows

the X-ray photoelectron spectra of SZ_{cord}, before and after hydrothermal reactions, at different temperatures.
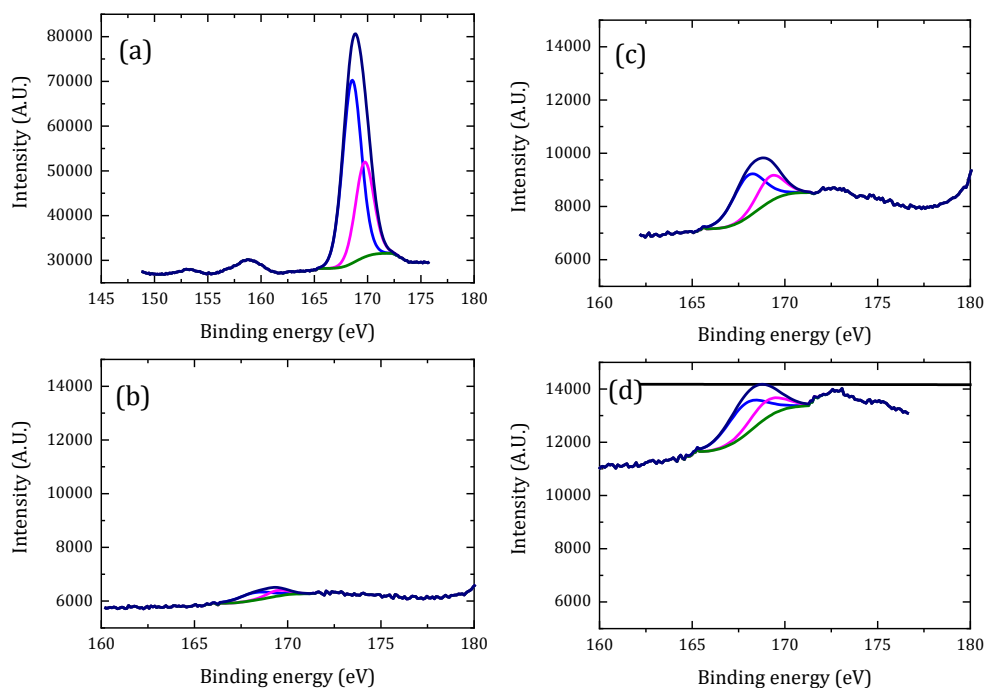
Figure 14. *XPS S 2p spectra of SZ on cordierite before (a) and after hydrothermal reaction at different temperatures: (b) 170 °C; (c) 190° C; (d) 210 °C.*

In Table 7, the binding energy values and surface atomic composition of metal oxides, before and after hydrothermal reaction, are shown. The amount of sulphur at the surface in the sample before hydrothermal reaction is 15% (SZ_{fresh}), and the amounts of sulphur in the samples after hydrothermal reaction – SZ_{170}, SZ_{190} and SZ_{210} – are 0.1, 0.7 and 0.7, respectively. It was inferred from Table 7 that leaching of the acid sites occurred. This means that the acid sites found in the fresh sample leached out into the aqueous solution under the reaction conditions presented in this research work. In the dehydration of xylose, the leaching of S and the accumulation of by-products are the main factors that cause the deactivation of the catalyst. The results shown in Table 7, from samples SZ on cordierite before and after hydrothermal reaction, correlate with the catalytic activity tests in Figure 11. Under the above-mentioned experimental conditions, once FUR is formed, it decomposes, as does xylose. The decomposition products evolve, forming humins on the surface of the catalysts (Figure 25), which is obviously detrimental to the reaction.

The samples of spent SZ on cordierite were characterised after the highest FUR yield was reached at every temperature level. Hence, the highest FUR yield in each temperature level was reached at different reaction times (Figure 11). The highest FUR yields at reaction temperatures of 170, 190 and 210 °C were reached in 60, 10 and 2 min, respectively. Therefore, surface concentrations of Zr and S are lower at 170 °C and 60 min than at 210 °C in 2 min.

Table 7. XPS data of SZ on cordierite before and after the hydrothermal reaction at differ-ent temperatures (170, 190 and 210 °C).

Sample	Name	Binding Energy (eV)	Element	% At Conc
SZ$_{fresh}$	O 1s	531.9	O	52.9
	C 1s	279.7	C	29.4
	S 2p	168.5	S	15.1
	Zr 3d	182.4	Zr	2.7
SZ$_{170}$	O 1s	531.7	O	23.6
	C 1s	284.2	C	75.8
	S 2p	169.0	S	0.1
	Zr 3d	182.3	Zr	0.5
SZ$_{190}$	O 1s	531.8	O	30.4
	C 1s	284.3	C	67.1
	S 2p	168.3	S	0.7
	Zr 3d	182.3	Zr	1.8
SZ$_{210}$	O 1s	531.7	O	36.2
	C 1s	283.8	C	60.6
	S 2p	168.2	S	0.7
	Zr 3d	182.4	Zr	2.5
SZ$_{reused}$	O 1s	532.2	O	48.8
	C 1s	284.2	C	48.9
	Zr 3d	182.4	Zr	2.3

5.1.4   Auto-catalyzed dehydration of birch hydrolysate into furfural

Hydrothermal reactions of birch hydrolysate were determined, under auto-catalysed con-ditions, in a monophasic (aqueous) phase. In addition to xylose and arabinose, birch hy-drolysate contains xylo-oligosaccharides and C6-sugars. The initial composition of the birch hydrolysate liquor is given in Table 8.

Table 8. *Initial composition of the birch hydrolysate after filtration.*

	Monomeric form, g l^{-1}	Total, g l^{-1}
Arabinose	0.63	0.66
Rhamnose	0.47	0.83
Galactose	0.50	1.29
Glucose	0.16	1.12
Xylose	8.05	26.15
Mannose	0.17	1.63
Lignin		4.20
HMF		0.04
Furfural		2.43

Figure 15 displays the FUR yield, pentose (xylose and arabinose) conversion and selectivity to FUR under various reaction times (between 10 min and 180 min) at temperatures of 170, 190 and 210 °C.

As can be seen in Figure 15a, FUR yield and pentose conversion are significantly influenced by the reaction time and temperature, which is in accordance with previous reports in this field (Chen, X. J. et al. 2012; Danon, B. et al. 2014; Gómez Millán et al. 2018; Hongsiri et al. 2015; Kootstra et al. 2009; Sahu and Dhepe 2012).

In the monophasic system, the highest FUR yield (46%) was reached at 190 °C in 60 min. The maximum selectivities to FUR (Figure 15c) formation were 65%, 51% and 43% at temperatures of 170, 190 and 210 °C, respectively. In comparison to the experiments using 186 mmol l^{-1} of an aqueous xylose solution, the highest FUR yield (48-49%) was obtained after the first 60 min at 210 °C, which corresponds to a xylose conversion of 94%. The decrease of FUR yield in prolonged reaction times occurs faster when using hydrolysate liquor than when employing the pure aqueous xylose solution; this is due to the degradation reactions occurring between the formed FUR and the complex matrix of C5- and C6-sugars contained in the hydrolysate liquor.
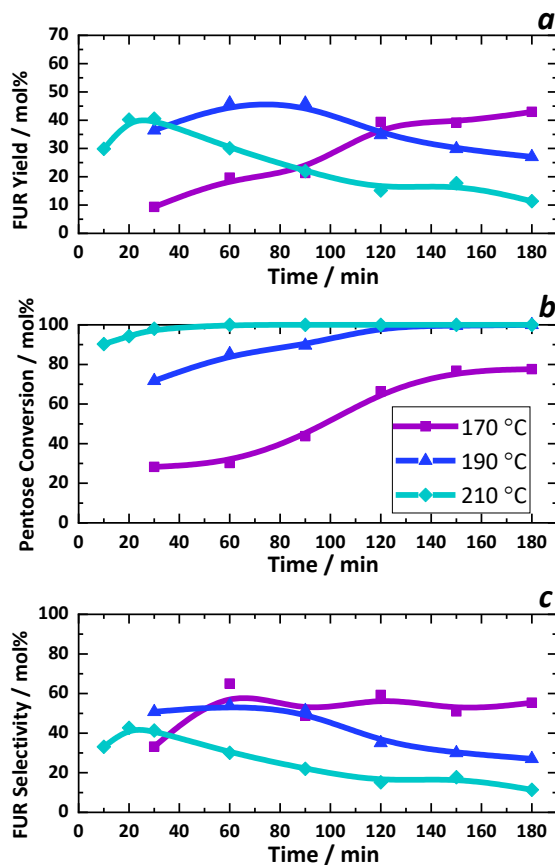
Figure 15. *Effect of temperature and reaction time on (a) FUR yield, (b) xylose conversion, (c) selectivity to FUR during auto-catalyzed conversion of birch hydrolysate liquor. Lines are to guide the eye.*

When birch hydrolysate liquor is used and dehydrated under auto-catalysed conditions at 210 °C, the FUR yield does not surpass that obtained at 190 °C. Under high reaction temperature (210 °C), it is possible that degradation of the complex sugar mix (pentoses and hexoses) contained in the hydrolysate liquor takes place faster. Hence, FUR is prone to degrade in a shorter reaction time at high temperatures, via condensation or resinification.

5.2 Biphasic system

Even though aqueous (monophasic) systems are less expensive than biphasic systems and have been widely studied for furan synthesis from lignocellulosic biomass, biphasic systems have demonstrated higher yields and selectivity towards furans. Furthermore, the use of biphasic systems continuously extracts furans during the reaction and could potentially reduce the energy demand associated with product recovery due to increased furan yields (Lange et al. 2012; Romo, Joelle E. et al. 2018).

5.2.1 Characterization of the organic water-immiscible solvents
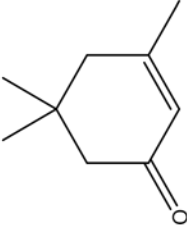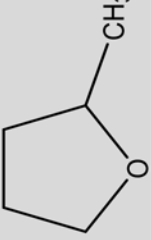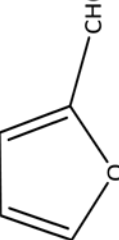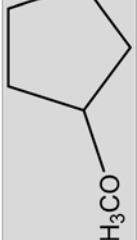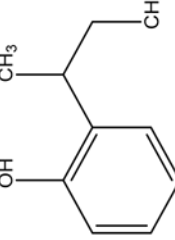
Previous studies about catalytic conversion of xylose into FUR have mainly focused on aqueous systems (Antal et al. 1991; Gómez Millán et al. 2018; Sievers et al. 2016). Recently, monophasic, solvent mixtures have been explored for auto-catalytic FUR production (Romo, Joelle et al. 2019). To our knowledge, auto-catalysed conversion of xylose into FUR in biphasic systems has not been previously explored (**Paper II**).

Solvent selection plays a key role in boosting FUR yields. Hansen Solubility Parameters (HSP) include functions of both solvent mixture and temperature, which at times are overlooked in biphasic systems (Doherty et al. 2010; Hansen 2007). HSP is a three-dimensional solubility parameter considering δ_d, dispersion forces, δ_p, polar forces, and δ_h, hydrogen bonding. Thus, the solubility parameter of a given solvent can be located in the three-dimensional space given by Equation 8.

$$\delta^2 = \delta_d^2 + \delta_p^2 + \delta_h^2 \qquad\qquad\qquad \text{(Eq. 8)}$$

Hence, if a solvent point is within the boundaries of a solute volume space, then the solute may be dissolved by the solvent. If the solvent point is placed outside the solubility sphere, such a solvent does not dissolve the solute (Gharagheizi et al. 2006; Hansen 2007). In the present work, four organic solvents with low miscibility in water have been selected: cyclopentyl methyl ether (CPME), isophorone, 2-methyltetrahydrofuran (MTHF) and 2-sec-butylphenol (SBP). Table 9 shows the HSP polarity values for solvents studied in the present work. The effect of time, temperature, organic solvent, FUR partition coefficient and the aqueous to organic phase ratio were studied in biphasic systems with these organic solvents. The results obtained when MTHF was used as an organic solvent in the biphasic system can be found in **Paper II**.

Table 9. HSP polarity values for solvents used in the present work.

Solvent	Structure	CAS	HSP (δ)	δ$_d$	δ$_p$	δ$_h$	Reference	Paper
Isophorone		78-59-1	9.7	8.1	4.0	3.6	(Hansen 1967)	=
			19.4	17	8	5	(Abbott 2019)	
			19.9	16.6	8.2	7.4	(Gharagheizi et al. 2006; Zeng et al. 2007)	
MTHF		96-47-9	18.1	16.9	5	4.3	(Abbott 2019)	=
FUR		98-01-1	24.4	18.6	14.9	5.1	(Abbott 2019)	I-IV
CPME		5614-37-9	17.8	16.7	4.3	4.3	(Abbott 2019)	II, IV
SBP		89-72-5	24.0	19.3	4.4	13.7	(Birajdar 2015)	III

[a] Measured at 25 °C.

45

As illustrated in Figure 16, Figure 17, Figure 18 and Figure 19 and discussed in **Paper II** and **Paper IV**, the effect of reaction temperature and time were studied when using CPME, isophorone, SBP and MTHF as organic solvents. Previous studies were conducted to determine partition coefficients, effect of aqueous to organic phase ratio, reaction temperature and distribution of FUR formed from xylose. These effects are explained in greater detail in **Paper II** and **Paper IV**.

The effect of reaction time on the production of FUR was studied by conducting reactions between 30 to 180 min at 170, 190 and 210 °C with CPME, isophorone, SBP and MTHF with a xylose solution of 186 mmol l^{-1}. This single containing xylose solution was used in a concentration typically found for birch hydrolysate (Table 8). Figure 16 shows the effect of reaction time when using CPME as an organic solvent in an aqueous to organic phase ratio of 1:1 (by volume) on FUR yield, xylose conversion and selectivity to FUR at 170, 190 and 210 °C. The highest FUR yield, 78%, was reached at 190 °C in 3 h.

As can be seen when using CPME, isophorone, SBP and MTHF (Figure 16, Figure 17, Figure 18 and a Figure 19, respectively), the FUR yield obtained at 190 °C eventually surpasses the FUR yield obtained at 210 °C. Under high reaction temperatures (210 °C), it was assumed that FUR tends to stay in the aqueous phase rather than in the organic phase; hence, degradation reactions of FUR take place more quickly.
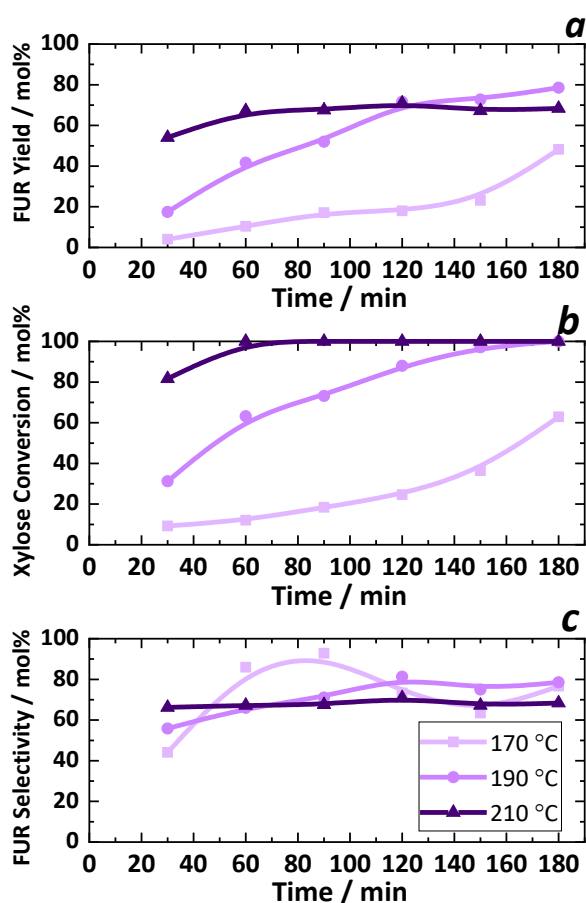
Figure 16. *Effect of reaction temperature and time on FUR yield (a), xylose conversion (b), selectivity to FUR (c) in the dehydration of 186 mmol l^{-1} xylose when using CPME as organic solvent with an aqueous to organic phase ratio of 1:1. Lines are to guide the eye.*

When isophorone is used as an organic solvent, the results occur as shown in Figure 17. The highest FUR yield (48%) was reached at 190 °C in 3 h. This low FUR yield was assumed to happen due to Diels-Alder reaction between the isophorone and FUR. In order to have a deeper understanding of the cause of low FUR yields when isophorone is used as an organic solvent, NMR studies were completed, and further details can be seen in **Paper II**. These NMR studies show that:

- water does have a significant effect on the condensation of FUR
- isophorone may allow for increased miscibility with water at higher temperatures, which may lead to increased degradation kinetics of FUR
- co-polymerisation of isophorone and FUR is likely occurring, which may lead to increased losses of both FUR and isophorone to some degree. This may be highly temperature dependent

In comparison to the performance of isophorone to CPME (Figure 16), it might be that FUR enters the organic phase but undergoes degradation in the presence of the solubilised water within isophorone. Afterwards, FUR precipitates out once a certain molecular weight of condensation or resinification reactions occur in the presence of water.

Figure 17. *Effect of reaction temperature and time on furfural yield (a), xylose conversion (b), selectivity to furfural (c) in the dehydration of 186 mmol l^{-1} xylose when using isophorone as organic solvent with an aqueous to organic phase ratio of 1:1. Lines are to guide the eye.*

47

Figure 18 shows FUR yield, xylose conversion and selectivity to FUR when employing 2-sec-butylphenol (SBP). The highest FUR yield (59%) was obtained at 190 °C in 3 h, which corresponds to a complete xylose conversion and a selectivity to FUR of 55%.
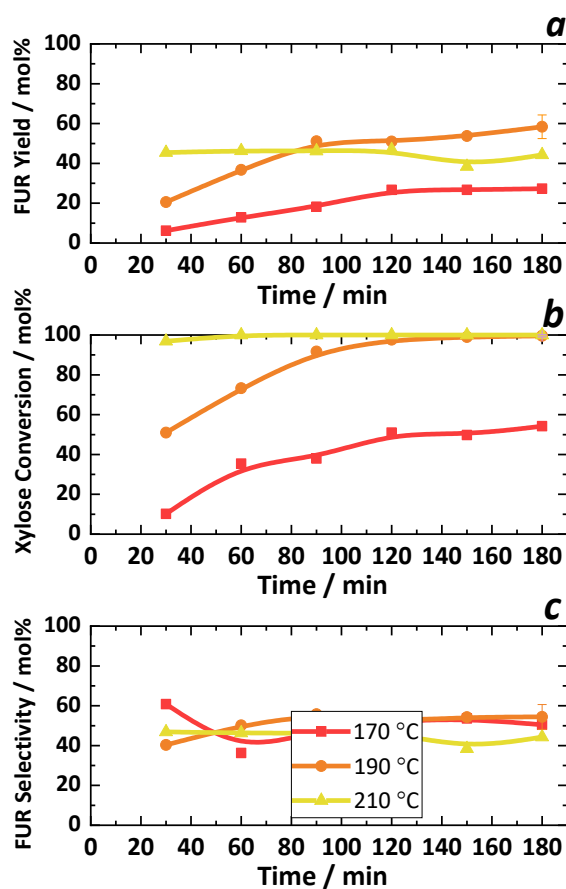
Figure 18. *Effect of reaction temperature and time on FUR yield (a), xylose conversion (b), selectivity to FUR (c) in the dehydration of 186 mmol l^{-1} xylose when using SBP as organic solvent with an aqueous to organic phase ratio of 1:1. Lines are to guide the eye.*

Figure 19 shows FUR yield, xylose conversion and selectivity to FUR when employing MTHF. Figure 19 shows that the first 60 min of the treatment the FUR yield was increased up to two times by increasing the temperature from 170 to 190 °C when employing an MTHF to aqueous fraction ratio of 1:1. The highest FUR yield (71%) was reached at 190 °C in 3 h. The maximum selectivity (Figure 19c) to FUR formation was 58% and 80% at temperatures of 170 and 190 °C, respectively.
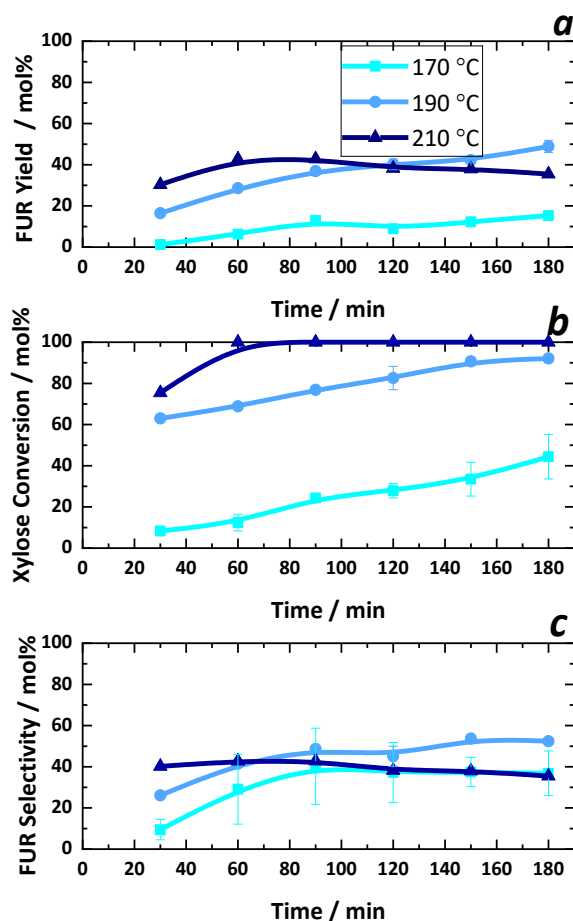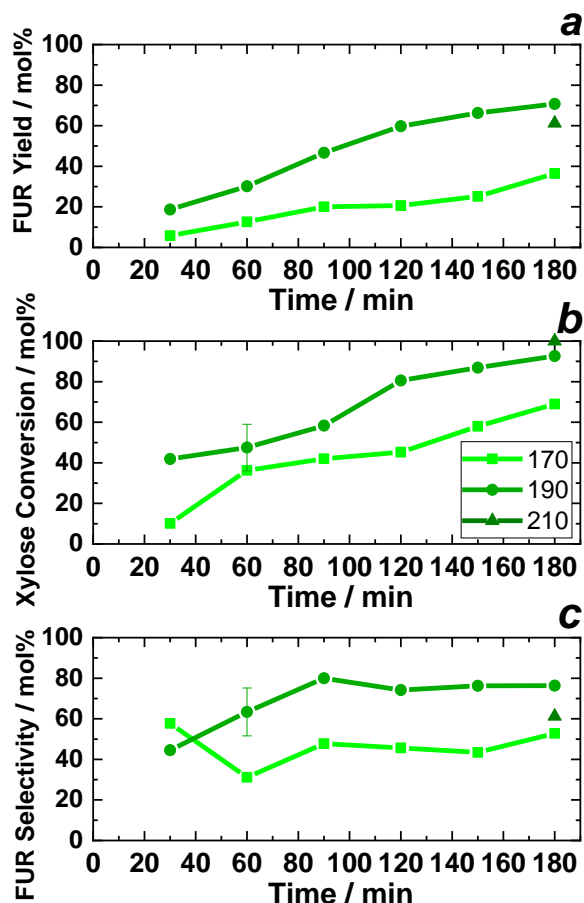
Figure 19. *Effect of temperature and reaction time on (a) FUR yield, (b) xylose conversion, (c) selectivity to FUR in the dehydration of 186 mmol l^{-1} xylose when using MTHF as organic solvent with an aqueous to organic phase ratio of 1:1. Lines are to guide the eye.*

Due to the high vapor pressure of MTHF, 136 mbar (Graziano et al. 2013), only one reaction using this organic solvent at 210 °C in 180 min could be performed.

Romo et al. (Romo, Joelle et al. 2019) developed a semi-empirical model that estimates xylose conversion and FUR yield based in reaction severity and HSP. The authors employed sulfolane, gamma-butyrolactone (GBL), gamma-valerolactone (GVL), gamma-hexalactone (GHL) and tetrahydrofuran (THF) in auto-catalytic reactions. Under auto-catalytic conditions, the highest FUR yield (61%) was reached using 50/50 w/w sulfolane and water with 93% xylose conversion at 190 °C.

5.2.2   Furfural production from birch hydrolysate in the biphasic system

The production of FUR from birch hydrolysate was studied under optimised conditions for the dehydration of C$_5$ sugars (190 °C, 1:1 aqueous to organic phase ratio, under microwave irradiation). Two organic solvents were used for this aim, CPME and SBP.

When using CPME, the FUR yield increased from 37 mol% to 68% with an increasing time from 30 to 90 min at 190 °C when employing an aqueous to CPME phase ratio of 1:1 (Figure 20).

The highest mole fraction of hydroxymethylfurfural (HMF) was 0.01 mmol, which is in agreement with previous studies when using birch hydrolysate to produce FUR from pentoses (Ershova, Olga et al. 2017).

When using SBP as an organic solvent, the highest FUR yield (54%) was reached at 190 °C in 3 h using an aqueous to SBP phase ratio of 1:1 (by volume) (Figure 20). Pentose conversion increased from 80% to 94% when increasing reaction time from 0.5 h to 1 h at 190 °C.
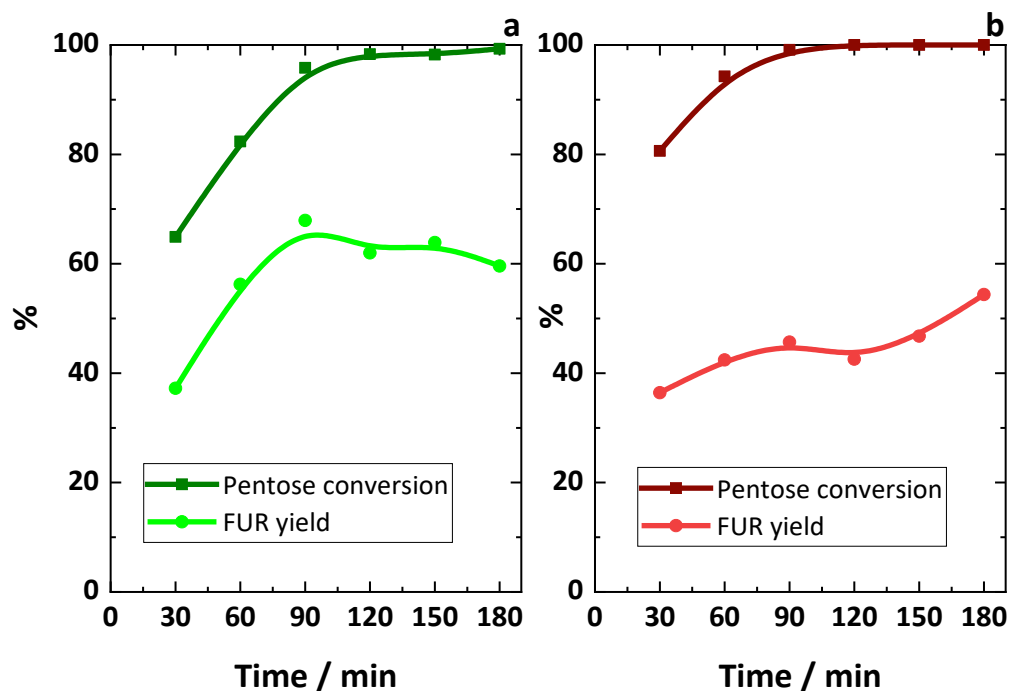
Figure 20. Pentose conversion and FUR yield from birch hydrolysate as a function of time at 190 °C under microwave irradiation. Biphasic reaction system: Aqueous phase = hydrolysate liquor after filtration (1.5 ml), organic phase (1.5 ml): (a) CPME, (b) SBP. The lines are to guide the eye.

In comparison to the monophasic system, where the highest FUR yield (46%) was reached at 190 °C in 60 min, the effect of the addition of a water-immiscible organic solvent is visible. When a biphasic system was used in a reaction temperature of 190 °C, the FUR yield incremented to 68% and 54% when using CPME and SBP, respectively. These FUR yield values confirm the positive effect of water-immiscible organic solvents in the conversion of pentoses.

5.2.3 Solid acid-catalyzed dehydration of xylose into furfural in biphasic system

A design of experiments was developed using a 1:3 water-to-CPME phase ratio (v/v) and 1 mg of Starbon®450-SO$_3$H/ 1 mg xylose at various reaction temperatures and times (Table 10).

Table 10. *Selected conditions based on statistical design and experimental values. Each experiment consisted of Starbon®450-SO₃H using an aqueous to CPME phase ratio of 1:3 H2O:CPME (v/v) at various reaction temperatures (150, 175 and 200 °C) and times (1, 12.5 and 24 h).*

Exp. No	T (°C)	t (h)	Furfural Yield (%)	Xylose Conversion (%)	Selectivity to Furfural (%)
1	150	1	0.7	1.3	53.1
2	200	1	69.5	95.9	72.5
3	150	24	52.2	79.5	65.6
4	200	24	21	100	21.0
5	150	12.5	54.4	78.5	69.2
6	200	12.5	50.3	100	50.3
7	175	1	20	30.8	64.8
8	175	24	60.2	100	60.2
9	175	12.5	61.8	100	61.8
10	175	12.5	63.2	100	63.2
11	175	12.5	64.6	100	64.6

Based on the results, practically all xylose was converted at 200 °C in 1 h. FUR yield varied from 0.7% to 70%. Prediction models for xylose conversion, FUR yield and selectivity were also successfully determined based on the results. R^2 values indicated that the models explained 92–99% of variation in the sample properties. The obtained models were then used to predict xylose conversion and FUR yield of the samples within the experimental design range. Longer reaction times significantly decreased the FUR yield at higher temperatures (Figure 21b).

The overlay contour plot in Figure 21 also suggested that a local optimum, where both xylose conversion and FUR yield were maximised, existed within the experimental design range. A verification experiment was thus performed by combining a reaction temperature of 175 °C with a reaction time of 18 h. The obtained results indicated that 100% of the xylose was converted to 69.3% FUR during the first cycle (Table 11). The verification results were in good agreement with the model predictions, which suggested that 101 ± 25.0% of xylose would be converted to 66.9 ± 10.5% (α=0.10) FUR (Gómez Millán, Phiri et al. 2019).

Table 11. *Selected conditions based on statistical design and experimental values. Each experiment consisted of Starbon®450-SO₃H using an aqueous to CPME phase ratio of 1:3 H2O:CPME (v/v) at various reaction temperatures (150, 175 and 200 °C) and times (1, 12.5 and 24 h).*

Exp. No	T (°C)	t (h)	Furfural Yield (%)	Xylose Conversion (%)	Selectivity to Furfural (%)
1	175	18	69.3	100	69.3
2	175	18	70.4	100	70.4
3	175	18	70.0	100	70.0

The analyses of variance are summarised in the Supplementary Information of **Paper III**.
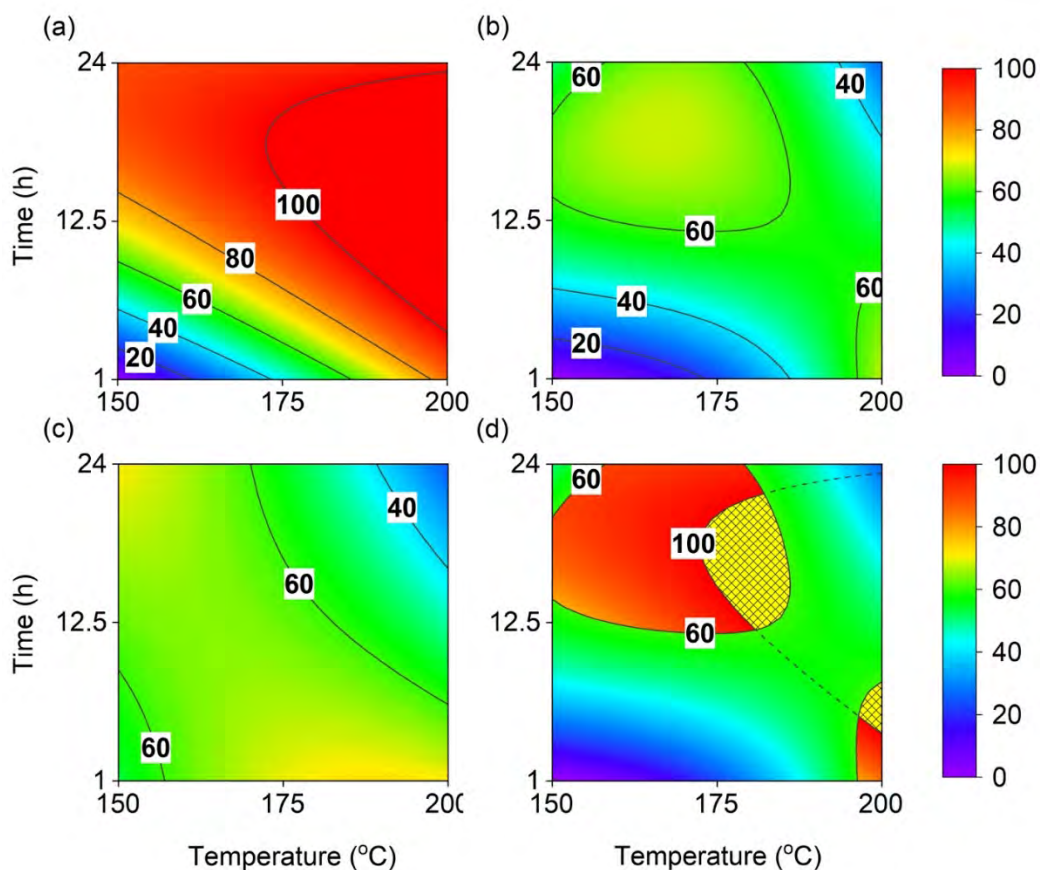
Figure 21. *Contour plots based on model prediction for (a) conversion of xylose (%, R^2 = 0.92); (b) furfural yield (%, R^2 = 0.99); (c) selectivity (%, R^2 = 0.92), and; (d) an overplay plot of xylose conversion and furfural yield. The yellow patterned area in (d) indicates 100% xylose conversion and a furfural yield of >60% based on the model predictions. Each experiment consisted of 21 mg of Starbon®450-SO₃H using an aqueous to CPME phase ratio of 1:3 (v/v) at various reaction temperatures (150, 175 and 200 °C) and times (1, 12.5 and 24 h).*

5.2.4   Catalyst characterization (Paper IV)

For the purpose of demonstrating various properties related to surface topography and chemical composition, scanning electron microscopy (SEM) and energy-dispersive X-ray (EDX) deliver simple, non-destructive analyses. Figure 22 corresponds to a representative image of Starbon®450-SO₃H catalyst powder before hydrothermal reaction, revealing the characteristic morphology of particles with sharp edges similar to that reported in the literature (Aldana-Pérez et al. 2012). Particles are compact, and their size is in the range of 50–100 μm.
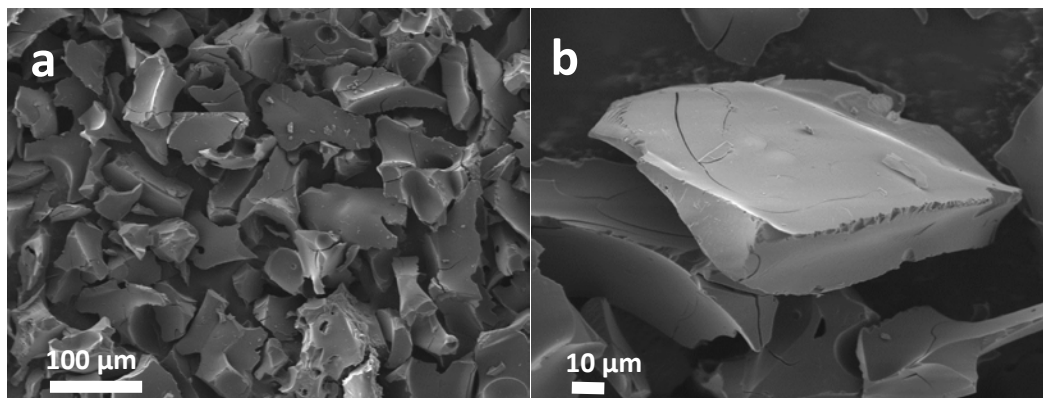
Figure 22. *SEM images of the Starbon®450-SO₃H catalyst powder obtained at different magnifications, (a) 180X and (b) 650X (Paper IV).*

A detailed X-ray photoelectron spectroscopy (XPS) analysis was performed to get deeper insight into the surface composition of Starbon®450-SO₃H before and after hydrothermal reaction. In Figure 23 and Table 12, the binding energy values of the surface atomic composition of Starbon®450-SO₃H before and after hydrothermal reaction are shown. As is demonstrated, there were no significant changes in the chemical composition of the surface of Starbon®450-SO₃H before and after hydrothermal reaction. The continuous catalytic activity of Starbon®450-SO₃H after various reusability cycles is consistent with the XPS results.
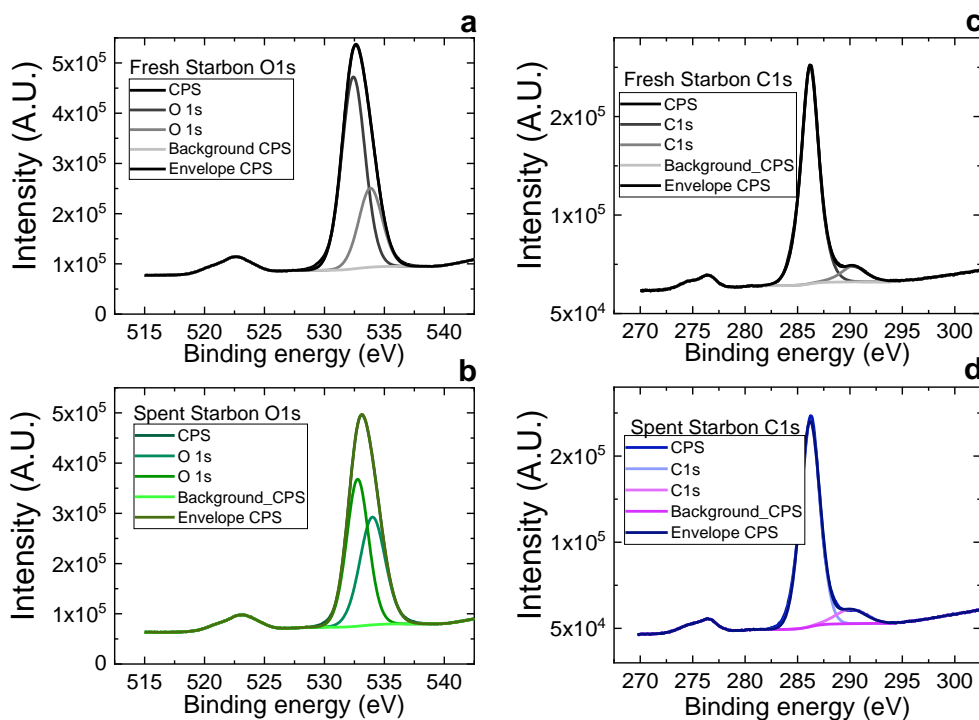
Figure 23. *XPS (a, b) O 1s and (c, d) C 1s spectra of Starbon®450-SO₃H (a, c) before and (b, d) after hydrothermal reaction at 175 °C in 18 h.*

53

Table 12. *XPS data of Starbon®450-SO3H before and after hydrothermal reaction at 175 °C in 18 h.*

Sample	Name	Binding Energy (eV)	Atomic conc. (%)
Starbon®450-SO$_3$H —fresh	O 1s	532.4	59.0
	C 1s	286.2	41.0
Starbon®450-SO$_3$H —1	O 1s	534	54.1
	C 1s	286.2	45.9

5.3 Furfural degradation

Insoluble polymeric structures, the so-called humins, are formed during the thermal treatment of lignocellulose in aqueous solution and acidic conditions in the subcritical range (van Zandvoort 2015; van Zandvoort et al. 2013). Humin formation under the auto-catalysed dehydration of birch hydrolysate liquor (3 ml) at 190 °C in 1 h can be seen in Figure 24. Under these experimental conditions, 5.3 mg of humins were obtained. The formation of these carbonaceous deposits is detrimental to the FUR formation reaction (Eifert and Liauw 2016). Nevertheless, recent interesting endeavours to valorise these polymers show significant market applications (as stabilisers, supercapacitor electrodes, templates and combustible agents) due to their various functionalities and their broad range of molecular weights (Chernysheva et al. 2018; Filiciotto et al. 2018).

Figure 24. *Humin formation under auto-catalyzed dehydration of hydrolysate liquor at 190 °C in 60 min (Paper IV).*

In Figure 25, humin formation can be observed on the surface of SZ$_{cord}$ after hydrothermal reaction at 210 °C for 2 min. On the surface of the spent samples, the characteristic structure of these spherical particles of 2 – 3 µm in size (marked by arrows) are typically formed from acid-catalysed dehydration of xylose (van Zandvoort et al. 2013).
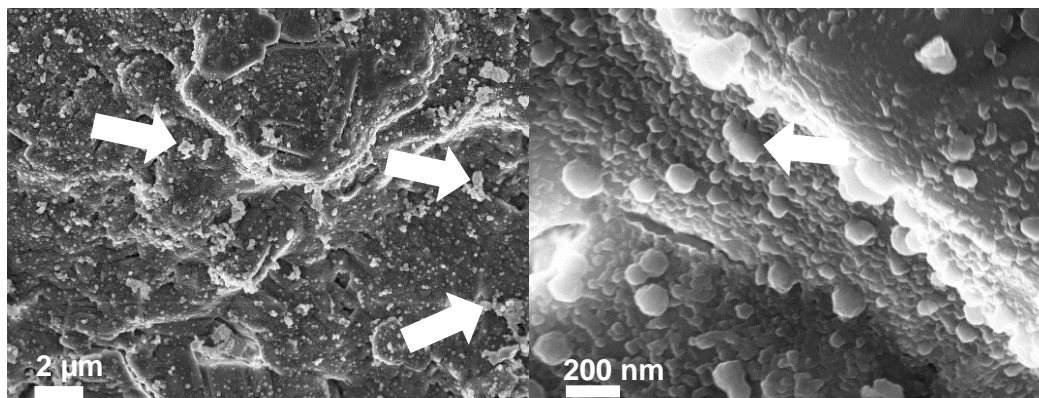
Figure 25. *SEM images of SZ on cordierite after hydrothermal reaction at 210 °C in 2 min (Paper I).*

In order to have a better understanding of the behaviour of FUR in the presence of an organic solvent, it is essential to study its degradation rate. Figure 26 illustrates the effect of the reaction temperature, time and usage of a 1:1 (v/v) aqueous to organic phase ratio on the degradation rate of FUR when adding CPME (Figure 26a), SBP (Figure 26b) and isophorone (Figure 26c). The results show a clear dependency of FUR degradation on the reaction temperature. It can be seen that when increasing the reaction temperature, FUR degradation increases. Additionally, the results show that FUR is degraded more rapidly in the presence of isophorone>SBP>CPME. The highest degree of FUR degradation, 38%, was observed at 210 °C in 180 min when adding isophorone. When adding SBP, the highest degree of FUR degradation was 29% under similar experimental conditions. In the case of CPME, the highest degree of degradation was below 12%.
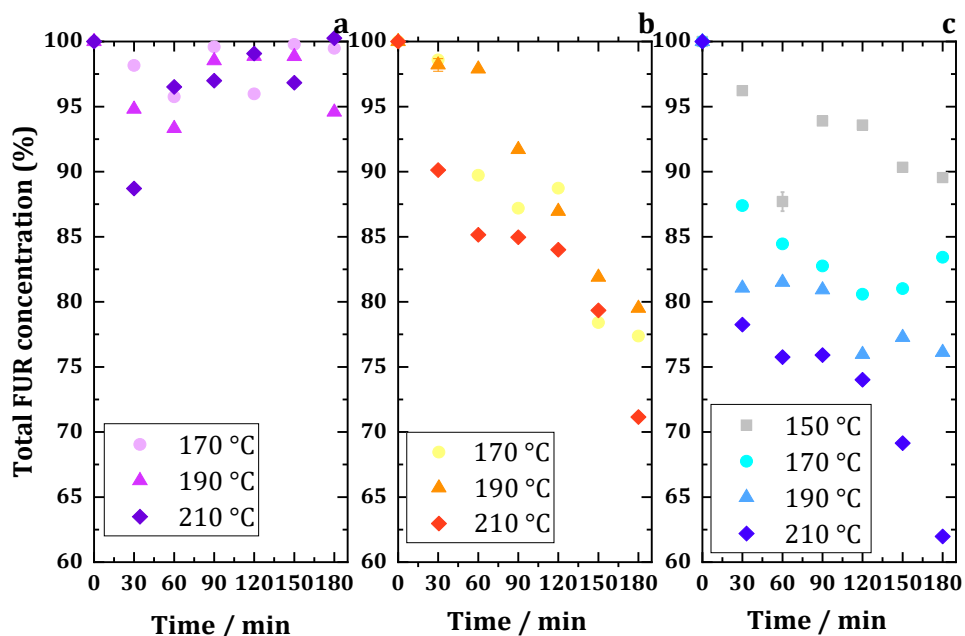
Figure 26. *The remaining furfural at various reaction times during auto-catalyzed degradation when employing CPME (a), SBP (b) and isophorone (c) to aqueous phase of 1:1 (v/v). The degradation of furfural was determined for a solution of 5 wt% furfural (squares – 150 °C, circles – 170 °C, triangles – 190 °C, diamonds – 210 °C) (Paper II and Paper IV).*

Even though FUR is mostly found in the organic phase, the presence of water does have a significant effect on the condensation of FUR. Isophorone and SBP may allow for increased miscibility with water at higher temperatures, which may lead to increased degradation kinetics of FUR. Co-polymerisation of SBP and FUR, isophorone and FUR is likely occurring, which may lead to increased losses of FUR, SBP and isophorone to some degree (Gómez Millán et al. 2019).

A comparison study has been completed for FUR degradation in the aqueous phase and biphasic system using SBP. Based on experiments completed in just aqueous phase by Ershova et al. (Ershova, O. et al. 2015) at reaction temperatures of 180, 200 and 220 °C, the results were interpolated and extrapolated by estimating the activation energy and frequency factors from Ershova's paper to temperatures of 170, 190 and 210 °C (Table 13). The rate constant for the degradation of FUR (k_1) in the auto-catalyzed system was calculated in the monophasic and biphasic system (eq. 9).

$$\text{Furfural} \xrightarrow{k_1} \text{Degradation products} \hspace{3cm} \text{(Eq. 9)}$$

Table 13. *Kinetic rate constants k_1 (min^{-1}) at each experimental temperature for furfural degradation in aqueous phase.*

T, (°C)	k_1	Reference
170	0.0014	This study
180	0.0019	(Ershova, O. et al. 2015)
190	0.0026	This study
200	0.0034	(Ershova, O. et al. 2015)
210	0.0045	This study
220	0.0059	(Ershova, O. et al. 2015)

After these values were calculated, the biphasic and monophasic results were compared at reaction temperatures of 170, 190 and 210 °C (Figure 27). As can be seen, degradation of FUR is dependent on temperature. Furthermore, FUR degradation in the monophasic system is clearly higher than in the biphasic system. This is a confirmation that the organic solvent extracts FUR from the aqueous phase, largely avoiding FUR degradation reactions. The highest observable difference is at 210 °C in 180 min, where, in the biphasic system, FUR degradation reaches 29%; whereas in the monophasic system, FUR degradation reaches more than two-fold this value (66%).
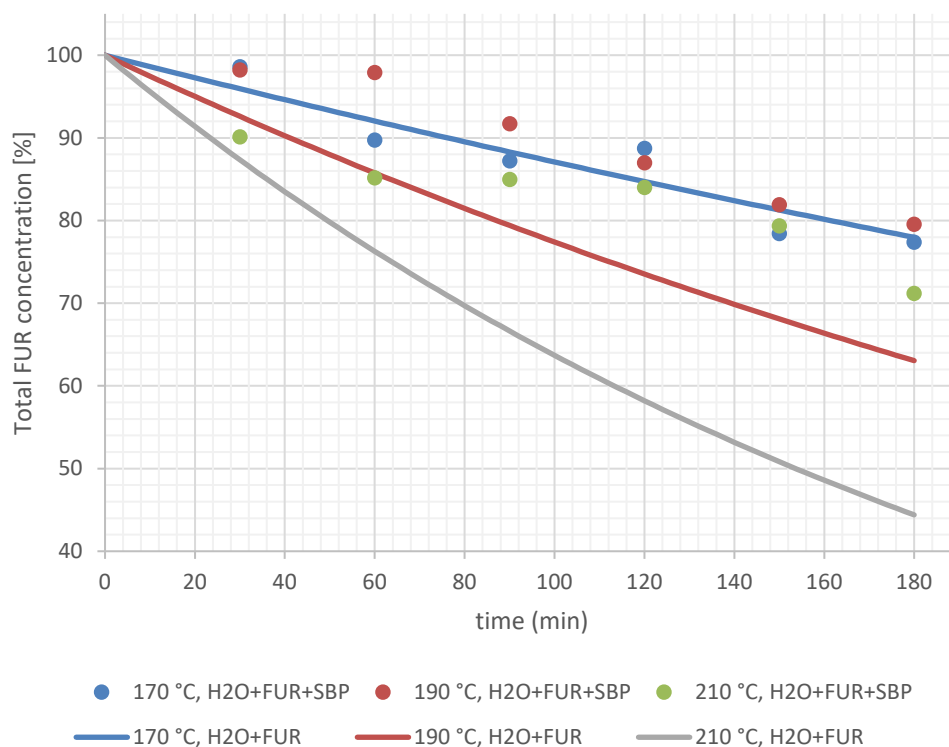
Figure 27. *The remaining furfural at various reaction times during auto-catalyzed degradation in mono- and biphasic systems when employing SBP to aqueous phase 1:1 (v/v; dots – experimental values, lines – interpolated and extrapolated values at 170, 190 and 210 °C).*

5.4 Catalyst reusability

Different approaches to measure the stability and reusability of solid catalysts have been under discussion in recent years. In order to design stable catalysts with practical applications, Christopher W. Jones (Jones 2010) highlighted the need for understanding deactivation mechanisms of solid catalysts. In this way, catalysis as a kinetic phenomenon should be used to assess recyclability, stability and deactivation. In the present set-up, it was not possible to withdraw samples and analyse them periodically from the reactor, as was performed in the referred literature. Nevertheless, experimental conditions, such as reaction time and temperature, were included in the present research work besides the number of reusability cycles and yields of FUR. This adds consistency to the study of hydrothermal stability, reusability and deactivation of the solid catalysts.

Hydrothermal stability of solid acid catalysts was investigated by employing the same catalyst in a series of xylose dehydration reactions. Prior to each reusability cycle, the catalyst was washed with deionised water and dried at 105 °C overnight. Figure 28 shows five consecutive reaction runs of SZ on cordierite (at 190 °C in 9 min using 50 mg of sample in 3 ml of 186 mmol l^{-1} xylose solution). After this, the catalyst was washed, dried, calcined and impregnated again with 1 M H_2SO_4 (cycle 6). After 5 cycles, the FUR yield of the reused catalyst decreased from 38% to 7%, as did the conversion of xylose (from 97% to 37%). The catalytic activity of the solid acid catalyst in cycle 5 decreased to a level that could be compared to the auto-catalysed system. However, the activity of the catalyst can be recovered by calcination and acid impregnation, and a FUR yield of 39% would again be

obtained. This result indicates that the observed progressive catalyst deactivation might be related to the accumulation of insoluble organic matter, which could be blocking the surface of the catalyst, hence leading to disabled acid sites. The catalyst deactivation also includes leaching of the active sites (**Paper I**).
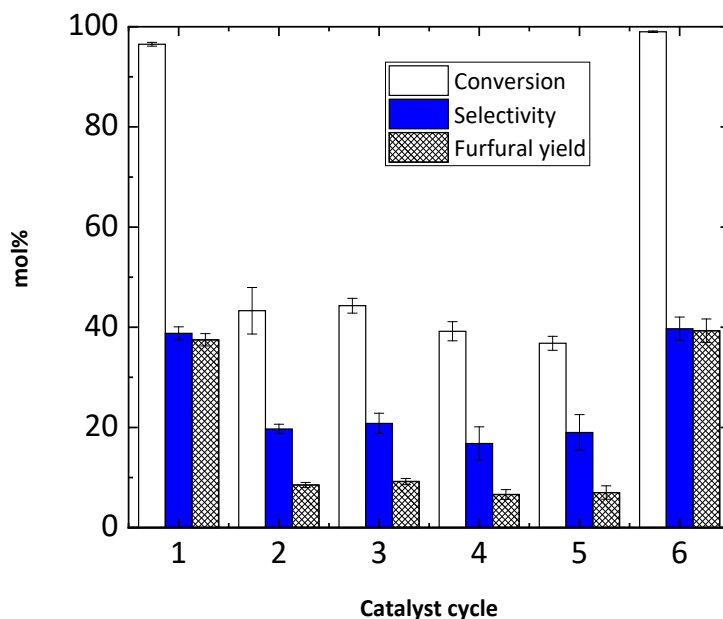
Figure 28. *Reusability of SZ on cordierite for the dehydration of xylose (186 mmol l^{-1}) to furural using 50 mg of catalyst at 190 °C for 9 min (xylose conversion (white bar), FUR yield (blue bar) and selectivity to FUR (striped bar)).*

Figure 29 shows three consecutive reaction runs of Starbon®450-SO$_3$H (at 175 °C in 18 h using 21 mg of Starbon®450-SO$_3$H in 0.75 ml of 186 mmol l^{-1} xylose concentration and 2.25 ml of CPME). After 3 cycles, the catalytic activity of the reused catalyst stayed stable, yielding 70% FUR at complete xylose conversion. Even though more cycles were planned to test the hydrothermal stability of Starbon®450-SO$_3$H, it was not possible to complete due to lack of material available in the time span given.

Under similar conditions (175 °C, 18 h and 1:3 aqueous to CPME phase ratio), the auto-catalysed system reaches 100% xylose conversion and 59% FUR yield. Prior to each cycle, the catalyst was filtered, washed with deionised water and dried at 105 °C overnight.
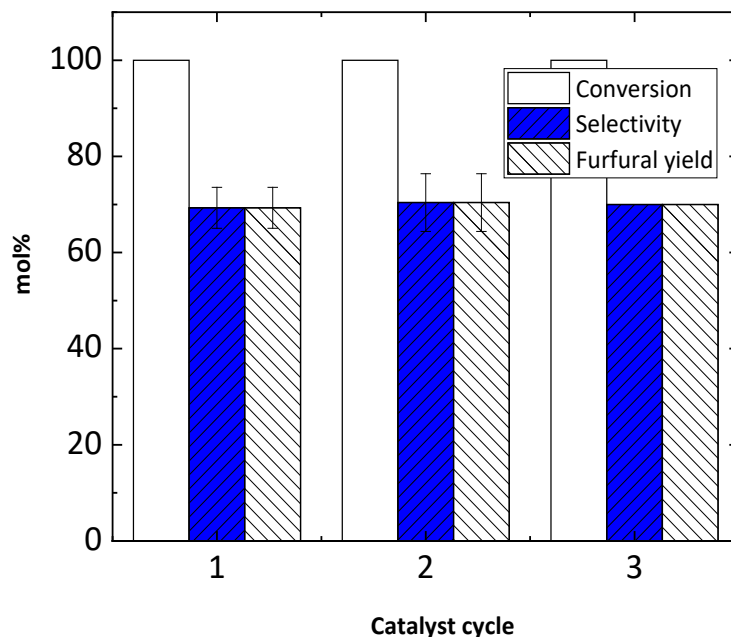
Figure 29. *Reusability of Starbon®450-SO₃H for the dehydration of xylose (186 mmol l⁻¹) to furfural using 21 mg of catalyst at 175 °C for 18 h using an aqueous to CPME phase ratio of 1:3 (v/v) (xylose conversion (white bar), furfural yield (blue bar) and selectivity to furfural (striped bar)).*

5.5 Preliminary techno-economic feasibility studies

A techno-economic feasibility assessment was completed of a FUR-based biorefinery concept employing a side-stream from the dissolving pulp production.

This section presents a techno-economic feasibility study to produce FUR from a hydrolysate liquor from the pulp and paper industry integrated into a biorefinery. Figure 30 illustrates the simplified process for the simulation with the specifications:

1. The process employs a hydrolysate stream from the biorefinery or pulp mill as a raw material and therefore, upon regeneration of the process, it is assumed that the hydrolysate cost is negligible and not taken into consideration when estimating the annual operating cost.
2. The plant is operated in continuous mode (8000 h/a).
3. The FUR reactor is energy-intensive, and it is therefore assumed that the energy demands for the reactor are met by utilising the excess energy available in the pulp mill or biorefinery.
4. A FUR production capacity of 5 kt/a.
5. A project lifetime of 20 years with 100% equity financing has been assumed.
6. Furthermore, it is assumed that the lignin removal from the hydrolysate is carried out in the pulp mill or biorefinery, and as such costs related to this are not taken into consideration in the techno-economic analysis.

A process simulation model was developed in Aspen Plus® v8.8 (Aspen Technology Inc. 2013) by using the universal quasi-chemical (UNIQUAC) thermodynamic method. The pre-

59

hydrolysate stream (S1) from the biorefinery after lignin separation consists mostly of xylo-oligosaccharides (64%) and monomeric xylose (36%). Water is introduced into the reactor operating at a temperature of 190 °C and 12.1 bar pressure. The stoichiometric reactor model (RSTOIC) available in Aspen Plus is used to simulate the auto-catalysed reaction of xylose to yield FUR. The outlet stream from the reactor is cooled to 50 °C and sent to an extraction column, where FUR is extracted into the organic phase using SBP as a solvent. The aqueous phase, predominantly consisting of water (99 wt. %), is separated and can be reused in the biorefinery for pre-hydrolysis.
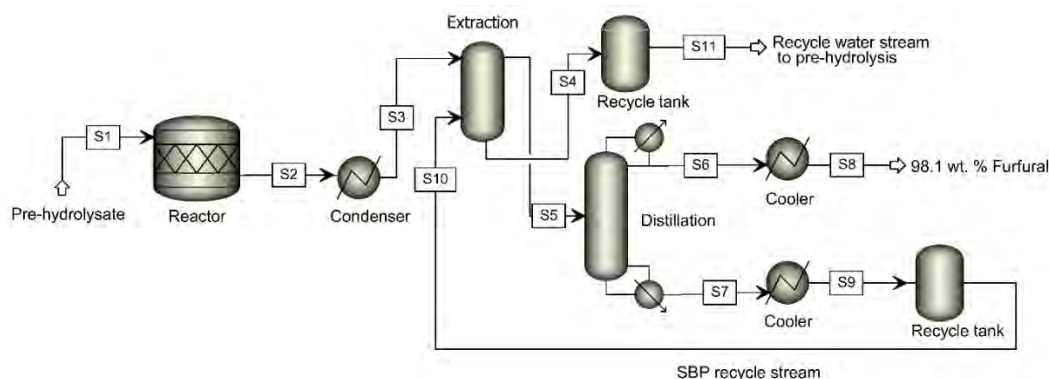
Figure 30. *Process simulation diagram for the production of furfural from birch wood pre-hydrolysate.*

The organic phase consisting of FUR and SBP is introduced into a distillation column operating with 30 ideal stages at atmospheric pressure. The RADFRAC rigorous distillation column in Aspen Plus is used to model the distillation process: 98 wt% FUR is recovered in the top fraction at 161 °C, and the bottom fraction consisting of pure SBP is recycled back for reuse in the extraction step. The mass balance is shown in Figure 31.
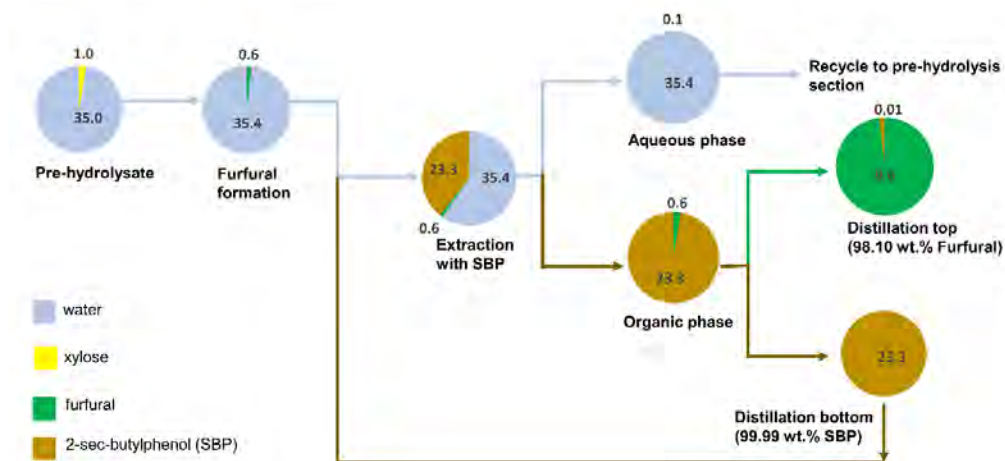
Figure 31. *Mass balance for the production of FUR from birch wood hydrolysate (5 kt per year). The reagents used are given a unique color and the proportion of reagents is displayed using a pie chart. Flow of streams is indicated with the color of the majority component.*

The project lifetime is assumed as 20 years, and the minimum selling price of FUR was found to be 1.33 € kg⁻¹. A detailed estimation of fixed capital, total investment and further information can be found in **Paper IV**. In the techno-economic evaluation of producing

chemicals and biofuels studied by Olcay et al., they included process simulations for seven biorefinery models designed to convert red maple wood into chemicals, among them FUR and HMF (Olcay et al. 2018). A FUR minimum selling price of 1.53 € kg^{-1}, which is comparable to our findings, was reported. Besides the primary contributors to the equipment cost include reactors, similar to our study. Furthermore, Bbosa et al. completed a techno-economic analysis of a 2000 metric tonne per day corn stover ethanol biorefinery producing 61 million gallons per year of ethanol (Bbosa et al. 2018). They reported a price of FUR 0.93 € kg^{-1}.

6. Conclusions

In this research, FUR formation from xylose in various systems was studied. In order to produce this attractive platform molecule, xylose was used as a model compound. In a later stage, birch hydrolysate liquor was employed as feedstock to form FUR. Pentosans were the dominant hemicelluloses in the birch hydrolysate liquor, especially xylan, which can be converted to FUR (Table 14). Besides, hexoses found also in the liquor can be used as feedstock to form HMF. Furthermore, acetic acid can also be recovered from the system.

The presented work describes the formation of FUR from xylose in heterogeneously catalysed systems in comparison to auto-catalysed and mineral acid-catalysed dehydration reactions. Metal oxides, polymeric resins and functionalised carbon-based catalysts were used, and the results are discussed. These catalysts were selected since they were assumed to have good hydrothermal stability and high acid site density. Even though SZ on cordierite showed deactivation due to leaching and fouling from humins of the acid sites, its catalytic activity can be recovered by impregnation with H_2SO_4. This differs to preparing a new catalyst, due to the changes in morphology and textural characteristics that might have occurred in the reactor, such as surface area. On the other side, the carbon-based catalyst (Starbon®450-SO$_3$H) displayed high hydrothermal stability in biphasic conditions and can be reused under similar experimental conditions for several cycles.

The results throughout this thesis emphasise the fact that acid site density has a meaningful role in FUR production. The nature, Lewis or Brønsted, and strength of acid site density found in the solid acid catalyst determines the reaction mechanism of FUR formation from xylose. Hence, attention should be paid to this characteristic, especially when studying real biomass or process side streams.

Biphasic systems for biomass reaction to increase furanic yields offer many advantages over monophasic systems. Organic solvents with low miscibility show benefits, excluding phase modifiers. However, degradation reactions between some organic solvents and FUR could take also place. Hence, FUR yields could suffer. In the present research work, four organic solvents were used in the synthesis and continuous extraction of FUR from pentoses: MTHF, isophorone, CPME and SBP. Table 14 exhibits the overall FUR yields reached under different experimental conditions in the present research work.

Table 14. *Overall furfural yields obtained in the present research work.*

Feedstock	Catalyst	Solvent	FUR yield	Tempera-ture (°C)	Time (min)	Paper
Xylose	Auto-catalyzed	H_2O	48%[a]	210	60	I
Xylose	SZ on cordierite	H_2O	41%[b]	210	2	I
Xylose	Starbon®450-SO_3H	H_2O/CPME	70%[c]	175	1080	IV
Xylose	Auto-catalyzed	H_2O/Iso-phorone	49%[d]	190	180	II
Xylose	Auto-catalyzed	H_2O/CPME	78%[d]	190	180	II
Xylose	Auto-catalyzed	H_2O/SBP	59%[d]	190	180	III
Birch hydroly-sate liquor	Auto-catalyzed	H_2O/CPME	68%[e]	190	90	II
Birch hydroly-sate liquor	Auto-catalyzed	H_2O/SBP	54%[f]	190	180	III

(a) 3 ml of 186 mmol l^{-1} xylose solution.

(b) 50 mg of SZ on cordierite in 3 ml of 186 mmol l^{-1} xylose solution.

(c) 21 mg of Starbon®450-SO_3H using a water to CPME phase ratio of 1:3 (v/v). The aqueous fraction consisted of 186 mmol l^{-1} xylose solution.

(d) When using an aqueous to organic phase ratio of 1:1 (v/v). The aqueous fraction consisted of 186 mmol l^{-1} xylose solution.

(e) When using an aqueous to CPME phase ratio of 1:1 (v/v).

(f) When using an aqueous to SBP phase ratio of 1:1 (v/v).

Based on the techno-economic analysis, the MSP of FUR is found to be 1.44 €/kg for a plant operating with a production capacity of 5 kt/yr. With a FUR selling price of 1.87 €/kg, the payback period is calculated as 5 years, resulting in a positive NPV of 13.4 M€ at the end of the project lifetime and an internal rate of return of 20.9%, making the process profitable.

7. Future work and outlook

Recent years have witnessed the first steps towards a bio-based economy. Nevertheless, robust systems based on the innovative and cost-efficient use of lignocellulosic materials in highly integrated biorefinery facilities are needed to ensure competitiveness and stability in the long term.

Catalytic conversion of C5-sugars, especially xylose, has demonstrated a high economic potential for the production of FUR. This is a promising route to add value to side-streams from the pulp and paper industry. The principal issues related to the heterogeneously catalytic conversion of pentoses into FUR, which require further examination, are:

a) development of hydrothermally stable solid acid catalysts at high temperature (~200 °C) and pressure (~15 bar);
b) design of high acid site density on the catalyst
c) finding commercially effective catalyst separation and recycling concepts

Even though the present work reports significant findings in the formation of FUR from xylose and birch hydrolysate liquor from the pulp and paper industry, as FuOH attractiveness increases in the market, new approaches are needed. A step forward has been recently taken into producing FuOH from xylose in one-pot reactions. However, the development of hydrothermally stable and highly active catalysts is still in development. A breakthrough in this field could shape the production process of furanic compounds.

Furthermore, in order to step forward in reaching the biorefinery paradigm, humin valorisation offers a significant appeal to industry and academia due to its wide range of applications. These insoluble polymers are associated with a meaningful number of processes related to lignocellulosic biomass processing, and its application market should therefore not be overlooked.

To summarise, for both the heterogeneous catalysis of biomass feedstock and organic solvents, future work must focus primarily on inexpensive, innovative processes enabling effective reusability and recycling of the catalysts and the organic solvents.

References

Abbott S. Hansen Solubility Parameter [cited 2019 July 2019]. Available from: https://www.stevenabbott.co.uk/practical-solubility/hsp-basics.php .

Agirrezabal-Telleria I., Requies J., Güemez M. B., Arias P. L. Pore size tuning of functionalized SBA-15 catalysts for the selective production of furfural from xylose. 2012. Appl Catal , B 115–116(0):169-78.

Agirrezabal-Telleria I., Gandarias I., Arias P. L. Heterogeneous acid-catalysts for the production of furan-derived compounds (furfural and hydroxymethylfurfural) from renewable carbohydrates: A review. 2014. Catal Today 234(0):42-58.

Agirrezabal-Telleria I., Requies J., Güemez M. B., Arias P. L. Dehydration of d-xylose to furfural using selective and hydrothermally stable arenesulfonic SBA-15 catalysts. 2014. Appl Catal , B 145(0):34-42.

Agirrezabal-Telleria I., Hemmann F., Jäger C., Arias P. L., Kemnitz E. Functionalized partially hydroxylated MgF2 as catalysts for the dehydration of d-xylose to furfural. 2013. J Catal 305(0):81-91.

Agirrezabal-Telleria I., Larreategui A., Requies J., Güemez M. B., Arias P. L. Furfural production from xylose using sulfonic ion-exchange resins (amberlyst) and simultaneous stripping with nitrogen. 2011. Bioresour Technol 102(16):7478-85.

Agirrezabal-Telleria I., García-Sancho C., Maireles-Torres P., Arias P. L. Dehydration of xylose to furfural using a lewis or brönsted acid catalyst and N2 stripping. 2013. Chin J Catal 34(7):1402-6.

Akiya N. and Savage P. E. Roles of water for chemical reactions in high-temperature water. 2002. Chem Rev 102(8):2725-50.

Aldana-Pérez A., et al. 2012. Sulfonic groups anchored on mesoporous carbon starbons-300 and its use for the esterification of oleic acid. Fuel 100:128-38.

Al-Hazmi M. and Apblett A. W. Benzylation of benzene over sulfated zirconia supported in MCM-41 using a single source precursor. 2011. Catal Sci Technol 1(4):621-30.

Alibaba. Factory wholesale low price furfural [cited 2019 9/10]. Available from: https://www.alibaba.com/product-detail/Factory-wholesale-low-price-furfural_1264137027.html?spm=a2700.7724857.normalList.63.73cf6033C7RiNK .

Antal M. J., Leesomboon T., Mok W. S., Richards G. N. Mechanism of formation of 2-furaldehyde from d-xylose. 1991. Carbohydr Res 217:71-85.

Antonyraj C. A. and Haridas A. A lignin-derived sulphated carbon for acid catalyzed transformations of bio-derived sugars. 2018. Catal Commun 104:101-5.

Aspen Technology Inc. 2013. **Aspen Plus** [computer program]. Version 2013. .

Barrett E. P., Joyner L. G., Halenda P. P. The determination of pore volume and area distributions in porous substances. I. computations from nitrogen isotherms. 1951. J Am Chem Soc 73:373.

Bbosa D., Mba-Wright M., Brown R. C. More than ethanol: A techno-economic analysis of a corn stover-ethanol biorefinery integrated with a hydrothermal liquefaction process to convert lignin into biochemicals. 2018. Biofuels, Bioprod Bioref 12(3):497-509.

Besson M., Gallezot P., Pinel C. Conversion of biomass into chemicals over metal catalysts. 2014. Chem Rev 114(3):1827-70.

Bhaumik P., Kane T., Dhepe P. L. Silica and zirconia supported tungsten, molybdenum and gallium oxide catalysts for the synthesis of furfural. 2014. Catal Sci Technol 4(9):2904-7.

Birajdar SD. 2015. A new paradigm for recovery of biologically produced 2, 3-butanediol using thermodynamically screened solvents in an intensified extraction system. India: Savitribai Phule Pune University.

Boehm H. 2008. Chapter thirteen - surface chemical characterization of carbons from adsorption studies. In: Adsorption by carbons. Bottani EJ, ,Tascón JMD, editors. Amsterdam: Elsevier. 301 p.

Brunauer S., Emmett P. H., Teller E. Adsorption of gases in multimolecular layer. 1938. J Am Chem Soc 35(60):309.

Campos Molina M. J., Mariscal R., Ojeda M., López Granados M. Cyclopentyl methyl ether: A green co-solvent for the selective dehydration of lignocellulosic pentoses to furfural. 2012. Bioresour Technol 126:321-7.

Carlos Serrano-Ruiz J. and Dumesic J. A. Catalytic upgrading of lactic acid to fuels and chemicals by dehydration/hydrogenation and C-C coupling reactions. 2009. Green Chem 11(8):1101-4.

CCM. CCM: China's market price of furfural bounces back in April.

Centi G., Lanzafame P., Perathoner S. Analysis of the alternative routes in the catalytic transformation of lignocellulosic materials. 2011. Catalysis Today 167(1):14-30.

Chen L., Janssens T. V. W., Skoglundh M., Grönbeck H. Interpretation of NH3-TPD profiles from cu-CHA using first-principles calculations. 2019. Top Catal 62(1):93-9.

Chen X. J., Liu X. Q., Xu F. L., Bai X. P. Degradation kinetics of xylose and arabinose in subcritical water in unitary and binary system. 2012. Advanced Materials Research 450-451:710-4.

Chen Z., Zhang W., Xu J., Li P. Kinetics of xylose dehydration into furfural in acetic acid. 2015. Chin J Chem Eng 23(4):659-66.

Chernysheva D. V., Chus Y. A., Klushin V. A., Lastovina T. A., Pudova L. S., Smirnova N. V., Kravchenko O. A., Chernyshev V. M., Ananikov V. P. Sustainable utilization of biomass refinery wastes for accessing activated carbons and supercapacitor electrode materials. 2018. ChemSusChem 11(20):3599-608.

Chheda J. N., Huber G. W., Dumesic J. A. Liquid-phase catalytic processing of biomass-derived oxygenated hydrocarbons to fuels and chemicals. 2007. Angew Chem , Int Ed 46(38):7164-83.

Choudhary V., Sandler S. I., Vlachos D. G. Conversion of xylose to furfural using lewis and brönsted acid catalysts in aqueous media. 2012. ACS Catal 2(9):2022-8.

Choudhary V., Pinar A. B., Sandler S. I., Vlachos D. G., Lobo R. F. Xylose isomerization to xylulose and its dehydration to furfural in aqueous media. 2011. ACS Catal 1(12):1724-8.

DalinYebo. Furfural Market [cited 2015 30/November]. Available from: http://www.da-linyebo.com/furfuralmarket .

Danon B., Hongsiri W., van der Aa L., de Jong W. Kinetic study on homogeneously catalyzed xylose dehydration to furfural in the presence of arabinose and glucose. 2014. Biomass Bioenergy 66(0):364-70.

Danon B., Marcotullio G., de Jong W. Mechanistic and kinetic aspects of pentose dehydration towards furfural in aqueous media employing homogeneous catalysis. 2014. Green Chem 16(1):39-54.

De Oliveira Vigier K. and Jerome F. 2010. Heterogeneously-catalyzed conversion of carbohydrates. Springer, Berlin, Heidelberg.

Delbecq F., Wang Y., Muralidhara A., El Ouardi K., Marlair G., Len C. Hydrolysis of hemicellulose and derivatives – A review of recent advances in the production of furfural. 2018. Frontiers in Chemistry 6.

Deng A., et al. 2016. A feasible process for furfural production from the pre-hydrolysis liquor of corncob via biochar catalysts in a new biphasic system. Bioresource Technology 216:754-60.

Dhepe P. L. and Sahu R. A solid-acid-based process for the conversion of hemicellulose. 2010. Green Chem 12(12):2153-6.

Dias A. S., Pillinger M., Valente A. A. Liquid phase dehydration of d-xylose in the presence of keggin-type heteropolyacids. 2005a. Appl Catal , A 285(1–2):126-31.

Dias A. S., Pillinger M., Valente A. A. Mesoporous silica-supported 12-tungstophosphoric acid catalysts for the liquid phase dehydration of d-xylose. 2006. Microporous Mesoporous Mater 94(1):214-25.

Dias A. S., Pillinger M., Valente A. A. Dehydration of xylose into furfural over micro-mesoporous sulfonic acid catalysts. 2005b. J Catal 229(2):414-23.

Dias A. S., Lima S., Pillinger M., Valente A. A. Modified versions of sulfated zirconia as catalysts for the conversion of xylose to furfural. 2007. Catal Lett 114(3):151-60.

Dias A. S., Lima S., Pillinger M., Valente A. A. Acidic cesium salts of 12-tungstophosphoric acid as catalysts for the dehydration of xylose into furfural. 2006. Carbohydr Res 341(18):2946-53.

Doherty T. V., Mora-Pale M., Foley S. E., Linhardt R. J., Dordick J. S. Ionic liquid solvent properties as predictors of lignocellulose pretreatment efficacy. 2010. Green Chem 12(11):1967-75.

Domalski E. S. and Hearing E. D. Heat capacities and entropies of organic compounds in the condensed phase. volume III. 1996. Journal of Physical and Chemical Reference Data 25(1):1-525.

Eifert T. and Liauw M. A. Process analytical technology (PAT) applied to biomass valorisation: A kinetic study on the multiphase dehydration of xylose to furfural. 2016. React Chem Eng 1(5):521-32.

Ershova O., Kanervo J., Hellsten S., Sixta H. The role of xylulose as an intermediate in xylose conversion to furfural: Insights via experiments and kinetic modelling. 2015. RSC Adv 5(82):66727-37.

Ershova O., Nieminen K., Sixta H. The role of various chlorides on xylose conversion to furfural: Experiments and kinetic modeling. 2017. ChemCatChem 9:3031-40.

Ershova O., et al. 2018. Vapor pressure, vapor-liquid equilibria, liquid-liquid equilibria and excess enthalpy of the system consisting of isophorone, furfural, acetic acid and water. Chemical Engineering Science 176(Supplement C):19-34.

Escobar A., Sathicq Á, Pizzio L., Blanco M., Romanelli G. Biomass valorization derivatives: Clean esterification of 2-furoic acid using tungstophosphoric acid/zirconia composites as recyclable catalyst. 2015. Process Saf Environ Prot 98:176-86.

Filiciotto L., Balu A. M., Van der Waal J. C., Luque R. Catalytic insights into the production of biomass-derived side products methyl levulinate, furfural and humins. 2018. Catal Today 302:2-15.

García-Sancho C., Agirrezabal-Telleria I., Güemez M. B., Maireles-Torres P. Dehydration of d-xylose to furfural using different supported niobia catalysts. 2014. Appl Catal , B 152–153(0):1-10.

Gharagheizi F., Sattari M., Angaji M. T. Effect of calculation method on values of hansen solubility parameters of polymers. 2006. Polymer Bulletin 57(3):377-84.

Goertzen S. L., Thériault K. D., Oickle A. M., Tarasuk A. C., Andreas H. A. Standardization of the boehm titration. part I. CO2 expulsion and endpoint determination. 2010. Carbon 48(4):1252-61.

Gómez Millán G., Hellsten S., Llorca J., Luque R., Sixta H., Balu A. M. Recent advances in the catalytic production of platform chemicals from holocellulosic biomass. 2019. ChemCatChem 11(8):2022-42.

70

Gómez Millán G., Phiri J., Mäkelä M., Maloney T., Balu A. M., Pineda A., Llorca J., Sixta H. Furfural production in a biphasic system using a carbonaceous solid acid catalyst. 2019. Appl Catal , A .

Gómez Millán G., Hellsten S., King A. W. T., Pokki J., Llorca J., Sixta H. A comparative study of water-immiscible organic solvents in the production of furfural from xylose and birch hydrolysate. 2019. J Ind Eng Chem 72:354-363.

Gómez Millán G., El Assal Z., Nieminen K., Hellsten S., Llorca J., Sixta H. Fast furfural formation from xylose using solid acid catalysts assisted by a microwave reactor. 2018. Fuel Process Technol 182:56-67.

Graziano B., Jakob M., Kremer F., Pischinger S., Lee C. and Fernandes R. X. 2013. Investigation on the ignition sensitivity of 2-MTHF, heptane and di-n-butylether. ; 25-28.6.2013; Lund, Sweden. .

Guenic S. L., Delbecq F., Ceballos C., Len C. Microwave-assisted dehydration of D-xylose into furfural by diluted inexpensive inorganic salts solution in a biphasic system. 2015. J Mol Catal A: Chem 410:1-7.

Gürbüz E., Bond J. Q., Dumesic J. A., Román-Leshkov Y. 2013. Chapter 8 - role of acid catalysis in the conversion of lignocellulosic biomass to fuels and chemicals. In: The role of catalysis for the sustainable production of bio-fuels and bio-chemicals. Triantafyllidis KS, Lappas AA,Stöcker M, editors. Amsterdam: Elsevier. 261 p.

Hansen C. M. 2007. Hansen solubility parameters: A user's handbook, second edition . CRC Press.

Hansen CM. 1967. The three dimensional solubility parameter and solvent diffusion coefficient, their importance in surface coating formulation. Copenhagen, Denmark: Technical University of Denmark.

Heng Z. and Grinstaff M. W. Recent advances in glycerol polymers: Chemistry and biomedical applications. 2014. Macromol Rapid Commun 35(22):1906-24.

Hinman N. D., Wright J. D., Hoagland W., Wyman C. E. Xylose fermentatio:
an economic analysis 1989. Applied Biochernistry and Biotechnology 20/21:391.

Holladay JE, Bozell JJ, White JF, Johnson D. 2007. Top value-added chemicals from biomass volume II—Results of screening for potential candidates from biorefinery lignin. . Report nr 16983.

Hongsiri W., Danon B., de Jong W. The effects of combined catalysis of oxalic acid and seawater on the kinetics of xylose and arabinose dehydration to furfural. 2015. Int J Energy Environ Eng 6(1):21-30.

Jalili R., Esrafilzadeh D., Aboutalebi S. H., Sabri Y. M., Kandjani A. E., Bhargava S. K., Della Gaspera E., Gengenbach T. R., Walker A., Chao Y., et al. Silicon as a ubiquitous contaminant in graphene derivatives with significant impact on device performance. 2018. Nat Commun 9(1):5070.

Jeong G. H., Kim E. G., Kim S. B., Park E. D., Kim S. W. Fabrication of sulfonic acid modified mesoporous silica shells and their catalytic performance with dehydration reaction of d-xylose into furfural. 2011. Microporous Mesoporous Mater 144(1–3):134-9.

Jones C. W. On the stability and recyclability of supported metal-ligand complex catalysts: Myths, misconceptions and critical research needs. 2010. Top Catal 53(13):942-52.

Kaiprommarat S., Kongparakul S., Reubroycharoen P., Guan G., Samart C. Highly efficient sulfonic MCM-41 catalyst for furfural production: Furan-based biofuel agent. 2016. Fuel 174:189-96.

Kamm B., Gerhardt M., Dautzenberg G. 2013. Chapter 5 - catalytic processes of lignocellulosic feedstock conversion for production of furfural, levulinic acid, and formic acid-based fuel components. In: New and future developments in catalysis. Suib SL, editor. Amsterdam: Elsevier. 91 p.

Karinen R., Vilonen K., Niemelä M. Biorefining: Heterogeneously catalyzed reactions of carbohydrates for the production of furfural and hydroxymethylfurfural. 2011. ChemSusChem 4(8):1002-16.

Kim S. B., You S. J., Kim Y. T., Lee S., Lee H., Park K., Park E. D. Dehydration of D-xylose into furfural over H-zeolites. 2011. Korean Journal of Chemical Engineering 28(3):710-6.

Kootstra A. M. J., Mosier N. S., Scott E. L., Beeftink H. H., Sanders J. P. M. Differential effects of mineral and organic acids on the kinetics of arabinose degradation under lignocellulose pretreatment conditions. 2009. Biochem Eng J 43(1):92-7.

Lam E., Majid E., Leung A. C. W., Chong J. H., Mahmoud K. A., Luong J. H. T. Synthesis of furfural from xylose by heterogeneous and reusable nafion catalysts. 2011. ChemSusChem 4(4):535-41.

Lam E., Chong J. H., Majid E., Liu Y., Hrapovic S., Leung A. C. W., Luong J. H. T. Carbocatalytic dehydration of xylose to furfural in water. 2012. Carbon 50(3):1033-43.

Lamminpää K. 2015. Formic acid catalysed xylose dehydration into furfural. University of Oulu.

Lamminpää K., Ahola J., Tanskanen J. Kinetics of furfural destruction in a formic acid medium. 2014. RSC Adv 4(104):60243-8.

Lamminpää K., Ahola J., Tanskanen J. Acid-catalysed xylose dehydration into furfural in the presence of kraft lignin. 2015. Bioresour Technol 177:94-101.

Lange J., van der Heide E., van Buijtenen J., Price R. Furfural - A promising platform for lignocellulosic biofuels. 2012. ChemSusChem 5(1):150-66.

Lê HQ. 2018. Wood biorefinery concept based on γ-valerolactone/water fractionation. Espoo, Finland: Aalto University.

Ledesma C. and Llorca J. Hydrogen production by steam reforming of dimethyl ether over Cu–Zn/CeO2–ZrO2 catalytic monoliths. 2009. Chem Eng J 154(1–3):281-6.

Legras A., et al. 2015. Inverse gas chromatography for natural fibre characterisation: Identification of the critical parameters to determine the Brunauer–Emmett–Teller specific surface area. Journal of Chromatography A 1425:273-9.

Lessard J., Morin J., Wehrung J., Magnin D., Chornet E. High yield conversion of residual pentoses into furfural via zeolite catalysis and catalytic hydrogenation of furfural to 2-methylfuran. 2010. Top Catal 53(15-18):1231-4.

Li H., Deng A., Ren J., Liu C., Wang W., Peng F., Sun R. A modified biphasic system for the dehydration of d-xylose into furfural using SO42−/TiO2-ZrO2/La3+ as a solid catalyst. 2014a. Catal Today 234(0):251-6.

Li H., Deng A., Ren J., Liu C., Wang W., Peng F., Sun R. A modified biphasic system for the dehydration of d-xylose into furfural using SO42−/TiO2-ZrO2/La3+ as a solid catalyst. 2014b. Catal Today 234:251-6.

Lima S., Pillinger M., Valente A. A. Dehydration of D-xylose into furfural catalysed by solid acids derived from the layered zeolite nu-6(1). 2008. Catal Commun 9(11–12):2144-8.

Lima S., Antunes M. M., Fernandes A., Pillinger M., Ribeiro M. F., Valente A. A. Catalytic cyclodehydration of xylose to furfural in the presence of zeolite H-beta and a micro/mesoporous beta/TUD-1 composite material. 2010. Appl Catal , A 388(1–2):141-8.

Lima S., Fernandes A., Antunes M. M., Pillinger M., Ribeiro F., Valente A. A. Dehydration of xylose into furfural in the presence of crystalline microporous silicoaluminophosphates. 2010. Catal Lett 135(1):41-7.

Lin L., Ma S., Li P., Zhu T., Chang H. Mutual solubilities for the water-2-sec-butylphenol system and partition coefficients for furfural and formic acid in the water-2-sec-butylphenol system. 2015. J Chem Eng Data 60(6):1926-33.

Mäki-Arvela P., Salmi T., Holmbom B., Willför S., Murzin D. Y. Synthesis of sugars by hydrolysis of hemicelluloses- A review. 2011. Chem Rev 111(9):5638-66.

Mariscal R., Maireles-Torres P., Ojeda M., Sadaba I., Lopez Granados M. Furfural: A renewable and versatile platform molecule for the synthesis of chemicals and fuels. 2016. Energy Environ Sci 9(4):1144-89.

Martel F., Estrine B., Plantier-Royon R., Hoffmann N., Portella C. 2010. Development of agriculture left-overs: Fine organic chemicals from wheat hemicellulose-derived pentoses. Rauter AP, Vogel P,Queneau Y, editors. Springer, Berlin, Heidelberg. 79 p.

Mazzotta M. G., Gupta D., Saha B., Patra A. K., Bhaumik A., Abu-Omar M. M. Efficient solid acid catalyst containing lewis and brønsted acid sites for the production of furfurals. 2014. ChemSusChem 7(8):2342-50.

Mellmer M. A., Sener C., Gallo J. M. R., Luterbacher J. S., Alonso D. M., Dumesic J. A. Solvent effects in acid-catalyzed biomass conversion reactions. 2014. Angewandte Chemie International Edition 53(44):11872-5.

Mittal A., Black S. K., Vinzant T. B., O'Brien M., Tucker M. P., Johnson D. K. Production of furfural from process-relevant biomass-derived pentoses in a biphasic reaction system. 2017. ACS Sustainable Chem Eng .

Molina M. J. C., Granados M. L., Gervasini A., Carniti P. Exploitment of niobium oxide effective acidity for xylose dehydration to furfural. 2015. Catal Today 254:90-8.

Moreau C., Durand R., Peyron D., Duhamet J., Rivalier P. Selective preparation of furfural from xylose over microporous solid acid catalysts. 1998. Ind Crops Prod 7(2–3):95-9.

Mukherjee A., Dumont M., Raghavan V. Review: Sustainable production of hydroxymethylfurfural and levulinic acid: Challenges and opportunities. 2015. Biomass Bioenergy 72:143-83.

Oefner P. J., Lanziner A. H., Bonn G., Bobleter O. Quantitative studies on furfural and organic acid formation during hydrothermal, acidic and alkaline degradation ofD-xylose. 1992. Monatshefte Für Chemie / Chemical Monthly 123(6):547-56.

Ojeda M., Balu A. M., Romero A. A., Esquinazi P., Ruokolainen J., Sixta H., Luque R. MAGBONS: Novel magnetically separable carbonaceous nanohybrids from porous polysaccharides. 2014. ChemCatChem 6(10):2847-53.

Olcay H., Malina R., Upadhye A. A., Hileman J. I., Huber G. W., Barrett S. R. H. Techno-economic and environmental evaluation of producing chemicals and drop-in aviation biofuels via aqueous phase processing. 2018. Energy Environ Sci .

O'Neill R., Ahmad M. N., Vanoye L., Aiouache F. Kinetics of aqueous phase dehydration of xylose into furfural catalyzed by ZSM-5 zeolite. 2009. Ind Eng Chem Res 48(9):4300-6.

Pineda A., Balu A. M., Campelo J. M., Luque R., Romero A. A., Serrano-Ruiz J. C. High alkylation activities of ball-milled synthesized low-load supported iron oxide nanoparticles on mesoporous aluminosilicates. 2012. Catal Today 187(1):65-9.

Pirola C., Rossetti I., Ragaini V. Are conversion, selectivity and yield terms unambiguously defined in chemical and chemical engineering technology? 2013. La Chimica & L'Industria 2:136-145.

Rinaldi R. and Schuth F. Design of solid catalysts for the conversion of biomass. 2009. Energy Environ Sci 2(6):610-26.

Rodriguez-Chiang L., et al. 2017. New alternative energy pathway for chemical pulp mills: From traditional fibers to methane production. Bioresource Technology 235:265-73.

Romo J., Miller K., Sundsted T., Job A., Hoo K., Wettstein S. G. The effect of solvent polarity on autocatalytic furfural production confirmed by multivariate statistical analysis. 2019. ChemCatChem 0.

Romo J. E., Bollar N. V., Zimmermann C. J., Wettstein S. G. Conversion of sugars and bio-mass to furans using heterogeneous catalysts in biphasic solvent systems. 2018. ChemCatChem 10(21):4805-16.

Sahu R. and Dhepe P. L. A one-pot method for the selective conversion of hemicellulose from crop waste into C5 sugars and furfural by using solid acid catalysts. 2012. ChemSusChem 5(4):751-61.

Sairanen E., Vilonen K., Karinen R., Lehtonen J. Functionalized activated carbon catalysts in xylose dehydration. 2013. Top Catal 56(9-10):512-21.

Schlosser P. M., Bale A. S., Gibbons C. F., Wilkins A., Cooper G. S. Human health effects of dichloromethane: Key findings and scientific issues. 2015. Environ Health Perspect 123:114-9.

Serrano-Ruiz J., Luque R., Sepulveda-Escribano A. Transformations of biomass-derived platform molecules: From high added-value chemicals to fuels via aqueous-phase processing. 2011. Chem Soc Rev 40(11):5266-81.

Serrano-Ruiz J., et al. 2012. Continuous-flow processes in heterogeneously catalyzed transformations of biomass derivatives into fuels and chemicals. Challenges 3(2).

Sheldon R. A., Arends I. W. C. E., Hanefeld U. 2007. Introduction: Green chemistry and catalysis. In: Green chemistry and catalysis. Wiley-VCH Verlag GmbH & Co. KGaA. 1 p.

Sievers C., Noda Y., Qi L., Albuquerque E. M., Rioux R. M., Scott S. L. Phenomena affecting catalytic reactions at Solidâ€"Liquid interfaces. 2016. ACS Catal 6(12):8286-307.

Sievers C., Musin I., Marzialetti T., Valenzuela Olarte M. B., Agrawal P. K., Jones C. W. Acid-catalyzed conversion of sugars and furfurals in an ionic-liquid phase. 2009. ChemSusChem 2(7):665-71.

Sigma-Aldrich. Furfural [cited 2019 July 2019]. Available from: https://www.sigmaaldrich.com/MSDS/MSDS/DisplayMSDSPage.do?country=DE&language=EN-generic&productNumber=185914&brand=SIAL&PageToGoToURL=https%3A%2F%2Fwww.sigmaaldrich.com%2Fcatalog%2Fproduct%2Fsial%2F185914%3Flang%3Dde .

Soler L., Casanovas A., Urrich A., Angurell I., Llorca J. CO oxidation and COPrOx over pre-formed au nanoparticles supported over nanoshaped CeO2. 2016. Applied Catalysis B: Environmental 197:47-55.

Stephenson R. M. and Malanowski S. 1987. Properties of organic compounds. In: Handbook of the thermodynamics of organic compounds. Stephenson RM and Malanowski S, editors. Dordrecht: Springer Netherlands. 1 p.

Talvitie H. and Pitkänen P. Cellunolix® ethanol plant to be built in Finland.

Tenne S., et al. 2013. 2-methyltetrahydrofuran and cyclopentylmethylether: Two green solvents for efficient purification of membrane proteins like FhuA. Journal of Chromatography B 937:13-7.

Termvidchakorn C., Itthibenchapong V., Songtawee S., Chamnankid B., Namuangruk S., Faungnawakij K., Charinpanitkul T., Khunchit R., Hansupaluk N., Sano N., et al. Dehydration of D-xylose to furfural using acid-functionalized MWCNTs catalysts. 2017. Adv Nat Sci : Nanosci Nanotechnol 8(3):035006.

Timokhin B. V., Baransky V. A., Eliseeva G. D. Levulinic acid in organic synthesis. 1999. Russ Chem Rev 68(1):73.

Toor S. S., Rosendahl L., Rudolf A. Hydrothermal liquefaction of biomass: A review of subcritical water technologies. 2011. Energy 36(5):2328-42.

van Zandvoort I. 2015. Towards the valorization of humin by-products: Characterization, solubilization and catalysis. The Netherlands: University of Utrecht.

van Zandvoort I., Wang Y., Rasrendra C. B., van Eck E. R. H., Bruijnincx P. C. A., Heeres H. J., Weckhuysen B. M. Formation, molecular structure, and morphology of humins in biomass conversion: Influence of feedstock and processing conditions. 2013. ChemSusChem 6(9):1745-58.

Verma S., Baig R. B. N., Nadagouda M. N., Len C., Varma R. S. Sustainable pathway to furanics from biomass via heterogeneous organo-catalysis. 2017. Green Chem 19(1):164-8.

vom Stein T., Grande P. M., Leitner W., Domínguez de María P. Iron-catalyzed furfural production in biobased biphasic systems: From pure sugars to direct use of crude xylose effluents as feedstock. 2011. ChemSusChem 4(11):1592-4.

Wang Y., et al. 2017. Application of sulfonated carbon-based catalyst for the furfural production from d-xylose and xylan in a microwave-assisted biphasic reaction. Mol Catal 438:167-72.

Watanabe K., Yamagiwa N., Torisawa Y. Cyclopentyl methyl ether as a new and alternative process solvent. 2007. Org Process Res Dev 11(2):251-8.

Weingarten R., Tompsett G. A., Conner Jr. W. C., Huber G. W. Design of solid acid catalysts for aqueous-phase dehydration of carbohydrates: The role of lewis and brønsted acid sites. 2011. J Catal 279(1):174-82.

Weingarten R., Cho J., Conner J.,Wm.Curtis, Huber G. W. Kinetics of furfural production by dehydration of xylose in a biphasic reactor with microwave heating. 2010. Green Chem 12(8):1423-9.

Werpy T and Petersen G. 2004. Top value added chemicals from biomass: Volume I -- results of screening for potential candidates from sugars and synthesis gas; sponsor org.: US department of energy (US). United States: .

Wojcieszak R., Santarelli F., Paul S., Dumeignil F., Cavani F., Gonçalves R. V. Recent developments in maleic acid synthesis from bio-based chemicals. 2015. Sustainable Chem Processes 3(1):9.

Xing R., Qi W., Huber G. W. Production of furfural and carboxylic acids from waste aqueous hemicellulose solutions from the pulp and paper and cellulosic ethanol industries. 2011. Energy Environ Sci 4(6):2193-205.

Xiong H., Pham H. N., Datye A. K. Hydrothermally stable heterogeneous catalysts for conversion of biorenewables. 2014. Green Chem 16(11):4627-43.

Yan K., Jarvis C., Gu J., Yan Y. Production and catalytic transformation of levulinic acid: A platform for speciality chemicals and fuels. 2015. Renewable Sustainable Energy Rev 51:986-97.

Yang Y., Hu C., Abu-Omar M. M. Synthesis of furfural from xylose, xylan, and biomass using AlCl3-6H2O in biphasic media via xylose isomerization to xylulose. 2012. ChemSusChem 5(2):405-10.

Yepez A., Garcia A., Climent M. S., Romero A. A., Luque R. Catalytic conversion of starch into valuable furan derivatives using supported metal nanoparticles on mesoporous aluminosilicate materials. 2014. Catal Sci Technol 4(2):428-34.

Zeitsch K. J. 2000. 1. introduction. In: The chemistry and technology of furfural and its many by-products. Zeitsch KJ, editor. Elsevier. 1 p.

Zeitsch K. J. 2000a. A. properties of furfural. In: The chemistry and technology of furfural and its many by-products. Zeitsch KJ, editor. Elsevier B.V. 234 p.

Zeitsch K. J. 2000b. 6. furfural loss reactions. In: The chemistry and technology of furfural and its many by-products. Zeitsch KJ, editor. Elsevier B.V. 19 p.

Zeitsch K. J. 2000c. 9. raw materials. In: The chemistry and technology of furfural and its many by-products. Zeitsch KJ, editor. Elsevier. 34 p.

Zeitsch K. J. 2000d. 14. applications of furfural. In: The chemistry and technology of furfural and its many by-products. Zeitsch KJ, editor. Elsevier B.V. 98 p.

Zeitsch K. J. 2000e. 10. furfural processes. In: The chemistry and technology of furfural and its many by-products. Zeitsch KJ, editor. Elsevier. 36 p.

Zeng W., Du Y., Xue Y., Frisch H. L. 2007. Solubility parameters. In: Physical properties of polymers handbook. Mark JE, editor. New York, NY: Springer New York. 289 p.

Zhang J., Li J., Lin L. Dehydration of sugar mixture to HMF and furfural over SO42-/ZrO2-TiO2 catalyst. 2014. BioResources 9:4194.

Zhang H. Liquid–liquid phase equilibria of the quaternary system {water (1)+acrylic acid (2)+acetic acid (3)+cyclopentyl methyl ether (4)}: Measurement, correlation, and comparative study. 2015. Fluid Phase Equilibria 403:23-9.

I

Gómez Millán, G., El Assal, Z., Nieminen, K., Hellsten, S., Llorca, J., Sixta, H. (2018) Fast Furfural Formation from Xylose Using Solid Acid Catalysts Assisted by a Microwave Reactor. *Fuel Processing Technology* **182**, 56-67.

Fast furfural formation from xylose using solid acid catalysts assisted by a microwave reactor

Gerardo Gómez Millán[a,b], Zouhair El Assal[c], Kaarlo Nieminen[a], Sanna Hellsten[a], Jordi Llorca[b], Herbert Sixta[a,*]

[a] Department of Bioproducts and Biosystems, Aalto University, Vuorimiehentie 1, 02150 Espoo, Finland
[b] Department of Chemical Engineering, Institute of Energy Technologies and Barcelona Research Center in Multiscale Science and Engineering, Universitat Politècnica de Catalunya, Eduard Maristany 10-14, 08019 Barcelona, Spain
[c] Department of Environmental and Chemical Engineering, Faculty of Technology, University of Oulu, P.O. Box 4300, 90014 Oulu, Finland

ARTICLE INFO

ABSTRACT

The production of furfural (FUR) from xylose was carried out using sulfated zirconia (SZ) on cordierite, alumina on cordierite and commercially-available polymeric solid catalysts (Amberlyst DT and Nafion NR40) to provide insights into the reaction pathways and kinetics for the dehydration of xylose in aqueous phase. Experiments conducted at three temperatures were investigated (170, 190 and 210 °C) in a stirred microwave-assisted batch reactor, which established the optimal conditions to obtain the highest FUR yield as well as extensive and fast xylose conversion. The maximum FUR yields obtained from xylose were 41 mol% when using SZ on cordierite in 2 min (at 210 °C), 43 mol% when using alumina on cordierite in 30 min (at 210 °C) and 48 mol% for an auto-catalyzed system in 60 min (at 210 °C). Based on the experimental results, a reaction mechanism was proposed considering the formation of an intermediate from xylose when solid acid catalysts were added. After five reusability cycles using SZ on cordierite, this catalyst can be regenerated with a similar performance and similar FUR yield on the 6th cycle.

1. Introduction

Furfural (furan-2-carbaldehyde, FUR) is the dehydration product of xylose and other pentoses, C_5-sugars typically found in hemicellulose in lignocellulosic biomass. A wide range of FUR derivatives with high potential for applications has been identified. FUR is considered a selective solvent for organic compounds and serves as a building block for its hydrogenation to furfuryl alcohol, for components of P-series fuels or liquid alkanes, and in the manufacture of foundry resins [1–3]. Tetrahydrofuran and tetrahydrofurfuryl alcohol are the other two main chemicals obtained from FUR that have wide applications in the chemical industry. The rest of the FUR is employed in oil refining, pharmaceutical, plastics and agrochemical industries (as fungicide and nematicide) [4]. Although xylan and xylose have not yet been fully utilized in the paper industry, a significant amount of xylose, from the hydrolysis of woody biomass, is mixed with lignin-derived compounds and burned to provide process heat [5]. Therefore, valorization of these compounds offers a new economic approach for new ideas and new markets.

The commercial process for the production of FUR involves several environmental issues, such as toxic effluents derived from mineral acids (sulfuric or phosphoric acid) at temperatures of approximately 200 °C and the consumption of high stripping-steam to FUR ratios, especially related to important energy and environmental concerns regarding the fuel employed to generate the steam. Homogeneous acids (in the form of dilute aqueous solutions) achieve a one-step hemicellulose deconstruction and xylose dehydration in the same reactor. However, the utilization of these corrosive homogeneous mineral acids leads to challenges in product separation, equipment corrosion, mineral acid loss, high amounts of acidic and toxic waste, as well as a significant amount of side reactions that limit FUR yields to ca. 50% [6]. New methodologies based on the use of easily-separable solid catalysts including zeolites [7–14], aluminosilicates supported with metals [15], modified silica [16–23], alumina [12], zirconia [12,24] solid acids like layered zeolite Nu-6 [25], sulfonated graphenes [26], heteropolyacids [27–29], coated activated carbon [30] and resins [20,31,32] to yield xylose dehydration are currently being explored to improve FUR yields in a much more environmentally friendly and efficient industrial process.

Previous published literature has described the high catalytic

---

activity of metal oxides in the dehydration of xylose into FUR. However, the hydrothermal stability of these materials has not been properly addressed. Furthermore, the reaction times to reach the highest FUR yields usually require from 2 [12] up to 20 h [21,23,27–29,33]. Dias et al. [29] studied various sulfated zirconias in the formation of FUR from xylose in an aqueous-toluene system at 160 °C in 4 h. They are able to identify a correlation of the catalytic activity with the sulphur content of the sulfated zirconia. Nevertheless, a significant amount of sulphur leaching is observed in the reusability tests. Zhang et al. [34] used a SO_4^{2-}/ZrO_2-TiO_2 catalyst in a sugar mixture employing an aqueous-n-butanol biphasic system. The maximum FUR yield (48 mol%) was reached at 170 °C in 2 h. Even though the authors performed a reusability test, two cycles might not be enough to observe hydrothermal stability of the catalyst. Li et al. [24] employed a SO_4^{2-}/TiO_2-ZrO_2/La^{3+} catalyst in a biphasic system to form FUR from xylose. The highest FUR yield reported (3563 μmol of FUR/g of xylose) was reached in 12 h at 180 °C. However, the article lacks hydrothermal stability studies and the reusability potential of the metal oxide catalyst.

The ongoing discussion of the proper reaction mechanisms of FUR formation has generated proposals for different formation pathways under homogeneous and heterogeneous catalysis. O'Neill and co-workers claim that xylose could be isomerized to lyxose via adsorption onto the acidic active sites of ZSM-5 zeolite [8]. These steps would occur through the formation of the linear open chain of xylose molecules caused by the acid-catalyzed hydrolysis. On the other hand, Verma et al. [35] proposed a mechanism via the formation of 2,5-anhydoxylose furanose cyclic intermediate using a sulfonated graphitic carbon nitride. Xylulose, a xylose isomer, has been under discussion as possible intermediate on FUR formation [36,37]. However, there is no conclusive information on either pathway.

In this work, we aimed to employ solid acid catalysts for the dehydration of xylose to produce FUR in short times (< 2 h). In addition, the kinetic model for this reaction was further investigated and a reaction mechanism is proposed for heterogeneously catalyzed systems. The hydrothermal stability of the solid catalysts is also addressed in the present paper. Due to their high acid site density [38,39], solid acid catalysts were developed (Al_2O_3 and $ZrO_2(SO_4^{2-})$ on cordierite) and compared to commercially available polymeric resins (Amberlyst DT and Nafion NR40). Their textural properties and acid site density were analyzed.

2. Materials and methods

D-Xylose powder (99%, Sigma Aldrich) was used in the experiments without further purification. Formic acid (98%), levulinic acid (99%) and acetic acid (99%) were purchased from Sigma Aldrich and used for the preparation of calibration standards for HPLC analysis. Millipore grade water was used for preparing the solutions. Cordierite was obtained from Corning (Germany) and Disperal from Sasol Germany GmbH (Hamburg, Germany). Amberlyst DT was purchased from Rohm and Haas (France). Nafion NR40 beads were purchased from Ion Power GmbH (Germany).

2.1. Catalyst preparation

Pieces of cordierite (1–4 mm) were used as support. Sulfated zirconia (SZ, $ZrO_2(SO_4^{2-})$) and Al_2O_3 were prepared by impregnation of $ZrOCl_2 \cdot 8H_2O$ and boehmite suspensions as precursors over cordierite following the method of Ledesma et al. [40]. The notation for SZ over cordierite is SZ_{cord} and for Al_2O_3 over cordierite is Al_2O_{3cord}. The resulting samples were dried at 105 °C and then calcined in air for 2–5 h to obtain the corresponding active oxides (SZ_{cord} at 500 °C; Al_2O_{3cord} at 450 °C). Saez et al. [38] found that cordierite presented no appreciable reactivity. The inclusion of cordierite in the catalyst preparation is to provide the catalyst a physical support for practical application.

Reaction tests were conducted over Nafion NR40 and Amberlyst DT for the sake of comparison. Nafion NR40 was purified by treatment with hot hydrogen peroxide (5%) to remove organic impurities and soaked in 5 wt% hot hydrochloric acid to remove cations and exchange them by protons. It was dried overnight at 105 °C. Amberlyst DT was also dried overnight at 105 °C prior experimental tests.
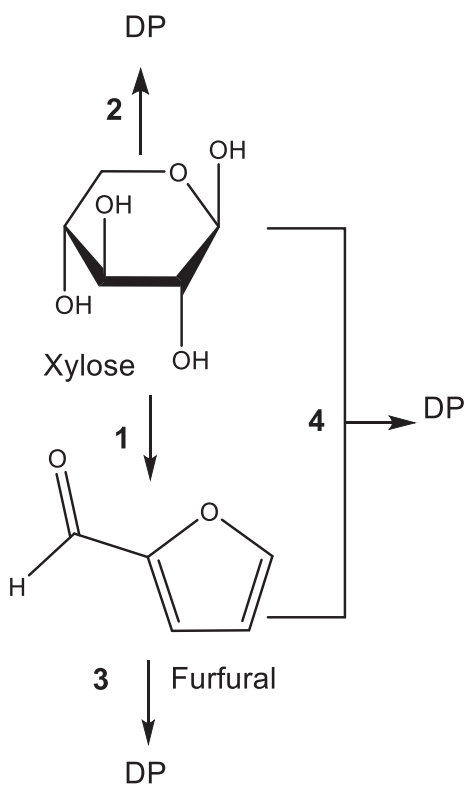
2.2. Catalytic activity tests

Single component solution of D-xylose (186 mmol l^{-1}) were freshly prepared before the experiments. This specific xylose concentration was found to be in the prehydrolysate liquor from birch wood [41]. The first set of experiments was performed in the absence of solid acid catalysts. The second set of experiments was performed using 50 mg of Al_2O_{3cord}, SZ_{cord}, Amberlyst DT or Nafion NR40 as a catalyst. In a typical experiment, the glass reactor was loaded with 3 ml of the xylose solution and heated using a borosilicate glass reactor (V = 10 cm^3) with magnetic stirring (600 min^{-1}) and microwave-assisted heating (Monowave 300, Anton Paar GmbH, Graz, Austria). After the reaction, the reactor was rapidly cooled to room temperature by utilizing compressed air. The highest temperature and the longest reaction time studied at the present work were 210 °C and 180 min, respectively. After reaction, the solutions were tested for FUR yield, selectivity and xylose conversion at the reaction temperatures of 170, 190 and 210 °C with different reaction times in the range of 2–180 min.

In a typical experiment with solid acid catalyst, the glass reactor was loaded with 3 ml of an aqueous solution of 186 mmol l^{-1} xylose and 50 mg of the catalyst. The reactor was placed in the microwave, heated to the set reaction temperature with an irradiation power of ≤ 850 W for maximum 1.5 min and kept at the reaction temperature for the set time. After the reaction, the reactor was rapidly cooled to room temperature by utilizing compressed air. For the reusability experiments, SZ_{cord} was collected after each use. It was washed with deionized water several times at room temperature and dried at 105 °C prior to reuse. All catalytic activity tests were performed in duplicate with a standard deviation below 10% (except for Nafion NR40, which its standard deviation is up to 33%).
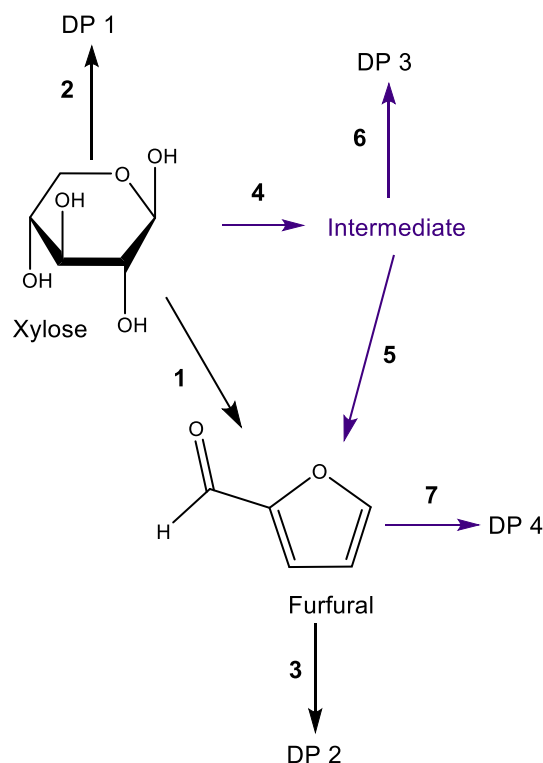
2.3. Reaction mechanism

The kinetic modeling of xylose dehydration and FUR formation were based on the obtained experimental results following three possible reaction mechanisms. These reaction mechanisms were screened in order to find the optimal kinetic model explaining the xylose dehydration and FUR formation. Even though the reaction mechanism of FUR formation has been under discussion, these reaction mechanisms consider a pathway of FUR formation via an intermediate or xylose itself, a reaction mechanism did not consider a pathway solely via an intermediate. Using the xylose conversion data only in the modeling resulted in multiple equally well-fitting models with different mechanistic assumptions. The tested reaction mechanism considering the intermediate formation from xylose is as follows:

In the reaction model presented in Scheme 1, xylose can be converted to FUR directly (k_1). In Scheme 2, FUR can be formed from xylose either stepwise with an intermediate product ($k_4 + k_5$), or via a direct or pseudo-direct reaction pathway (k_1). In the reaction model presented in Scheme 3, FUR is formed stepwise via an intermediate ($k_4 + k_5$) [41] or via a direct or pseudo-direct reaction pathway (k_1). The latter scheme proposes a parallel reaction model from the intermediate. The produced FUR further forms degradation products (DP). DP 2 is formed in the auto-catalyzed reaction and DP 4 formation is promoted by solid acid catalysts. Simultaneously, some fraction of xylose and intermediates (isomers or epimers of xylose) form also degradation products (DP 1 and DP 3). The HPLC analysis did not identify any significant amount from products originating from side reactions between xylose and FUR, as well as the isomerization of the

Scheme 1. FUR formation with direct xylose decomposition.

Scheme 2. FUR formation with side reaction between intermediate and FUR.

Scheme 3. Parallel FUR formation with side reaction decomposition.

3. Results and discussion

3.1. Auto-catalyzed dehydration of xylose

Kinetic studies for auto-catalyzed xylose dehydration were performed at various reaction times at temperatures of 170, 190 and 210 °C. Fig. 1 shows the FUR yield, xylose conversion and selectivity to FUR under these reaction conditions. The experimental tests can be considered as auto-catalyzed, since water is self-ionized to H^+ and OH^- ions that act as acid or base catalysts at the given temperature [45]. Later on, the carboxylic acids (formic, levulinic and acetic acid) or intermediates formed during the reaction, may have a catalytic effect [32,41,46]. The influence of the reaction temperature on the FUR yield and xylose conversion has been observed previously in similar work [37,47]. As Fig. 1a displays, the FUR yield increased with reaction temperature up to 4 times from 170 to 190 °C after the first 60 min. When the reaction temperature was further increased from 190 to 210 °C, a 2-fold increase can be seen. It was observed that at the highest temperature investigated in the present study (210 °C) the FUR yield firstly increases and thereafter decreases, as the reaction time prolongs. The decrease of FUR yield in prolonged reaction time occurs due to decomposition and polymerization with humins production [48,49]. Under the present experimental conditions, the maximum FUR yield (48–49%) was reached after the first 60 min at 210 °C, which corresponds to a xylose conversion of 94% (Fig. 1b) and a FUR selectivity of 52% (Fig. 1c).

At reaction temperatures of 170 and 190 °C, no distinct FUR yield culmination point, with subsequent rapid decrease was perceived during the reaction time range investigated. However, a yield decrease similar to that observed at 210 °C could be possibly observed at lower reaction temperatures (170 and 190 °C) during prolonged reaction times. Nevertheless, the maximum yield unmistakably shifts to a longer reaction time with a decline of the reaction temperature. Furthermore, the FUR yield (and thus also the selectivity) decreases with decreasing the reaction temperature, this is in agreement with literature [50]. It is worth noting that the maximum selectivity to FUR observed in the auto-

intermediate back to xylose.

Previous kinetic studies have used either Scheme 1 [42] or Scheme 2 [41,43,44] using homogeneous catalysts. Different formation pathways include isomerization of xylose to other pentoses such as lyxose and xylulose. Dias et al. [29] proposed a similar reaction mechanism for sulfated zirconia as Scheme 2 shown in the present study, however there was no kinetic studies reported on the pathway of FUR formation from the intermediate.
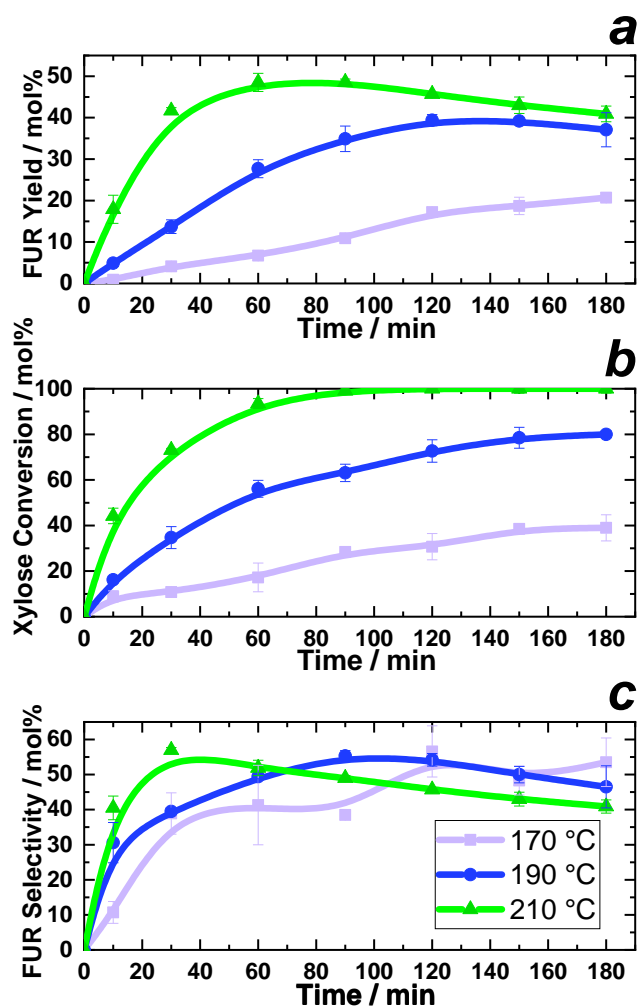
Fig. 1. FUR yield (a), xylose conversion (b) and selectivity to FUR (c) at various reaction times during auto-catalyzed conversion of xylose 186 mmol l^{-1} (purple square — 170 °C, blue circle — 190 °C, green triangle — 210 °C, lines are to guide the eye). (For interpretation of the references to color in this figure legend, the reader is referred to the web version of this article.)

catalyzed conversion of xylose was 56–58% in the present studied range of reaction temperatures. These results agree with previously published papers [37].

3.2. Catalyzed dehydration of xylose by solid acids

Fig. 2a, b and c shows the FUR yield, xylose conversion and selectivity to FUR at various reaction times at 170, 190 and 210 °C when Al$_2$O$_{3cord}$ is present in the dehydration of xylose. For SZ$_{cord}$-catalyzed conversion of xylose Fig. 2d, e and f shows the FUR yield, xylose conversion and selectivity to FUR, respectively. Similarly to the auto-catalyzed process, the FUR yield and the xylose conversion are visibly influenced by the reaction temperature. When using Al$_2$O$_{3cord}$, the maximum FUR yield is clearly influenced by the reaction temperature: at 170 °C starts from 26%, it increases furthermore up to 43% at 210 °C (Fig. 2a). This is similar to the effect observed when adding SZ$_{cord}$, the maximum FUR yield increases from 36 to 41% when the reaction temperature is increased from 170 °C to 210 °C (Fig. 2d). After the maximum FUR yield has been reached, selectivity decreases because the FUR formed reacts further, via condensation and resinification [12]. Hence, humin formation was observed. These FUR yield losses were observed at reaction temperatures of 190 and 210 °C.

Similarly as in the auto-catalyzed process, conversion of xylose to FUR needs relatively high temperatures (Fig. 2b and e). When using Al$_2$O$_{3cord}$ in the dehydration reaction of xylose, the maximum FUR yield (43%, Fig. 2a) was reached in 30 min at 210 °C, corresponding to a xylose conversion of 91% (Fig. 2b) and a FUR selectivity of 48% (Fig. 2c). The maximum FUR yield (41%) was reached after 2 min at 210 °C during the SZ$_{cord}$-catalyzed reaction, corresponding to a xylose conversion of 96% (Fig. 2e) and a FUR selectivity of 43% (Fig. 2f). During the SZ$_{cord}$-catalyzed reaction, the maximum selectivity to FUR was 43% (at 210 °C in 2 min) in contrast to 57% (at 210 °C in 30 min) obtained in the auto-catalyzed reaction system. When comparing the present results with the catalyzed system using H$_2$SO$_4$ [37] and a xylose concentration of 196 mmol l^{-1}, the highest selectivity to FUR is 68% (at 180 °C in 5 min) and 65% (at 200 °C in 1 min, and at 220 °C in 2 min).

The FUR yield, xylose conversion and selectivity to FUR at various reaction times at 170 °C during conversion of xylose conducted with Amberlyst DT are shown in Fig. S1. Amberlyst DT was only tested at 170 °C (maximum operational temperature) due to its limited hydrothermal stability as stated by the manufacturer. The maximum FUR yield (30%) was reached in 60 min at 170 °C with a xylose conversion of 70%.

The FUR yield, xylose conversion and selectivity to FUR at 170, 190 and 210 °C at various reaction times during xylose conversion conducted with Nafion NR40 are shown in Fig. S2. In the same way that reaction temperature strongly influences FUR yield and xylose conversion in the auto-catalyzed process, the effect can be also observed when adding Nafion NR40. When adding Nafion NR40 pellets to the aqueous system, the maximum FUR yield is determined by the reaction temperature: at 170 °C starts from 33%, furthermore it increases up to 41% at 210 °C (Fig. S2a). Due to the nature of the catalysts, the standard deviation increased at high reaction times and at high temperatures (> 190 °C), even though the manufacturer guarantees its stability from 220 to 240 °C in aqueous systems. The catalysts clogged into each other making a barrier in the middle of the reactor. Therefore, the FUR and xylose concentration do not follow a smooth tendency. Nevertheless, xylose conversion behaves similarly to the auto-catalyzed system, since it requires longer reaction times to convert the same amount of xylose at a lower reaction temperature (Fig. S2b). In the case of Nafion NR40, the maximum FUR yield (41%, Fig. S2a) was reached in 8 min at 210 °C, resulting on a xylose conversion of 70% (Fig. S2b) and a FUR selectivity of 60% (Fig. S2c). During the Nafion NR40-catalyzed reaction, the maximum selectivity to FUR was 67% (at 210 °C in 2 min) in contrast to 43% (at 210 °C in 2 min) obtained in the SZ$_{cord}$-catalyzed reaction system, and 52% (at 210 °C in 60 min) in the auto-catalyzed reaction system.

Control experiments for cordierite were performed at 170 °C and 210 °C for 60 min. Xylose conversion, FUR yield and pH values can be considered comparable for systems in the presence of cordierite and in the auto-catalyzed system. In contrast, experiments employing 0.1 mol l^{-1} H$_2$SO$_4$ were performed in earlier work [37]. These experiments show that the highest FUR yield (65%) is reached at 220 °C in 2 min. At 200 °C, the highest FUR yield (59%) is reached in 5 min. At 180 °C the highest FUR yield (55%) is reached in 25 min.

The xylulose formation, a possible key intermediate [36,51,52], was monitored by means of HPLC utilizing a pure xylulose solution as a reference. No detectable amounts of xylulose were observed in the initial xylose solutions. Under auto-catalyzed conditions at temperature reactions of 170–210 °C, xylulose formation was not detectable. This is in accordance with the low amount of xylulose yield (< 3 mol%) reported by Ershova et al. [37] when employing a 196 mmol l^{-1} xylose solution at reactions temperatures of 180, 200 and 220 °C.

Fig. S3a shows that the highest amount of xylulose (18 mol%) was formed when employing alumina as catalyst in the dehydration of xylose at 170 °C in 120 min. At this temperature, some amount of xylulose was still present even after 3 h of treatment. When adding SZ$_{cord}$ (Fig. S3b), 46 mol% was the highest amount of xylulose formed at 170 °C in
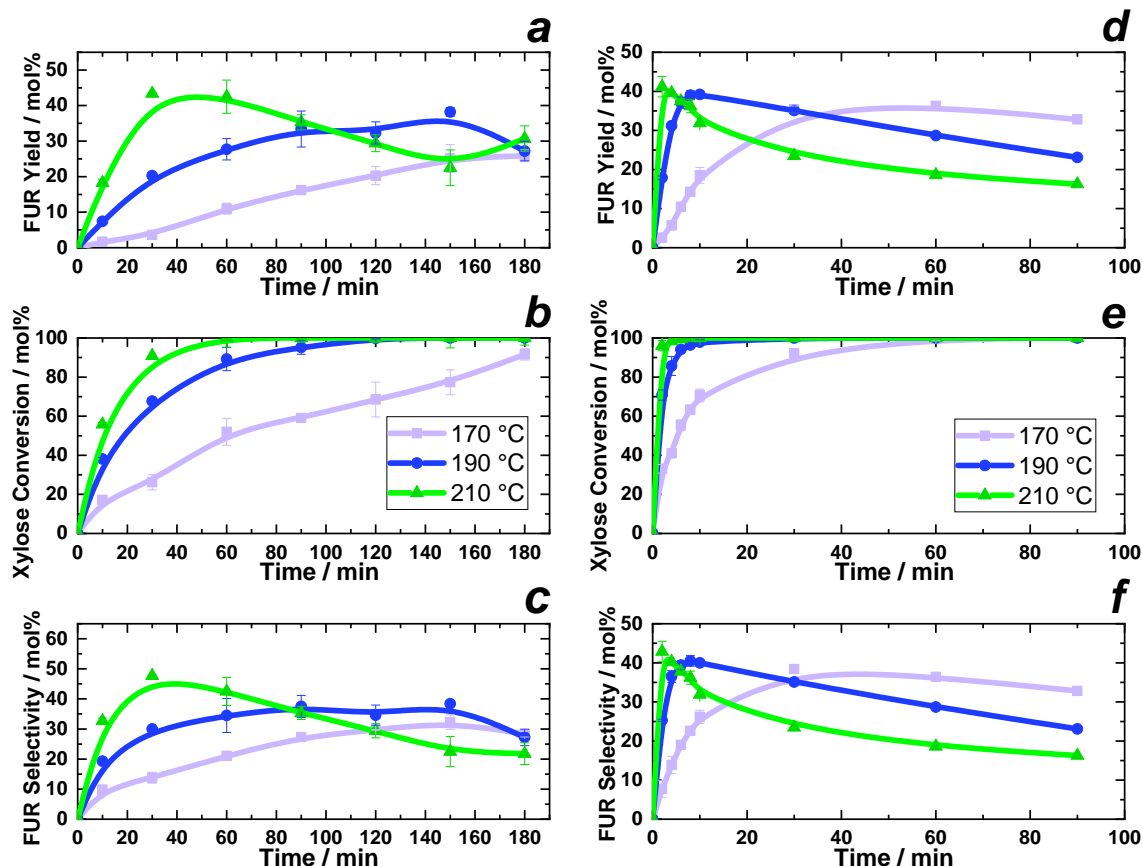
Fig. 2. FUR yield (a, d), xylose conversion (b, e) and selectivity to FUR (c, f) at various reaction times during conversion of xylose 186 mmol l^{-1} using Al$_2$O$_{3\text{cord}}$ (a, b, c) and SZ$_{\text{cord}}$ (d, e, f), respectively (purple square — 170 °C, blue circle — 190 °C, green triangle — 210 °C, lines are to guide the eye). (For interpretation of the references to color in this figure legend, the reader is referred to the web version of this article.)

6 min. When the reaction temperature increased to 190 °C, the amount of yielded xylulose decreased (27%). At 210 °C, 2% of xylulose was yielded in 2 min. The extent of xylulose formation was highest at the lowest reaction temperature (170 °C) used in the present paper.

Xylulose was not identified at any experimental temperature employed in the present paper when polymeric resins (Amberlyst DT and Nafion NR40) were added into the system.

3.3. Mathematical modeling

Assuming a sequence of predominantly pseudo-first order reactions, the reactions of the model are assumed to follow the rate equations for similar elementary reactions. When the reactions are carried out in a batch reactor, the component mass balance for Scheme 1 (assuming that the k_3 rate constant describes that the reaction consumes equal amount of moles of xylose and FUR) are: Eqs. (1) and (2);

$$\frac{d[Xylose]}{dt} = -(k_1 + k_2)[Xylose] - (k_4)[Xylose][FUR] \tag{1}$$

$$\frac{d[FUR]}{dt} = k_1[Xylose] - ((k_3)[FUR] + (k_4)[Xylose][FUR]) \tag{2}$$

for Scheme 2 the component mass balance are shown in Eqs. (3), (4) and (5);

$$\frac{d[Xylose]}{dt} = -(k_1 + k_2 + k_4)[Xylose] + k_{-4}[Intermediate] \tag{3}$$

$$\frac{d[Intermediate]}{dt} = k_4[Xylose] - (k_{-4} + k_5 + k_6)[Intermediate] \tag{4}$$

$$\frac{d[FUR]}{dt} = k_5[Intermediate] + k_1[Xylose] - k_3[FUR] \tag{5}$$

For Scheme 3 for the auto-catalyzed system Eqs. (6) and (7) show the component mass balance:

$$\frac{d[Xylose]}{dt} = -(k_1 + k_6)[Xylose] \tag{6}$$

$$\frac{d[FUR]}{dt} = k_1[Xylose] - k_3[FUR] \tag{7}$$

And for the solid acid-catalyzed system Eqs. (8), (9) and (10):

$$\frac{d[Xylose]}{dt} = -(k_1 + k_2 + k_4)[Xylose] \tag{8}$$

$$\frac{d[Intermediate]}{dt} = k_4[Xylose] - (k_5 + k_6)[Intermediate] \tag{9}$$

$$\frac{d[FUR]}{dt} = k_1[Xylose] + k_5[Intermediate] - (k_3 + k_7)[FUR] \tag{10}$$

where k_1, k_2, k_3, k_4, k_5, k_6, and k_7 are rate constants and [*Xylose*], [*Intermediate*], and [*FUR*] are concentrations (in mol l^{-1}) for xylose, intermediate and FUR, respectively.

The fittings of the kinetic models of the experimental results with pure xylose solution and solid acid catalysts corresponding to Scheme 3 are shown in Figs. 3–5. The fittings show that the chemical intermediate concentration is strongly influenced by the reaction temperature and the presence of the solid acid catalysts. As it can be seen in Figs. 4 and 5, the concentration of the intermediate decreases when the reaction temperature increases. In the case of the Al$_2$O$_{3\text{cord}}$ (Fig. 5), the concentration of the chemical intermediate reaches up to 32 mmol l^{-1} at
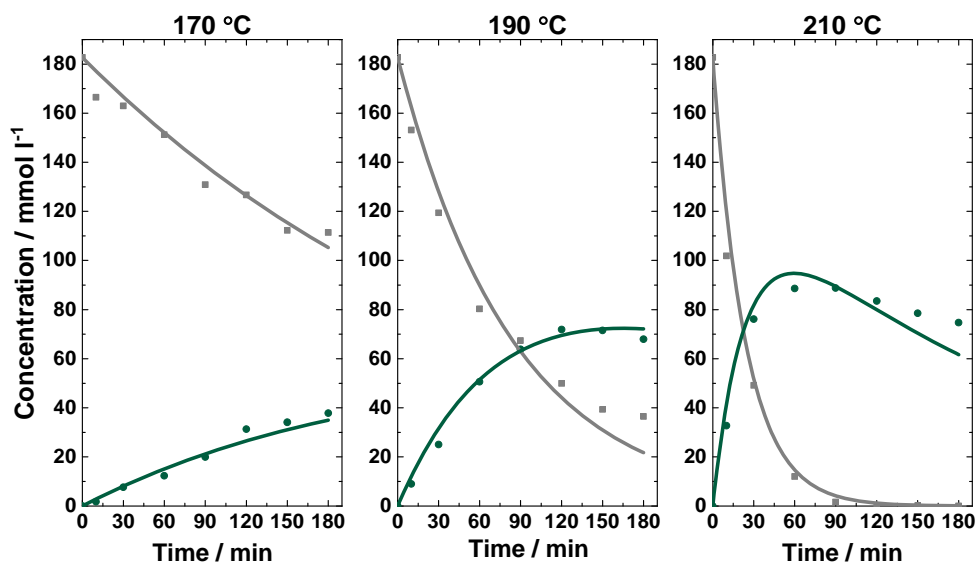
Fig. 3. Scheme 3 and concentrations of FUR (green) and xylose (grey) at temperatures of 170, 190 and 210 °C in auto-catalyzed system. (Experimental-circle, modeled-solid lines). (For interpretation of the references to color in this figure legend, the reader is referred to the web version of this article.)

170 °C. When adding SZ$_{cord}$, this concentration increases up to 86 mmol l^{-1} (Fig. 4) also at 170 °C.

It has been reported previously that SZ$_{cord}$ possesses Brønsted acid (BA) sites, while Al$_2$O$_{3cord}$ presents a combination of BA and Lewis acid (LA) sites. BA are linked to direct pentose dehydration into FUR, and LA tend to isomerize pentoses into chemical intermediates, such as xylulose [12,20,36,53–55]. However, the discussion on the co-existence of BA and LA sites on the surface of SZ$_{cord}$ and how to properly measure it still continues [56–58]. Furthermore, the discussion on the relationship between LA and BA sites effect on the dehydration mechanism is largely unclear [59]. The extent of sulfation on the SZ$_{cord}$ was low (Table 5), which might favor the presence of LA [56], thus promoting reaction pathways with chemical intermediates, such as xylulose. For both systems employing solid acid catalysts (SZ$_{cord}$ and Al$_2$O$_{3cord}$), the highest concentration of xylulose is reached at the lowest temperature (170 °C). This is in agreement with previous studies [36,37], which highlighted that the reaction of xylulose to FUR is favored at low temperatures in the presence of LA over the reaction of xylose to FUR. In contrast, at

high temperatures LA catalysts lose the pathway via xylulose, due to gradual transformation of LA into BA, which can be seen in Figs. 4 and 5 where xylulose disappears as temperature increases. Their presence also involves the formation of degradation products such as carboxylic acids (formic, acetic and levulinic acid). These compounds were identified but not quantified. The figures corresponding to the models following scheme 1 and scheme 2 are displayed on Figs. S4–S11.

3.4. Model fitting

The Figs. 3–5 show that Scheme 3 predicts xylose and FUR concentrations properly. The models fit all the xylose conversion experimental data as well as FUR formation. The main difference between the three models is that Scheme 3 includes a parallel reaction when the solid acid catalyst is added, thus describing the formation of an intermediate (xylulose). The best fitting of the model to experimental data was obtained considering a parallel pathway via an intermediate compound leading to the formation of FUR when using solid acid

Fig. 4. Scheme 3 and concentrations of FUR (green), xylose (grey) and xylulose (blue) at temperatures of 170, 190 and 210 °C with SZ$_{cord}$. (Experimental-circle, modeled-solid lines). (For interpretation of the references to color in this figure legend, the reader is referred to the web version of this article.)
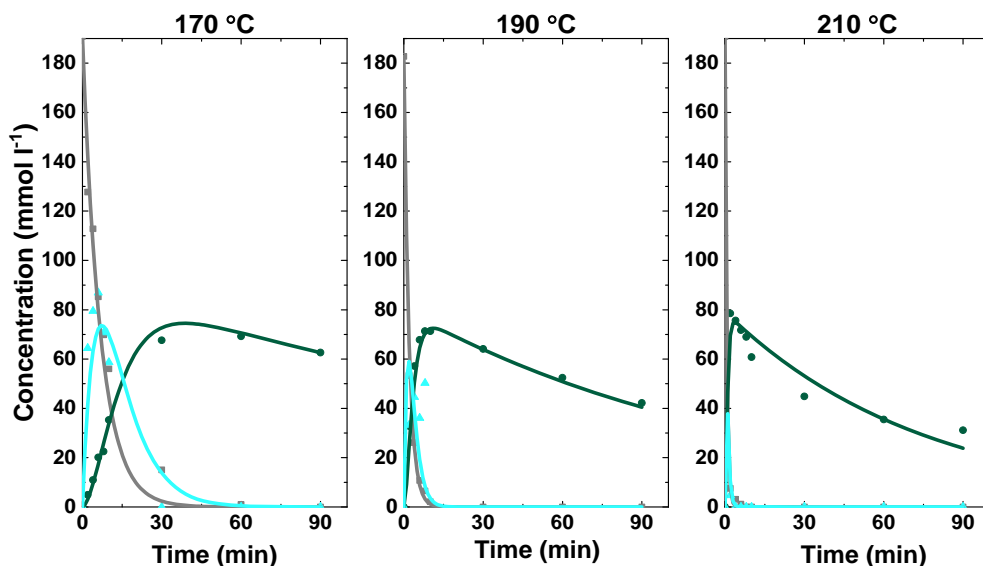
Fig. 5. Scheme 3 and concentrations of FUR (green), xylose (grey) and xylulose (blue) at temperatures of 170, 190 and 210 °C with Al_2O_{3cord}. (Experimental-circle, modeled-solid lines). (For interpretation of the references to color in this figure legend, the reader is referred to the web version of this article.)
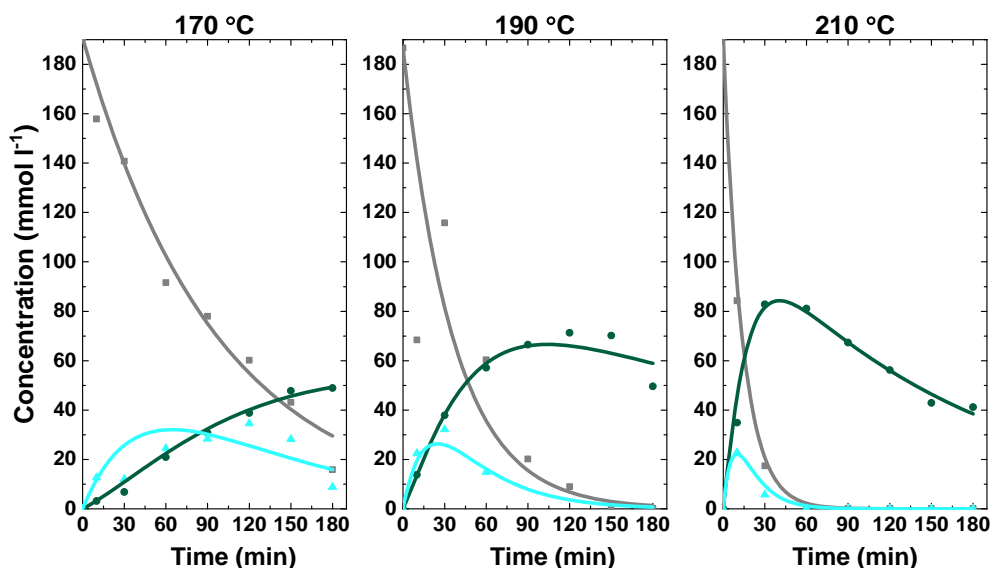
catalysts (Scheme 3) and a direct formation of FUR from xylose in the auto-catalyzed system.

In order to be able to elucidate relative contributions of individual steps (Table 1), the pre-exponential factor and the activation energy values were evaluated by fitting the models to the data. The rate constants were then calculated from the pre-exponential factor and the activation energy according to the Arrhenius equation. When SZ_{cord} and Al_2O_{3cord} are added the temperature dependence of k_i is more pronounced, indicating that the reaction rates in the presence of solid acid catalyst are subtler to the reaction temperature. Tables 1–3 display the obtained kinetic parameters and the activation energy for each reaction step.

As Table 1 reveals, the rate constants for the xylose dehydration into FUR (k_1) increase as the temperature increases in the auto-catalyzed system. Similar to this, the rate constants for the decomposition of xylose (k_2) and FUR (k_3) also increase as the reaction temperature increases. The addition of SZ_{cord} and Al_2O_{3cord} as solid acid catalysts adds a reaction for the xylose isomerization (k_4), its dehydration to FUR (k_5) and the further decomposition products from the chemical intermediate (k_6) and from FUR (k_7). This observation is supported by the fact that sugar isomerization reactions are catalyzed by the presence of LA sites [36,37,53,59,60]. The addition of SZ_{cord} and Al_2O_{3cord}, increases the xylose decomposition (k_2). These results are in agreement with You et al. [61], which confirms that LA sites are involved in the formation of humin from xylose dehydration. The rate constant for the decomposition of FUR (k_3, k_7) in the auto-catalyzed and catalyzed systems with SZ_{cord} and Al_2O_{3cord} are negligible. At the studied conditions when

SZ_{cord} and Al_2O_{3cord} are added to the system, the formation of decomposition products is found to decrease in the order $k_6 > k_2 > k_7 > k_3$. This could be due to the introduction of BA sites, which increase the decomposition rate of pentoses [38].

This is in line with the activation energy values presented in Table 3. The ratio of the reaction rate k_1/k_2 indicates that the dehydration of xylose is faster than the formation of decomposition products (Table 2). At the same time, the high ratio of k_1/k_3 shows that the reaction to FUR from xylose is much faster than the decomposition of FUR. When adding SZ_{cord}, the low ratio values of k_5/k_6 indicate that the intermediate decomposes faster than FUR is formed from it. This could be due to the introduction of LA sites, which are known to promote humin formation and decomposition into C_1–C_3 products [36,61]. Nevertheless, in the case of Al_2O_{3cord}, the opposite is true except at high temperatures (210 °C). This could be explained by the presence of LA sites that at high temperatures are transformed into BA sites [10,57]. Furthermore, the ratio k_1/k_4 demonstrates that the addition of solid acid catalysts, which present LA sites isomerize xylose into other pentoses (xylulose) as other authors have previously reported [12,20,36,55,60,62]. Furthermore, when SZ_{cord} is added to the reaction the ratio k_3/k_7 decreases as temperature increases. However, in the case of Al_2O_{3cord}, the rate of decomposition products forming from FUR in the auto-catalyzed system is faster than in the solid acid-catalyzed system. Nevertheless, k_3 and k_7 values are negligible as Table 1 shows.

The frequency factors and activation energy values for each reaction step are shown in Table 3. For comparison reasons, some published data related to similar reaction steps are also shown in Table S1. To the

Table 2
Ratio of selected kinetic rate constants at each experimental temperature for auto-catalyzed and solid acid-catalyzed systems following Scheme 3.

T, (°C)	Solid acid	k_1/k_2	k_1/k_3	k_5/k_6	k_1/k_4	k_3/k_7
170	–	1.07	1.23			
190	–	1.51	2.84			
210	–	2.11	6.33			
170	SZ_{cord}	1.07	1.23	0.70	0.01	0.81
190	SZ_{cord}	1.51	2.84	0.67	0.01	0.66
210	SZ_{cord}	2.11	6.33	0.65	0.01	0.54
170	Al_2O_{3cord}	1.07	1.23	1.77	0.21	0.62
190	Al_2O_{3cord}	1.51	2.84	1.36	0.44	1.09
210	Al_2O_{3cord}	2.11	6.33	0.97	0.92	1.73

Table 1
Kinetic rate constants k_i (min^{-1}) at each experimental temperature for auto-catalyzed and acid-catalyzed systems following Scheme 3.

T, (°C)	Solid acid catalysts	k_1	k_2	k_3	k_4	k_5	k_6	k_7
170	–	0.002	0.002	0.001				
190	–	0.007	0.005	0.002				
210	–	0.028	0.014	0.004				
170	SZ_{cord}	0.002	0.002	0.001	0.13	0.065	0.093	0.002
190	SZ_{cord}	0.007	0.005	0.002	0.54	0.43	0.64	0.004
210	SZ_{cord}	0.028	0.014	0.004	2.02	2.41	3.71	0.008
170	Al_2O_{3cord}	0.002	0.002	0.001	0.008	0.006	0.003	0.002
190	Al_2O_{3cord}	0.007	0.005	0.002	0.016	0.015	0.011	0.002
210	Al_2O_{3cord}	0.028	0.014	0.004	0.031	0.036	0.037	0.003

Table 3

Frequency factors ($A_{ref,i}$ min^{-1}) and activation energy values (E_{ai}, kJ mol^{-1}) for the kinetic model proposed in Scheme 3; auto-catalyzed system, SZ_{cord}- and Al_2O_{3cord}-catalyzed system.

Scheme number		$A_{ref,i}$ (auto-catalyzed)	E_{ai} (auto-catalyzed)	$A_{ref,i}$ (SZ_{cord})	E_{ai} (SZ_{cord})	$A_{ref,i}$ (Al_2O_{3cord})	E_{ai} (Al_2O_{3cord})
Scheme 3	(1)	$3.2 \times 10^{+11}$	121				
	(2)	$1.9 \times 10^{+9}$	103				
	(3)	2900	53.7				
	(4)			$3.42 \times 10^{+13}$	122	$1.92 \times 10^{+5}$	63
	(5)			$5.85 \times 10^{+17}$	161	$3.8 \times 10^{+7}$	83
	(6)			$1.99 \times 10^{+18}$	164	$3.54 \times 10^{+10}$	111
	(7)			$7.02 \times 10^{+5}$	73	0.031	10

authors' knowledge, the frequency factors and activation energy values of xylose isomerization to the intermediate, to FUR and degradation products formation from the intermediate following Scheme 3 have not been previously reported in literature for neither auto-catalyzed nor catalyzed reactions with solid acid catalysts present. In comparison to the auto-catalyzed system, when using SZ_{cord} and Al_2O_{3cord} in the system the activation energy values increased. The activation energy calculated when employing SZ_{cord} and Al_2O_{3cord} in the present study are higher than those published before the present study. These divergences between data could be possibly explained by either implementation of simplified reaction mechanism [2,53,63–66] or utilization of subcritical and supercritical reaction condition in earlier studies [67].

Confidence intervals for the kinetic parameters in Table 3 are shown in Table S2 in the Supplementary Information. As expected, the ranges of the intervals are significant; the frequency factors vary with several orders of magnitude, which is in agreement with the exponential nature of the quantity. For Reaction (1) it was not possible to calculate the confidence interval for the activation energy in the case of Al_2O_{3cord} due to the proximity of zero.

Reaction rate constants, frequency factors and activation energy values when using Nafion NR40 can be seen in Tables S3, S4 and S5. Frequency factors and activation energy values for the kinetic models (Schemes 1 and 2); in the auto-catalyzed system and when using SZ_{cord} and Al_2O_{3cord} can be seen in Table S7. Due to the absence of xylulose when the polymeric resins were employed, Scheme S1 shows the model use to fit the experimental data when using the resins in the present system.

3.5. Catalyst characterization

Solid acid catalysts before and after hydrothermal reaction were characterized based on the highest FUR yield reached at the three selected temperatures (170, 190 and 210 °C). The notation for SZ_{cord} and Al_2O_{3cord} after hydrothermal reaction at 170 °C includes a hyphen, e.g. $SZ_{cord-170}$ (where the highest FUR yield was reached).

3.5.1. Morphology of the solid acid catalysts

Fig. 6 shows, as an example, the scanning electron micrographs of $Al_2O_{3cord-fresh}$ and $Al_2O_{3cord-210}$ catalyst samples. On the $Al_2O_{3cord-fresh}$ sample, Fig. 6(a), the alumina plates can be seen on the surface. Fig. 6(c) corresponds to $Al_2O_{3cord-210}$ on cordierite sample (210 °C after 30 min). Fig. 6(b, d) correspond to $Al_2O_{3cord-fresh}$ and $Al_2O_{3cord-210}$ on cordierite sample at a higher magnification. It can be seen on Fig. 6(c, d) humin formation on the surface of the metal oxide catalyst samples (see spheres marked with arrows).

SZ_{cord} can be seen on Fig. 7(a, b), the SEM images show similitude of the SZ_{cord} characteristically cylindrical-like structure as reported by Al-Hazmi and Apblett [68]. $SZ_{cord-210}$ on cordierite catalyst sample is shown on Fig. 7(c, d) after the hydrothermal reaction at 210 °C for 2 min. On the surface of the spent samples appeared spheres (marked by arrows in Fig. 7(c, d)), which are humins formed in the hydrothermal reaction.

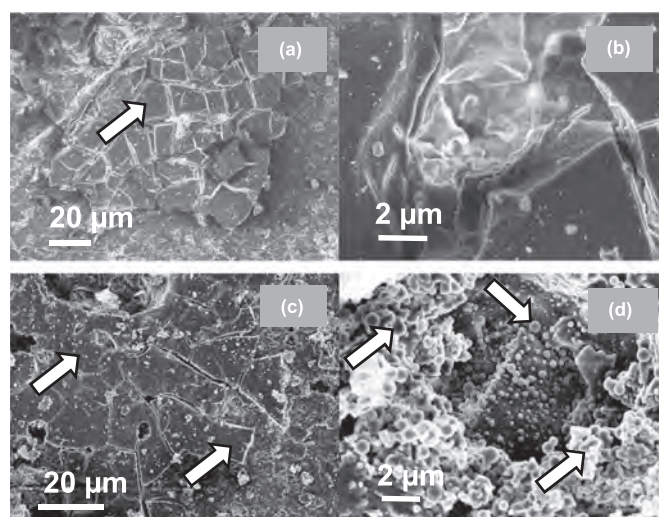SEM images of Nafion NR40$_{fresh}$ and Nafion NR40$_{210}$, Amberlyst

Fig. 6. SEM images of (a, b) Al_2O_{3cord}, (c, d) $Al_2O_{3cord-210}$.
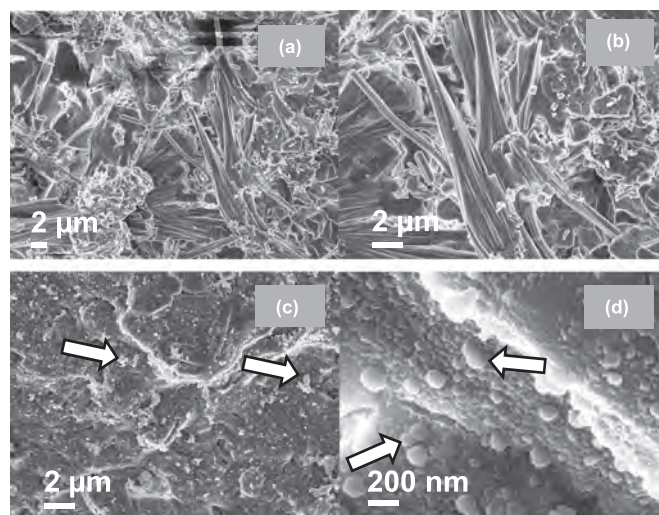
Fig. 7. SEM images of (a, b) SZ_{cord}, (c, d) $SZ_{cord-210}$.

DT$_{fresh}$ and Amberlyst DT$_{170}$, as well as $SZ_{cord-170}$, $SZ_{cord-190}$ and $SZ_{cord-reused}$ can be seen in Figs. S12, S13 and S14, respectively. The structure of these spherical particles 2–3 μm in size agree with the findings of Van Zandvoort et al. [48], who studied humin formation from acid-catalyzed dehydration of xylose under standard reaction conditions of 180 °C, 1 M solution of sugar and 0.01 M H_2SO_4. These insoluble polymeric structures are formed by aqueous acidic media of most lignocellulosic biomass valorization processes [2,59,69]. The formation of carbonaceous deposits is detrimental to the reaction as can be seen in Figs. 1 and 2.

Table 4

Textural properties of solid acid catalysts (i.e., BET (A_{BET}), pore volume (V_p) and pore diameter (d_p).

Catalysts	A_{BET} (m^2 g^{-1})	V_p (cm^3 g^{-1})	d_p (nm)
Al$_2$O$_{3cord}$	11.8	10^{-2}	4.4
SZ$_{cord}$	0.8	10^{-3}	5.0
Nafion NR40	0.2	4×10^{-5}	1.4
Amberlyst DT	0.2	$1o^{-4}$	1.1

3.5.2. N$_2$-sorption

The BET (Brunauer-Emmett-Teller) specific surface areas and pore volumes obtained by the nitrogen physisorption are compiled in Table 4. Both polymeric resins (Amberlyst DT and Nafion NR40) show low BET specific surface area (0.2 m^2 g^{-1}), but Al$_2$O$_{3cord}$ sample exhibits a higher surface area (11.8 m^2 g^{-1}). SZ$_{cord}$ sample also shows a low BET of 0.8 m^2 g^{-1} (as reported by Casanovas et al. [70] the A_{BET} of the support (cordierite) is 0.1 m^2 g^{-1}). The pore width distributions shown in Fig. S15 reveal a narrow pore width of approximately 45 Å in Al$_2$O$_{3cord}$. These pores occupy a large part of the total pore volume in Al$_2$O$_{3cord}$. There are three other broader pore widths at 115, 153 and 311 Å with high pore volumes. There can be seen two similar pore width distributions in SZ$_{cord}$ at 193 and 310 Å with high pore volumes. The pore volume for both commercial polymeric resins is below 4×10^{-5} cm^3 g^{-1}. The pore width distributions of Amberlyst DT reveal a broad pore width of approximately 604 Å. Nafion NR40 shows a small pore width at 513 Å.

As reported by other researchers [59,71], a large surface area is preferable to ease accessibility of xylose (for adsorption and further dehydration purposes). The effect of a higher A_{BET}, hence a higher amount of active sites available in the reaction to dehydrate xylose, in the case of Al$_2$O$_{3cord}$ could be observed in Fig. 2 with a higher selectivity (48%) in comparison to SZ$_{cord}$ (43%). The pore widths of solid acid catalysts used in the present study are larger than optimal pore widths reported previously to provide accessibility for xylose and FUR molecules [71].

3.6. Catalyst stability

3.6.1. NH$_3$-TPD

To obtain insight into the catalytic activity tendency, Table 5 shows the total density of acid sites determined by temperature-programmed desorption profile of NH$_3$ (NH$_3$-TPD). Even though there are continuing discussions about the acidity of SZ [72,73] and Al$_2$O$_3$, clearly, the acidity of Al$_2$O$_{3cord}$ (137.2 µmol of NH$_3$ g^{-1}) was much higher than that of SZ$_{cord}$ (38.4 µmol of NH$_3$ g^{-1}). This comparison agrees with that reported by Saez et al. [38], which confirms that Al$_2$O$_{3cord}$ have higher total acid sites than SZ$_{cord}$. This is in contrast with the acid site density of SZ and Al$_2$O$_3$ reported by other researchers [2,12,74], the reported values could be due to the synthesis method employed.

After hydrothermal reaction at 210 °C in 30 min, Al$_2$O$_{3cord}$ lost more than half of its total acid sites (41.9 µmol of NH$_3$ g^{-1}), as well as SZ$_{cord}$ after hydrothermal reaction at 190 °C in 10 min (27.8 µmol of NH$_3$ g^{-1}). It is assumed that the loss of acid sites under experimental conditions is due to high pressure (> 12 bar) and hydrothermal conditions in the reactor.

Table 5

Total acid site density of calcined catalysts determined by temperature-programmed desorption (TPD) of NH$_3$ from 100 °C to 600 °C.

Catalyst	Total acid sites (µmol of NH$_3$ g^{-1})
Al$_2$O$_{3cord}$	137.2
Al$_2$O$_{3cord-210}$	41.9
SZ$_{cord}$	38.4
SZ$_{cord-190}$	27.8

Table 6

XPS data of SZ$_{cord}$ and Al$_2$O$_{3cord}$ on cordierite before and after the hydrothermal reaction at different temperatures.

Sample	Name	Binding energy (eV)	Atomic conc., %
SZ$_{cord-fresh}$	O 1s	531.9	52.9
	C 1s	279.7	29.4
	S 2p	168.5	15.1
	Zr 3d	182.4	2.7
SZ$_{cord-170}$	O 1s	531.7	23.6
	C 1s	284.2	75.8
	S 2p	169.0	0.1
	Zr 3d	182.3	0.5
SZ$_{cord-190}$	O 1s	531.8	30.4
	C 1s	284.3	67.1
	S 2p	168.3	0.7
	Zr 3d	182.3	1.8
SZ$_{cord-210}$	O 1s	531.7	36.2
	C 1s	283.8	60.6
	S 2p	168.2	0.7
	Zr 3d	182.4	2.5
SZ$_{cord-reused}$	O 1s	532.2	48.8
	C 1s	284.2	48.9
	Zr 3d	182.4	2.3
Al$_2$O$_{3cord-fresh}$	O 1s	528.3	43.8
	C 1s	281.7	23.6
	Al 2s	118.7	19.5
	Mg 2p	48.4	13.0
Al$_2$O$_{3cord-210}$	O 1s	527.6	26.2
	C 1s	283.5	59.0
	Al 2s	118.7	1.8
	Mg 2p	49.9	13.0

The ion exchange capacities of the polymeric resins were verified by back-titration following the method reported by Goertzen et al [75]. Table S6 shows that Amberlyst DT (a macroreticular, sulfonic acid polymeric catalyst) has three times more acid sites (3.1 meq g^{-1}) than Nafion NR40 in bead form (1.0 meq g^{-1}). According to the manufacturer, Nafion NR40 in bead-form has an ion exchange capacity of 1.0 meq g^{-1}. Amberlyst DT (a macroreticular, sulfonic acid polymeric catalyst) has a concentration of acid sites of ≥ 3.1 meq g^{-1}.

3.6.2. XPS

Apart from the thorough microstructural analysis of the above samples, a detailed XPS analysis was performed to get a deeper insight about the surface composition of the materials. In Table 6 the binding energy values and surface atomic composition of metal oxides before and after hydrothermal reaction are shown.

The amount of sulphur at the surface in the sample SZ$_{fresh}$ is 15%, and the amount of sulphur in the samples SZ$_{170}$, SZ$_{190}$ and SZ$_{210}$, is 0.1, 0.7 and 0.7, respectively. For the sample SZ$_{reused}$ there was no measurable sulphur traces. It is inferred from Tables 5 and 6 that there is leaching of the acid sites of both Al$_2$O$_{3cord}$ and SZ$_{cord}$. This means that the acid sites found in the fresh sample have leached out into the aqueous solution under the reaction conditions presented in this paper. It is also shown that the atomic concentration of C is lower on the surface of the fresh sample (29%) than the atomic concentration of C on the spent samples SZ$_{cord-170}$ (76%), SZ$_{cord-190}$ (67%), SZ$_{cord-210}$ (61%) and SZ$_{cord-reused}$ (49%). This means that there is carbon deposition on the surface of the catalyst after hydrothermal reaction, in accordance to the humins imaged by SEM (Fig. 7c and d).

The amount of aluminum at the surface in the sample Al$_2$O$_{3cord-fresh}$ is 19.5%, and the amount of aluminum in the sample Al$_2$O$_{3cord-210}$ is 1.8%. This shows the leaching of the acid sites found in the fresh sample have also leached out from the catalyst into the aqueous solution. The sample of Al$_2$O$_{3cord-fresh}$ contains a lower C amount (24%) than the sample Al$_2$O$_{3cord-210}$ after hydrothermal reaction (59%). This also evidences the formation of carbon deposits on the surface (Fig. 6c and d) of the catalyst after hydrothermal reaction.

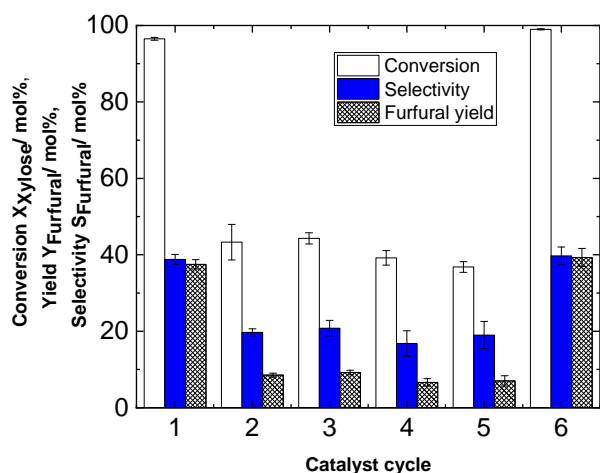Table S7 shows the binding energy and the atomic concentration

Fig. 8. Reusability of SZ$_{cord}$ for the dehydration of xylose to FUR using 50 mg of catalyst at 190 °C for 9 min (xylose conversion (white bar), FUR yield (blue bar) and selectivity to FUR (striped bar)). (For interpretation of the references to color in this figure legend, the reader is referred to the web version of this article.)

percentages of Nafion NR40 before and after hydrothermal reaction at 210 °C, and Amberlyst DT before and after hydrothermal reaction at 170 °C. Under those conditions, both catalysts suffer a sulphur loss. In addition, Amberlyst DT loses Cl and Nafion NR 40 loses F. Hence, leaching of acid sites under these conditions was seen from all solid acid catalysts tested.

Figs. S16 and S17 show the X-ray photoelectron spectra of SZ$_{cord}$ and Al$_2$O$_{3cord}$, respectively, before and after hydrothermal reactions at different temperatures. Figs. S18 and S19 show the X-ray photoelectron spectra of Amberlyst DT and Nafion NR40, respectively, before and after hydrothermal treatment. Figs. S20 and S21 show the TCD of SZ$_{cord}$ and Al$_2$O$_{3cord}$ before and after hydrothermal reaction.

In the dehydration of xylose, the degradation of acid concentration, the leaching of S and the accumulation of by-products are the main factors that cause the deactivation of the catalyst. The results shown in Tables 5 and 6 from samples SZ$_{cord}$ and Al$_2$O$_{3cord}$ before and after hydrothermal reaction correlate with the catalytic activity tests in Figs. 1 and 2 and the models shown in Figs. 3–5. Under the above-mentioned experimental conditions FUR, once it is formed, it decomposes as well as the xylose. The decomposition products evolve forming humins on the surface of the catalysts (Figs. 6 and 7), which is obviously detrimental to the reaction.

Besides, the proposed kinetic model (Scheme 3) was applied also to a purely homogeneous catalyzed dehydration reaction (employing H$_2$SO$_4$) in order to exclude the effect of leaching acidic species on the reaction mechanism of SZ$_{cord}$ (this information can be found in the Supplementary Information). The proposed kinetic model simulates heterogeneous- and homogeneous-catalyzed systems very well (Figs. S22 and S23, Tables S1 and S2). Furthermore, the acid content in the sulfuric acid-catalyzed reaction (Fig. S24) was almost one order of magnitude higher, both xylose concentration and FUR formation can be simulated with the same kinetic model (Fig. S4).

3.7. Reusability

The stability of the SZ$_{cord}$ under reaction conditions was investigated by employing this catalyst in a series of xylose dehydration reactions. Prior to each cycle, the SZ$_{cord}$ was washed with deionized water and dried at 105 °C. Fig. 8 shows five consecutive reaction runs of SZ$_{cord}$ at 190 °C in 9 min. After this, the catalyst was washed, dried at 105 °C, calcined and impregnated again with 1 M H$_2$SO$_4$ (cycle 6).

After 5 cycles, the catalytic activity of the reused catalyst decreased

from 38% to 7%, as well as the conversion of xylose (from 97% to 37%). At the same time, the activity of the catalyst can be recovered by calcination and a FUR yield of 39% is obtained again. These results are in accordance with the XPS results, since the catalytic activity of the reused catalysts decreased in each cycle without regeneration. This result indicates that the observed progressive catalyst deactivation might be related to the accumulation of insoluble organic matter, which could be blocking the surface of the catalyst, hence leading to disabled acid sites. The catalyst deactivation includes also leaching of the active sites (Table 6).

4. Conclusions

A kinetic model for the auto-catalyzed and solid acid-catalyzed decomposition of xylose using SZ$_{cord}$, Al$_2$O$_{3cord}$ on cordierite and Nafion NR40 at temperatures from 170 to 210 °C in aqueous phase was developed. Reaction rate constants for xylose and FUR decomposition were also determined in the temperature range of 170 to 210 °C. The major product of auto-catalyzed and solid acid-catalyzed xylose dehydration was FUR, the maximum mole fraction yield of which was 49% in 60 min at 210 °C. When using SZ$_{cord}$, the fastest time to reach the maximum mole fraction yield (41%) was in 2 min (at 210 °C). When adding Al$_2$O$_{3cord}$, the fastest time to reach the maximum mole fraction yield (43%) was in 30 min (at 210 °C). When adding Nafion NR40 and Amberlyst DT, the maximum mole fraction yield of FUR was 41% in 8 min at 210 °C and 30% in 60 min at 170 °C, respectively. Under the experimental conditions used, leaching of S, F, and Cl was evidenced from SZ$_{cord}$, Nafion NR40 and Amberlyst DT, respectively. Besides, the acid site density of spent samples shows lower values than those of fresh catalysts. It was also seen deposition of C on the surface of samples after hydrothermal reaction, which means that humins were formed on the solid acid catalysts, affecting the solid acid catalysts' performance.

There was no xylulose formation detected under auto-catalyzed conditions, xylulose was only formed when adding SZ$_{cord}$ and Al$_2$O$_{3cord}$. This could be due to the presence of Lewis acid sites contained in the solid acid catalysts.

Overall, hydrothermal stability should be further improved in future work, as well as their acid site density. In addition, it is crucial to avoid the decomposition of FUR once it is formed, either by a secondary process such as nitrogen-stripping or on-site extraction systems such as organic solvents included in a bi-phasic set-up.

Appendix A. Supplementary data

Supplementary data to this article can be found online at https://doi.org/10.1016/j.fuproc.2018.10.013.

References

[1] J.N. Chheda, G.W. Huber, J.A. Dumesic, Liquid-phase catalytic processing of

biomass-derived oxygenated hydrocarbons to fuels and chemicals, Angew. Chem. Int. Ed. 46 (2007) 7164–7183.

[2] R. Weingarten, J. Cho, J. Conner, W.M. Curtis, G.W. Huber, Kinetics of furfural production by dehydration of xylose in a biphasic reactor with microwave heating, Green Chem. 12 (2010) 1423–1429.

[3] J. Carlos Serrano-Ruiz, J.A. Dumesic, Catalytic upgrading of lactic acid to fuels and chemicals by dehydration/hydrogenation and C-C coupling reactions, Green Chem. 11 (2009) 1101–1104.

[4] K.J. Zeitsch, 14. Applications of furfural, in: K.J. Zeitsch (Ed.), The Chemistry and Technology of Furfural and its Many By-products, Elsevier B.V., 2000, pp. 98–103.

[5] L. Yang, J. Su, S. Carl, J.G. Lynam, X. Yang, H. Lin, Catalytic conversion of hemi-cellulosic biomass to lactic acid in pH neutral aqueous phase media, Appl. Catal. B Environ. 162 (2015) 149–157.

[6] A.S. Mamman, J. Lee, Y. Kim, I.T. Hwang, N. Park, Y.K. Hwang, et al., Furfural: hemicellulose/xylosederived biochemical, Biofuels Bioprod. Biorefin. 2 (2008) 438–454.

[7] C. Moreau, R. Durand, D. Peyron, J. Duhamet, P. Rivalier, Selective preparation of furfural from xylose over microporous solid acid catalysts, Ind. Crop. Prod. 7 (1998) 95–99.

[8] R. O'Neill, M.N. Ahmad, L. Vanoye, F. Aiouache, Kinetics of aqueous phase dehy-dration of xylose into furfural catalyzed by ZSM-5 zeolite, Ind. Eng. Chem. Res. 48 (2009) 4300–4306.

[9] R. Sahu, P.L. Dhepe, A one-pot method for the selective conversion of hemicellulose from crop waste into C5 sugars and furfural by using solid acid catalysts, ChemSusChem 5 (2012) 751–761.

[10] S. Lima, A. Fernandes, M.M. Antunes, M. Pillinger, F. Ribeiro, A.A. Valente, Dehydration of xylose into furfural in the presence of crystalline microporous sili-coaluminophosphates, Catal. Lett. 135 (2010) 41–47.

[11] S. Lima, M.M. Antunes, A. Fernandes, M. Pillinger, M.F. Ribeiro, A.A. Valente, Catalytic cyclodehydration of xylose to furfural in the presence of zeolite H-Beta and a micro/mesoporous Beta/TUD-1 composite material, Appl. Catal. A Gen. 388 (2010) 141–148.

[12] R. Weingarten, G.A. Tompsett, W.C. Conner Jr., G.W. Huber, Design of solid acid catalysts for aqueous-phase dehydration of carbohydrates: the role of Lewis and Brønsted acid sites, J. Catal. 279 (2011) 174–182.

[13] L.R. Ferreira, S. Lima, P. Neves, M.M. Antunes, S.M. Rocha, M. Pillinger, et al., Aqueous phase reactions of pentoses in the presence of nanocrystalline zeolite beta: identification of by-products and kinetic modelling, Chem. Eng. J. 215–216 (2013) 772–783.

[14] E.I. Gürbüz, J.M.R. Gallo, D.M. Alonso, S.G. Wettstein, W.Y. Lim, J.A. Dumesic, Conversion of hemicellulose into furfural using solid acid catalysts in γ-valer-olactone, Angew. Chem. Int. Ed. 52 (2013) 1270–1274.

[15] A. Yepez, A. Garcia, M.S. Climent, A.A. Romero, R. Luque, Catalytic conversion of starch into valuable furan derivatives using supported metal nanoparticles on me-soporous aluminosilicate materials, Catal. Sci. Technol. 4 (2014) 428–434.

[16] M.J.C. Molina, M.L. Granados, A. Gervasini, P. Carniti, Exploitment of niobium oxide effective acidity for xylose dehydration to furfural, Catal. Today 254 (2015) 90–98.

[17] G.H. Jeong, E.G. Kim, S.B. Kim, E.D. Park, S.W. Kim, Fabrication of sulfonic acid modified mesoporous silica shells and their catalytic performance with dehydration reaction of D-xylose into furfural, Microporous Mesoporous Mater. 144 (2011) 134–139.

[18] S. Kaiprommarat, S. Kongparakul, P. Reubroycharoen, G. Guan, C. Samart, Highly efficient sulfonic MCM-41 catalyst for furfural production: furan-based biofuel agent, Fuel 174 (2016) 189–196.

[19] I. Agirrezabal-Telleria, J. Requies, M.B. Güemez, P.L. Arias, Pore size tuning of functionalized SBA-15 catalysts for the selective production of furfural from xylose, Appl. Catal. B Environ. 115–116 (2012) 169–178.

[20] I. Agirrezabal-Telleria, C. García-Sancho, P. Maireles-Torres, P.L. Arias, Dehydration of xylose to furfural using a Lewis or Brönsted acid catalyst and N2 stripping, Chin. J. Catal. 34 (2013) 1402–1406.

[21] I. Agirrezabal-Telleria, J. Requies, M.B. Güemez, P.L. Arias, Dehydration of D-xylose to furfural using selective and hydrothermally stable arenesulfonic SBA-15 cata-lysts, Appl. Catal. B Environ. 145 (2014) 34–42.

[22] P. Bhaumik, T. Kane, P.L. Dhepe, Silica and zirconia supported tungsten, mo-lybdenum and gallium oxide catalysts for the synthesis of furfural, Catal. Sci. Technol. 4 (2014) 2904–2907.

[23] A.S. Dias, M. Pillinger, A.A. Valente, Dehydration of xylose into furfural over micro-mesoporous sulfonic acid catalysts, J. Catal. 229 (2005) 414–423.

[24] H. Li, A. Deng, J. Ren, C. Liu, W. Wang, F. Peng, et al., A modified biphasic system for the dehydration of D-xylose into furfural using SO₄²⁻/TiO₂-ZrO₂/La³⁺ as a solid catalyst, Catal. Today 234 (2014) 251–256.

[25] S. Lima, M. Pillinger, A.A. Valente, Dehydration of D-xylose into furfural catalysed by solid acids derived from the layered zeolite Nu-6(1), Catal. Commun. 9 (2008) 2144–2148.

[26] E. Lam, J.H. Chong, E. Majid, Y. Liu, S. Hrapovic, A.C.W. Leung, et al., Carbocatalytic dehydration of xylose to furfural in water, Carbon 50 (2012) 1033–1043.

[27] A.S. Dias, M. Pillinger, A.A. Valente, Liquid phase dehydration of D-xylose in the presence of Keggin-type heteropolyacids, Appl. Catal. A Gen. 285 (2005) 126–131.

[28] A.S. Dias, M. Pillinger, A.A. Valente, Mesoporous silica-supported 12-tungstopho-sphoric acid catalysts for the liquid phase dehydration of D-xylose, Microporous Mesoporous Mater. 94 (2006) 214–225.

[29] A.S. Dias, S. Lima, M. Pillinger, A.A. Valente, Modified versions of sulfated zirconia as catalysts for the conversion of xylose to furfural, Catal. Lett. 114 (2007) 151–160.

[30] E. Sairanen, K. Vilonen, R. Karinen, J. Lehtonen, Functionalized activated carbon

[31] E. Lam, E. Majid, A.C.W. Leung, J.H. Chong, K.A. Mahmoud, J.H.T. Luong, Synthesis of furfural from xylose by heterogeneous and reusable nafion catalysts, ChemSusChem 4 (2011) 535–541.

[32] I. Agirrezabal-Telleria, A. Larreategui, J. Requies, M.B. Güemez, P.L. Arias, Furfural production from xylose using sulfonic ion-exchange resins (Amberlyst) and si-multaneous stripping with nitrogen, Bioresour. Technol. 102 (2011) 7478–7485.

[33] A.S. Dias, S. Lima, M. Pillinger, A.A. Valente, Acidic cesium salts of 12-tung-stophosphoric acid as catalysts for the dehydration of xylose into furfural, Carbohydr. Res. 341 (2006) 2946–2953.

[34] J. Zhang, J. Li, L. Lin, Dehydration of sugar mixture to HMF and furfural over SO₄²⁻/ZrO₂-TiO₂ catalyst, Bioresources 9 (2014) 4194.

[35] S. Verma, R.B.N. Baig, M.N. Nadagouda, C. Len, R.S. Varma, Sustainable pathway to furanics from biomass via heterogeneous organo-catalysis, Green Chem. 19 (2017) 164–168.

[36] V. Choudhary, S.I. Sandler, D.G. Vlachos, Conversion of xylose to furfural using Lewis and Brönsted acid catalysts in aqueous media, ACS Catal. 2 (2012) 2022–2028.

[37] O. Ershova, J. Kanervo, S. Hellsten, H. Sixta, The role of xylulose as an intermediate in xylose conversion to furfural: insights via experiments and kinetic modelling, RSC Adv. 5 (2015) 66727–66737.

[38] B. Saez, A. Santana, E. Ramírez, J. Maçaira, C. Ledesma, J. Llorca, et al., Vegetable oil transesterification in supercritical conditions using co-solvent carbon dioxide over solid catalysts: a screening study, Energy Fuel 28 (2014) 6006–6011.

[39] N. Katada, J. Endo, K. Notsu, N. Yasunobu, N. Naito, M. Niwa, Superacidity and catalytic activity of sulfated zirconia, J. Phys. Chem. B 104 (2000) 10321–10328.

[40] C. Ledesma, J. Llorca, Hydrogen production by steam reforming of dimethyl ether over Cu–Zn/CeO₂-ZrO₂ catalytic monoliths, Chem. Eng. J. 154 (2009) 281–286.

[41] O. Ershova, K. Nieminen, H. Sixta, The role of various chlorides on xylose con-version to furfural: experiments and kinetic modeling, ChemCatChem 9 (2017) 3031–3040.

[42] M.A. Mellmer, C. Sener, J.M.R. Gallo, J.S. Luterbacher, D.M. Alonso, J.A. Dumesic, Solvent effects in acid-catalyzed biomass conversion reactions, Angew. Chem. Int. Ed. 53 (2014) 11872–11875.

[43] B. Danon, G. Marcotullio, W. de Jong, Mechanistic and kinetic aspects of pentose dehydration towards furfural in aqueous media employing homogeneous catalysis, Green Chem. 16 (2014) 39–54.

[44] K. Lamminpää, J. Ahola, J. Tanskanen, Acid-catalysed xylose dehydration into furfural in the presence of kraft lignin, Bioresour. Technol. 177 (2015) 94–101.

[45] N. Akiya, P.E. Savage, Roles of water for chemical reactions in high-temperature water, Chem. Rev. 102 (2002) 2725–2750.

[46] Z. Chen, W. Zhang, J. Xu, P. Li, Kinetics of xylose dehydration into furfural in acetic acid, Chin. J. Chem. Eng. 23 (2015) 659–666.

[47] B. Danon, W. Hongsiri, L. van der Aa, W. de Jong, Kinetic study on homogeneously catalyzed xylose dehydration to furfural in the presence of arabinose and glucose, Biomass Bioenergy 66 (2014) 364–370.

[48] I. van Zandvoort, Y. Wang, C.B. Rasrendra, E.R.H. van Eck, P.C.A. Bruijnincx, H.J. Heeres, et al., Formation, molecular structure, and morphology of humins in biomass conversion: influence of feedstock and processing conditions, ChemSusChem 6 (2013) 1745–1758.

[49] C. Sievers, I. Musin, T. Marzialetti, M. Valenzuela-Olarte, P. Agrawal, C. Jones, Acid-catalyzed conversion of sugars and furfurals in an ionic-liquid phase, ChemSusChem 2 (2009) 665–671.

[50] K.J. Zeitsch, o. Furfural as a solvent, Sugar Ser. 13 (2000) 317–318.

[51] Y. Yang, C. Hu, M.M. Abu-Omar, Synthesis of furfural from xylose, xylan, and biomass using AlCl₃·6H₂O in biphasic media via xylose isomerization to xylulose, ChemSusChem 5 (2012) 405–410.

[52] J.B. Binder, J.J. Blank, A.V. Cefali, R.T. Raines, Synthesis of furfural from xylose and xylan, ChemSusChem 3 (2010) 1268–1272.

[53] J. Iglesias, J.A. Melero, G. Morales, M. Paniagua, B. Hernández, Dehydration of xylose to furfural in alcohol media in the presence of solid acid catalysts, ChemCatChem 8 (2016) 2089–2099.

[54] M. Paniagua, S. Saravanamurugan, M. Melian-Rodriguez, J.A. Melero, A. Riisager, Xylose isomerization with zeolites in a two-step alcohol–water process, ChemSusChem 8 (2015) 1088–1094.

[55] M.G. Mazzotta, D. Gupta, B. Saha, A.K. Patra, A. Bhaumik, M.M. Abu-Omar, Efficient solid acid catalyst containing Lewis and Brønsted acid sites for the pro-duction of furfurals, ChemSusChem 7 (2014) 2342–2350.

[56] G.D. Yadav, J.J. Nair, Sulfated zirconia and its modified versions as promising catalysts for industrial processes, Microporous Mesoporous Mater. 33 (1999) 1–48.

[57] B.T. Loveless, A. Gyanani, D.S. Muggli, Discrepancy between TPD- and FTIR-based measurements of Brönsted and Lewis acidity for sulfated zirconia, Appl. Catal. B Environ. 84 (2008) 591–597.

[58] G.G. Volkova, S.I. Reshetnikov, L.N. Shkuratova, A.A. Budneva, E.A. Paukshtis, n-Hexane skeletal isomerization over sulfated zirconia catalysts with different Lewis acidity, Chem. Eng. J. 134 (2007) 106–110.

[59] L. Filiciotto, A.M. Balu, J.C. Van der Waal, R. Luque, Catalytic insights into the production of biomass-derived side products methyl levulinate, furfural and hu-mins, Catal. Today. 302 (2018) 2–15.

[60] V. Choudhary, A.B. Pinar, S.I. Sandler, D.G. Vlachos, R.F. Lobo, Xylose isomeriza-tion to xylulose and its dehydration to furfural in aqueous media, ACS Catal. 1 (2011) 1724–1728.

[61] S.J. You, Y.T. Kim, E.D. Park, Liquid-phase dehydration of D-xylose over silica-alumina catalysts with different alumina contents, React. Kinet. Mech. Catal. 111 (2014) 521–534.

[62] S. Lima, M.M. Antunes, A. Fernandes, M. Pillinger, M.F. Ribeiro, A.A. Valente,

Catalytic cyclodehydration of xylose to furfural in the presence of zeolite H-Beta and a micro/mesoporous Beta/TUD-1 composite material, Appl. Catal. A Gen. 388 (2010) 141–148.

[63] S.B. Kim, M.R. Lee, E.D. Park, S.M. Lee, H. Lee, K.H. Park, et al., Kinetic study of the dehydration of D-xylose in high temperature water, React. Kinet. Mech. Catal. 103 (2011) 267–277.

[64] P.J. Oefner, A.H. Lanziner, G. Bonn, O. Bobleter, Quantitative studies on furfural and organic acid formation during hydrothermal, acidic and alkaline degradation of D-xylose, Monatsh. Chem. 123 (1992) 547–556.

[65] Q. Jing, X. Lü, Kinetics of non-catalyzed decomposition of D-xylose in high temperature liquid water, Chin. J. Chem. Eng. 15 (2007) 666–669.

[66] K. Lamminpää, J. Ahola, J. Tanskanen, Kinetics of xylose dehydration into furfural in formic acid, Ind. Eng. Chem. Res. 51 (2012) 6297–6303.

[67] T.M. Aida, N. Shiraishi, M. Kubo, M. Watanabe, R.L. Smith Jr., Reaction kinetics of D-xylose in sub- and supercritical water, J. Supercrit. Fluids 55 (2010) 208–216.

[68] M. Al-Hazmi, A.W. Apblett, Benzylation of benzene over sulfated zirconia supported in MCM-41 using a single source precursor, Catal. Sci. Technol. 1 (2011) 621–630.

[69] T. Eifert, M.A. Liauw, Process analytical technology (PAT) applied to biomass valorisation: a kinetic study on the multiphase dehydration of xylose to furfural, React. Chem. Eng. 1 (2016) 521–532.

[70] A. Casanovas, C. de Leitenburg, A. Trovarelli, J. Llorca, Catalytic monoliths for ethanol steam reforming, Catal. Today 138 (2008) 187–192.

[71] R. Karinen, K. Vilonen, M. Niemelä, Biorefining: heterogeneously catalyzed reactions of carbohydrates for the production of furfural and hydroxymethylfurfural, ChemSusChem 4 (2011) 1002–1016.

[72] Y. Wang, K. Lee, S. Choi, J. Liu, L. Wang, C.H.F. Peden, Grafting sulfated zirconia on mesoporous silica, Green Chem. 9 (2007) 540–544.

[73] H. Yang, R. Lu, J. Zhao, X. Yang, L. Shen, Z. Wang, Sulfated binary oxide solid superacids, Mater. Chem. Phys. 80 (2003) 68–72.

[74] M. Haneda, K. Takamura, Y. Doi, N. Bion, L. Vivier, Synthesis of ordered porous zirconia containing sulfate ions and evaluation of its surface acidic properties, J. Mater. Sci. 52 (2017) 5835–5845.

[75] S.L. Goertzen, K.D. Thériault, A.M. Oickle, A.C. Tarasuk, H.A. Andreas, Standardization of the Boehm titration. Part I. CO_2 expulsion and endpoint determination, Carbon 48 (2010) 1252–1261.

Supplementary Information

Gerardo Gómez Millán[a,b,*], Zouhair El Assal[c], Kaarlo Nieminen[a], Sanna Hellsten[a], Jordi Llorca[b], Herbert Sixta[a,*]

[a]Department of Bioproducts and Biosystems, Aalto University, Vuorimiehentie 1, 02150 Espoo, Finland
[b]Department of Chemical Engineering, Institute of Energy Technologies and Barcelona Research Center in Multiscale Science and Engineering, Universitat Politècnica de Catalunya, Eduard Maristany 10-14, 08019 Barcelona, Spain
[c]Department of Environmental and Chemical Engineering, Faculty of Technology, University of Oulu, P.O. Box 4300, 90014 Oulu, Finland

*Corresponding author at: Department of Bioproducts and Biosystems, Aalto University, Vuorimiehentie 1, 02150 Espoo, Finland.
Gerardo Gómez Millán: gerardo.gomezmillan@aalto.fi, Herbert Sixta: herbert.sixta@aalto.fi

1. Determination of FUR and by-products

The liquid samples were analysed by High Performance Liquid Chromatography (HPLC) operating a Dionex UltiMate 3000 HPLC (Dionex, Sunnyvale, CA, USA) device equipped with refractive index (RI) and ultraviolet (UV) diode array detectors. Product separation was achieved on a HyperRez XP Carbohydrate Ca^{2+} column (Thermo Scientific, Waltham, MA, USA). Aqueous sulfuric acid (0.0025 mol l^{-1}) was used as an eluent with a flow rate of 0.8 ml min^{-1}. The column temperature and the RI-detector temperature were set to 70 °C and 55 °C, respectively. The FUR concentration was determined by the UV-detector at a wavelength of 280 nm. The xylose concentration was analysed simultaneously by the RI-detector and the UV-detector at 210 nm for a crosscheck[1]. For calibration of the HPLC, a series of calibration standards was prepared from the following chemicals: xylose (99%, Sigma Aldrich), 5-hydroxymethylfurfural (HMF) (99%, Sigma Aldrich), FUR (99%, Sigma Aldrich), formic acid (98%, VWR), acetic acid (99%, Sigma Aldrich), levulinic acid (99%, Sigma Aldrich). From a parent standard solution (0.1 g diluted in 100 ml of Milli-Q water) calibration standards in four concentrations (0.1 ml, 0.5 ml, 1 ml and 1.5 ml 10 ml of Milli-Q) were prepared. The HPLC system was calibrated within the concentration ranges of 10 to 150 mg l^{-1}.

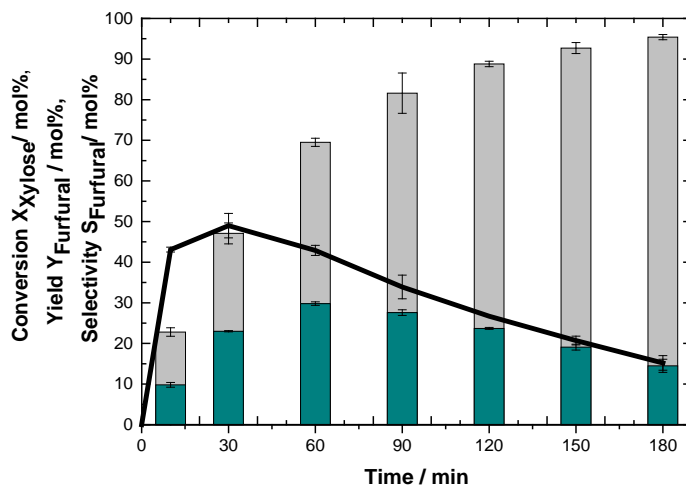## 2. Catalytic conversion of xylose into FUR using polymeric resins

Figure S1. Xylose conversion (grey bar), FUR yield (green bar) and selectivity to FUR (black line) at various reaction times during conversion of xylose using Amberlyst DT at 170 °C.
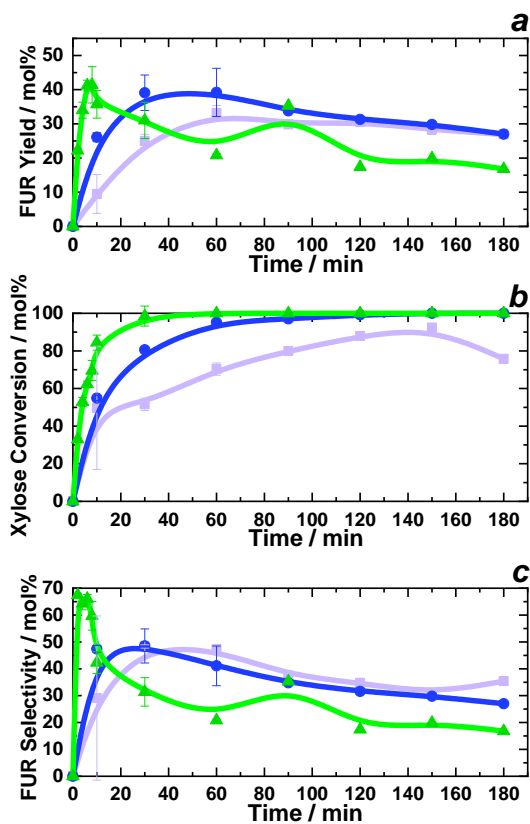

Figure S2. FUR yield (a), xylose conversion (b) and selectivity to FUR (c) at various reaction times during conversion of xylose using Nafion NR40 (purple square – 170 °C, blue circle – 190 °C, green triangle – 210 °C, lines are to guide the eye).

3. Xylulose formation

Under auto-catalyzed conditions at temperature reactions of 170 to 210 °C, xylulose formation was not detectable. This is in accordance with the low amount of xylulose (< 3 mol%) reported by Ershova et al[11] employing a 196 mmol l⁻¹ xylose solution at reactions temperatures of 180, 200 and 220 °C.

However, when adding alumina and SZ_cord the presence of xylulose was observed (Figure S3a and S3b, respectively).
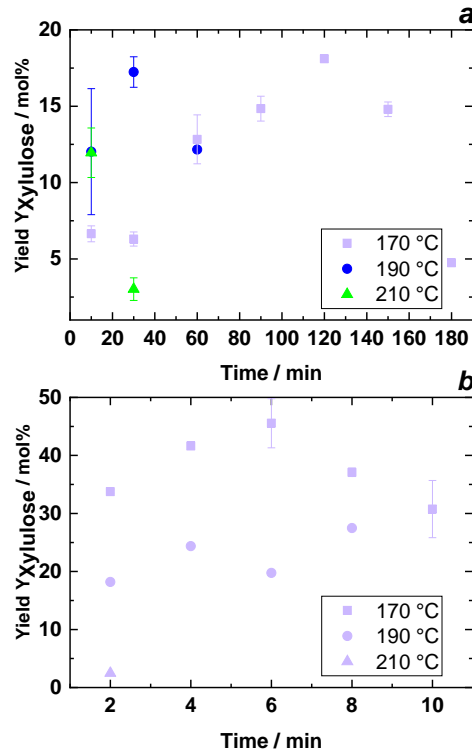

Figure S3. Xylulose yield when adding 50 mg of alumina (a), xylulose yield when adding 50 mg of SZ_cord (b) at various reaction times during conversion of xylose (purple square – 170 °C, blue circle – 190 °C, green triangle – 210 °C, lines are to guide the eye).

4. Modelling

In this study conversion is defined in terms of moles of reactant converted per unit volume of reactor. Selectivity, at an instant, is the generated amount of a desired product relative to the generation of some undesired product on a molar basis. Yield is the amount in moles of desired product (FUR) produced related to the amount of the key reactant (xylose)[2]. The following equations have been used for the mathematical evaluation of the obtained results:

$$X_{xyl} = \frac{c_{xyl}^{in} - c_{xyl}^{f}}{c_{xyl}^{in}} \times 100 \ [\%] \qquad (1),$$

$$S_{xyl}^{fur} = \frac{c_{fur}}{c_{xyl}^{in} - c_{xyl}^{f}} \times 100 \ [\%] \qquad (2),$$

$$Y_{fur} = \frac{c_{fur}}{c_{xyl}} \times 100 \ [\%] \hspace{4cm} (3),$$

where X, S, Y are the– conversion of xylose, selectivity to FUR and FUR yield, respectively; c is the– concentration in mmol l^{-1} (the subscripts to be read as follows: *xyl, fur, in, f* are the– xylose, FUR, initial, final).

The Arrhenius equation has been used to describe the dependence of rate constants on the absolute temperature:

$$k_i = A_i \cdot \exp\left(-\frac{E_{a,i}}{RT}\right) \ [min^{-1}] \hspace{3cm} (4),$$

For the optimization purposes of this study, the following equivalent form is numerically more convenient:

$$k_i = A_{ref,i} \cdot exp\left(-\frac{E_{a,i}}{R} \cdot \left(\frac{1}{T} - \frac{1}{T_{ref}}\right)\right) \ [min^{-1}] \hspace{1.5cm} (5),$$

where T_{ref} and T [K] are the– reference temperature (200 °C) and experimental temperature respectively, $E_{a,i}$ [kJ mol^{-1}] is the– activation energy, $A_{ref,i}$ [min^{-1}] is the– temperature-mean-centered Arrhenius pre-exponential constant. The relation between A_{ref} and A is:

$$A_{ref} = A \cdot exp\left(-\frac{E_a}{RT_{ref}}\right) \hspace{3cm} (6),$$

The analysis was performed using the Wolfram Mathematica software, version 11. The frequency factor and the activation energy for the different reactions were estimated. The rate constants were calculated from the obtained Arrhenius parameters. Since the presence of the second order reaction prevented the analytic solution of the differential equations to define the model, the model was calculated numerically with Mathematica's ParametricNDSolveValue function. The fit was performed using the NonLinearModelFit function.

4.1 Kinetic model fitted to scheme 1 from experimental results

Figure S4. Experimental (circle) and modeled according to scheme 1 (solid lines) concentrations of xylose, FUR and intermediate at different temperatures in auto-catalyzed conditions. (green-xylose, red-FUR, dark blue-DP2 intermediate, light blue-DP3 intermediate, cyan-DP4 intermediate).

Figure S5. Experimental (circle) and modeled according to scheme 1 (solid lines) concentrations of xylose, FUR and intermediate at different temperatures in solid-acid conditions (SZ_{cord}). (green-xylose, red-FUR, dark blue-DP2 intermediate, light blue-DP3 intermediate, cyan-DP4 intermediate).
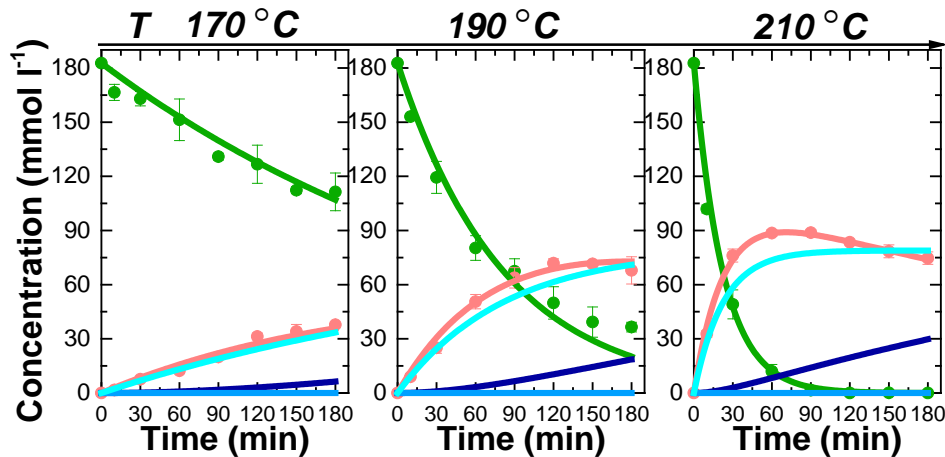

Figure S6. Experimental (circle) and modeled according to scheme 1 (solid lines) concentrations of xylose, FUR and intermediate at different temperatures in solid-acid conditions (Al_2O_{3cord}).

(green-xylose, red-FUR, dark blue-DP2 intermediate, light blue-DP3 intermediate, cyan-DP4 intermediate).

Figure S7. Experimental (circle) and modeled according to scheme 1 (solid lines) concentrations of xylose, FUR and intermediate at different temperatures in solid-acid conditions (Amberlyst DT) at 170 °C. (green-xylose, red-FUR, dark blue-DP2 intermediate, light b blue-DP3 intermediate, cyan-DP4 intermediate)
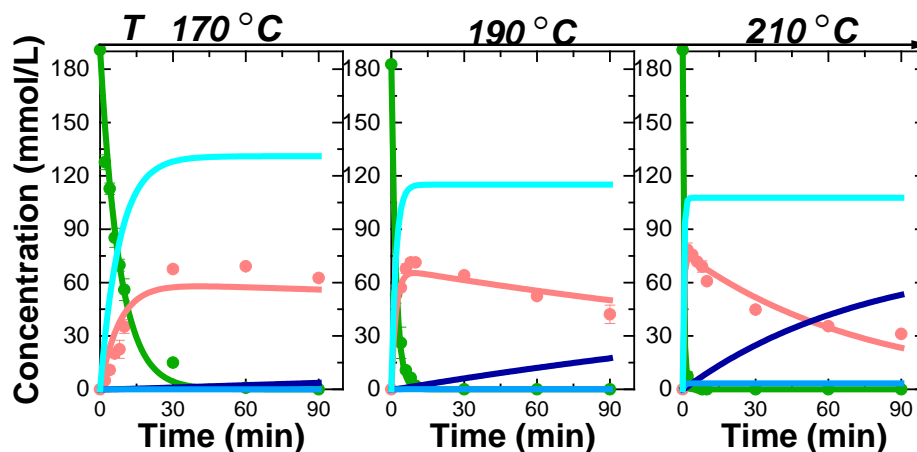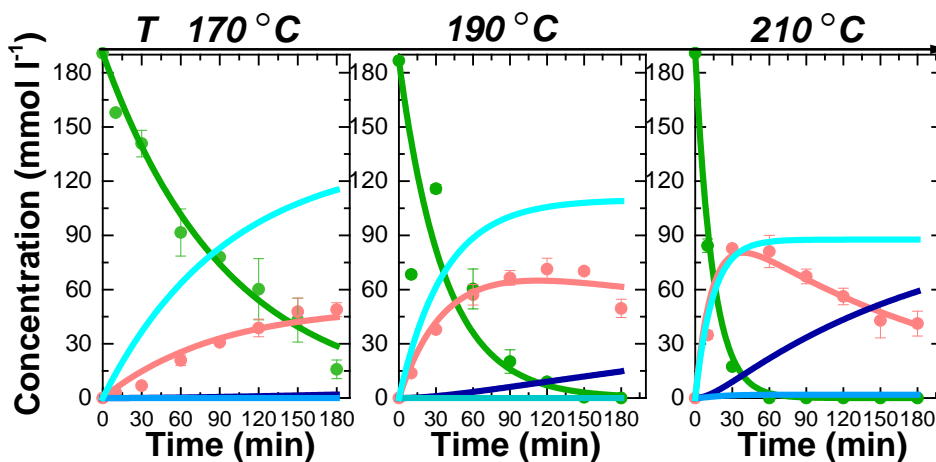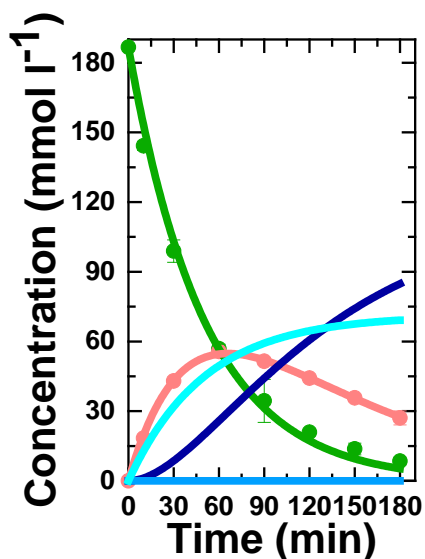

Figure S8. Experimental (circle) and modeled according to scheme 1 (solid lines) concentrations of xylose, FUR and intermediate at different temperatures in solid-acid conditions (Nafion NR40). (green-xylose, red-FUR, dark blue-DP2 intermediate, light blue-DP3 intermediate, cyan-DP4 intermediate)

SCHEME 2

Figure S9. Experimental (circle) and modelled (solid lines) according to scheme 2 concentrations of xylose, FUR and intermediate at different temperatures in auto-catalyzed conditions. (Green-xylose, red-FUR, blue-intermediate)

Figure S10. Experimental (circle) and modeled (solid lines) concentrations of xylose, FUR and intermediate at different temperatures in solid acid-catalyzed conditions (SZ$_{cord}$) according to scheme 2. (Green-xylose, red-FUR, blue-intermediate)
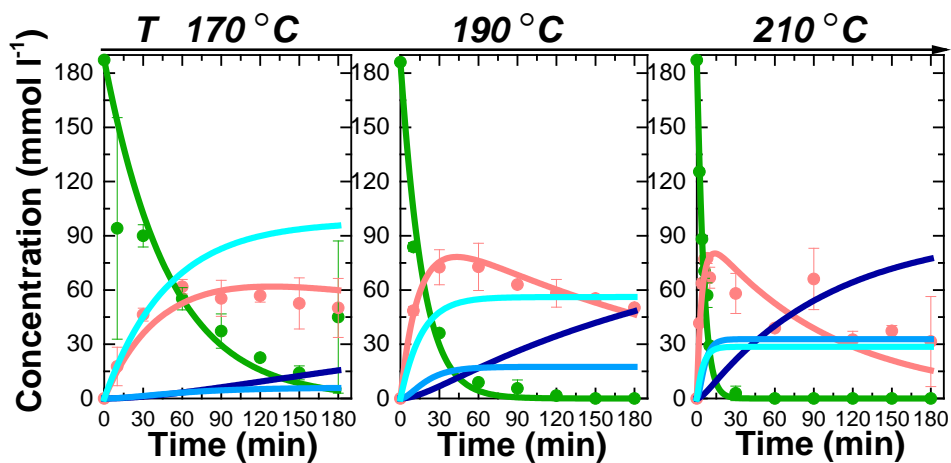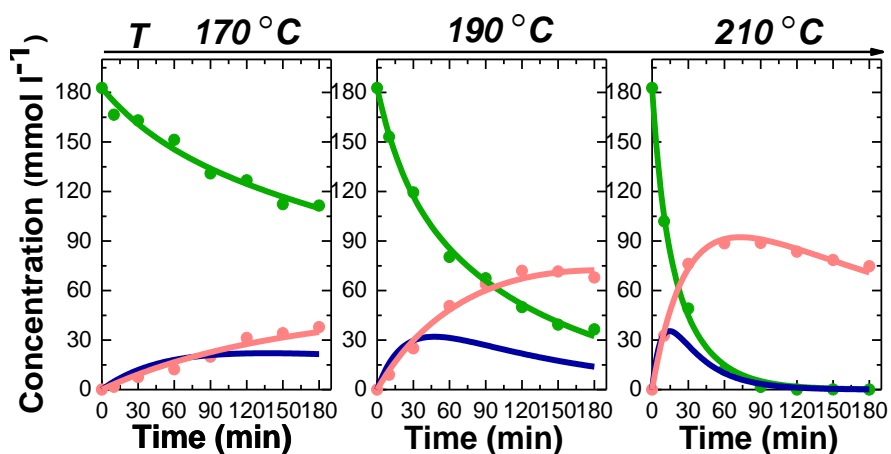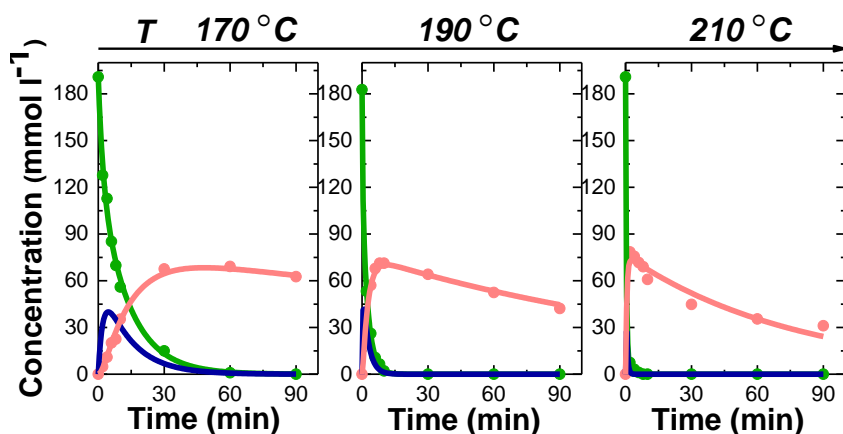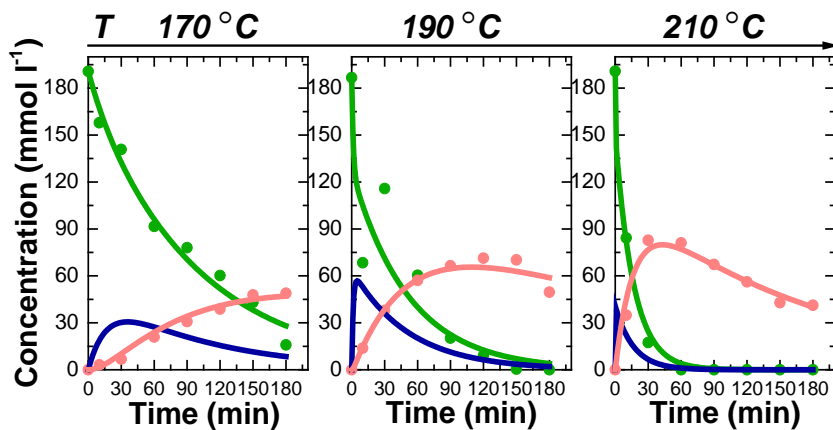
Figure S11. Experimental (circle) and modeled (solid lines) concentrations of xylose, FUR and intermediate at different temperatures in solid acid-catalyzed conditions (Al_2O_{3cord}) according to scheme 2. (Green-xylose, red-FUR, blue-intermediate).

4.2 Frequency factors and activation energies of SZ_{cord}, Al_2O_{3cord} and auto-catalyzed system for schemes 1 and 2

Table S1. Frequency factors ($A_{ref,i}$ min^{-1}) and activation energies (E_{ai}, kJ mol^{-1}) for the kinetic models proposed (scheme 1 and 2); in the auto-catalyzed system and when using SZ_{cord} and Al_2O_{3cord}.

Scheme Number		$A_{ref,i}$(auto-catalyzed)	E_{ai}(auto-catalyzed)	$A_{ref,i}$(SZ_{cord})	E_{ai}(SZ_{cord})	$A_{ref,i}$(Al_2O_{3cord})	E_{ai}(Al_2O_{3cord})	E_{ai}, Literature data
Scheme 1	(1)	$3.53 \times 10^{+11}$	121.5	$6.65 \times 10^{+14}$	138	$4.76 \times 10^{+10}$	112	68.5[6], 76.6[7], 108.6[8], 110-127[9], 111.5[10], 13.2[11], 119.4[12], 117.9-129.9[13], 133.3[14]
	(2)	0.0298	10.6	$6.86 \times 10^{+11}$	127	$5.5 \times 10^{+10}$	120.3	24.2[7], 53.5[11], 58.8[10], 63.4[8], 75.5[15], 57.9-77.2[13], 102.1[14]
	(3)	0	0	$1.06 \times 10^{+51}$	500	$1.66 \times 10^{+49}$	500	56.2-88.8[13], 105[8]
	(4)	$1.65 \times 10^{+11}$	119.6	$4.14 \times 10^{+12}$	116	$3.75 \times 10^{+5}$	65.3	58.8[7], 101-119[16], 119.8[11], 125.8[14], 143.1[10]
Scheme 2	(1)	$1 \times 10^{+11}$	114.8	$1.64 \times 10^{+19}$	170	$1.72 \times 10^{+27}$	247	150.0-157.7[15]
	(2)	$5.14 \times 10^{+20}$	208.6	$1.11 \times 10^{+15}$	136	6600	48	118-191[15], 183.6[17]
	(3)	$3.51 \times 10^{+10}$	112.6	$7.4 \times 10^{+45}$	440	$1.65 \times 10^{+46}$	440	--
	(4)	0.007	2.783	$6 \times 10^{+5}$	71	580	46	75.5[15]
	(5)	$3.11 \times 10^{+14}$	147.1	$4.6 \times 10^{+48}$	460	0.028	3.7×10^{-4}	--
	(6)	0	0	$4 \times 10^{+15}$	143	$4.7 \times 10^{+49}$	470	367.2[17]
	(7)	2980	45.1	$2.59 \times 10^{+19}$	170	$7.6 \times 10^{+34}$	312	99.7[17]

4.3 Statistical analysis of the kinetic model

Monte Carlo method was used for calculating the confidence intervals.

Table S2. Confidence intervals for the kinetic parameters of Scheme 3.

	$A_{ref,i}$(auto-catalyzed)		E_{ai}(auto-catalyzed)		$A_{ref,i}$(SZ$_{cord}$)		E_{ai}(SZ$_{cord}$)		$A_{ref,i}$(Al$_2$O$_{3cord}$)		E_{ai}(Al$_2$O$_{3cord}$)	
	Low	High	Low	High	Low	High	Low	High	Low	High	Low	High
(1)	$2.9\times10^{+10}$	$1.6\times10^{+12}$	111	127								
(2)	$1.6\times10^{+8}$	$6.4\times10^{+12}$	94	134								
(3)	1000	6600	49	57								
(4)					$1.3\times10^{+12}$	$5\times10^{+4}$	110	132	1.6	$4\times10^{+9}$	20	99
(5)					$2.6\times10^{+15}$	$1.3\times10^{+21}$	140	190	71000	$1.6\times10^{+11}$	60	110
(6)					$2.5\times10^{+15}$	$1.4\times10^{+22}$	140	200	37000	$2.4\times10^{+26}$	60	250
(7)					200	$2.4\times10^{+13}$	42	140	0.023	0.069	x	x

4.4 Model Fitting for Nafion NR40

Since there was no xylulose present when Nafion NR40 was added to the system, the parallel FUR formation from Scheme 3 was modified as follows (Scheme S1).
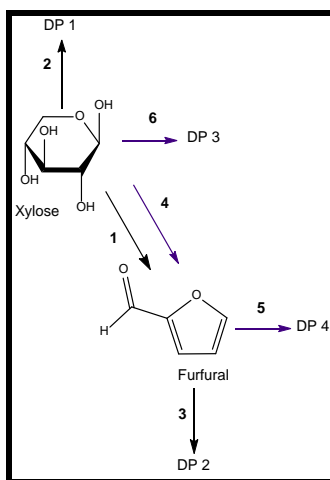
Scheme S1. Parallel FUR Formation with Side Reaction Decomposition

Table S3. Kinetic rate constants k_i (min^{-1}) at each experimental temperature for Nafion-catalyzed systems following Scheme S1.

T, (°C)	Solid acid	k_4	k_5	k_6
170	Nafion NR40	0.008	0.000	0.013
190	Nafion NR40	0.024	0.001	0.033
210	Nafion NR40	0.068	0.041	0.035

Table S4. Ratio of selected kinetic rate constants at each experimental temperature for Nafion-catalyzed systems following Scheme S1.

T, (°C)	Solid acid	k_2/k_6	k_4/k_6	k_5/k_6	k_1/k_4	k_3/k_5
170	Nafion NR40	0.154	0.615	0	0.25	-
190	Nafion NR40	0.152	0.727	0.030	0.292	2
210	Nafion NR40	0.4	1.943	1.171	0.411	0.098

4.5 Frequency factors and activation energies of Nafion NR40

Table S5. Frequency factors ($A_{ref,i}$ min^{-1}) and activation energies (E_{ai}, kJ mol^{-1}) for the kinetic models proposed (scheme 1, 2 and S1); when using Nafion NR40.

i		$A_{ref,i}$(Nafion NR40)	E_{ai}(Nafion NR40)
Scheme 1	(1)	$9.43 \times 10^{+11}$	119
	(2)	$4.24 \times 10^{+6}$	80
	(3)	$3.03 \times 10^{+4}$	163
	(4)	$2.67 \times 10^{+3}$	46
Scheme 2	(1)	$3.85 \times 10^{+50}$	472
	(2)	$2.90 \times 10^{+42}$	393
	(3)	$1.49 \times 10^{+11}$	112
	(4)	$2.35 \times 10^{+9}$	104
	(5)	$9.54 \times 10^{+24}$	228
	(6)	$2.70 \times 10^{+7}$	79
	(7)	$4.86 \times 10^{+7}$	53
Scheme 3	(4)	$2.0 \times 10^{+9}$	97
	(5)	$1.6 \times 10^{+7}$	89
	(6)	$2.4 \times 10^{+7}$	79

5. Catalyst characterization

5.1 SEM images taken of Nafion NR40, Amberlyst DT and SZ$_{cord}$

Scanning electron microscopy (SEM) images were recorded at 2 kV (for Amberlyst DT and Nafion NR40) and at 5 kV (for Al$_2$O$_{3cord}$ and SZ$_{cord}$ on cordierite) using a Zeiss Neon40Crossbeam Station instrument equipped with a field emission source[3]. Samples were deposited on conductive carbon tabs.

Fig. S12(a,c) show a low-magnification view of Nafion NR40 before and after (at 210 °C in 8 min) the hydrothermal reaction has taken place, respectively. Fig. S12(b,d) correspond to SEM images recorded at a higher magnification. The sample shows how this nafion perfluorosulfonic acid (PFSA) super acid resin changes its elipse-like structure post-reaction, even though the manufacturer reports a stability in aqueous systems at higher temperatures (220 ° to 240 °C) than those used in this case (<210 °C).

Fig. S13(a,d) show a general view of Amberlyst DT before and after (170 °C in 60 min) the hydrothermal reaction has taken place, respectively. Fig. S13(a) shows half of an Amberlyst DT-sphere. Fig. S13(d) is virtually identical to the sample before the hydrothermal reaction, since there is no major fragmentation evidence on the surface of organic polymeric formation. Fig. S13(b,c) relate to images recorded at a higher magnification of the Amberlyst DT beads before

hydrothermal reaction. Fig. S13(e,f) correspond to SEM images recorded at a higher magnification.

The spent SZ$_{cord}$ catalyst sample is shown on Fig. S14(a,b) after the hydrothermal reaction at 170 °C for 60 minutes. Fig. S14(c,d) corresponds to the SZ$_{cord}$ catalyst sample after the hydrothermal reaction at 190 °C for 10 min. Fig. S14(e,f) relate to SEM images taken of the SZ$_{cord}$ catalyst sample after the 5th reuse cycle (190 °C for 9 min).
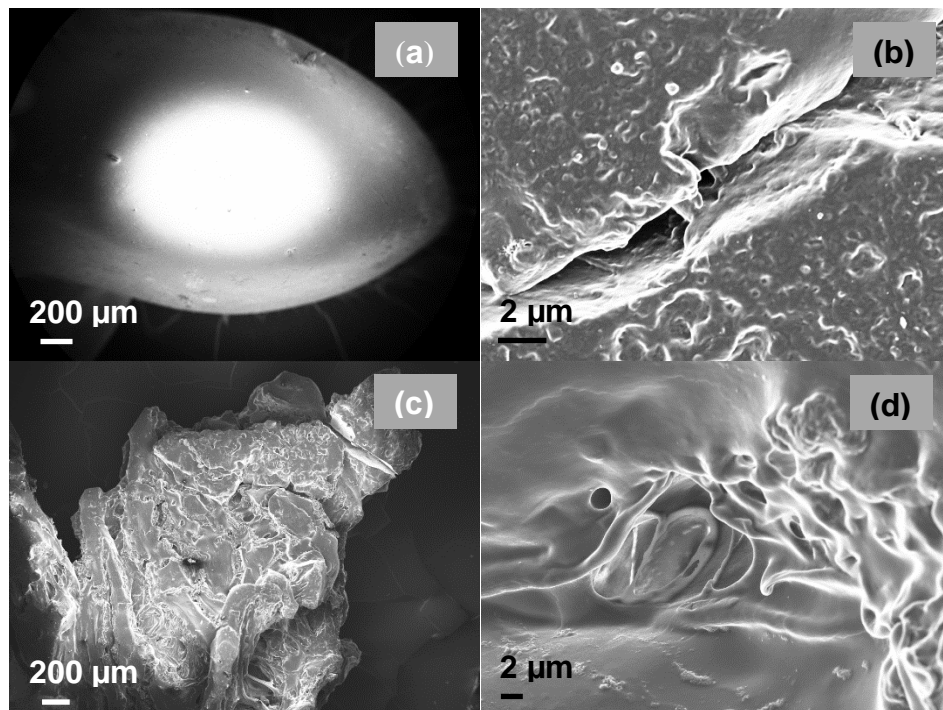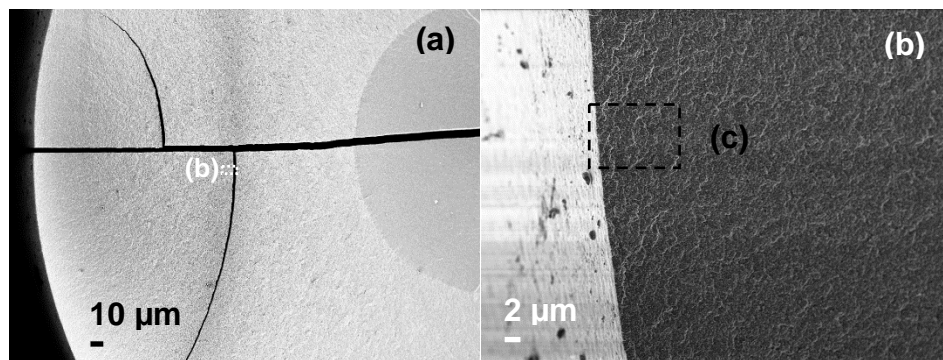

Figure S12. SEM images of (a,b) Nafion NR40 and (c,d) Nafion NR40 after hydrothermal reaction at 210 °C for 8 min.
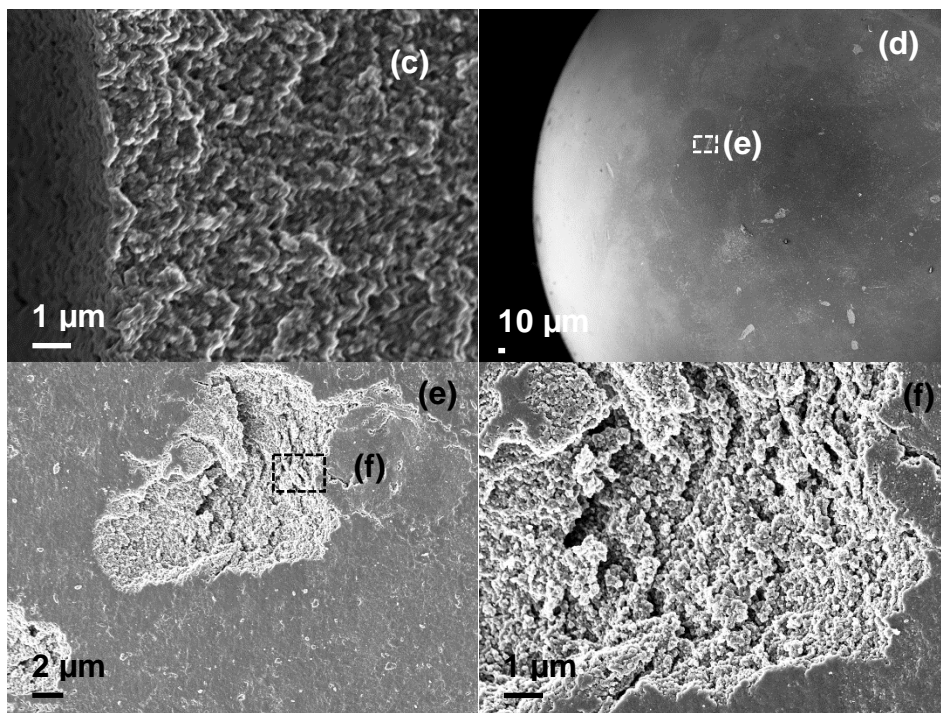
Figure S13. SEM images of (a-c) Amberlyst DT and (d-f) Amberlyst DT after hydrothermal reaction at 170 °C for 60 min.
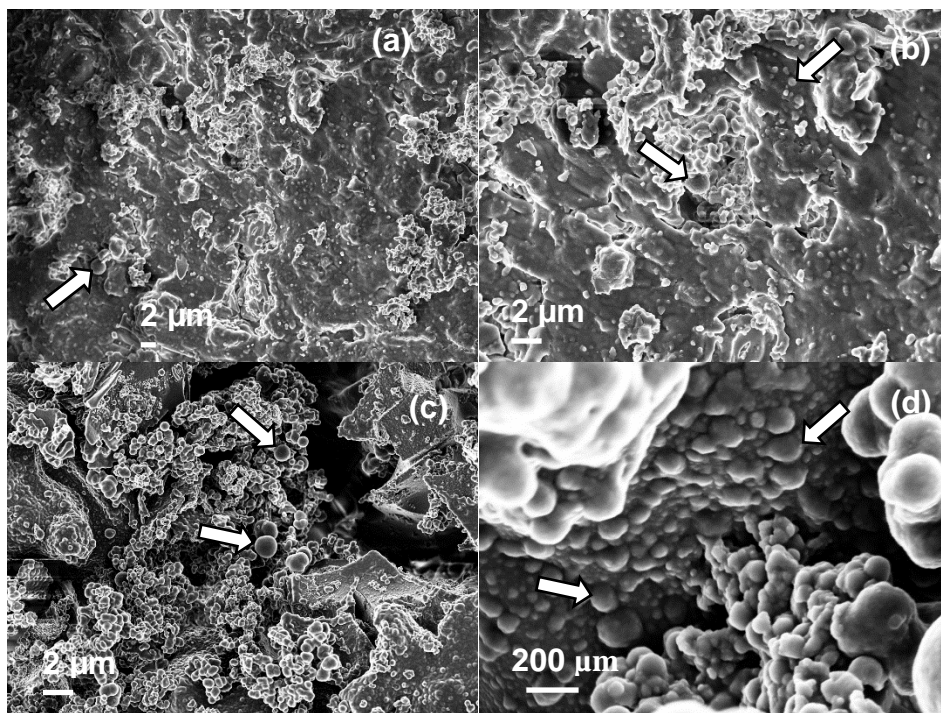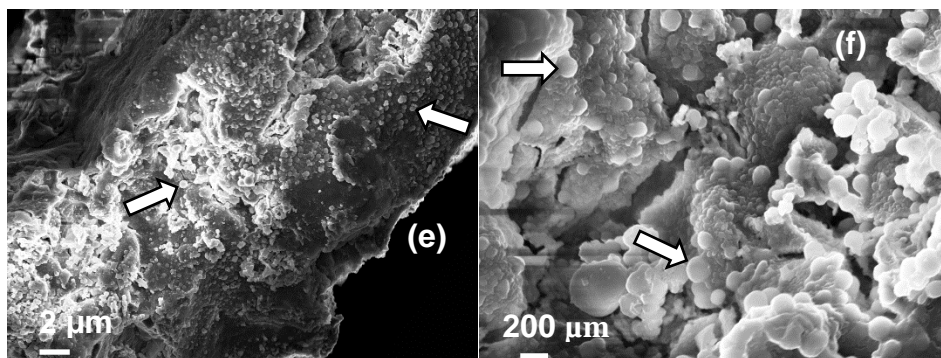
Figure S14. SEM images of (a,b) SZ on cordierite after hydrothermal reaction at 170 °C for 60 min, (c,d) SZ on cordierite after hydrothermal reaction at 190 °C for 10 min, (e,f) SZ on cordierite after the 5th cycle of reusability at 190 °C for 9 min.

5.2 N_2-physisorption

A Micromeritics Tristar II-Physisorption Analyzer was utilized to record the nitrogen sorption isotherms for fresh and spent catalysts. All samples were dried at 105 °C and exposed to nitrogen gas for 12 h before measurement and the isotherms were taken at 77 K. The samples were exposed to ~20 % humid room air for about 1 minute during the transfer to the holders. The specific surface area (A_{BET}) was determined by the Brunauer-Emmett-Teller (BET) model[4] at relative pressures between 5 and 35% where the data points were observed to arrange linearly. The specific pore volume (V_p) was estimated from N_2 uptake at a p/p_0 value of 0.99 while recording approximately 150 equilibrium data points. The pore width distribution (d_p) was deduced from the desorption branch using the Barrett-Joyner-Halenda (BJH) method[5].
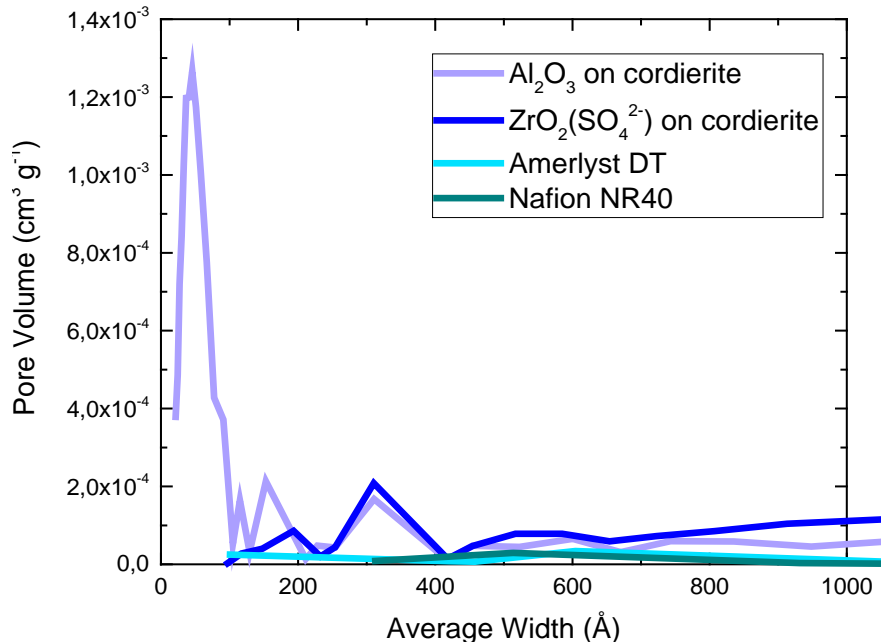
Figure S15. Pore size distribution curves of the samples.

5.3 Ion exchange capacities of polymeric resins

For the polymeric resins, the general titration procedure was carried out based on Boehm's method [18,19]. A known mass of the catalyst was added to 50 ml of one of 0.02 M concentration: NaOH (Sigma-Aldrich, 99.998%). The samples were agitated by shaking for 24 h and then filtered to remove the solid, and 10 ml aliquots were taken by pipette from the sample into three different flasks. Each of the three aliquots of the reaction base NaOH were then acidified by the addition of 10 ml of 0.02 M HCl (Sigma–Aldrich, 99.999%). The acidified solutions were then back-titrated with 0.02 M NaOH, the titrator base.

The ion exchange capacities provided by the manufacturer were verified by back-titration following the method reported by Goertzen et al[19]. Table S6 includes both manufacturer's value of the ion exchange capacities and the experimental ion exchangeable H^+ concentration in meq g^{-1} of the dry resin, as well as the % difference involved in the experimental results. It is showed that the experimental values obtained in this laboratory agree with the manufacturer's specifications. Amberlyst DT (a macroreticular, sulfonic acid polymeric catalyst) has three times more acid sites (3.1 meq g^{-1}) than Nafion NR40 in bead-form (1.0 meq g^{-1}).

Table S6. Ion exchange titration data for Amberlyst DT and Nafion NR40 resins.

Catalyst	Manufacturer's meq g^{-1}	Experimental meq g^{-1}	% Difference
Amberlyst DT	≥3.1	3.4	9.2
Nafion NR40	1.0	1.1	9.5

5.4 XPS

The surface characterization was done with X-ray photoelectron spectroscopy (XPS) on a SPECS system equipped with an Al anode XR50 source operating at 150 mW and a Phoibos 150 MCD-9 detector. The pressure in the analysis chamber was always below 10^{-7} Pa. The area analyzed was about 2 mm x 2 mm. The pass energy of the hemispherical analyzer was set at 25 eV and the energy step was set at 0.1 eV. The sample powders were pressed to self-consistent disks for XPS analysis.

Peak fitting and quantification analysis were performed using the software package CasaXPS (Casa Software Ltd., UK). Binding energy (BE) values for SZ_{cord} were referred to the adventitious Zr 3d signal, for Al_2O_{3cord} BE values were referred to Al 2s signal, for Nafion NR40 they were referred to F 1s and for Amberlyst DT they were referred to C 1s. Atomic surface ratios were obtained by using peak areas normalized on the basis of acquisition parameters after background subtraction, experimental sensitivity factors and transmission factors provided by the manufacturer.

5.5   Total Acid Site density

The total acid site density was calculated following the method published by El Assal et al[20]. The following equation has been used to calculate the amount of total acid sites of metal oxide on cordierite:

$$TAS_{MO} = \frac{AS}{D} \times 100 \ [\%]$$

where *TAS*, *AS*, *D* are the– total acid site density of metal oxide in µmol g^{-1}, acid sites in 1 g of sample in µmol g^{-1} and percentage of coated cordierite, respectively; the subscript to be read: *MO* is the metal oxide.

5.6 XPS values

Table S7. XPS data of fresh Nafion NR40 and Amberlyst DT before and after the hydrothermal reaction at 210 and 170 °C, respectively.

Sample	Name	Position (eV)	% At Conc
Nafion$_{fresh}$	O 1s	527.9	17.3
	C 1s	290.4	47.4
	S 2p	169.8	1.4
	F 1s	689.0	33.8
Nafion$_{210}$	O 1s	528.6	21.7
	C 1s	292.0	46.9
	S 2p	169.0	0.9
	F 1s	688.9	30.4
Amb$_{fresh}$	O 1s	532.4	21.5
	C 1s	284.8	64.9
	S 2p	168.8	4.9
	Cl 2p	200.5	8.6
Amb$_{170}$	O 1s	532.2	24.3
	C 1s	284.9	71.5
	S 2p	168.4	1.5
	Cl 2p	200.3	2.7
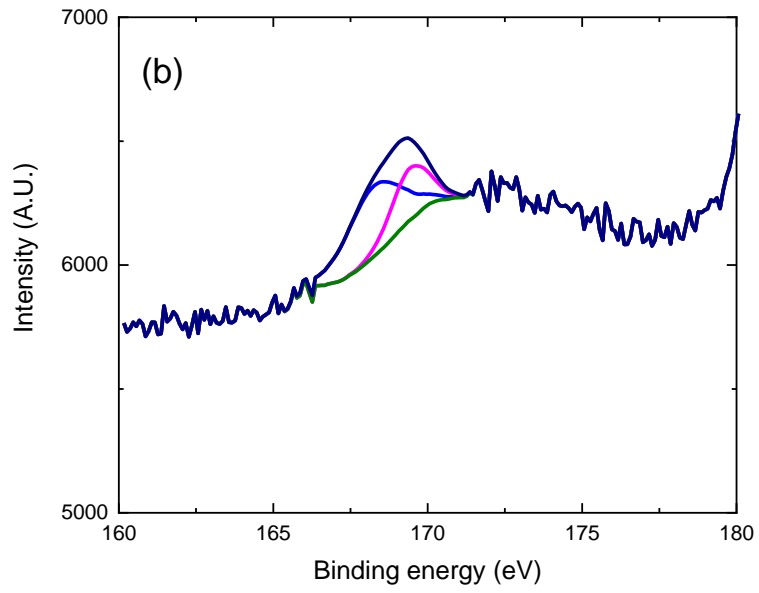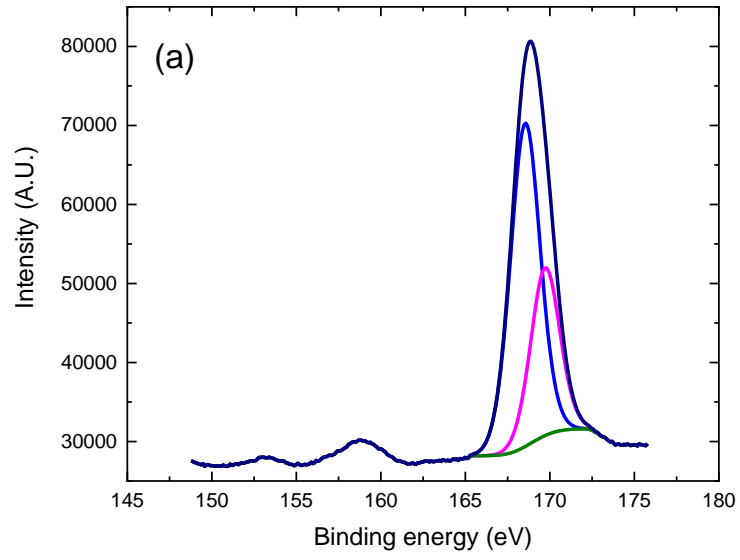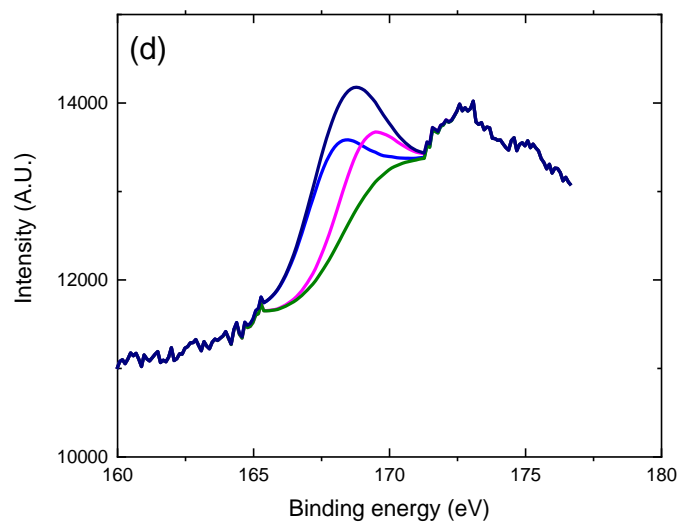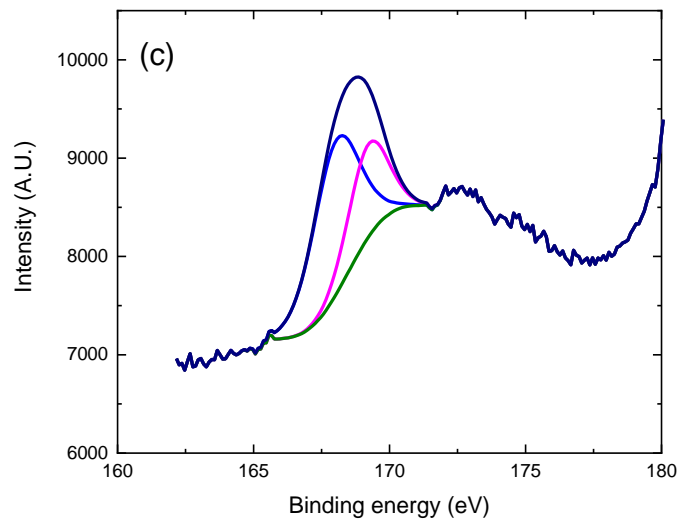
Figure S16. XPS S 2p spectra of SZ$_{cord}$ before (a) and after hydrothermal reaction at different temperatures: (b) 170 °C; (c) 190 °C; (d) 210 °C.
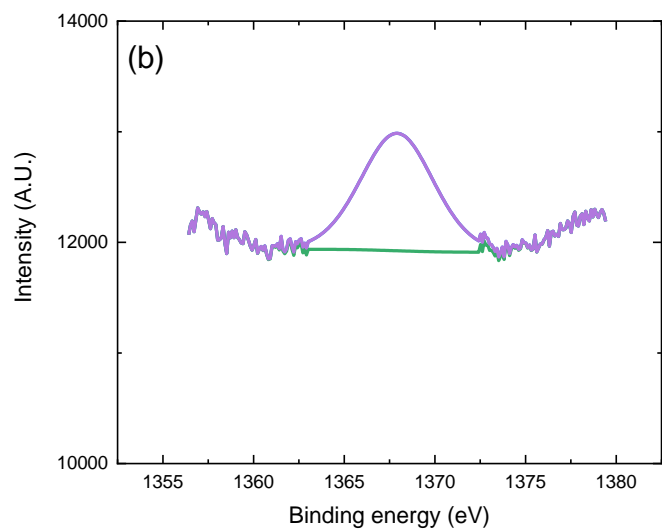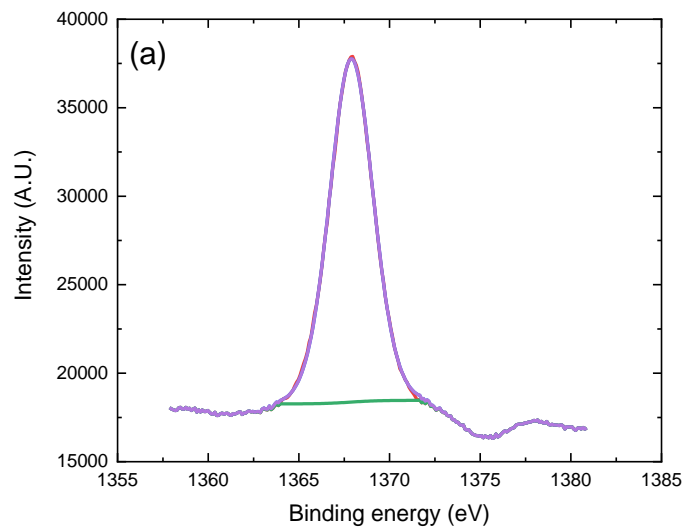
Figure S17. XPS Al 2s spectra of Al_2O_{3cord} before (a) and after hydrothermal reaction at 210 °C (b).
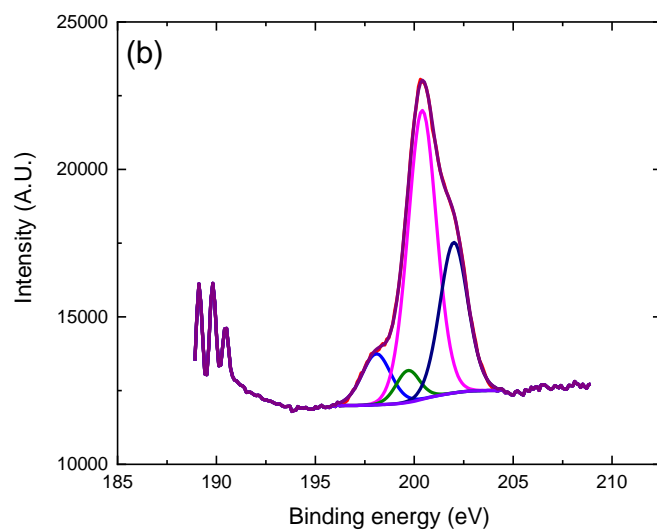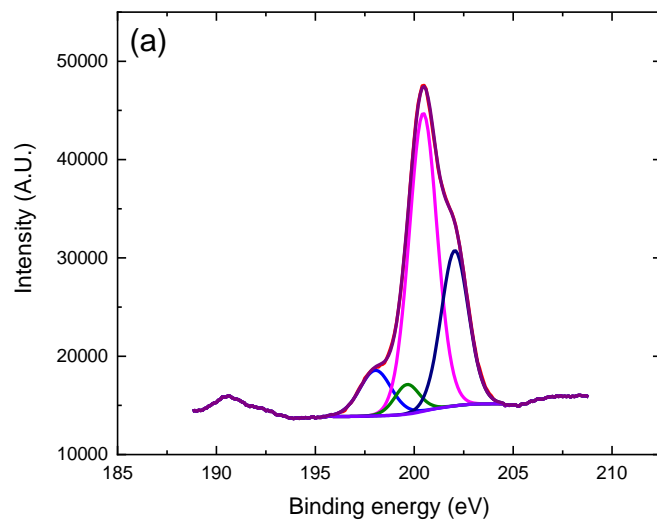
Figure S18. XPS Cl 2p^3 spectra of Amberlyst DT before (a) and after hydrothermal reaction at 170 °C (b).
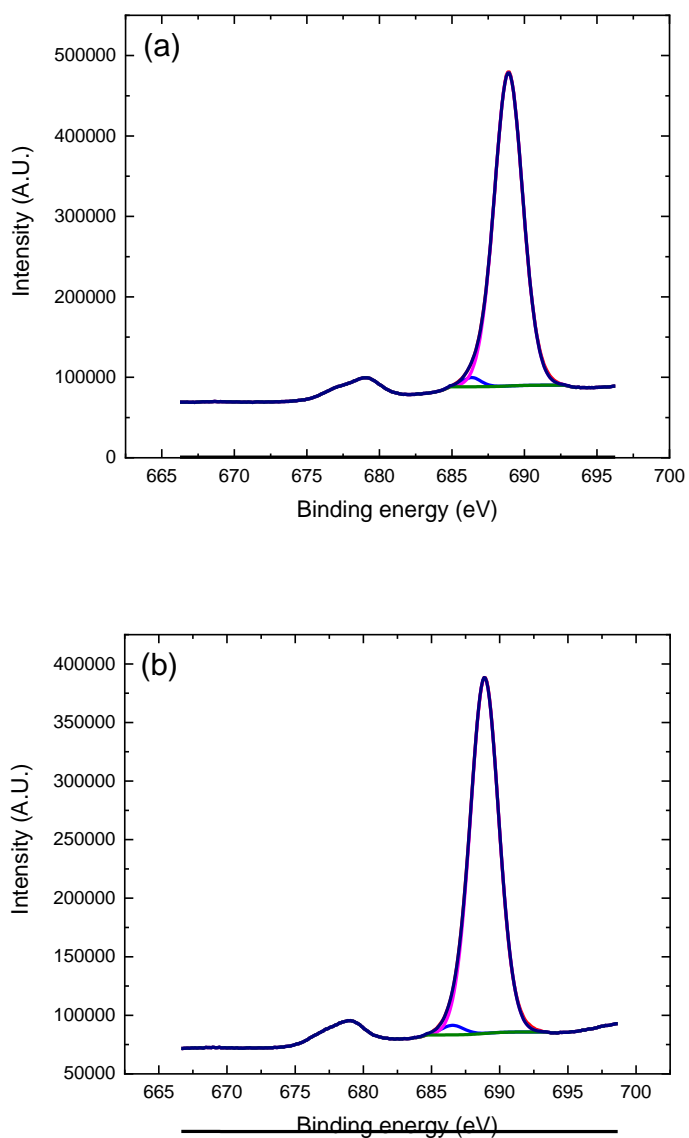
Figure S19. XPS F 1s spectra of Nafion NR40 before (a) and after hydrothermal reaction at 170 °C (b).

5.7   NH₃-TPD

The temperature-programmed desorption profile of NH_3 (NH_3-TPD) study was performed with an AutoChem II 2920 chemisorption analyser equipped with a TCD detector to measure the total acidity of the samples before and after hydrothermal reaction. Prior to the adsorption of NH_3, ca. 100 mg of sample were first preheated at 110 °C under flowing He with a heating rate of 10 K min^{-1} for 0.5 h to remove undesirable physisorbed species, followed by heating under He environment at 600 °C for 1 h, then cooled to room temperature. Consequently, the sample was exposed to flowing ammonia gas mixture (15% NH_3 in He with a flow of 50 ml min^{-1}) for 1 h, then

purged by He gas for 30 min to remove excessive physisorbed ammonia. The NH_3-TPD of the samples was carried out by increasing the reactor temperature linearly to 600 °C with a heating rate of 10 K min^{-1}.
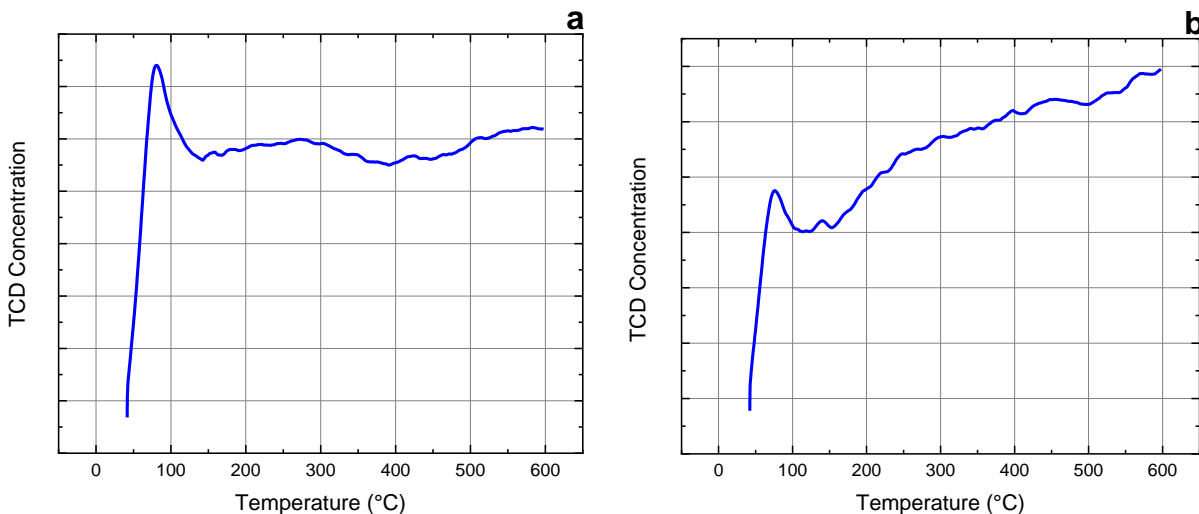
Figure S20. TCD of SZ_{cord} before (a) and after hydrothermal reaction at 190 °C (b).
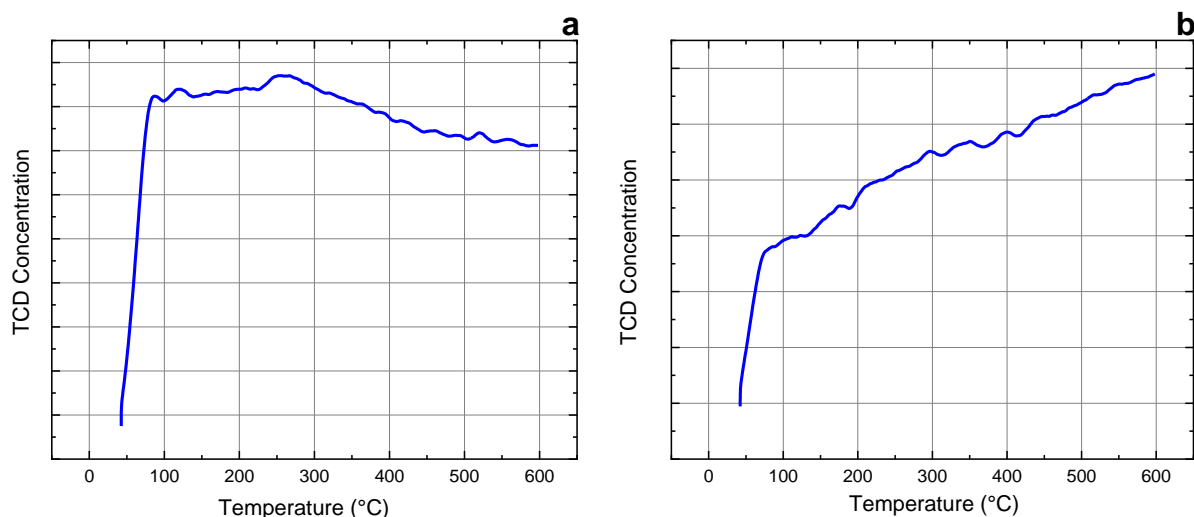
Figure S21. TCD of Al_2O_{3cord} before (a) and after hydrothermal reaction at 210 °C (b).

5.8   Kinetic model comparison with homogeneous catalysis

To investigate the effect of acid species leaching on the reaction mechanism of the sulfated zirconia-catalyzed dehydration reaction of xylose, the kinetic model described in Scheme 3 was also applied to a purely homogeneously catalyzed dehydration reaction. This study was conducted as follows:

The conditions for homogeneous catalysis were 0.1 M H_2SO_4, Temperature=180, 200 and 220 °C, time= 0 to 60 min, initial xylose concentration of 85 mmol L^{-1}.

As can be seen from Figures S22 and S23, the results imply that the same model scheme (Scheme 3) fits to both, the purely homogeneous and the mixed heterogeneous/homogeneous (through leaching) catalyzed reactions.
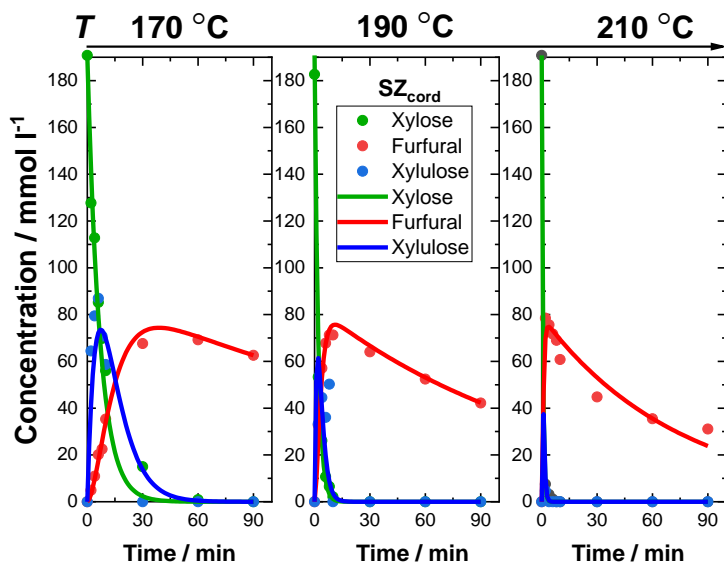
Figure S22. Scheme 3 and concentrations of FUR, xylose, and xylulose at temperatures of 170, 190 and 210 °C when employing SZ_{cord} (Experimental-circle, modeled-solid lines).
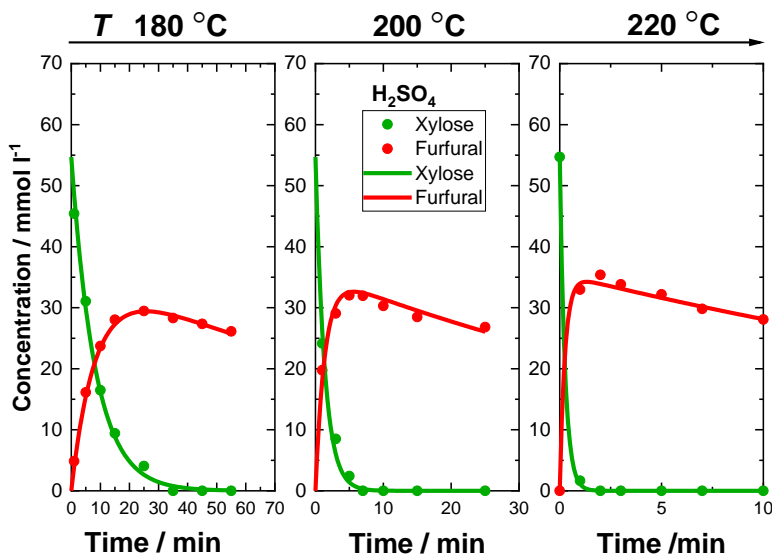
Figure S23. Scheme 3 and concentrations of FUR and xylose at temperatures of 180, 200 and 220 °C when using H_2SO_4 (Experimental-circle, modeled-solid lines).

Owing to the high acidity of the sulfuric acid catalysis, very high rate constants for the degradation of the intermediate (k_5 and k_6) were observed when employing H_2SO_4 (Table S8 and S9). Besides, the activation energy in this case for k_5 and k_6 are very low which explains why xylulose intermediate was not observed.

Table S8. Frequency factors (A, min^{-1}) and activation energies (E$_a$, kJ mol^{-1}) for the kinetic model proposed.

	Catalyst	k_4	k_5	k_6	k_7
A (min^{-1})	H$_2$SO$_4$	6.5×10^{17}	4.4×10^5	1.4×10^5	9.4×10^4
	SZ$_{cord}$	3.4×10^{13}	5.9×10^{17}	2.0×10^{18}	7.0×10^5
Ea (kJ mol^{-1})	H$_2$SO$_4$	163	6.5	3.4	64
	SZ$_{cord}$	122	161	164	73

Table S9. Kinetic rate constants (min^{-1}) at each experimental temperature when employing H$_2$SO$_4$ and SZ$_{cord}$ following the kinetic model proposed.

Catalyst	T (°C)	k_4 (min^{-1})	k_5 (min^{-1})	k_6 (min^{-1})	k_7 (min^{-1})
H$_2$SO$_4$	180	0.11	101000	58000	0.0044
	200	0.71	108000	61000	0.0091
	220	3.81	114000	63000	0.0175
SZ$_{cord}$	170	0.13	0.065	0.093	0.002
	190	0.54	0.43	0.64	0.004
	210	2.02	2.02	3.71	0.008

5.9 pH values of heterogeneous and homogeneous catalysis

Final pH values of both systems were measured to understand the acid species leached in the aqueous phase. Although the acid content in the sulfuric acid-catalyzed reaction was almost one order of magnitude higher, both xylose concentration and furfural formation can be simulated with the same kinetic model as in the heterogeneous case (Figure S4). The pH values after the catalyzed reactions stay fairly constant as a funtion of reaction time.
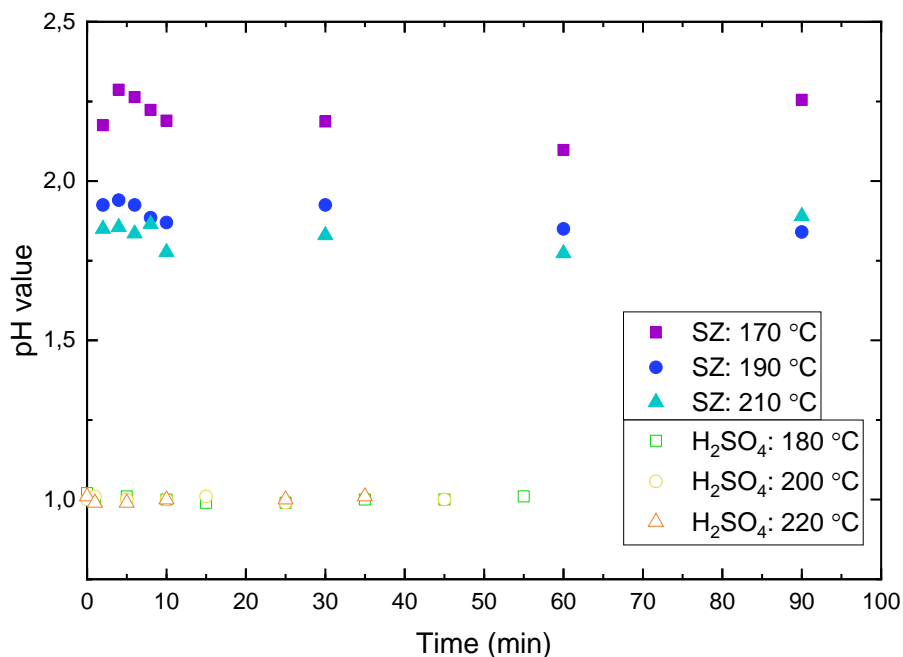
Figure S24. pH values of H$_2$SO$_4$ catalysis

The initial dominating heterogeneous catalysis implies that the present kinetic model cannot be attributed to a purely heterogeneous-catalyzed reaction. There is leaching of S species from sulfated zirconia into the aqueous phase. Nevertheless, there is a significant difference with the purely homogeneously catalyzed reaction when using H_2SO_4, based on the pH final values and the kinetic information when applying Scheme 3.

References

[1] S. Givry, C. Bliard, F. Duchiron, Selective ketopentose analysis in concentrate carbohydrate syrups by HPLC, Carbohydr. Res. 342 (2007) 859-864.

[2] C. Pirola, I. Rossetti, V. Ragaini, Are conversion, selectivity and yield terms unambiguously defined in chemical and chemical engineering technology? La Chimica & L'Industria. 2 (2013) 136-145.

[3] L. Soler, A. Casanovas, A. Urrich, I. Angurell, J. Llorca, CO oxidation and COPrOx over preformed Au nanoparticles supported over nanoshaped CeO2, Applied Catalysis B: Environmental. 197 (2016) 47-55.

[4] S. Brunauer, P.H. Emmett, E. Teller, Adsorption of gases in multimolecular layer, Journal of the American Chemical Society. 35 (1938) 309.

[5] E.P. Barrett, L.G. Joyner, P.P. Halenda, The determination of pore volume and area distributions in porous substances. I. Computations from nitrogen isotherms, Journal of the American Chemical Society. 73 (1951) 373.

[6] D. Hua, Y. Wu, Y. Liu, Y. Chen, M. Yang, X. Lu, et al., Preparation of furfural and reaction kinetics of xylose dehydration to furfural in high-temperature water, Petroleum Science. 13 (2016) 167-172.

[7] S.B. Kim, M.R. Lee, E.D. Park, S.M. Lee, H. Lee, K.H. Park, et al., Kinetic study of the dehydration of d-xylose in high temperature water, Reaction Kinetics, Mechanisms and Catalysis. 103 (2011) 267-277.

[8] Z. Chen, W. Zhang, J. Xu, P. Li, Kinetics of xylose dehydration into furfural in acetic acid, Chin. J. Chem. Eng. 23 (2015) 659-666.

[9] X.J. Chen, X.Q. Liu, F.L. Xu, X.P. Bai, Degradation Kinetics of Xylose and Arabinose in Subcritical Water in Unitary and Binary System, Advanced Materials Research. 450-451 (2012) 710-714.

[10] Q. Jing, X. Lü, Kinetics of Non-catalyzed Decomposition of D-xylose in High Temperature Liquid Water, Chinese Journal of Chemical Engineering. 15 (2007) 666-669.

[11] O. Ershova, J. Kanervo, S. Hellsten, H. Sixta, The role of xylulose as an intermediate in xylose conversion to furfural: insights via experiments and kinetic modelling, RSC Adv. 5 (2015) 66727-66737.

[12] P.J. Oefner, A.H. Lanziner, G. Bonn, O. Bobleter, Quantitative studies on furfural and organic acid formation during hydrothermal, acidic and alkaline degradation ofD-xylose, Monatshefte für Chemie / Chemical Monthly. 123 (1992) 547-556.

[13] R. Weingarten, J. Cho, J. Conner Wm.Curtis, G.W. Huber, Kinetics of furfural production by dehydration of xylose in a biphasic reactor with microwave heating, Green Chem. 12 (2010) 1423-1429.

[14] B. Danon, W. Hongsiri, L. van der Aa, W. de Jong, Kinetic study on homogeneously catalyzed xylose dehydration to furfural in the presence of arabinose and glucose, Biomass Bioenergy. 66 (2014) 364-370.

[15] K. Lamminpää, J. Ahola, J. Tanskanen, Kinetics of Xylose Dehydration into Furfural in Formic Acid, Ind Eng Chem Res. 51 (2012) 6297-6303.

[16] T.M. Aida, N. Shiraishi, M. Kubo, M. Watanabe, R.L. Smith Jr., Reaction kinetics of d-xylose in sub- and supercritical water, The Journal of Supercritical Fluids. 55 (2010) 208-216.

[17] J. Iglesias, J.A. Melero, G. Morales, M. Paniagua, B. Hernández, Dehydration of Xylose to Furfural in Alcohol Media in the Presence of Solid Acid Catalysts, ChemCatChem. 8 (2016) 2089-2099.

[18] H. Boehm, Chapter Thirteen - Surface Chemical Characterization of Carbons from Adsorption Studies, in: E.J. Bottani, , J.M.D. Tascón (Eds), Adsorption by Carbons, Elsevier, Amsterdam, 2008, pp. 301-327.

[19] S.L. Goertzen, K.D. Thériault, A.M. Oickle, A.C. Tarasuk, H.A. Andreas, Standardization of the Boehm titration. Part I. CO2 expulsion and endpoint determination, Carbon. 48 (2010) 1252-1261.

[20] Z. El Assal, S. Ojala, S. Pitkäaho, L. Pirault-Roy, B. Darif, J. Comparot, et al., Comparative study on the support properties in the total oxidation of dichloromethane over Pt catalysts, Chemical Engineering Journal. 313 (2017) 1010-1022.

II

Gómez Millán, G., Hellsten, S., King, A. W. T., Pokki, J. P., Llorca, J., Sixta, H. (2019) A Comparative Study of Water-Immiscible Organic Solvents in the Production of Furfural from Xylose and Birch Hydrolysate. *Journal of Industrial and Engineering Chemistry. 72*, 354-363.

A comparative study of water-immiscible organic solvents in the production of furfural from xylose and birch hydrolysate

Gerardo Gómez Millán[a,b], Sanna Hellsten[a], Alistair W.T. King[c], Juha-Pekka Pokki[d], Jordi Llorca[b], Herbert Sixta[a,*]

[a] Department of Bioproducts and Biosystems, School of Chemical Engineering, Aalto University, Vuorimiehentie 1, 02150 Espoo, Finland
[b] Department of Chemical Engineering, Institute of Energy Technologies and Barcelona Research Center in Multiscale Science and Engineering, Universitat Politècnica de Catalunya, Eduard Maristany 10-14, 08019 Barcelona, Spain
[c] Materials Chemistry Division, Chemistry Department, University of Helsinki, AI Virtasen Aukio 1, Helsinki, Finland
[d] Department of Chemical and Metallurgical Engineering, School of Chemical Engineering, Aalto University, PL 16100, 00076 Espoo, Finland

ABSTRACT

Furfural (FUR) was produced from xylose using a biphasic batch reaction system. Water-immiscible organic solvents such as isophorone, 2-methyltetrahydrofuran (2-MTHF) and cyclopentyl methyl ether (CPME) were used to promptly extract FUR from the aqueous phase in order to avoid the degradation to humins as largely as possible. The effect of time, temperature, organic solvent and organic-to-aqueous ratio on xylose conversion and FUR yield were investigated in auto-catalyzed conditions. Experiments at three temperatures (170, 190 and 210 °C) were carried out in a stirred microwave-assisted batch reactor, which established the optimal conditions for achieving the highest FUR yield. The maximum FUR yields from xylose were 78 mol% when using CPME, 48 mol% using isophorone and 71 mol% in the case of 2-MTHF at an aqueous to organic phase ratio of 1:1 (v/v). Birch hydrolysate was also used to show the high furfural yield that can be obtained in the biphasic system under optimized conditions. The present study suggests that CPME can be used as a green and efficient extraction solvent for the conversion of xylose into furfural without salt addition.

© 2019 The Korean Society of Industrial and Engineering Chemistry. Published by Elsevier B.V. All rights reserved.

Introduction

Hemicellulose, one of the three major components in lignocel-lulosic biomass including cellulose and lignin, is a cross-linked fibrous amorphous heteropolysaccharide, consisting mostly of different pentoses (C_5) with some hexoses and uronic acids sugar monomers [1]. Hemicelluloses are the second most abundant natural polymer [2]. The main C_5 sugars found in hemicellulose are xylose and arabinose. Xylan, which is degraded during kraft pulping of hardwood, is currently valorized to sugar-based products in very small quantities. In these cases, xylan is typically hydrolysed to xylose and then further reduced to xylitol. In a typical hardwood kraft pulping process, about 50% of the xylan in the wood is degraded to carboxylic acids, which are enriched in the black liquor together with the degraded lignin. After thermal concentration to thick liquor, the organic matter is burnt and the energy obtained is used for the pulping process [3]. Therefore,

valorization of these attractive industrial streams extends the possibility to create new markets and new economic models.

According to the United States Department of Energy, furfural (furan-2-carbaldehyde, FUR) is one of the top 10 most rewarding bio-based platform molecules [4]. FUR is industrially produced by the dehydration of xylose and other C_5-sugars in aqueous solutions usually found in hemicellulosic fractions of lignocellulosic biomass. The FUR application range varies from the chemical industry, where is used as solvent and extracting agent, to the agrochemical sector, where it is employed as nematicide, fungicide and herbicide; it can also be involved in processes in the pharmaceutical and cosmetic industries [5]. Furthermore, FUR serves as a platform molecule to produce furfuryl alcohol (via hydrogenation) [6,7] with applications in the food industry as flavoring agent, for the synthesis of furan resins and in the biofuel sector. Other important molecules that can be potentially synthesized from FUR are: tetrahydrofurfuryl alcohol, furan as a diene in Diels–Alder reactions, tetrahydrofuran, dihydropyran and furoic acid [8]. Besides, FUR has been identified as a direct or indirect feedstock to more than 80 chemicals [9,10]. Consequently,

FUR plays a major role as a platform molecule in future bio-refineries developments [1].

In the commercial process, FUR yield does not exceed 50 mol% and is associated with various environmental problems, such as toxic effluents derived from mineral acids (sulfuric or hydrochloric acid) and high energy demand due to the need of high temperatures of approximately 200 °C. In order to avoid the formation of high salt loads resulting from the neutralization of mineral acid catalysts, the development of easily-separable solid acid catalysts is being undertaken (e.g. zeolites [11–20], sulfonated graphenes [21–24], sulfated zirconia [6,25], alumina [26], coated activated carbon [15,27], among others [1]) and ionic liquids [5]. These recent advances suggest operational improvements involving green principles [28]. However, solid catalysts might face deactivation, fouling or low catalytic activity after the first cycle of reuse. Moreover, the unknown consequences of long-term use of ionic liquids, together with their elevated cost and yet inefficient recovery and recycling, set significant drawbacks to scale up their development [5].

In addition, the limited FUR yields are partly due to the formation of insoluble polymers (humins). These humins are decomposition products of both xylose and FUR, which react via resinification or condensation [1,29–32]. A recent article showed limited FUR yields of 49% in aqueous phase at 210 °C in 1 h using a xylose solution of 186 mmol l^{-1} [33]. Several studies have suggested ways to inhibit the formation of humins and subsequently increase the FUR yield. One approach is to selectively extract the FUR instantaneously from the aqueous solution into an organic phase [34]. Trimble and Dunlop were the pioneers to implement this idea using ethyl acetate as the extracting media [35]. Subsequent research included studies on various organic solvents such as 2-s-butylphenol, 4-n-hexylphenol, 2-methoxy-4-propylphenol [36], 1-butanol [37], γ-valerolactone [13,38], cyclohexanol [39], methyl isobutyl ketone (MIBK) [34,39], dimethyl sulfoxide (DMSO) [40,41], 1,3-Dimethyl-2-imidazolidinone (DMI) [42] and widely-used toluene [39]. However, most of these studies involve the addition of salts (used as phase modifiers) due to the high solubility of organic solvents in water, in order to increase the partition coefficient. Hence producing high salt waste after work-up, corrosion of the reactor and possible deactivation of acid sites on solid acid catalysts [43,44]. Besides, several solvents are toxic and are not ideal for industrial application. In contrast, green solvents from renewable sources such as 2-MTHF and CPME [45–47] are commercially available offering sustainable alternatives in order to extract FUR without the addition of salts due to its aqueous-immiscibility nature and provide a superior phase separation at the organic-water interface without forming emulsions [48]. An organic solvent with similar properties, isophorone, has been recently reported, which claims a higher distribution coefficient of FUR at 25 °C in a quaternary mixture of FUR + water + isophorone + acetic acid (14) [49] than CPME (8.5) and 2-MTHF (8) [50]. Under normal conditions, isophorone has a solubility in water of 1.2 g/100 g at 20 °C [49], CPME of 1.1 g/100 g at 23 °C [47] and 2-MTHF of 14 g/100 g at 20 °C [51].

The aim of this work is to evaluate the production of FUR from xylose using a biphasic system including a novel promising water-immiscible solvent, isophorone, in which FUR is extracted thus increasing the FUR yield by reducing FUR decomposition reactions via condensation and resinification. The performance of isophorone is compared with other known water-immiscible organic solvents like CPME and 2-MTHF. An additional advantage of this system is the prevention of salt addition that offers a greener perspective in the FUR production. Furhtermore, a liquid–liquid extraction (LLE) model was developed in order to predict the mass fractions of formed FUR in aqueous and organic phases under experimental conditions.

Experimental

Materials

D-Xylose powder (99%), isophorone (97%), 2-MTHF (99%) and CPME (99%) were purchased from Sigma Aldrich.

D-Xylose powder was used in the experiments without further purification. Millipore grade water was used for preparing the solutions.

The birch hydrolysate was supplied by Stora Enso (Stora Enso, Imatra, Finland), which was used for the dehydration reaction experiments.

Methods

Xylose dehydration reaction experiments in biphasic system

Single containing D-xylose solution in a concentration typical for biomass hydrolysate (186 mmol l^{-1}) was freshly prepared before the experiments (Table A1 in the Supporting Information). These experiments can be considered as an auto-catalyzed reaction system where some side products (namely carboxylic acids) or intermediates, formed during the reaction, may have a catalytic effect [52,53]. In a typical experiment, the samples were prepared by heating 3 ml of an aqueous solution of 186 mmol l^{-1} xylose using a borosilicate glass reactor (V = 10 cm^3) with magnetic stirring (600 min^{-1}), an irradiation power of ≤850 W for maximum 2 min and microwave-assisted heating (Monowave 300, Anton Paar GmbH, Graz, Austria). The prepared solutions were tested for FUR yield, selectivity and xylose conversion at the reaction temperatures of 170, 190 and 210 °C with different reaction times in the range of 30–240 min. The reaction vial was rapidly cooled after the reaction by compressed air inside the reactor until it reached 60 °C. The highest temperature and the longest reaction time studied at the present work were 210 °C and 180 min, respectively.

Birch hydrolysate dehydration reaction experiments in biphasic system

The birch hydrolysate was filtered by using a glass filter with porosity 4 (Duran). The composition of the liquor was determined according to the analytical method NREL/TP-510-42623 [54]. The concentration of monomeric sugars was measured by high-performance anion exchange chromatography with pulse amperometric detection (HPAEC-PAD) by using a Dionex ICS-3000 column.

Determination of xylose, FUR and by-products

Samples for analysis were drawn from both the organic phase (top) and aqueous phase (bottom) after microwave heating. Xylose and FUR from aqueous phase were analyzed separately by High Performance Liquid Chromatography (HPLC) operating a Dionex UltiMate 3000 HPLC (Dionex, Sunnyvale, CA, USA) device equipped with refractive index (RI) and ultraviolet (UV) diode array detectors. Product separation was achieved on a HyperRez XP Carbohydrate Ca$^+$ column (Thermo Scientific, Waltham, MA, USA). Aqueous sulfuric acid (0.005 mol l^{-1}) was used as eluent with a flow rate of 0.8 ml min^{-1}. The column temperature and the RI-detector temperature were set to 70 °C and 55 °C, respectively. The FUR and hydroxymethylfurfural (HMF) concentration was determined by the UV-detector at a wavelength of 280 nm. The xylose concentration was analyzed simultaneously by the RI-detector and the UV-detector at 210 nm for a crosscheck [55].

FUR from the organic phase was analyzed by gas chromatography with a flame ionization detector (GC-FID) relative to iso-butanol as internal standard (IS). The column used was a DB-WAXetr (30 m, 0.32 mm i.d., 1 μm film thickness) from Agilent

Technologies Inc. The injected samples (0.5 μL) were subjected to a split ratio of 20:1 in the inlet maintained at 250 °C and pressure of 12.967 psi. Helium was used as the carrier gas. The oven was initially maintained at 80 °C for 1 min, after which the temperature was increased to 250 °C at 30 °C min^{-1}. The FID was operated at 250 °C with hydrogen, air, and helium delivered at 30 ml min^{-1}, 380 ml min^{-1}, and 29 ml min^{-1}, respectively.

In this study conversion is defined in terms of moles of reactant converted per unit volume of reactor (Eq. (1)) Selectivity, at an instant, is the generated amount of moles of desired product referred to the moles of reactant converted (Eq. (2)). Yield is the amount in moles of desired product, FUR, produced relative to the amount of the key reactant, xylose (Eq. (3)) [56]. The following equations have been used for the mathematical evaluation of the obtained results:

$$X_{xyl} = \frac{c_{xyl}^{in} - c_{xyl}^{f}}{c_{xyl}^{in}} \times 100[\%] \qquad (1),$$

$$S_{xyl}^{fur} = \frac{c_{fur}}{c_{xyl}^{in} - c_{xyl}^{f}} \times 100[\%] \qquad (2),$$

$$Y_{fur} = \frac{c_{fur}}{c_{xyl}} \times 100[\%] \qquad (3),$$

where X, S, Y are the – conversion of xylose, selectivity to FUR and FUR yield, respectively; c is the – concentration in mmol (the subscripts to be read as follows: xyl, fur, in, f are the – xylose, FUR, initial, final).

Furfural decomposition reaction experiments in biphasic system.

FUR decomposition reactions were conducted using a 10 ml borosilicate glass reactor with magnetic stirring (600 min^{-1}) and microwave-assisted heating (Monowave 300, Anton Paar GmbH, Graz, Austria). The vials were filled with 1.5 ml of 5 wt% FUR solution and 1.5 ml of the organic solvent. The prepared solutions in the biphasic system were tested for FUR concentration at the reaction temperatures of 170, 190 and 210 °C with different reaction times in the range of 30–180 min. The reaction vial was rapidly cooled down to 60 °C after the reaction via a stream of compressed air that was blown onto the reactor. Samples were stored at 0 °C until analyzed.

Results and discussion

Furfural partitioning in a biphasic reactor system.

The partitioning of FUR in different organic solvents was investigated by conducting hydrothermal reactions wherein a solution of 5 wt% FUR in water was heated with isophorone, 2-MTHF, and CPME for 30 min at 190 °C at five different ratios of aqueous to organic solvent: 1:5, 1:2, 1:1, 2:1 and 5:1 (v/v). Fig. 1 shows the FUR partition coefficients (P) obtained with the three organic solvents, where P was calculated using Eq. (4) [39].

$$P = \frac{[FUR]_{org}}{[FUR]_{aq}} \qquad (4)$$

A FUR partition coefficient of 9.1 was obtained with an aqueous to isophorone fraction ratio of 1:5. This value decreased to 7.5, 8.4, 6.9 and 6.6 as the aqueous to isophorone fraction ratio increased to 1:2, 1:1, 2:1 and 5:1, respectively. For 2-MTHF (4.6) and CPME (3.8) lower partition coefficients were obtained compared to isophorone.
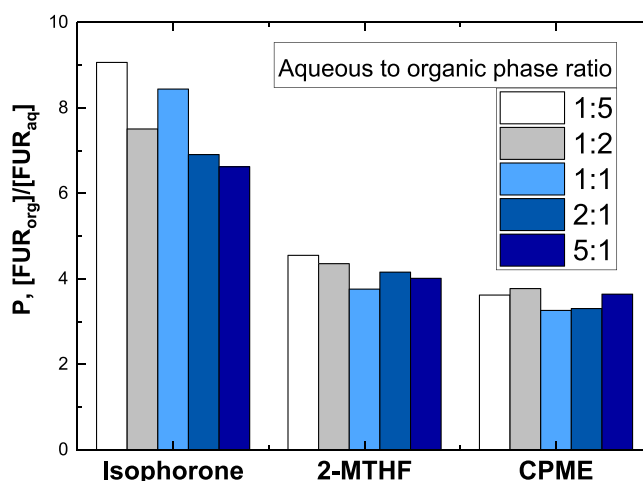
Fig. 1. Partition coefficients for furfural among isophorone, 2-MTHF and CPME. Partition coefficients were determined for a solution of 5 wt% furfural in water heated for 30 min at 190 °C (and then cooled down to 60 °C) at five different ratios of aqueous to organic solvent: 1:5, 1:2, 1:1, 2:1 and 5:1 (v/v).

In a recent article using isophorone [49], the partition coefficient of FUR in a ternary system was studied (FUR + isophorone + water). It can be observed that when the FUR fraction and temperature increase, the partition coefficient tends to decrease. However, under the experimental conditions of the present paper, the partition coefficient does not vary significantly (low mass fractions of FUR). Even though the partition coefficient of FUR when CPME and 2-MTHF tends to increase, when the FUR fraction and the temperature increase [57], its values do not vary significantly under the presented experimental conditions, due to the low mass fractions of FUR formed.

Furfural production from xylose

The effect of xylose dehydration on FUR production was studied in biphasic systems made with isophorone, 2-MTHF or CPME serving as the organic phase and an aqueous xylose solution.

Effect of organic phase and aqueous to organic phase ratio

Solubility of water in the organic solvents has been measured in recent papers for isophorone [49], 2-MTHF and CPME [57]. It is observed that solubility of water in the three organic solvents used in the present paper is minimal under the given experimental conditions.

The effect of different organic solvents and an aqueous solution of 186 mmol l^{-1} was studied in biphasic systems at 190 °C in 30 min. For this, three water-immiscible solvents were studied: isophorone, 2-MTHF and CPME. Simultaneously, the effect of aqueous-to-organic phase ratio on xylose conversion and FUR production was investigated. Consequently, five ratios of aqueous to organic phase (1:5, 1:2, 1:1, 2:1, 5:1; v/v) were planned. The FUR yields are shown in Fig. 2 and are calculated using Eq.(3).

Fig. 2 shows that the FUR yield increases as the aqueous to organic ratio increases from 1:5 up to 1:1 (v/v), regardless of the organic solvent. At ratios of aqueous to organic volumes of 2:1 to 5:1, we suggest that a higher FUR yield is prevented through the generation of increased decomposition products. The highest FUR yield (14%, Fig. 2a) is reached (at 190 °C in 30 min) when employing isophorone in an aqueous to organic phase ratio of 1:1. When 2-MTHF is employed (Fig. 2b), the highest FUR yield (13%) is also reached in an aqueous to organic phase ratio of 1:1. When CPME is used (Fig. 2c), a FUR yield of 26% is reached at 190 °C in 30 min.
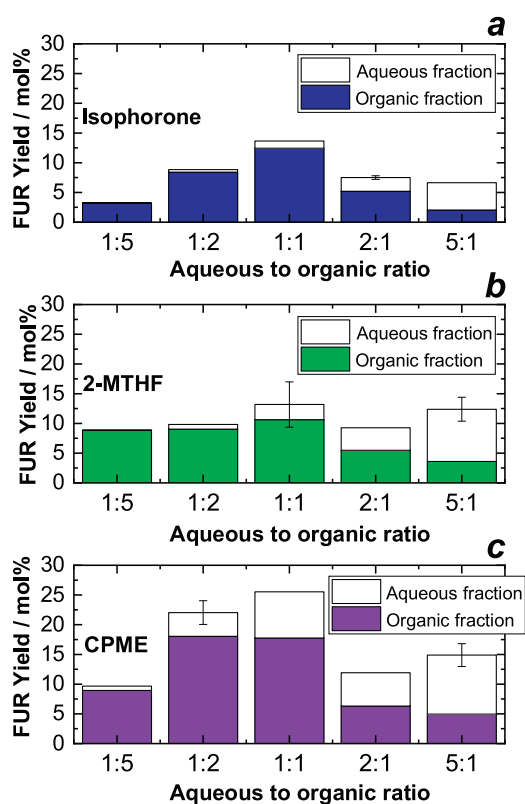
Fig. 2. Effect of aqueous-to-organic ratio on FUR yield when using isophorone (a), 2-MTHF (b) and CPME (c) as organic phase. The effect was determined for a solution of xylose (186 mmol l^{-1}) heated at 190 °C in 30 min at five different ratios of aqueous to organic solvent: 1:5, 1:2, 1:1, 2:1, 5:1 (v/v). The error bars shown are one standard deviation from duplicate analyses.

Figure A1 (in the Supporting Information) displays the xylose conversion and the FUR selectivity in the three biphasic systems. When employing isophorone, the xylose conversion varied from 36% to 41%. When using 2-MTHF, xylose conversion varied from 40% to 44%; and CPME, where xylose conversion fluctuated from 41% to 56%. Selectivity to FUR inceases as the aqueous to organic ratio increases from 1:5 to 1:1 (v/v), thereafter it decreases when increasing the aqueous to organic phase ratio to 5:1. The decrease of FUR selectivity could be due to saturation of the organic solvent to extract FUR.
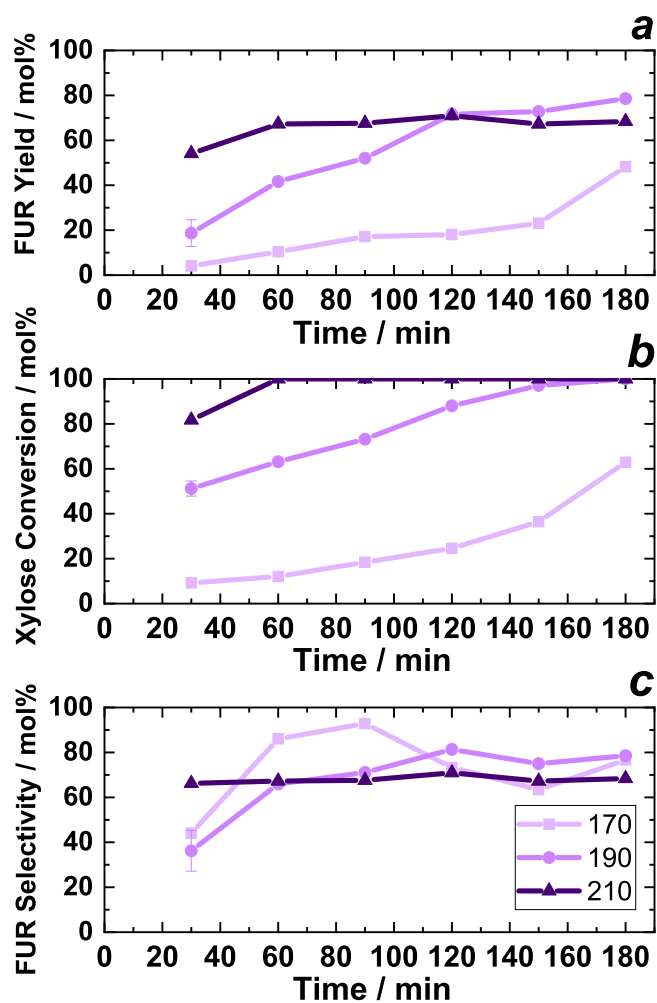
Effect of reaction temperature

The influence of the reaction temperature on the dehydration of xylose and the resulting FUR yield was studied by using a 186 mmol l^{-1} xylose concentration in a two-phase mixture at a temperature range between 100 and 200 °C for 30 min (water-organic solvent, 5:1 v/v) under microwave irradiation (Figure A2 in the Supporting Information). D-xylose is not soluble in the organic phase [49,57,58]. Thereby, the FUR yield varied between 0 and 23 mol% (Fig. A2a). The effect of reaction temperature on FUR yield, xylose conversion and selectivity to FUR when working with an aqueous to organic ratio of 5:1 was further investigated. A low FUR yield was obtained from 100 to 150 °C (approximately 0%). The reason for lower FUR yield at the low reaction temperature was due to incomplete xylose conversion (below 15%, Fig. A2b). The highest FUR yield when employing CPME and 2-MTHF is 23% (at a xylose conversion of 57% and 49%, respectively) in 30 min at 200 °C, and when using isophorone is 18% (at a xylose conversion of 50%) at 200 °C (in 30 min).

Effect of reaction time

The effect of reaction time on the production of FUR was studied by conducting reactions between 30 to 180 min at 170, 190 and 210 °C with isophorone, 2-MTHF and CPME with a xylose solution of 186 mmol l^{-1}. Due to the low vapor pressure of 2-MTHF, reactions using this organic solvent at reaction temperatures of 210 °C were not possible to perform. Fig. 3 shows the effect of reaction time when using CPME on FUR yield, xylose conversion and selectivity to FUR. In agreement with previous studies [59], FUR yield and xylose conversion were observed to be strongly influenced by the reaction temperature.

Fig. 3 displays the effect of reaction time on FUR yield, xylose conversion and selectivity to FUR at 170, 190 and 210 °C when using CPME as organic solvent in an aqueous to organic phase ratio of 1:1. As seen in Fig. 3a, after the first 60 min of the hydrothermal reaction the FUR yield was increased up to four times by increasing the temperature from 170 to 190 °C. The highest FUR yield (78%) was reached at 190 °C in 3 h. The maximum selectivity (Fig. 3c) to FUR formation was 93%, 81% and 71% at temperatures of 170, 190 and 210 °C, respectively.

It can be seen, that at times longer than 120 min, the FUR yield obtained at 190 °C surpasses the FUR yield obtained at 210 °C. Under high reaction temperatures (210 °C) we assume that CPME does not extract FUR as efficiently. Therefore FUR tends to stay in

Fig. 3. Effect of temperature and reaction time on (a) FUR yield, (b) xylose conversion, (c) selectivity to FUR in the dehydration of 186 mmol l^{-1} xylose when using CPME as organic solvent with an aqueous to organic phase ratio of 1:1. Lines are to guide the eye.

the aqueous phase rather than in the organic phase, hence decomposition reactions of FUR occur faster.

When isophorone is used as water-immiscible solvent, the results are shown in Fig. 4. For the first 60 min of the treatment the FUR yield was increased up to four times by increasing the temperature from 170 to 190 °C when employing isophorone to aqueous fraction ratio of 1:1 (Fig. 4a). The highest FUR yield (49%) was reached at 190 °C in 3 h. The maximum selectivity (Fig. 4c) to FUR formation was 48%, 54% and 43% at temperatures of 170, 190 and 210 °C, respectively. A similar phenomenon occurred when employing isophorone as observed with CPME. Under high reaction temperatures (210 °C), FUR tends to stay in the aqueous phase rather than in isophorone, hence decomposition of FUR occurs faster. In comparison to the performance of isophorone to 2-MTHF and CPME (Fig. 5), it might be that FUR enters the organic phase but undergoes degradation in the presence of the solubilized water within isophorone. Afterwards FUR precipitates out once a certain molecular weight is reached.

Fig. 5 shows FUR yield, xylose conversion and selectivity to FUR when employing 2-MTHF. Fig. 5a shows that the first 60 min of the treatment the FUR yield was increased up to two times by increasing the temperature from 170 to 190 °C when employing 2-MTHF to aqueous fraction ratio of 1:1. The highest FUR yield (71%) was reached at 190 °C in 3 h. The maximum selectivity (Fig. 5c) to
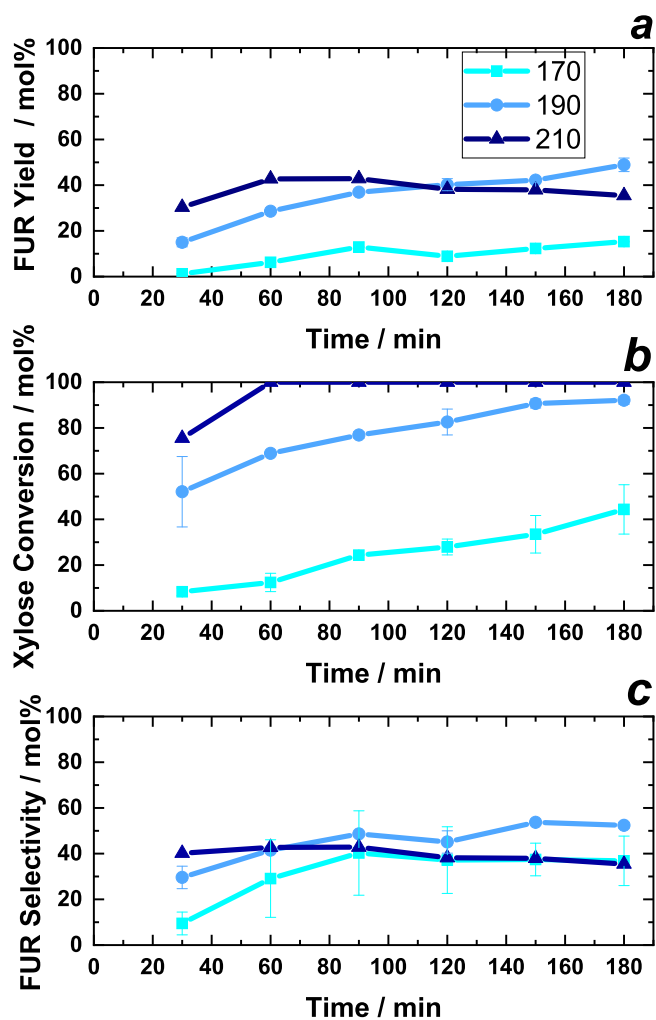
Fig. 4. Effect of temperature and reaction time on (a) FUR yield, (b) xylose conversion, (c) selectivity to FUR in the dehydration of 186 mmol l⁻¹ xylose when using isophorone as organic solvent with an aqueous to organic phase ratio of 1:1. Lines are to guide the eye.
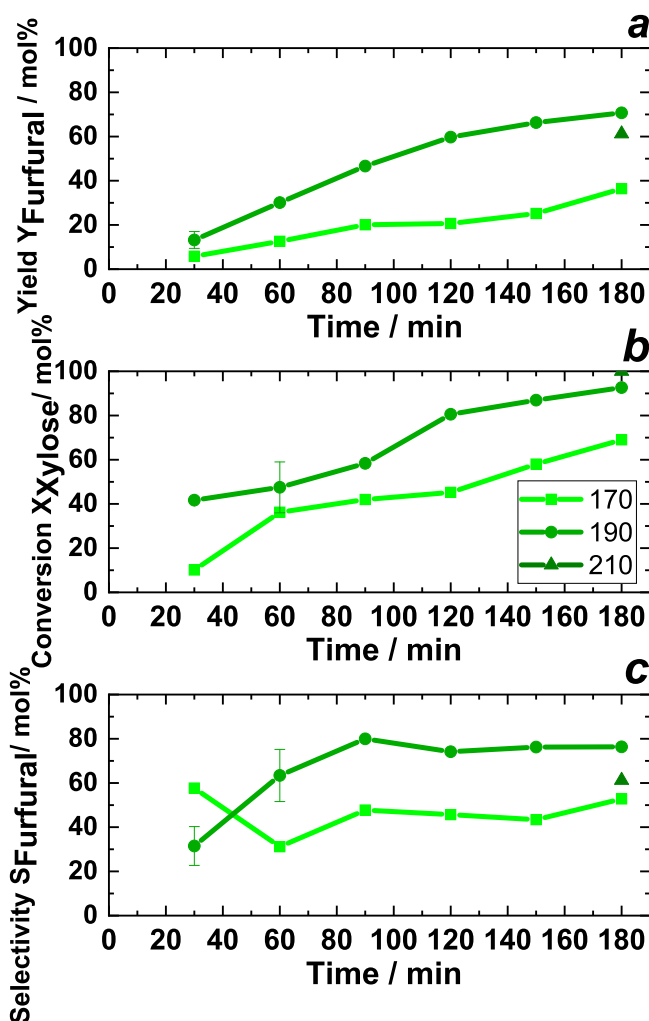
Fig. 5. Effect of temperature and reaction time on (a) FUR yield, (b) xylose conversion, (c) selectivity to FUR in the dehydration of 186 mmol l⁻¹ xylose when using 2-MTHF as organic solvent with an aqueous to organic phase ratio of 1:1. Lines are to guide the eye.

FUR formation was 58% and 80% at temperatures of 170 and 190 °C, respectively. Due to the low vapor pressure of 2-MTHF, reactions using this organic solvent at reaction temperatures of 210 °C were not possible to perform.

Recent research of the auto-catalyzed system in aqueous phase has been published under similar experimental conditions [33,60]. The maximum FUR yield (48–49%) was reached at reaction temperatures of 210 °C–220 °C in 1 h and 35 min, respectively, corresponding to a xylose conversion of 100% and 96%, respectively. It was observed that the FUR yield goes through a maximum and thereafter decreases with increasing reaction time. Decrease of FUR yield is due to the condensation and resinification reactions that take place between FUR and xylose [29,31,32], producing humins, which are detrimental to FUR yield. In contrast, when using pure organic solvent, recent studies have shown low solubility of xylose in CPME [57,61]. Le Guenic et al recently reported [61] a limited selectivity to FUR (2%) after the reaction took place at 170 °C in 40 min when using only CPME in monophase.

Furfural decomposition in the biphasic system

To increase understanding of the behavior of FUR under the conditions of microwave-assisted reaction in the presence of an

organic solvent, it is essential to know its degradation rate. The FUR degradation experiments were performed for the auto-catalyzed reactions using CPME and isophorone at the temperatures of 170, 190 and 210 °C. The experimental data showing the remaining fractions of FUR found in the aqueous and organic phases at various reaction times are presented in Fig. 6a and b, when adding isophorone and CPME, respectively. The figures illustrate the effect of the treatment temperature and the usage of 1:1 aqueous to organic phase ratio on the degradation rate of FUR. The results show a clear dependency of FUR degradation on the temperature, similarly to the data presented in earlier reports in monophasic systems [62–64]. It can be seen that when increasing the temperature the FUR degradation increases for both auto-catalyzed with isophorone and CPME. In addition, the results show that FUR is decomposed more rapidly in the presence of isophorone. The highest degree of degradation, 38%, was observed at 210 °C after 180 min. When CPME was employed as organic solvent, the highest degree of degradation was below 12%.

In order to confirm FUR decomposition in the presence of isophorone, a temperature level study was performed from 110 °C to 210 °C in 60 min when employing an aqueous to organic phase ratio of 1:1 (v/v). Fig. A3 (in the Supporting Information) shows that FUR decomposes linearly under the experimental conditions reaching the highest degree of degradation (24%) at 210 °C in 60 min.

Liquid–liquid equilibrium study

To get FUR from aqueous phase to organic phase the distribution should favor high solute distribution coefficients of FUR when defined as in Eq. (5)

$$K_i = \frac{w_{i,organic}}{w_{i,aqueous}} \tag{5}$$

where i refers to any component in the mixture. Isophorone-FUR-water data at 30, 50 and 70 °C was recently published by Ershova et al. [49] demonstrating that at the equilibrium state the aqueous phase contains around 1 wt% isophorone and around 0.8–3.8 wt% FUR, whereas the organic phase contains 4.5–6.4 wt% water. In contrast, CPME-FUR-water and 2-MTHF-FUR-water at 20, 50 and 70 °C have been recently reported [57]. At the equilibrium state of

2-MTHF-FUR-water the aqueous phase contains from 1 to 11 wt% 2-MTHF and approximately 1 to 9.9 wt% FUR, while the organic phase contains 4.8 to 8.8 wt%. In the case of CPME-FUR-water the aqueous phase contains less than 1 wt% CPME and around 1.7 to 11 wt% FUR, whereas the organic phase contains 0.8 to 6 wt% water.

In order to confirm the values predicted by the LLE model, one test in each biphasic system was performed at 190 °C in 120 min (black dot). These tests show the consistency of the model in both aqueous and organic phase in the three biphasic systems. Even though when CPME and 2-MTHF are employed, FUR in the aqueous phase is not fully in line with predicted data, the values are comparable to the predicted data. This small deviation could be due to small droplets of organic solvent in the aqueous sample. Figs. 7–9 summarize the measured (dots) and predicted (lines) LLE phase equilibrium.

From Figs. 7–9 it can be seen that the slope of tie-line changes from positive to negative as temperature increases. It means that the distribution coefficient of FUR is higher than one close to room temperature but at the reaction temperature of this work it is less than one. The calculated distribution coefficients are presented in Fig. 10.

Based only on liquid–liquid equilibria (LLE) 2-MTHF gives K values of FUR higher than one at 150 °C but CPME and isophorone less than one. At 170 °C and higher temperature all solvents give the K-value of FUR less than one. In industrial practice, this could mean that lower temperatures are preferred for the FUR to be extracted adequately by the organic phase.

In the present work from the three water-immiscible organic solvents studied, isophorone shows a higher distribution coefficient of FUR, however CPME demonstrates a higher selectivity towards FUR without decomposition. This suggests that FUR undergoes decomposition reactions, potentially including isophorone as a co-reactant. Alternatively, the rate of degradation of FUR may be increased by an increasing content of water at temperatures approaching 200 °C. These possibilities were investigated by NMR analysis of the degradation of FUR: isophorone molar ratios of 1:1 and 1:10 at 190 °C over 30 min and 120 min (Figures A4–A6 in the Supporting Information). Potential mechanisms for this degradation might be, for example, Diels–Alder cycloaddition (isophorone as hindered dienophile), Aldol condensation (isophorone C6 reacting as nucleophile at the FUR
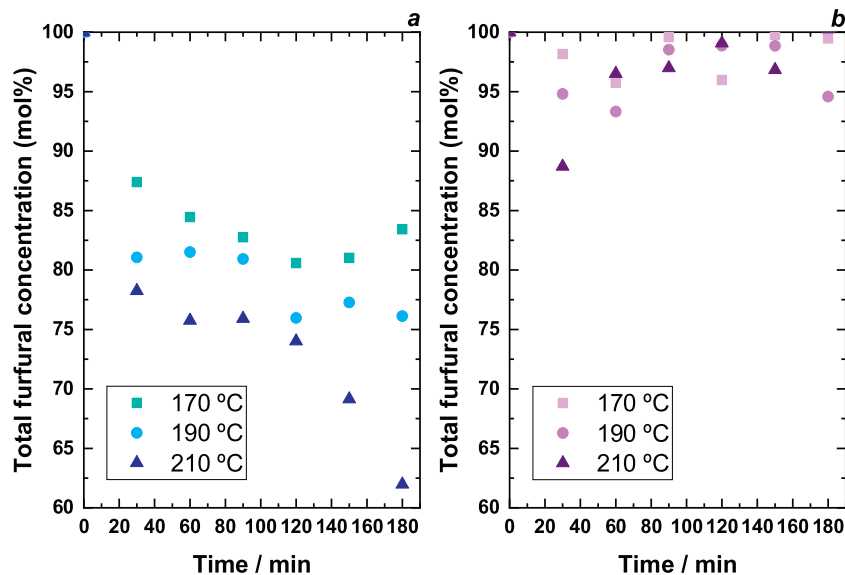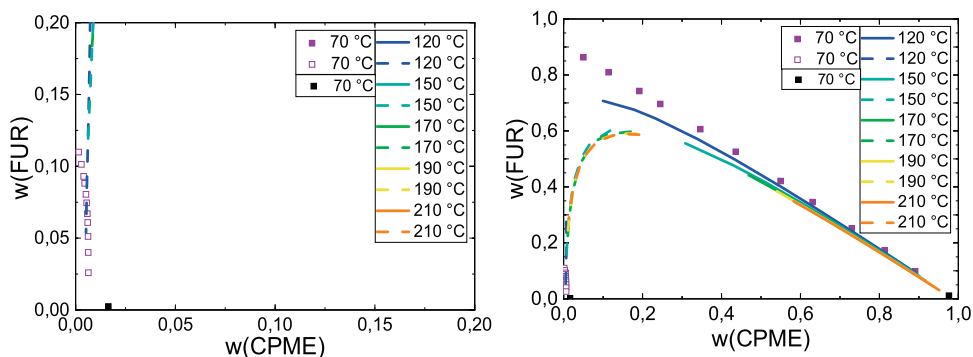

Fig. 6. The remaining furfural at various reaction times during auto-catalyzed degradation when employing isophorone (a) and CPME (b) to aqueous phase of 1:1 (v/v). The decomposition of furfural was determined for a solution of 5 wt% furfural (squares - 170 °C, circles - 190 °C, triangle - 210 °C).

Fig. 7. CPME and FUR binary LLE in mass fractions at atmospheric pressure. 70 °C Männisto et al., [50] 120–210 °C lines are extrapolated based on UNIQUAC model, filled symbol and solid line - organic (upper) phase, open symbol and dashed line - aqueous (lower) phase. Left figure shows the aqueous phase enlarged.
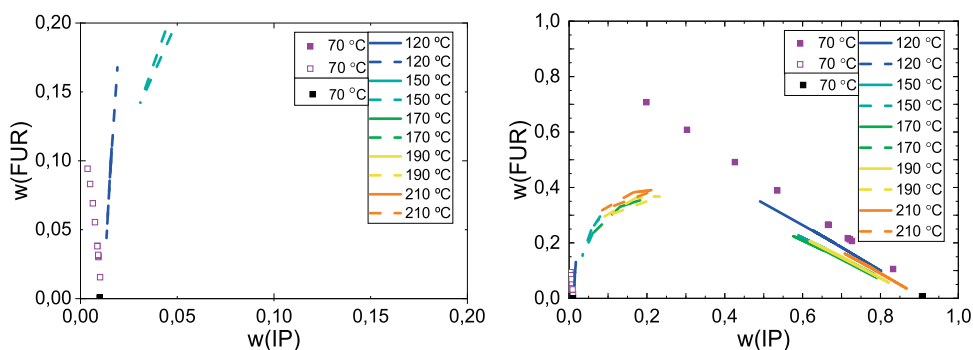
Fig. 8. Isophorone (IP) and FUR binary LLE in mass fractions at atmospheric pressure. 70 °C symbols from Ershova et al. [49], 120–210 °C lines are extrapolated based on UNIQUAC model, filled symbol and solid line − organic (upper) phase, open symbol and dashed line − aqueous (lower) phase. Left figure shows the aqueous phase enlarged.
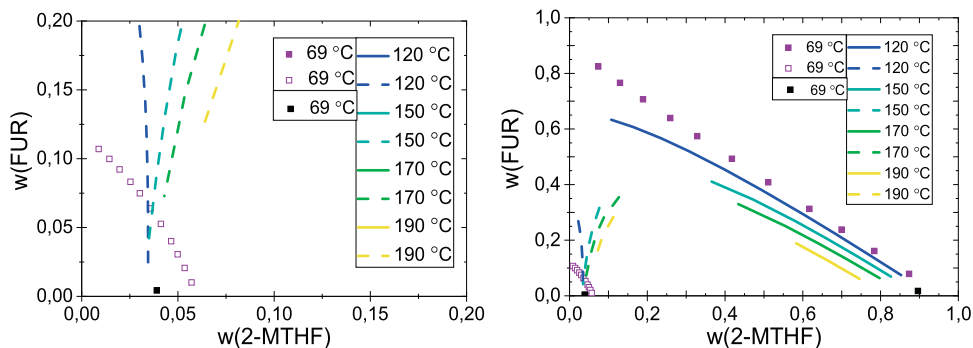
Fig. 9. 2-MTHF and FUR binary LLE in mass fractions at atmospheric pressure. 70 °C symbols from Männisto et al. [50], 120–210 °C lines are extrapolated based on UNIQUAC model, filled symbol and solid line − organic (upper) phase, open symbol and dashed line − aqueous (lower) phase. Left figure shows the aqueous phase enlarged.

aldehyde), Baylis–Hillman reaction (isophorone C2 reacting as nucleophile at the FUR aldehyde) and Michael addition (isophorone C3 as α-β unsaturated electrophile). Other reactivity may of course be possible [65–67].

Despite colourisation of the solutions after heating, ^{1}H NMR analysis (in DMSO-d_6 at 27 °C) showed that no new decomposition products were formed in significant quantities (Supporting Information Figures A7 and A8) and no precipitate was visible that might indicate significant condensation of FUR. Presence of water in the organic phase is another potential reason for losses of FUR. However, there is no literature LLE data available for water and isophorone at the higher temperatures studied. The maximum temperatures quoted in the literature are only up to 70 °C [49]. The changing miscibility of water and isophorone up to 190 °C was crudely assessed by heating a mixture of isophorone (1 ml) and water (1 ml) in sealed narrow bore sample vials from 110 °C to

190 °C, with 5 min equilibration time every 10 °C (Figure A7 in the Supporting Information). At room temperature and even up to 110 °C the mixtures clearly form separate phases. However, as the temperature exceeds 150 °C the organic phase becomes cloudy, indicating dispersion of water into the phase. This phenomenon may be a result of increased hydrate (hemiketal) formation at the elevated temperatures or simply kinetic dispersion of clusters into the organic phase. These explanations, however, are speculative in the absence of accurate LLE data and require further studies to understand this phenomenon.

Further NMR experiments were also carried out after heating equivolume mixtures of FUR:H$_2$O, FUR:isophorone, FUR:H$_2$O:isophorone and Xylose:H$_2$O:isophorone at 210 °C for 3 h. The FUR:H$_2$O mixtures quickly degraded and formed a dark precipitate, from condensation of the FUR. All other mixtures colourised to some degree but did not form precipitate. The organic phases of
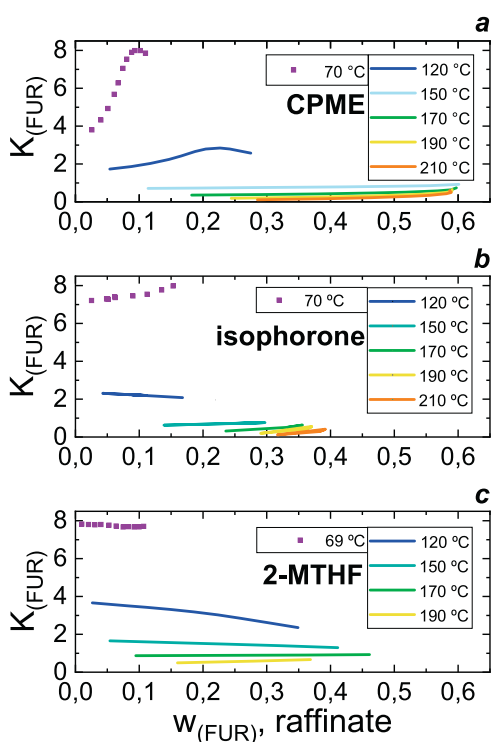
Fig. 10. Distribution coefficient K for FUR in raffinate in the system when: (a) CPME, (b) isophorone and (c) 2-MTHF are added to the system, where lines are extrapolated based on UNIQUAC model.

each reaction were separated and evaporated to almost complete dryness by heating with a heat-gun (<150 °C) under oil pump vacuum with N_2 trap, to remove the majority of the volatiles (trace water, FUR or isophorone). The residues and also the solids from the FUR:H_2O mixture were added to DMSO-d_6 for NMR analysis. A multiplicity-edited HSQC and HSQC-TOCSY were recorded for the FUR:isophorone residue (Figure A8). This showed resonances characteristic of trace FUR and isophorone, in addition to several other low molecular weight decomposition products or impurities. The main visible TOCSY correlations between the main aliphatic region (1–2.5 ppm in ^{1}H) and the FUR CH region (5.5–10 ppm in ^{1}H) seem to be between 2-CH and 3CMe or 4-CH_2 on isophorone, or related compounds. Thus, there does not see to be any low molecular weight species that show obvious linkages between FUR and isophorone. However, this is not absolute proof that they do not exist and further inspection of the ^{1}H spectrum (Figure A9, top) shows that the low molecular weight aldehyde (CHO) functionalities are largely missing indicating potential linkage at the aldehyde functionality on FUR.

When a diffusion-edited ^{1}H experiment for the same sample is measured, compared to the standard ^{1}H experiment (Figure A9), it is clear to see that there is polymeric material in the DMSO-d_6 solution. Diffusion-editing has the effect of removal of the low molecular weight resonances and retention of the polymeric resonances [68]. The retained signals in the soluble organic fraction from the FUR:isophorone reaction correspond to both polymerised FUR and isophorone. Unfortunately, relaxation of these polymeric signals are too fast and abundances are too low so that we do not see the correlations to any significant degree, by HSQC or HSQC-TOCSY. Therefore, this makes it unclear if the FUR and isophorone-derived resonances are present due to co-precipitation or covalent linkage between the two moieties. If we compare the ^{1}H spectrum from the isolated solids from the FUR:H_2O reaction against the diffusion-edited ^{1}H spectra for the soluble fractions in the FUR:H_2O and FUR:isophorone reactions

(Figure A10) it is clear that all mixtures contain polymeric material. In the case of the solids fraction from the FUR:H_2O reaction, the sample only partially dissolved in DMSO-d_6 indicating that there is a much higher molecular weight cross-linked polymer present. However, the spectrum looks very similar to that of the soluble fraction of the corresponding FUR:H_2O reaction, except for the presence of the H_2O and DMSO peaks (standard ^{1}H experiment – not diffusion-edited). The diffusion-edited ^{1}H spectrum for the soluble organic fraction of the FUR:isophorone reaction contains a similar FUR CH region but is missing the aldehyde (CHO), likely attributable to the FUR aldehyde functionality on a polymerised furan backbone. In addition, there is the major contribution of the aliphatics, attributable to isophorone moieties. This might indicate that the aldehydes are an attachment point for isophorone to the polymerised furans. Reaction of isophorone at the aldehyde functionality of FUR is most likely via a Baylis–Hillman or Aldol type reaction. However, some isophorone 2-CH (5.8 ppm) is clearly still present in the polymeric fraction, so a combination of these and other possible mechanisms may be responsible.

When the diffusion-edited ^{1}H spectra for FUR:isophorone, FUR:H_2O:isophorone and Xylose:H_2O:isophorone are compared (Figure A11) we see some further changes from the inclusion of water with organics. The peak shape of the aliphatics change indicating new mechanisms of polymerisation. Aldehydes, FUR CHs isophorone 2-CH and acetals are missing. However, this may be due to the formation of a rigid enough polymer backbone that the signals relax before the collection phase of the NMR experiments pulse sequence. Alternatively, a Diels–Alder-type or other cycloaddition reactions may be induced, which would lead to formation of aliphatic resonances. Water may have a significant effect here as formation of FUR hemiacetal would increase its reactivity, as a diene towards [4 + 2] cycloaddition, under the conventional Diels Alder HOMO-LUMO energy ordering. After all, water is well-known to have a rate-enhancing effect on the Diels–Alder reaction [69]. While this NMR result is inconclusive, clearly there is polymer forming to some degree from polymerisation of FUR and/or isophorone in the presence of water.

While none of these NMR studies give measures of increased degradation of FUR, it shows that:

1. water does have a significant effect on the condensation of FUR [31,32]
2. isophorone may allow for increased miscibility with water at higher temperatures, which may lead to increased degradation kinetics of FUR
3. *co*-polymerisation of isophorone and FUR is likely occurring, which may lead to increased losses of both FUR and isophorone to some degree. This may be highly temperature dependent

Clearly more in-depth studies are required to isolate suitable polymeric fractions that might allow for more detailed NMR studies, to trace spin-systems between FUR and isophorone moieties, and to avoid the effects of transverse relaxation (T_2) which reduces the quantity of the diffusion-edited ^{1}H experiment.

Furfural production from birch hydrolysate

The production of FUR from birch hydrolysate was studied under optimized conditions for the dehydration of C_5 sugars (190 °C, 1:1 aqueous to CPME phase ratio (v/v), under microwave irradiation). The initial composition of the birch hydrolysate is given in Table A1 (in the Supporting Information).

The FUR yield increased from 37% to 68% with an increasing time from 30 to 90 min at 190 °C when employing an aqueous to CPME phase ratio of 1:1 (v/v) (Fig. 11). The highest mole fraction of hydroxymethylfurfural (HMF) was 0.01 mmol (Figure A12 in the
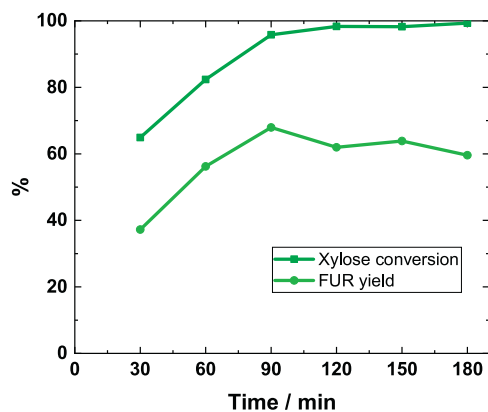
Fig. 11. Xylose conversion and FUR yield from birch hydrolysate as a function of time at 190 °C under microwave irradiation. Biphasic reaction system: Aqueous phase = hydrolysate liquor after filtration (1.5 ml), organic phase: CPME (1.5 ml). Lines are to guide the eye.

Supporting Information), which is in agreement with previous studies when using birch hydrolysate to produce FUR from pentoses [70].

Conclusion

In a two-phase system with three different water-immiscible organic solvents, the dehydration reaction of xylose and the resulting furfural yields were investigated under well-controlled conditions.

The optimum aqueous-to-organic phase ratio for all three tested organic solvents was 1:1 to extract FUR in the dehydration of xylose. The main product of auto-catalyzed and solid acid-catalyzed xylose dehydration was FUR, whose maximum mole fraction yield at 190 °C in 180 min was 78% in the case of CPME as an organic solvent phase. The highest selectivity to FUR, namely 93%, was achieved in 90 min at 170 °C when CPME was added.

In the case of birch hydrolysate as pentose source, a maximum FUR yield of 68% (and a xylose conversion of 96%) after 90 min in auto-catalyzed reaction at 190 °C was achieved under the optimized conditions of a two-phase dehydration reaction in the presence of CPME in a volume ratio of 1:1.

The results of the experiments when using isophorone as organic solvent allowed us to conclude that there are decomposition reactions between the solvent and FUR above 110 °C, which may or may not be linked to an increase on water solubility at elevated temperatures. Therefore, even though isophorone shows a higher partition coefficient in the biphasic system, it should be employed at temperatures below the conditions stated in the present study.

Studies on the in-situ extraction of FUR involving solvents that are not miscible with water show a high selectivity to FUR and thus its yield increases. This offers an interesting approach for a greener process and the avoidance of salt addition.

Acknowledgements

Appendix A. Supplementary data

Supplementary data associated with this article can be found, in the online version, at https://doi.org/10.1016/j.jiec.2018.12.037.

References

[1] L. Filiciotto, A.M. Balu, J.C. Van der Waal, R. Luque, Catal. Today 302 (2018) 2.
[2] A. Griebl, T. Lange, H. Weber, W. Milacher, H. Sixta, Macromol. Symp. 232 (2006) 107.
[3] L. Yang, J. Su, S. Carl, J.G. Lynam, X. Yang, H. Lin, Appl. Catal B: Environ. 162 (2015) 149.
[4] T. Werpy, G. Petersen, Top Value Added Chemicals from Biomass: Volume I – Results of Screening for Potential Candidates from Sugars and Synthesis Gas, Sponsor Org.: US Department of Energy (US), 2004.
[5] S. Peleteiro, S. Rivas, J.L. Alonso, V. Santos, J.C. Parajó, Bior. Technol. 202 (2016) 181.
[6] R.F. Perez, S.J. Canhaci, L.E.P. Borges, M.A. Fraga, Catal. Today 289 (2017) 273.
[7] X. Chen, L. Zhang, B. Zhang, X. Guo, X. Mu, Sci. Rep. 6 (2016) 28558.
[8] K.J. Zeitsch, in: K.J. Zeitsch (Ed.), The Chemistry and Technology of Furfural and its Many by-Products, Elsevier B.V, 2000, pp. 98.
[9] R. Mariscal, P. Maireles-Torres, M. Ojeda, I. Sadaba, M. Lopez Granados, Energy Environ. Sci. 9 (2016) 1144.
[10] B. Kamm, P.R. Gruber, M. Kamm, Biorefineries — Industrial Processes and Products: Status Quo and Future Directions, Wiley-VCH, 2010.
[11] S.B. Kim, S.J. You, Y.T. Kim, S. Lee, H. Lee, K. Park, E.D. Park, Korean J. Chem. Eng. 28 (2011) 710.
[12] F. Xue, C. Miao, Y. Yue, W. Hua, Z. Gao, Green Chem. 19 (2017) 5582.
[13] S.M. Bruce, Z. Zong, A. Chatzidimitriou, L.E. Avci, J.Q. Bond, M.A. Carreon, S.G. Wettstein, J. Mol. Catal. A: Chem. 422 (2016) 18.
[14] T. Ennaert, J. Van Aelst, J. Dijkmans, R. De Clercq, W. Schutyser, D. Verboekend, B.F. Sels, Chem. Soc. Rev. 45 (2016) 584.
[15] L.J. Konwar, P. Mäki-Arvela, E. Salminen, N. Kumar, A.J. Thakur, J. Mikkola, D. Deka, Appl. Catal. B: Environ. 176–177 (2015) 20.
[16] P.S. Metkar, E.J. Till, D.R. Corbin, C.J. Pereira, K.W. Hutchenson, S.K. Sengupta, Green Chem. 17 (2015) 1453.
[17] M. Paniagua, S. Saravanamurugan, M. Melian-Rodriguez, J.A. Melero, A. Riisager, ChemSusChem 8 (2015) 1088.
[18] J. Lessard, J. Morin, J. Wehrung, D. Magnin, E. Chornet, Top. Catal. 53 (2010) 1231.
[19] L.R. Ferreira, S. Lima, P. Neves, M.M. Antunes, S.M. Rocha, M. Pillinger, I. Portugal, A.A. Valente, Chem. Eng. J. 215–216 (215) (2013) 772.
[20] S. Lima, M.M. Antunes, A. Fernandes, M. Pillinger, M.F. Ribeiro, A.A. Valente, Appl. Catal. A: Gen. 388 (2010) 141.
[21] B. Garg, T. Bisht, Y. Ling, Molecules 19 (2014).
[22] E. Lam, J.H. Chong, E. Majid, Y. Liu, S. Hrapovic, A.C.W. Leung, J.H.T. Luong, Carbon 50 (2012) 1033.
[23] S. Suganuma, K. Nakajima, M. Kitano, H. Kato, A. Tamura, H. Kondo, S. Yanagawa, H. Hayashi, M. Hara, Microporous Mesoporous Mater. 143 (2011) 443.
[24] E. Lam, E. Majid, A.C.W. Leung, J.H. Chong, K.A. Mahmoud, J.H.T. Luong, ChemSusChem 4 (2011) 535.
[25] A.S. Dias, S. Lima, M. Pillinger, A.A. Valente, Catal. Lett. 114 (2007) 151.
[26] S.J. You, Y.T. Kim, E.D. Park, Mech. Catal. 111 (2014) 521.
[27] E. Sairanen, K. Vilonen, R. Karinen, J. Lehtonen, Top. Catal. 56 (2013) 512.
[28] V.K. Ahluwalia, M. Kidwai, in: V.K. Ahluwalia, M. Kidwai (Eds.), New Trends in Green Chemistry, Springer Netherlands, Dordrecht, 2004, pp. 5.
[29] I. vanZandvoort, Y. Wang, C.B. Rasrendra, E.R.H. vanEck, P.C.A. Bruijnincx, H.J. Heeres, B.M. Weckhuysen, ChemSusChem 6 (2013) 1745.
[30] H. Rasmussen, H.R. Sørensen, A.S. Meyer, Carbohydr. Res. 385 (2014) 45.
[31] C. Sener, A.H. Motagamwala, D.M. Alonso, J.A. Dumesic, ChemSusChem 11 (2018) 2321.
[32] M.A. Mellmer, C. Sener, J.M.R. Gallo, J.S. Luterbacher, D.M. Alonso, J.A. Dumesic, Angew. Chem. Int. Ed. 53 (2014) 11872.
[33] G. Gómez Millán, Z. El Assal, K. Nieminen, S. Hellsten, J. Llorca, H. Sixta, Fuel Process. Technol. 182 (2018) 56.
[34] R. Weingarten, J. Cho, J. Conner WmCurtis, G.W. Huber, Green Chem. 12 (2010) 1423.
[35] F. Trimble, A.P. Dunlop, Ind. Eng. Chem. Anal. Ed. 12 (1940) 721.
[36] E.I. Gürbüz, S.G. Wettstein, J.A. Dumesic, ChemSusChem 5 (2012) 383.
[37] J. Zhang, J. Zhuang, L. Lin, S. Liu, Z. Zhang, Biomass Bioenergy 39 (2012) 73.
[38] P.L. Dhepe, R. Sahu, Green Chem. 12 (2010) 2153.
[39] A. Mittal, S.K. Black, T.B. Vinzant, M. O'Brien, M.P. Tucker, D.K. Johnson, ACS Sustainable Chem. Eng. 5 (2017) 5694.
[40] A.S. Dias, S. Lima, M. Pillinger, A.A. Valente, Carbohydr. Res. 41 (2006) 2946.
[41] X. Guo, F. Guo, Y. Li, Z. Zheng, Z. Xing, Z. Zhu, T. Liu, X. Zhang, Y. Jin, Appl. Catal. A: Gen. 558 (2018) 18.
[42] H. Li, A. Deng, J. Ren, C. Liu, W. Wang, F. Peng, R. Sun, Catal. Today 234 (2014) 251.
[43] D.M. Argyle, H.C. Bartholomew, Catalysts 5 (2015).
[44] J.E. Romo, N.V. Bollar, C.J. Zimmermann, S.G. Wettstein, ChemCatChem 10 (2018) 4805.
[45] K. Watanabe, Molecules 18 (2013).

[46] S. Tenne, J. Kinzel, M. Arlt, F. Sibilla, M. Bocola, U. Schwaneberg, J. Chromatogr. B. 937 (2013) 13.
[47] M.J. Campos Molina, R. Mariscal, M. Ojeda, M. López Granados, Bioresour. Technol. 126 (2012) 321.
[48] S. Tenne, U. Schwaneberg, Int. J. Mol. Sci. 13 (2012).
[49] O. Ershova, J. Pokki, A. Zaitseva, V. Alopaeus, H. Sixta, Chem. Eng. Sci. 176 (2018) 19.
[50] M. Männistö, J. Pokki, V. Alopaeus, J. Chem. Thermodyn. 119 (2018) 61.
[51] V. Pace, W. Holzer, P. Hoyos, M.J. Hernáiz, A.R. Alcántara, in: P.L. Fuchs (Ed.), Encyclopedia of Reagents for Organic Synthesis, John Wiley & Sons Ltd., 2001, pp. 1.
[52] K. Lamminpää, J. Ahola, J. Tanskanen, Ind. Eng. Chem. Res. 51 (2012) 6297.
[53] K. Dussan, B. Girisuta, M. Lopes, J.J. Leahy, M.H.B. Hayes, ChemSusChem 9 (2016) 492.
[54] A. Sluiter, B. Hames, R. Ruiz, C. Scarlata, J. Sluiter, D. Templeton, Determination of Sugars, Byproducts, and Degradation Products in Liquid Fraction Process Samples, Technical Report NREL/TP-510-42623, (2008) .
[55] S. Givry, C. Bliard, F. Duchiron, Carbohydr. Res. 342 (2007) 859.
[56] C. Pirola, I. Rossetti, V. Ragaini, La Chimica L'Industria 2 (2013) 136.
[57] M. Männistö, J. Pokki, L. Fournis, V. Alopaeus, J. Chem. Thermodyn. 110 (2017) 127.
[58] S.L. Guenic, F. Delbecq, C. Ceballos, C. Len, J. Mol. Catal. A: Chem. 410 (2015) 1.
[59] B. Danon, W. Hongsiri, L. van der Aa, W. de Jong, Biomass Bioenergy 66 (2014) 364.
[60] O. Ershova, J. Kanervo, S. Hellsten, H. Sixta, RSC Adv. 5 (2015) 66727.
[61] S. Le Guenic, D. Gergela, C. Ceballos, F. Delbecq, C. Len, Molecules 21 (2016).
[62] G. Marcotullio, W. de Jong, Int. J. Chem. Reactor Eng. 7 (1) (2009) A67.
[63] B. Danon, L. van der Aa, W. de Jong, Carbohydr. Res. 375 (2013) 145.
[64] K. Lamminpää, J. Ahola, J. Tanskanen, RSC Adv. 4 (2014) 60243.
[65] S. Thiyagarajan, H.C. Genuino, M. Sliwa, Jan C. van der Waal, E. de Jong, J. van Haveren, B.M. Weckhuysen, P.C.A. Bruijnincx, D.S. van Es, ChemSusChem 8 (2015) 3052.
[66] T. Shanmugam, H.C. Genuino, J.C. van der Waal, E. de Jong, B.M. Weckhuysen, J. van Haveren, P.C. Bruijnincx, D.S. van Es, Angew. Chem. Int. Ed. 55 (2016) 1368.
[67] H.C. Genuino, T. Shanmugam, J.C. van der Waal, ChemSusChem 10 (2017) 277.
[68] A.W.T. King, V. Mäkelä, S.A. Kedzior, T. Laaksonen, G.J. Partl, S. Heikkinen, H. Koskela, H.A. Heikkinen, A.J. Holding, E.D. Cranston, I. Kilpeläinen, Biomacromol 19 (2018) 2708.
[69] D.C. Rideout, R. Breslow, J. Am. Chem. Soc. 102 (1980) 7817.
[70] O. Ershova, K. Nieminen, H. Sixta, ChemCatChem 9 (2017) 3031.

Supplementary Information

Gerardo Gómez Millán[a,b], Sanna Hellsten[a], Alistair W.T. King[c], Juha-Pekka Pokki[d], Jordi Llorca[b], Herbert Sixta[a,*]

[a]Department of Bioproducts and Biosystems, Aalto University, Vuorimiehentie 1, 02150 Espoo, Finland

[b]Department of Chemical Engineering, Institute of Energy Technologies and Barcelona Research Center in Multiscale Science and Engineering, Universitat Politècnica de Catalunya, Eduard Maristany 10-14, 08019 Barcelona, Spain

[c]Materials Chemistry Division, Chemistry Department, University of Helsinki, AI Virtasen Aukio 1, Helsinki, Finland

[d]Department of Chemical and Metallurgical Engineering, School of Chemical Engineering, Aalto University, PL 16100, 00076 Espoo, Finland

*Corresponding author at: Department of Bioproducts and Biosystems, Aalto University, Vuorimiehentie 1, 02150 Espoo, Finland.

Herbert Sixta: herbert.sixta@aalto.fi

1. Birch hydrolysate composition

Table A1. Initial composition of the birch hydrolysate after filtration

	Monomeric form, g l⁻¹	Total, g l⁻¹
Arabinose	0.63	0.66
Rhamnose	0.47	0.83
Galactose	0.50	1.29
Glucose	0.16	1.12
Xylose	8.05	26.15
Mannose	0.17	1.63
Lignin		4.20
HMF		0.04
Furfural		2.43

2. Modelling

The GC-analysis of the samples requires converting the peak areas into mass fractions through the response factors. These were made by weighing known quantities of isobutanol (i-BuOH) and they were added as an internal standard. This allowed connecting the peak areas of other components into the i-BuOH peak area. The response factors were calculated from the FID results. The response factors were calculated with Eq. (A1) and their uncertainty with Eq. (A2).

$$F_i = F_{std} \times \frac{A_{std}}{A_i} \times \frac{m_i}{m_{std}} \tag{A1}$$

$$\Delta F_i = \sqrt{\left(\frac{\delta F_i}{\delta A_i} \times \frac{\Delta A_i}{\mu V \cdot s}\right)^2 + \left(\frac{\delta F_i}{\delta A_{std}} \times \frac{\Delta A_{std}}{\mu V \cdot s}\right)^2 + \left(\frac{\delta F_i}{\delta m_i} \times \frac{\Delta m_{balance}}{g}\right)^2 + \left(\frac{\delta F_i}{\delta m_{std}} \times \frac{\Delta m_{balance}}{g}\right)^2} \tag{A2}$$

A_i, A_{std}, ΔA_i and ΔA_{std} refer to peak areas and calculated uncertainties for the component i and the standard respectively. F_{std} refers to i-BuOH response factor, which is set to 1. Notations m_i, m_{std} and $\Delta m_{balance}$ refer to masses of component i and standard and to the uncertainty of the mass in the weightings of the standards. The measured and predicted LLE area is based on the previous works[1, 2] where the ternary LLE from 298 K to 343 K was measured and the parameters of UNIQUAC activity coefficient model was optimized.

3. Furfural formation analysis
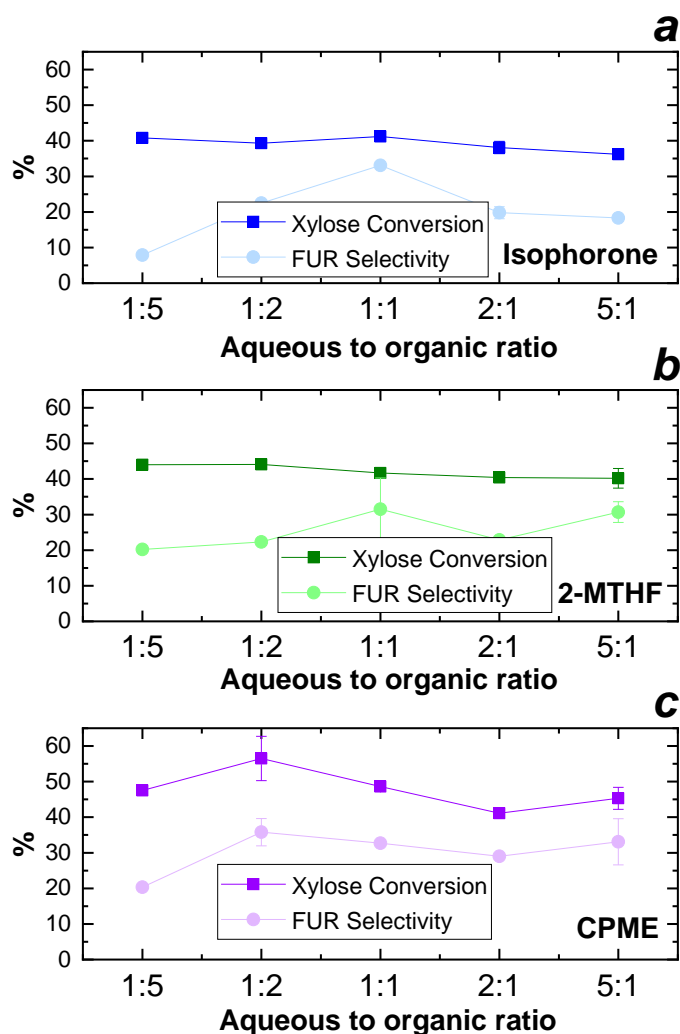
Figure A1. Effect of aqueous-to-organic ratio on xylose conversion and FUR selectivity when using (a) isophorone, (b) 2-MTHF and (c) CPME as organic phase. The effect was determined for a solution of xylose (186 mmol l^{-1}) heated at 190 °C in 30 min at five different ratios of aqueous to organic solvent: 1:5, 1:2, 1:1, 2:1, 5:1 (v/v). The error bars shown are one standard deviation from duplicate analyses.
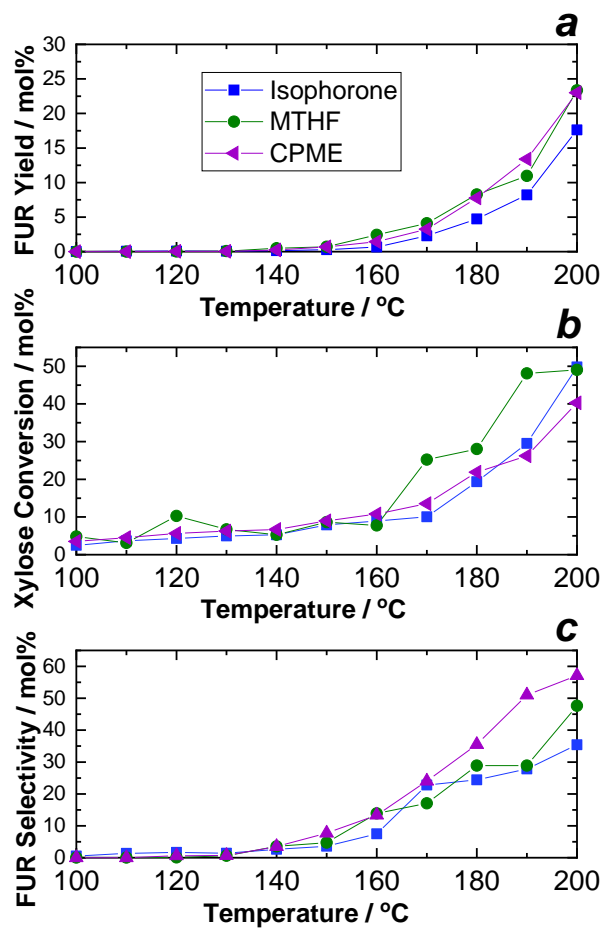
Figure A2. Effect of reaction temperature on (a) furfural yield, (b) xylose conversion, (c) selectivity to furfural in the dehydration of 186 mmol l^{-1}. Blue squares - isophorone, green circles – 2-MTHF, purple triangles – CPME. Aqueous ratio to organic solvent was 5:1, lines are to guide the eye.

4. Furfural decomposition
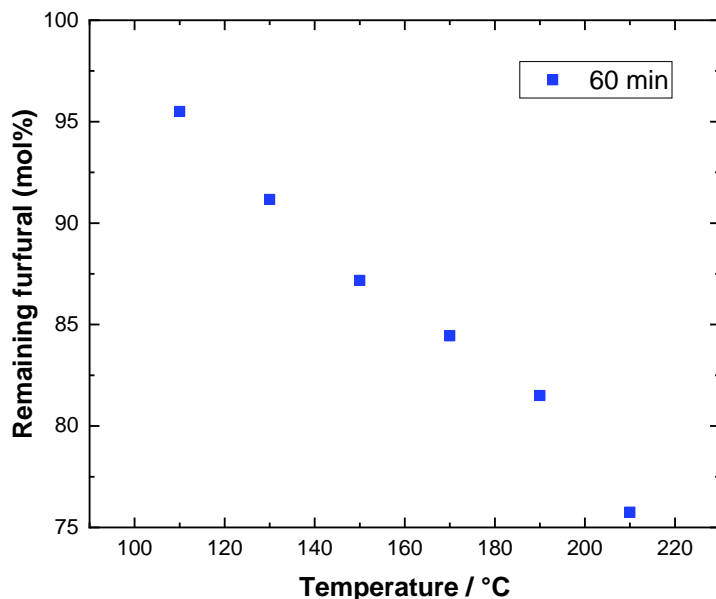
Figure A3. The remaining furfural (mol%) at various reaction temperatures (110, 130, 150, 170, 190 and 210 °C) during auto-catalyzed degradation when employing isophorone to aqueous phase ratio of 1:1 (v/v) in 60 min. The decomposition of furfural was determined for a solution of 5 wt% furfural.

5. ^{1}H NMR analysis

DMSO-d_6 (990 mg) was added to the sample (10 mg) in a sample vial. The mixture was shaken and then 600 μL was transferred to a 5 mm NMR tube for analysis. The experiments were performed using a Varian ^{UNITY} *INOVA* 600 MHz spectrometer equipped with 5 mm triple resonance probe-head. Spectral width was 6634 Hz. The transmitter offset was 5.5 ppm. The pulse flip angle was 45 °. The relaxation delay was 1 s and acquisition time was 1.25 s. DMSO-d_6 in the sample was used as locking solvent, and 32 transients were collected. The experiment temperature was maintained at 27 °C. The processed spectra, are shown in Figure A4-A6.
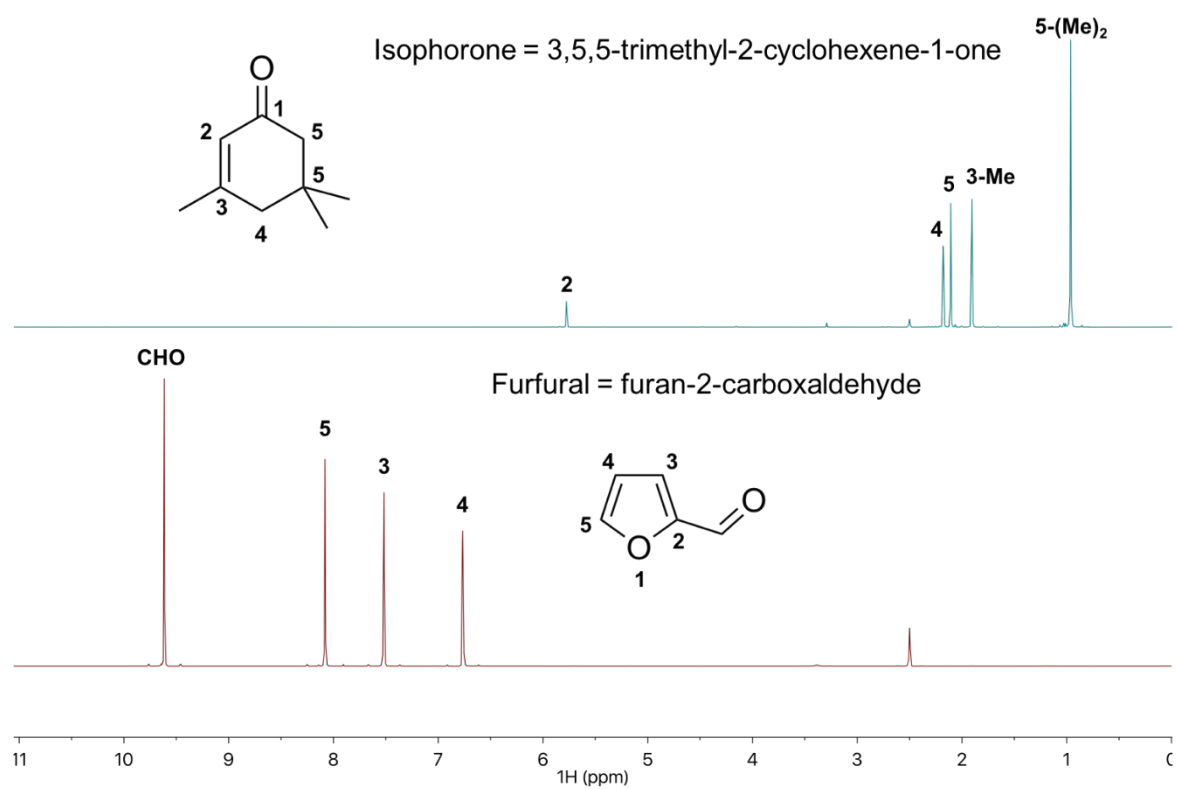
Figure A4. Initial assignment of furfural and isophorone peaks in the ¹H NMR spectra (DMSO-d₆ at 27 °C)
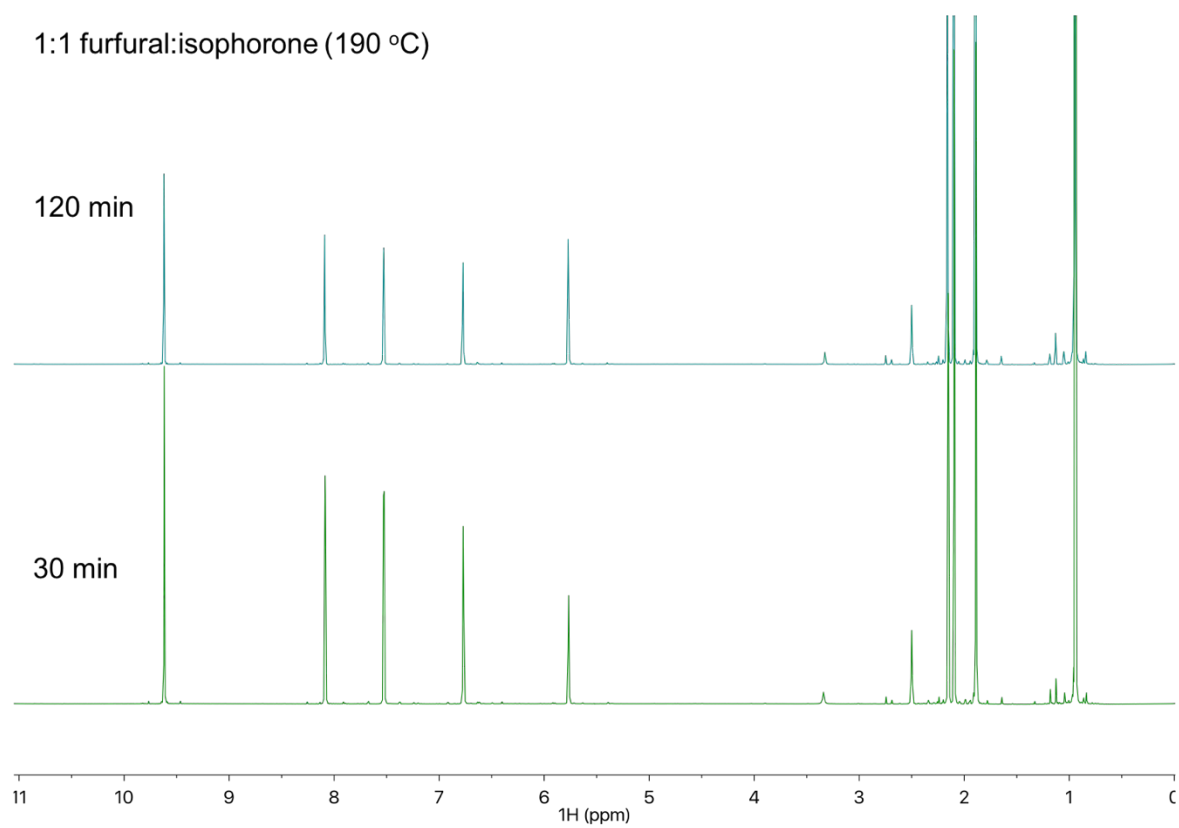
Figure A5. ^{1}H NMR spectra (DMSO-d$_6$ at 27 $^\circ$C) of 1:1 molar equivalents of FUR:isophorone heated at 190 $^\circ$C for 30 and 120 min.
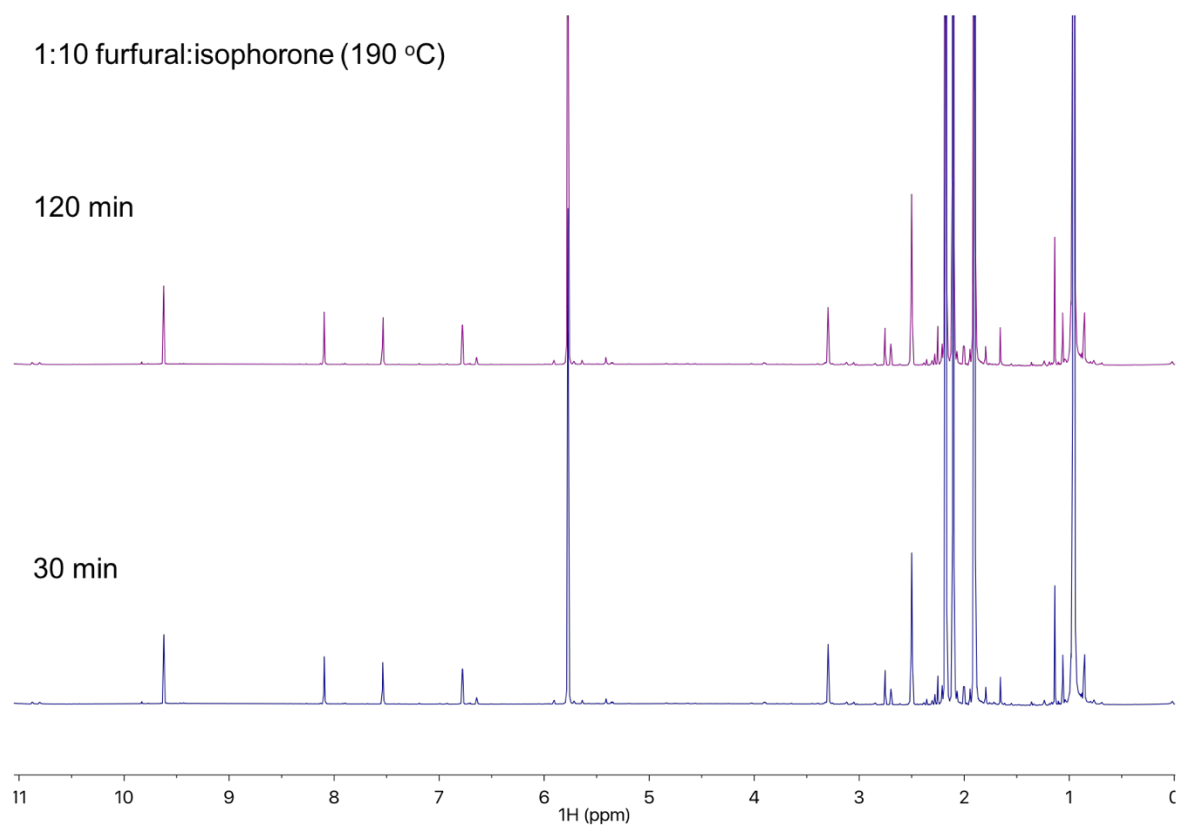
Figure A6. ^{1}H NMR spectra (DMSO-d_6 at 27 °C) of 1:10 molar equivalents of FUR:isophorone heated at 190 °C for 30 and 120 min.

6. Isophorone-water phase behaviour

The changing miscibility of water and isophorone up to 190 C was crudely assessed by heating a mixture of isophorone (1 ml) and water (1 ml) in sealed narrow bore sample vials (Fig. A7) from 110 °C to 190 °C, with 5 min equilibration time every 10 °C. At room temperature and even up to 110 °C the mixtures clearly form separate phases.
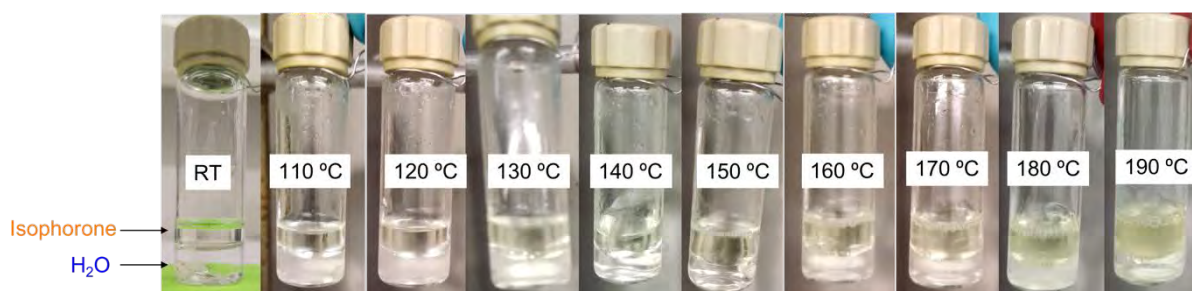
Figure A7. Phase-behaviour of 1:1 v/v FUR:isophorone from 110-190 °C.
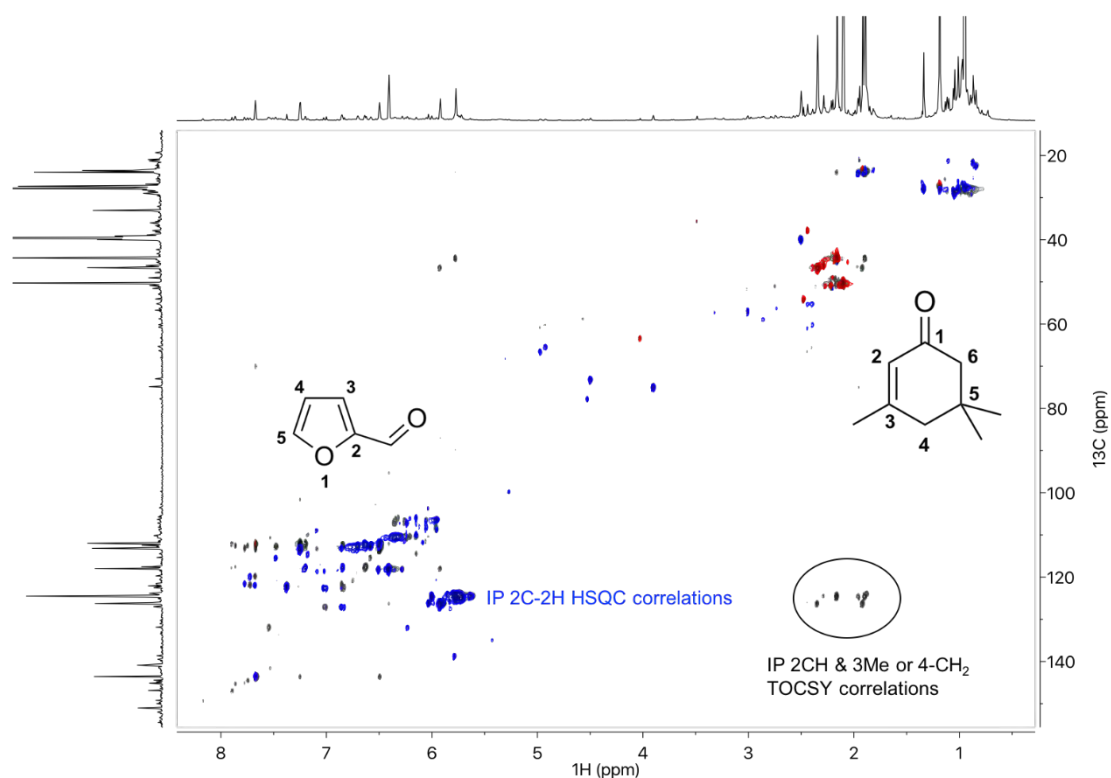
Figure A8. 2D [^{13}C,^{1}H] HSQC-TOCSY of FUR:isophorone 1:1 molar heated at 210 °C for 3 h.
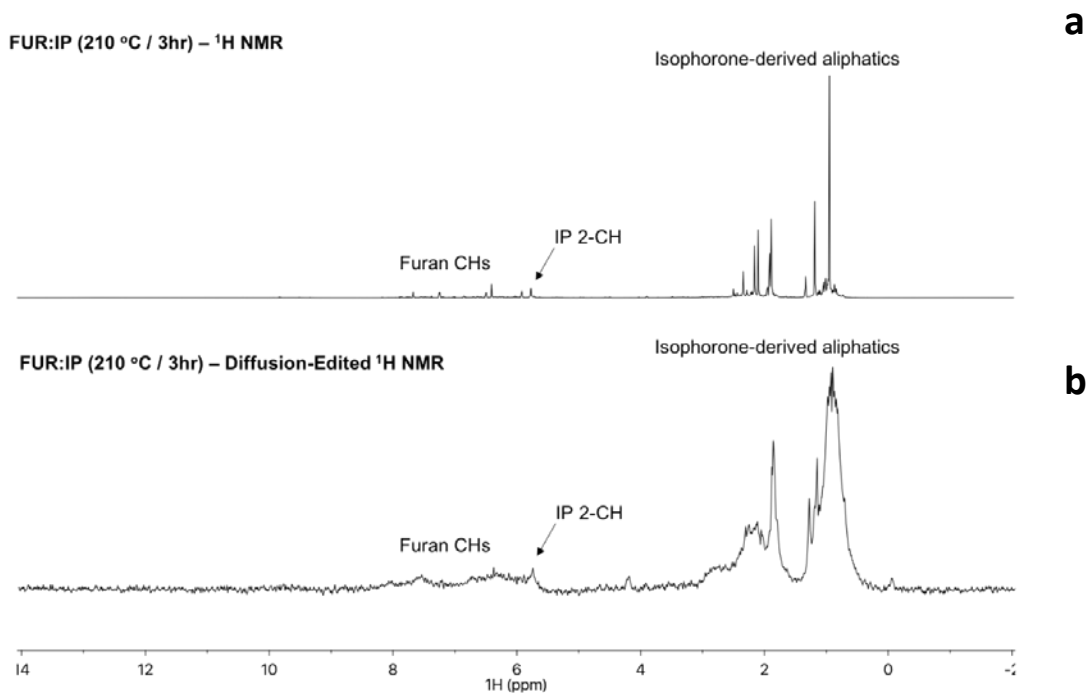
Figure A9. (a) ^{1}H NMR spectra and (b) Diffusion-edited ^{1}H NMR spectra (DMSO-d$_6$ at 27 $^\circ$C) of 1:1 molar equivalents of FUR:isophorone heated at 210 $^\circ$C for 3 h.
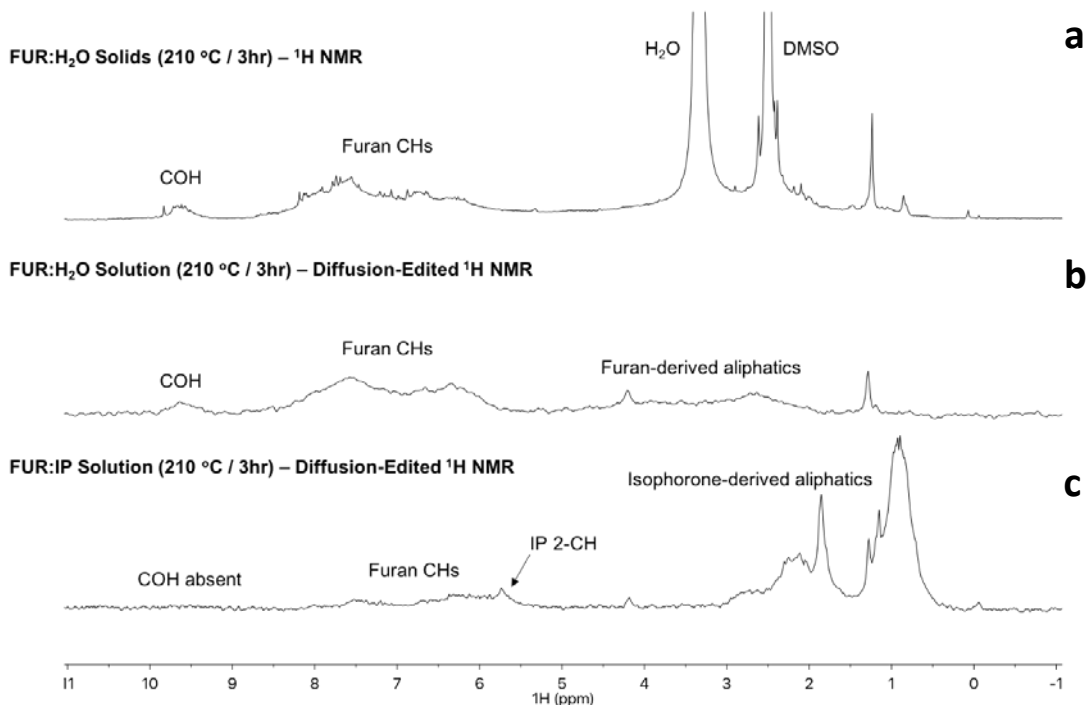
Figure A10. ^{1}H NMR spectra (DMSO-d$_6$ at 27 $^\circ$C) of 5 wt% FUR solution and isophorone 1:1 (v/v) heated at 210 $^\circ$C for 3 h.
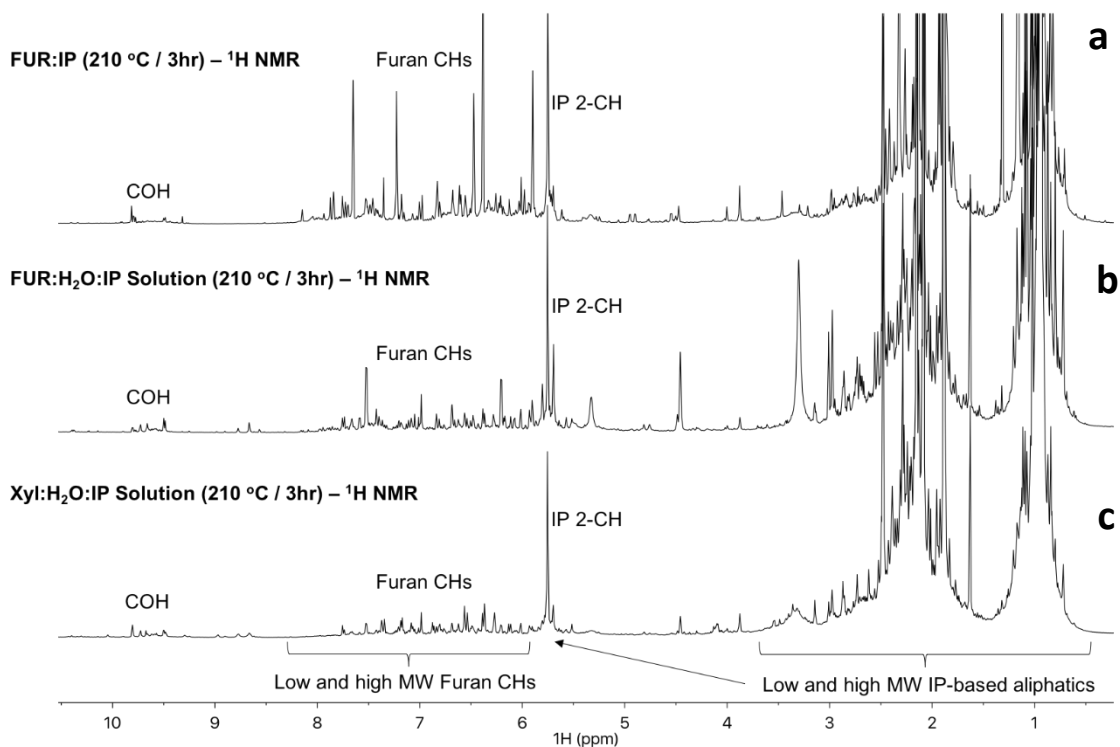
Figure A11. ^1H NMR spectra (DMSO-d_6 at 27 ^oC) of 1:10 molar equivalents of FUR:isophorone heated at 210 ^oC for 3 h.

7. HMF formation from birch hydrolysate

Figure A12. HMF (mmol) in the birch hydrolysate after hydrothermal auto-catalyzed reaction when employing CPME to aqueous phase ratio of 1:1 (v:v) at 190 °C.

References

[1] O. Ershova, J. Pokki, A. Zaitseva, V. Alopaeus, H. Sixta, *Chemical Engineering Science,* https://doi.org/10.1016/j.ces.2017.10.017.

[2] M. Männistö, J. Pokki, V. Alopaeus, *The Journal of Chemical Thermodynamics*, https://doi-org.recursos.biblioteca.upc.edu/10.1016/j.jct.2017.12.015.

III

Furfural production in a biphasic system using a carbonaceous solid acid catalyst

Gerardo Gómez Millán[a,b], Josphat Phiri[a], Mikko Mäkelä[a,c], Thad Maloney[a], Alina M. Balu[d], Antonio Pineda[d], Jordi Llorca[b], Herbert Sixta[a,*]

[a] Department of Bioproducts and Biosystems, School of Chemical Engineering, Aalto University, Vuorimiehentie 1, 02150, Espoo, Finland
[b] Department of Chemical Engineering, Institute of Energy Technologies and Barcelona Research Center in Multiscale Science and Engineering, Universitat Politècnica de Catalunya, Eduard Maristany 10-14, 08019, Barcelona, Spain
[c] Department of Forest Biomaterials and Technology, Swedish University of Agricultural Sciences, Skogsmarksgränd, 90183, Umeå, Sweden
[d] Departmento de Química Orgánica, Universidad de Cordoba, Campus Rabanales, Edificio Marie Curie (C-3), Ctra Nnal IV-A, km 396, Cordoba, Spain

ARTICLE INFO

ABSTRACT

The formation of furfural from xylose was investigated under heterogeneously catalyzed conditions with Starbon®450-SO₃H as a catalyst in a biphasic system. Experiments were performed based on a statistical experimental design. The variables considered were time and temperature. Starbon®450-SO₃H was characterized by scanning electron microscopy, N₂-physisorption, thermogravimetric analysis, diffuse reflectance infrared Fourier transform, Raman spectroscopy, pyridine titration and X-ray photoelectron spectroscopy. The results indicate that sulfonated Starbon®450-SO₃H can be an effective solid acid catalyst for furfural formation. A maximum furfural yield and selectivity of 70 mol% was achieved at complete xylose conversion under optimum experimental conditions. The present paper suggests that functionalized Starbon®450-SO₃H can be employed as an efficient solid acid catalyst that has significant hydrothermal stability and can be reused for several cycles to produce furfural from xylose.

1. Introduction

Furfural (FUR) has been highlighted as one of the top ten most rewarding bio-based building blocks by the United States Department of Energy. FUR can be employed directly as a chemical solvent and selective extractant, as a fungicide and component of disinfectors, in rust removers and pesticides [1,2]. Furthermore, FUR holds the potential to be further transformed directly or indirectly into more than 80 valuable chemicals [2,3]. Additionally FUR can be hydrogenated into furfuryl alcohol, which has applications in the biofuel and food industries (furfuryl alcohol represents around 60% of the FUR market [4]). It can further be used in the manufacturing of chemical resistant furanic resins. Other attractive chemicals that can be obtained from FUR are levulinic acid, 2-methyltetrahydrofuran, furan and furoic acid [2,5].

FUR is typically produced by dehydration of C₅-sugars (arabinose and xylose) contained in the hemicellulose of lignocellulosic biomass. The production of FUR on an industrial scale is associated with high reaction temperatures (approximately 200 °C) and mineral acids (usually sulphuric and hydrochloric acids) that have various process drawbacks, such as the production of toxic effluents, equipment

corrosion and the consumption of high stripping-steam-to-FUR ratios. Furthermore, the number of side reactions under these conditions limits FUR yields to approximately 50% [6]. Recent research in this field has focused on increasing the FUR yield with reusable solid acid catalysts to replace the typically used homogenous acid catalyzed conditions. A wide range of solid acid catalysts have been developed for the purpose of producing FUR from xylose; such as zirconia [7–10], alumina [10,11], zeolites [10,12–17], aluminosilicates supported with metals [18], modified silica [19–26], sulfonated graphenes [27], heteropolyacids [8,28,29], coated activated carbon [30], and resins [22,31,32]. However, one of the main challenges of heterogeneous catalysis is the hydrothermal stability of the solid catalysts and the blocking of active sites by humins (insoluble polymeric products formed via condensation and resinification of furanic compounds) [7,16,33].

Carbon-based catalysts offer high hydrothermal stability [34]. Carbon materials, such as functionalized activated carbon [30], provide exciting opportunities for the catalytic conversion of biomass into value-added chemicals due to their hydrothermal stability, their potential to be produced from biomass and ability to be functionalized by various methods. *Sairanen et al* [30] impregnated activated carbon with

---

H_2SO_4, HNO_3 and a combination of both in order to form FUR from xylose in aqueous media. Even though xylose conversion is complete under the reported experimental conditions, FUR yield is not shown in the paper and the reusability of the catalyst is not mentioned. In a similar way, *Termvidchakorn et al* [35] functionalized multi-wall carbon nanotubes with mineral and organic acids. They employed the functionalized catalysts to form FUR from xylose and achieved the highest xylose conversion (95%) when adding Co ($Co(NO_3)_2 \cdot 6H_2O$ was used as precursor) in 3 h at 170 °C. Nevertheless, FUR yield was not reported. Moreover, the carbon-based catalysts employed were not investigated for their hydrothermal stability or reusability potential. Unlike previous carbon-based catalysts, *Lam et al* [27] developed a sulfonated graphene oxide that yielded 62% FUR in 35 min at 200 °C in water. Nevertheless, the production of graphene oxide includes several steps and various chemicals. *Jalili* et al [36] reported in their recent paper that graphene derivatives contain silicon, which has a significant impact on their performance. Among these carbon-based catalysts, a mesoporous material derived from renewable bio-resources (potato and corn starches) known as Starbon®450-SO_3H has demonstrated superior selectivities and activities in various acid catalyzed aqueous phase reactions, such as the esterification of succinic acid [37–40]. In addition, Starbon®450-SO_3H functionalities, such as hydrophilicity, can be tuned which makes it possible to dehydrate xylose in aqueous phase.

The aim of the present paper was to employ Starbon®450-SO_3H as a solid acid catalyst for the dehydration of xylose to produce FUR. Cyclopentyl methyl ether (CPME) was added to the aqueous xylose solution to extract formed FUR into the organic phase as part of a biphasic system [41]. CPME was demonstrated to be an efficient green solvent, due to its lower toxicity in comparison to other ethers, in the extraction of FUR [42,43]. Furthermore, the hydrothermal stability of the solid acid catalyst and its reusability were thoroughly investigated. Under the experimental conditions provided in this paper, it is demonstrated that Starbon®40-SO_3H can produce high FUR yields in a biphasic system and its catalytic activity remains similar after 3 reusability cycles. Besides this, the characteristics of the solid catalyst were studied in detail by scanning electron microscopy (SEM), energy dispersive X-ray spectroscopy (EDX), N_2-physorption, Py-titration, thermogravimetric analysis (TGA), diffuse reflectance infrared fourier transform spectroscopy analysis (DRIFT), Raman spectroscopy and X-ray photoelectron spectroscopy (XPS).

2. Experimental

2.1. Materials

D-Xylose powder (99%, Sigma Aldrich), CPME (99.9%, Sigma Aldrich), furfural (99%, Sigma Aldrich), potato starch (Sigma Aldrich), and sulphuric acid (25%, HPLC grade, Sigma Aldrich) were used in the experiments without further purification. Formic acid (98%, Sigma Aldrich), levulinic acid (99%, Sigma Aldrich) and acetic acid (99%, HPLC grade, Sigma Aldrich) were used for the preparation of calibration standards for HPLC analysis. Iso-butanol (99.9%, Sigma Aldrich) was used as internal standard (IS) for gas chromatography (GC) analysis. Millipore-grade water was used for preparing the solutions.

2.2. Methods

2.2.1. Determination of FUR and by-products

From the biphasic system, samples for analysis were drawn from both the top (organic phase) and the bottom part (aqueous phase) after hydrothermal reaction. Xylose, carboxylic acids (formic, acetic and levulinic acids) and FUR from aqueous phase were analyzed separately by High Performance Liquid Chromatography (HPLC) operating a Dionex UltiMate 3000 HPLC (Dionex, Sunnyvale, CA, USA) device equipped with refractive index (RI) and ultraviolet (UV) diode array detectors. Product separation was achieved using a Rezex ROA-Organic Acid H$^+$

(8%) LC column (7.8 mm × 300 mm, Phenomenex, USA). Aqueous sulphuric acid (0.0025 mol l^{-1}) was used as an eluent with a flow rate of 0.5 ml min^{-1}. A temperature of 55 °C was set for the column temperature and the RI-detector. The FUR concentration was determined by the UV-detector at a wavelength of 280 nm. Xylose concentration was simultaneously analyzed by the RI-detector and the UV-detector at 210 nm [44]. The samples were filtered through a 0.45 µm syringe filter before the analysis. For calibration of the HPLC, a series of calibration standards were prepared from the following chemicals: xylose, furfural, formic acid, acetic acid, and levulinic acid. From a parent standard solution (0.1 g diluted in 100 ml of Milli-Q water) calibration standards in four concentrations (0.1 ml, 0.5 ml, 1 ml and 1.5 ml in 10 ml of Milli-Q water) were prepared.

FUR from the organic phase was analyzed by gas chromatography with a flame ionization detector (GC-FID) relative to iso-butanol as IS. The column used was a DB-WAXetr (30 m, 0.32 mm i.d., 1 µm film thickness) from Agilent Technologies Inc. The volume of injected samples was 0.5 µl and they were subjected to a splitless ratio of 20:1 in the inlet, which was maintained at 250 °C and a pressure of 13 psi. Helium was used as the carrier gas. The oven was initially maintained at 80 °C for 1 min, after which the temperature was increased to 250 °C at 30 °C min^{-1}. The FID was operated at 250 °C with hydrogen, air, and helium delivered at 30 ml min^{-1}, 380 ml min^{-1}, and 29 ml min^{-1}, respectively.

In this study conversion was defined in terms of moles of reactant converted per unit volume of reactor (Eq. 1). Selectivity, at an instant, was the generated number of moles of desired product referred to the moles of reactant converted (Eq. 2). Yield was calculated as the amount in moles of the desired product (FUR) produced related to the amount of xylose converted (Eq. 3) [45]. The following equations were used for deriving these parameters:

$$X_{xyl} = \frac{c_{xyl}^{in} - c_{xyl}^{f}}{c_{xyl}^{in}} \times 100 \, [\%] \tag{1}$$

$$Y_{fur} = \frac{c_{fur}}{c_{xyl}^{in}} \times 100 \, [\%] \tag{2}$$

$$S_{xyl}^{fur} = \frac{c_{fur}}{c_{xyl}^{in} - c_{xyl}^{f}} \times 100 \, [\%] \tag{3}$$

where *X*, *S*, *Y* are the– conversion of xylose, selectivity to FUR and FUR yield, respectively; *c* is the– concentration in mmol l^{-1} (the subscripts *xyl*, *fur*, *in*, *f* refer to xylose, FUR, initial, final).

Once the concentrations of FUR and xylose had been determined in each sample, individual prediction models were built for xylose conversion, FUR yield and selectivity to FUR separately by solving the general linear regression equation (Eq. 4) [46].

$$\mathbf{y} = \mathbf{Zb} + \mathbf{e} \tag{4}$$

by minimizing the sum of squares of model residuals through the least-squares estimate (Eq. 5):

$$\mathbf{b} = (\mathbf{Z^T Z})^{-1} \mathbf{Z^T y} \tag{5}$$

where *y* denoted a vector of response values, *Z* the mean-centered and coded design matrix including interaction and second-order terms, *b* a vector of model coefficients and *e* the model residuals. Statistically insignificant model terms (p > 0.10) were excluded based on an F-test that compared the effects with the respective model residuals. The performance of the models was expressed through the R^2 value, which indicated the proportion of data variation explained by each individual model.

2.2.2. Catalyst preparation

Starbon®450-SO_3H catalyst was synthesized according to known literature procedure with minor modifications [47]. First, the starting material (starch from potato, Sigma-Aldrich) was heated up in water to

140 °C for 2 h (150 g starch in 3 l deionized water). Upon cooling the warm solution was poured into a vial at room temperature, and it was further cooled down to 5 °C for 48 h until formation of a porous gel in water. To avoid the structure to collapse while drying, several solvent exchange steps were conducted until water was fully replaced by ethanol (5 times), and finally by acetone (2 times) to stabilize the porous network. The resulting materials were then filtered off and dried overnight at 50 °C under vacuum, rendering the mesoporous starch structure, subsequently calcined at 450 °C under inert atmosphere (N_2, 50 ml min^{-1}) by using the following heating conditions: from RT to 450 °C, heating rate 1 °C min^{-1}; temperature maintained for 1 h. A purge with nitrogen prior to carbonization was conducted to ensure the absence of oxygen in the first steps of carbonization.

For sulfonation, the calcined Starbon®450 material was suspended in H_2SO_4 of 95–97% purity (10 ml acid per gram of material and 4 h at 80 °C). After sulfonation, samples were thoroughly washed with distilled water until they reached a neutral pH value, and finally oven dried at 100 °C overnight. The resulting functionalized mesoporous acid material is denoted as Starbon®450-SO$_3$H (STARch carBONized at 450 °C with sulfonic acid groups).

2.2.3. Catalyst characterization

Scanning electron microscopy (SEM) images were recorded at 5 kV using a JEOL JSM-7800 F PRIME Schottky Field Emission Scanning Electron Microscope equipped with a high resolution Gentle Beam (GBSH). Samples were deposited on conductive carbon tabs. The instrument has a field emission gun and it is also equipped with an energy dispersive X-ray (EDX) detector for chemical analysis.

Thermogravimetric analysis (TGA) was carried out in a Setaram Setsys 12 using air as a carrier gas (50 ml min^{-1}). The sample was loaded in ceramic crucibles with α-Al_2O_3 used as reference compound and a Pt/Pt-Rh (10%) thermocouple. The heating rate employed was 10 K min^{-1} in all cases.

Infrared studies were conducted using Diffuse Reflectance Infrared Fourier Transform (DRIFT). Spectra were recorded on an ABB BOMEM MB 3000 Instrument equipped with an environmental chamber (Spectra Tech, P/N, 0030–100) placed in the diffuse reflectance attachment. The resolution was 8 cm^{-1} and 256 scans were averaged to obtain the spectra in the 4000-400 cm^{-1} range. Spectra were recorded by using KBr as a reference. The samples for DRIFTS studies were prepared by mechanically grinding all reactants to a fine powder (sample/KBr 1:5.7 ratio).

A Micromeritics Tristar II-Physisorption Analyzer was utilized to record the nitrogen sorption isotherms for Starbon®450-SO$_3$H. All samples were dried at 105 °C and exposed to nitrogen gas for 12 h before measurement and the isotherms were taken at 196.15 °C. The samples were exposed to ~20% humid room air for about 1 min during the transfer to the holders. The specific surface area (A_{BET}) was determined by the Brunauer-Emmett-Teller (BET) model [48] at relative pressures between 5% and 35% where the data points were observed to arrange linearly. The specific pore volume (V_p) was estimated from the N_2 uptake at a p/p$_0$ value of 0.99 while recording approximately 150 equilibrium data points. The pore width distribution (d_p) was deduced from the desorption branch using the Barrett-Joyner-Halenda (BJH) method [49].

Xylose adsorption tests were completed by stirring 3 ml of an aqueous solution of 186 mmol l^{-1} xylose using a borosilicate glass reactor (V = 10 cm^3) with magnetic stirring (600 m in^{-1}) and 50 mg of Starbon®450-SO$_3$H. Agitation of the suspension occurred for 24 h at room temperature (25 °C). Determination of xylose adsorption was performed by HPLC analysis.

Pyridine (Py) titration experiments were conducted by a similar method found in the literature with few modifications [50]. The experiments were performed at 200 °C via gas phase adsorption of the basic probe molecules utilising a pulse chromatographic titration methodology. Briefly, probe molecules (typically 2–5 μL) were injected

into a gas chromatograph (GC) through a microreactor in which the solid acid catalyst was previously placed. Basic compounds were adsorbed to full saturation, from which the peaks of the probe molecules in the gas phase were detected in the GC. The quantity of probe molecules adsorbed by the solid acid catalyst could subsequently be easily quantified.

Raman spectra were measured using a WITec alpha300 R Raman microscope (alpha 300, WITec, Ulm, Germany) equipped with a piezoelectric scanner using a 532 nm linear polarized excitation laser. The measurement was conducted directly on the powder catalyst after washing and drying.

The surface characterization was performed with X-ray photoelectron spectroscopy (XPS) on a SPECS system equipped with an Al anode XR50 source operating at 150 mW and a Phoibos 150 MCD-9 detector. The pressure in the analysis chamber was always maintained below 10^{-7} Pa. The area analyzed was about 2 mm × 2 mm. The pass energy of the hemispherical analyzer was set at 25 eV and the energy step was set at 0.1 eV.

Peak fitting and quantification analysis were performed using the software package CasaXPS (Casa Software Ltd., UK). Binding energy (BE) values for Starbon®450-SO$_3$H were referred to the adventitious C 1s signal at 284.8 eV. Atomic surface ratios were obtained by using peak areas normalized on the basis of acquisition parameters after background subtraction, experimental sensitivity factors and transmission factors provided by the manufacturer.

2.2.4. Catalytic activity tests

In a typical experiment, the glass reactor (V = 8 cm^3) was loaded with 0.75 ml of an aqueous D-xylose solution in a concentration typical for biomass hydrolysate (186 mmol l^{-1}) [43], 2.25 ml of CPME and 21 mg of the catalyst. The glass reactor included magnetic stirring (600 m in^{-1}) (Figure S1 in the Supplementary Information). The vials were heated up in a silicone oil bath until the desired temperature was reached. Time zero was set when the vials were immersed into the oil bath. Towards the reaction end time, vials were rapidly pulled up from the silicone oil bath and cooled in an ice bath. The prepared solutions were used for determining FUR yield, selectivity to FUR and xylose conversion in different reaction conditions. The individual experiments were organized according to a central composite design on two variables. This design enabled the determination of the effects, and statistical significance of the reaction conditions on sample properties. The variables, reaction temperature and time, were varied on three different levels. The design thus consisted of 11 experiments, including 3 replicated experiments at the design center (175 °C in 12.5 h) (Table 2).

3. Results and discussion

In order to know more about the unique characteristics of the carbonaceous acid catalyst, various analytical techniques were employed on Starbon®450-SO$_3$H and how its characteristics affect the production of FUR from xylose. The results of its analyses are described below.

3.1. Scanning electron microscopy (SEM) and energy-dispersive X-ray (EDX)

For the purpose of demonstrating various properties related to surface topography and chemical composition, scanning electron microscopy (SEM) and energy-dispersive X-ray (EDX) deliver simple, non-destructive analyses. Fig. 1 corresponds to a representative image of Starbon®450-SO$_3$H catalyst powder before hydrothermal reaction revealing the characteristic morphology of particles with sharp edges similar to those reported in the literature [51]. Particles are compact and their size is in the range of 50–100 μm.

EDX analyses showed that the catalyst had a very homogeneous composition. Table 1 compiles the mean values obtained in three different regions of the sample. They showed small variations in the
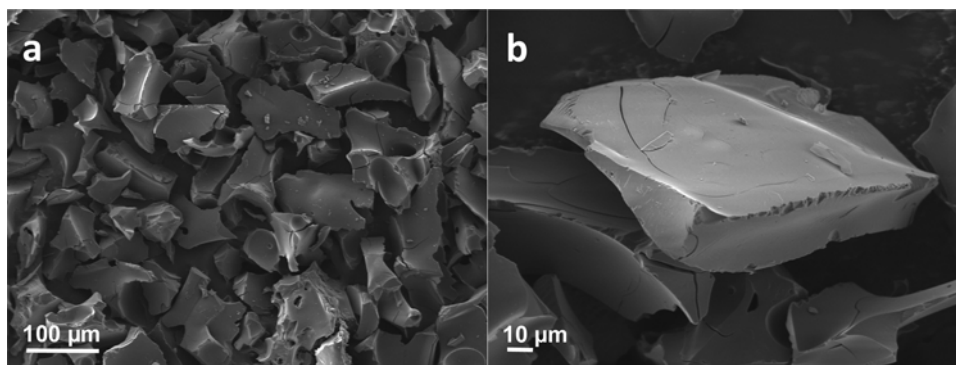
Fig. 1. SEM images of the Starbon®450-SO$_3$H catalyst powder obtained at different magnifications, (a) 180X and (b) 650X.

content of the elements detected (0.2%).

3.2. N$_2$-physisorption – Py TPD

As published in previous literature, a large surface area is preferable due to a high occurrence of available acid sites and to facilitate the accessibility of xylose [52]. Another important textural characteristic of the catalyst, the pore width, affects the diffusivity. Fast diffusion in large pores can prevent FUR decomposition, hence increased selectivity can be achieved [52]. Brunauer-Emmett-Teller (BET) specific surface area, pore volume, xylose adsorption capacity and acid site density of Starbon®450-SO$_3$H are compiled in Table 1. Starbon®450-SO$_3$H shows a BET of 264.5 m^2 g^{-1}, a pore volume of 0.4 cm^3 g^{-1} and a pore width of 3.5 nm; which are similar to previously reported literature on similar materials [40]. The pore width distribution shown in Figure S2 (in the Supplementary Information) reveals a narrow pore width of approximately 10 nm.

Xylose adsorption was investigated to determine the availability of the reaction starting material xylose at the surface. Adsorption of sugar solutions (xylose [30,53] and fructose [54]) in aqueous phase onto solid materials has been investigated by previous researchers. According to *Sairanen et al*, [30] if the amount of xylose adsorbed on the catalyst surface is higher than the amount of acid sites, it would indicate that xylose is adsorbed at sites other than the Brönsted sites as determined in our studies by pyridine titration. Brönsted acid sites are associated with direct dehydration of xylose into FUR, while Lewis acid sites are known to shift the equilibrium towards the isomers (especially to xylulose) [10,55,56]. Our results showed that the concentration of xylose adsorbed on the surface was slightly higher than the catalyst's acid site density, suggesting that acid sites other than Brönsted are present on the surface of the catalyst. Nevertheless, even if Lewis acid sites were present on the surface of Starbon®450-SO$_3$H, they did not play a significant role in the isomerization of xylose into xylulose, since xylulose was not detected by HPLC. Other literature mentioning materials including mesoporous silica SBA-15 have been reported to have lower
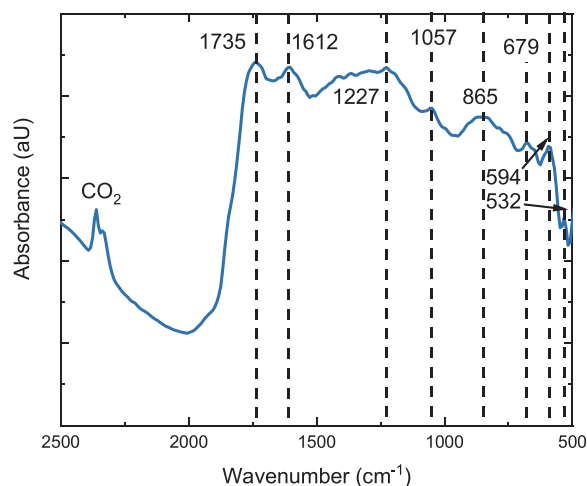
Fig. 2. Infrared spectrum of Starbon®450-SO$_3$H.

acid site densities (e.g. 0.16 mmol g^{-1}) [57].

3.3. Infrared spectroscopy (IR) and thermal gravimetric analysis (TGA)

The infrared (IR) spectrum of Starbon®450-SO$_3$H is shown in Fig. 2. It exhibits two maxima at 1735 cm^{-1} and 1612 cm^{-1} that could be assigned to asymmetric stretching vibrations of $-$COOH carboxyl and $-$COO- carbonyl and/or $-$C $=$ O ketone units and to the stretching vibrations of C $=$ C bonds in aromatic carbon rings, respectively [58]. There is also a peak at 1227 cm^{-1}, which can be assigned to asymmetric stretch of –C-C-C bridges in ketonic groups and/or to deformation vibrations of O$-$H vibration in the carboxylic acid and alcoholic groups from sugars present in the starch-based material, which have been formed during the carbonization of the starch precursor [59]. There is also a small peak at 1057 cm^{-1}, which could be assigned to

Table 1
Energy-dispersive X-ray spectroscopy (EDX) analysis of Starbon®450-SO$_3$H, textural properties (i.e., BET (A$_{BET}$), Pore volume (V$_p$) and Pore diameter (d$_p$)) and acid properties of Starbon®450-SO$_3$H.

Energy-dispersive X-ray spectroscopy (EDX)			Textural properties			Xylose adsorption[a] (mmol g^{-1})	Acid site density[b] (mmol Py g^{-1})
Element	Wt. %	Atomic %	A$_{BET}$ (m^2 g^{-1})	V$_p$ (cm^3 g^{-1})	d$_p$ (nm)		
C	68.9 ± 0.2	75.2 ± 0.2	264.5 ± 62.9	0.04 ± 0.004	3.5 ± 0.6	0.32	0.29
O	29.3 ± 0.2	24.0 ± 0.2					
S	1.8 ± 0.1	0.8 ± 0.0					
Total:	100.0	100.0					

[a] 50 mg of Starbon®450-SO$_3$H in 3 ml of a xylose solution (186 mmol l^{-1}). Agitation of the suspension for 24 h at room temperature (25 °C). Determination of xylose adsorption by HPLC analysis. Adsorbed amount of xylose per gram of catalyst.

[b] Pyridine (Py) titration value at 200 °C.

symmetric S = O stretching of sulfonic groups attached to the material [59–63]. Bands observed in a low region of 865 cm^{-1} could be related to symmetrical C−O−C stretching [59]. In the low frequency range, the line at 679 cm^{-1} indicates a S = O stretching mode of –SO$_3$H [59,64]. The peak at 594 cm^{-1} is assigned to the S−O stretching mode and 532 cm^{-1} was assigned to the C–S stretching mode, suggesting the existence of covalent sulfonic acid groups [64,65]. Starbon®450 before sulfonation was also analyzed with IR (Figure S3 in the Supplementary Information). Significant changes can be seen after Starbon®450 was sulfonated. Mena's synthesis of Starbon® carbonized at 300 °C reported a similar spectrum, which diverged at lower wavenumber regions, due to the use of p-toluenesulfonic acid [59].

In order to study the thermal stability and the decomposition rate of Starbon®450-SO$_3$H, DTA/TGA curves were recorded (Figure S4 in the Supplementary Information). The DTA curve for Starbon®450-SO$_3$H displays two endothermic peaks at 100 °C and 540 °C due to moisture in the sample and the combustion of the carbon matrix, respectively [41,59]. The TGA curve of Starbon®450-SO$_3$H showed a steep weight loss of nearly 70% between 350 °C and 600 °C, which could be associated with the combustion of the carbonaceous material.

3.4. Catalytic activity tests in monophasic system

Xylose dehydration into FUR in aqueous phase leads to the rapid decomposition of FUR and provides low product yields [7]. As Tables S1, S2 and Figure S5 display (in the Supplementary Information); the auto-catalyzed system of xylose dehydration (3 ml of a 186 mmol l^{-1} xylose solution) at 170 °C with various reaction times (1–6 h), the highest FUR yield was 38% with a xylose conversion of 58% after 6 h (Figure S5a). A selectivity to FUR (74%) was reached after 5 h, which decreased to 66% after 6 h (Figure S5c). The addition of Starbon®450-SO$_3$H (50 mg) to the aqueous xylose solution (3 ml of 186 mmol l^{-1}) at 170 °C with various reaction times (1–6 h), the highest FUR yield was 42% at a xylose conversion of 73% (after 6 h, Figure S5b). When adding Starbon®450-SO$_3$H, FUR yield and xylose conversion increase in comparison to the auto-catalyzed system. This is due to the addition of acid sites into the system. In a similar published system, a high selectivity to FUR (67%) was reached after 2 h at 170 °C, which gradually decreased with increasing reaction time. Under similar conditions (2 h at 170 °C), alumina on cordierite reached a selectivity to FUR of 30%; whereas polymeric resins, such as Nafion NR40 and Amberlyst DT showed a selectivity to FUR of 48% and 27%, respectively [7]. In order to avoid FUR decomposition, and to increase its yield, a biphasic system was developed adding an organic solvent that would protect the FUR formed.

3.5. Tests in biphasic system

3.5.1. Partition coefficient

The partitioning of FUR was determined by performing hydrothermal reactions employing a solution of 5 wt% FUR in water, which was heated with CPME for 60 min at 170 °C at five different ratios of CPME to aqueous: 5:1, 2:1, 1:1, 1:2 and 1:5 (v/v) and 25 mg of Starbon®450-SO$_3$H. Figure S6 displays the FUR partition coefficients (P) obtained with CPME, where ***P*** was determined by using Eq. 6 [66].

$$P = \frac{[FUR]_{org}}{[FUR]_{aq}} \qquad (6)$$

At an aqueous to CPME fraction ratio of 5:1, a FUR partition coefficient of 3.4 was obtained. This partition coefficient value declined to 3.3, 3.2, 3.0 and 2.8 as the aqueous to CPME fraction ratio experienced increments to 1:2, 1:1, 2:1 and 5:1, respectively. Similar values have been recently reported when studying the partition coefficient of FUR in CPME-aqueous phases at 190 °C for 30 min under auto-catalyzed conditions [43]. The selection of the aqueous to organic phase ratio in a
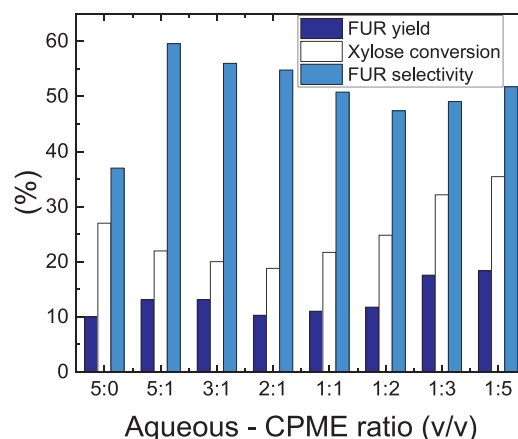
Fig. 3. Effect of aqueous to organic ratio on FUR yield when using CPME. The effect was determined for a solution of xylose (186 mmol l^{-1}) heated for 60 min at 170 °C with 25 mg of Starbon®450-SO$_3$H (and then cooled down to 4 °C) at eight different ratios of aqueous to organic solvent: 5:0, 5:1, 3:1, 2:1, 1:1, 1:2, 1:3 and 1:5 (v/v).

range of 1:5 to 5:1 has a rather low influence on the partition coefficient as highlighted in Figure S6 (in the Supplementary Information).

3.5.2. Effect of the ratio water-CPME on furfural yields

In order to evaluate the effect of the ratio water-CPME on catalyzed xylose conversion and furfural yields, eight ratios of aqueous to organic phase (5:0, 5:1, 3:1, 2:1, 1:1, 1:2, 1:3 and 1:5; v/v) were studied. When the reaction was performed in pure water (ratio 5:0), the yield of the produced FUR did not exceed 10%, and the selectivity was approximately 37% (Fig. 3), the conversion of xylose was around 27%. In the biphasic system, xylose conversion remained around 20% when the aqueous to CPME phase ratio decreased from 5:1 to 2:1 (v/v). However, when adding further CPME to decrease the aqueous to organic phase ratio from 1:1 to 1:5 xylose conversion increased from 22% to 35%. This could be due to xylose fragmentation into carboxylic acids [30]. Generated carboxylic acids (especially formic and acetic acid) during hydrothermal reaction concentrate in the aqueous phase with increasing CPME proportion, thus enhancing the acidity in the aqueous phase. Therefore xylose conversion increases as lower aqueous to CPME phase ratios are used. A similar effect has been reported in the literature [67]. By increasing the aqueous to organic phase ratio, the selectivity to FUR increased with values of 60%, 56%, 55% and 51% for water-CPME volumetric ratios of 5:1, 3:1, 2:1 and 1:1, respectively. Additionally, when the water-to-CPME volumetric ratios increased even more to 1:3 and 1:5, the FUR yield increased to 18%, due to a concomitant increase of the conversion rate. Experiments employing pure CPME were excluded from this study, since xylose has been proven to be almost insoluble in this organic solvent, hence FUR yields are generally minimal [67]. Even though the selectivity and xylose conversion are higher at water to CPME volumetric ratios of 1:5 than at 1:3, it is not practical for industrial applications due to high organic solvent requirements. Thus, the ratio of 1:3 was selected for further experiments. This is in accordance with published literature, since biphasic systems benefit from higher organic to aqueous phase ratios [68].

A design of experiments was developed using a 1:3 water-to-CPME phase ratio (v/v) and 21 mg of Starbon®450-SO$_3$H at various reaction temperatures and times. The original experimental design and the calculated results are illustrated in Table 2.

Based on the results, practically all xylose was converted at 200 °C in 1 h. At 150 °C only 1.3% of the xylose was dehydrated (Fig. 4a). Yield of FUR varied from 0.7% to 69.5%. Based on the results, FUR yield increased when reaction temperature and reaction time increased, but decreased when reaction times greater than 17 h at 200 °C were used (Fig. 4b). Selectivity to FUR ranged from 1.5% and 72.5%. Fig. 2c

Table 2

Variables and the calculated response values based on the experiments. Each experiment consisted of 21 mg of Starbon®450-SO₃H using an aqueous to CPME phase ratio of 1:3 (v/v) at various reaction temperatures (150, 175 and 200 °C) and times (1, 12.5 and 24 h).

Exp. No	T (°C)	t (h)	Furfural Yield (%)	Xylose Conversion (%)	Selectivity to Furfural (%)
1	150	1	0.7	1.3	53.1
2	200	1	69.5	95.9	72.5
3	150	24	52.2	79.5	65.6
4	200	24	21	100	21.0
5	150	12.5	54.4	78.5	69.2
6	200	12.5	50.3	100	50.3
7	175	1	20	30.8	64.8
8	175	24	60.2	100	60.2
9	175	12.5	61.8	100	61.8
10	175	12.5	63.2	100	63.2
11	175	12.5	64.6	100	64.6

shows that the highest selectivities were achieved at low reaction temperatures (150 °C – 170 °C) and long reaction times (> 10 h) or short reaction times (1–10 h) and high temperatures (170 °C – 200 °C).

Prediction models for xylose conversion, FUR yield and selectivity were also successfully determined based on the results. R^2 values indicated that the models explained 92–99% of variation in the sample properties. The obtained models were then used to predict xylose conversion and FUR yield of the samples within the experimental design range. As illustrated in Fig. 2, both reaction temperature and time were statistically significant for xylose conversion, FUR yield and selectivity. Interaction effects between reaction temperature and time were also significant based on the determined models. As an example, longer reaction times increased xylose conversion at lower temperatures, but the effect of time decreased at higher temperatures (Fig. 4a). Longer reaction times also decreased FUR yield significantly at higher temperatures (Fig. 4b). The highest selectivities were thus obtained by combining high reaction temperature with low reaction time, or low to medium reaction temperature with medium to high reaction time (Fig. 4c). The overlay contour plot in Fig. 4d also suggested that a local optimum, where both xylose conversion and FUR yield were
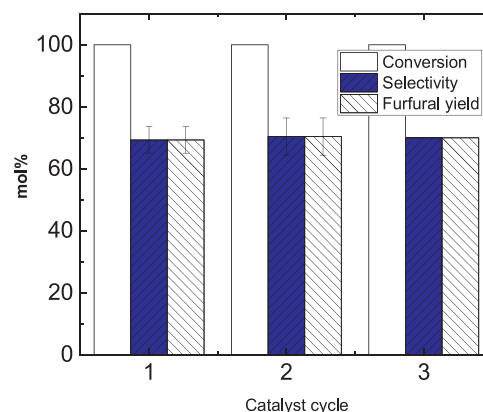
Fig. 5. Reusability of Starbon®450-SO₃H for the dehydration of xylose to FUR using 21 mg of catalyst using an aqueous to CPME phase ratio of 1:3 (v/v) at 175 °C for 18 h (xylose conversion (white bar), FUR yield (blue bar) and selectivity to FUR (striped bar)). (For interpretation of the references to colour in this figure legend, the reader is referred to the web version of this article).

maximized, existed within the experimental design range. Even though another optimum could be found at reaction temperatures above 200 °C and reaction times below 6 h (Fig. 4d), these conditions were not possible to perform in the present set-up. Furthermore, those experimental conditions could present a challenge for the hydrothermal stability of the catalyst. A verification experiment was thus performed by combining a reaction temperature of 175 °C with a reaction time of 18 h. The obtained results indicated that 100% of xylose was converted to 69.3% FUR during the first cycle. The verification results were well aligned with the model predictions, which suggested that 101 ± 25.0% of xylose would be converted to 66.9 ± 10.5% ($\alpha = 0.10$) FUR. The analyses of variance are summarized in Tables S4, S5 and S6 (in the Supplementary Information), for FUR yield, xylose conversion and selectivity to FUR, respectively.

3.5.3. Reusability

The hydrothermal stability of Starbon®450-SO₃H under the
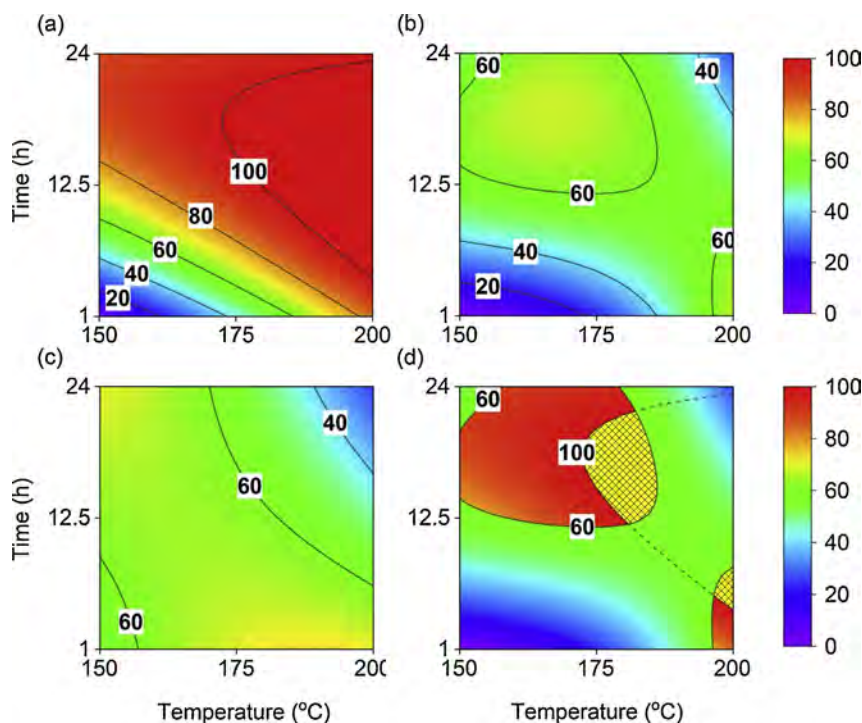
Fig. 4. Contour plots based on model prediction for (a) conversion of xylose (%, $R^2 = 0.92$); (b) furfural yield (%, $R^2 = 0.99$); (c) selectivity (%, $R^2 = 0.92$), and; (d) an overplay plot of xylose conversion and furfural yield. The yellow patterned area in (d) indicates 100% xylose conversion and a furfural yield of > 60% based on the model predictions. Each experiment consisted of 21 mg of Starbon®450-SO₃H using an aqueous to CPME phase ratio of 1:3 (v/v) at various reaction temperatures (150, 175 and 200 °C) and times (1, 12.5 and 24 h). (For interpretation of the references to colour in this figure legend, the reader is referred to the web version of this article).
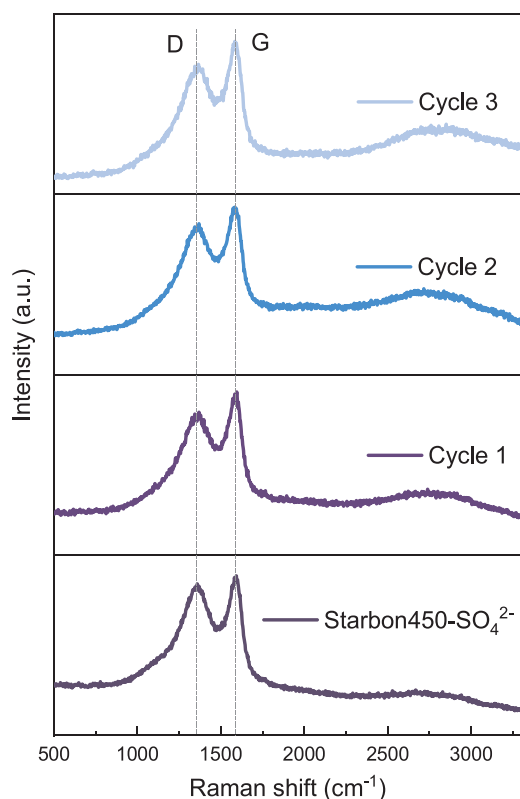
Fig. 6. Raman spectra of the catalyst before and after reusability cycles. Each reusability cycle consisted of adding 21 mg of catalyst to biphasic system employing an aqueous to CPME phase ratio of 1:3 (v/v) at 175 °C for 18 h. After each cycle, the catalyst was filtered, washed with deionized water and dried at 105 °C.

investigated reaction conditions was tested by employing the same catalyst in a series of xylose dehydration reactions. Prior to each cycle, the sample was washed with deionized water and dried at 105 °C. Fig. 5 shows three consecutive reaction runs of Starbon®450-SO$_3$H (at 175 °C in 18 h using 21 mg of Starbon®450-SO$_3$H in 0.75 ml of xylose concentration (186 mmol l^{-1}) and 2.25 ml of CPME). The notation for Starbon®450-SO$_3$H after the reusability test includes a hyphen and the reusability cycle number, e.g. Starbon®450-SO$_3$H$_{-1}$.

After 3 cycles, the catalytic activity of the reused catalyst stayed stable, yielding 70% FUR at complete xylose conversion. Under similar conditions (175 °C, 18 h and 1:3 aqueous to CPME phase ratio), the auto-catalyzed system reaches 100% xylose conversion and 59% FUR yield.

As a non-destructive method, Raman spectroscopy is commonly used to characterize the structure of carbon-based materials. As shown in Fig. 6, all the samples showed two pronounced bands: D and G bands, at around 1347 cm^{-1} and 1593 cm^{-1}, respectively, which are a typical characteristic for graphitic carbon and show the presence of aromatic carbon sheets [69]. The D-band is associated with the breathing modes of sp^3 atoms and is activated only in the presence of defects and disorder in the carbon structure, whilst the G-band is attributed to the vibrations of sp^2 bonded carbon atoms in the hexagonal lattice. The higher frequency position of the G-band and the broad and intense D-band indicate the presence of amorphous phase [69].

As shown in Fig. 6, the Raman spectra of the catalyst before and after the cycles were very similar. The intensity ratio of the G and D band, I_D/I_G can be used to estimate the defect level. The I_D/I_G ratios were virtually identical: 0.984, 0.961, 0.962 and 0.964 for Starbon®450-SO$_3$H$_{-fresh}$, Starbon®450-SO$_3$H$_{-1}$, Starbon®450-SO$_3$H$_{-2}$ and Starbon®450-SO$_3$H$_{-3}$, respectively. Therefore, the catalyst was stable and reusable, in accordance with the reusability tests which also

did not show any loss of yield and selectivity between the three cycles.

Apart from Raman spectra studies, a detailed X-ray photoelectron spectroscopy (XPS) analysis was performed to gain a deeper insight into the surface composition of the materials. In Figure S7 and Table S3 (in the Supplementary Information) the binding energy values and surface atomic composition of Starbon®450-SO$_3$H, before and after hydrothermal reaction, are shown. As can be demonstrated, there were no significant changes in the chemical composition of the surface of Starbon®450-SO$_3$H before and after hydrothermal reaction. Different approaches to measure stability and reusability of solid catalysts have been under discussion in recent years. In order to design stable catalysts with practical applications, *Christopher W. Jones* [70] highlighted the need of understanding deactivation mechanisms of solid catalysts. In this way, catalysis as a kinetic phenomenon should be used to assess recyclability, stability and deactivation. We agree with his approach. However, in the present set-up, it was not possible to withdraw samples and analyze them periodically from the reactor as it was conducted in the referred literature. We nevertheless not only report the number of reusability cycles and yield, but also included experimental conditions, such as reaction time and temperature. This adds consistency to the continuous catalytic activity of Starbon®450-SO$_3$H after various reusability cycles. We also agree that deactivation plays a key role in the improvement of solid catalysts. Deactivation studies of Starbon®450-SO$_3$H are not included in the present paper, nevertheless we certainly consider that they should be addressed in future work.

Starbon®450-SO$_3$H is a very attractive solid acid catalyst to form FUR from xylose due to its high BET surface area, excellent hydrothermal stability, and high acid site density. It is interesting to compare the performance of Starbon®450-SO$_3$H with those of other carbon-based catalysts employed in similar set-ups. *Wang et al* [71] developed a Miscanthus-based catalyst with sulfonic groups for the FUR formation from xylose and xylan in a CPME/H$_2$O 3:1 phase ratio (v/v). Under optimized conditions, they reported a FUR yield of 60% and 42% from xylose and xylan, respectively (at 190 °C in 1 h). A sulfated lignin-based catalyst was developed by *Antonyraj and Haridas* [72] to form FUR and hydroxymethylfurfural (HMF) from xylose and fructose, respectively, in a methyl isobutyl ketone (MIBK)/H$_2$O 7:3 phase ratio (v/v) system. They reported yields of up to 65% FUR at 175 °C in 3 h from xylose and 27% HMF at 150 °C in 3 h from fructose.

In this work, we have shown how higher FUR yields and complete xylose conversion can be achieved when using Starbon®450-SO$_3$H in comparison to similar systems using carbonaceous catalysts. Moreover, Starbon®450-SO$_3$H can be functionalized with sulphuric acid and has shown hydrothermal stability under the experimental conditions presented in this paper. Moreover, it can be easily separated from the reaction media and further reused without losing its catalytic activity. Additionally, statistical methods have rarely been employed to optimize reaction conditions in converting xylose to FUR. Among the few who have used design of experiments, Lamminpää [73] supported her research employing experimental design to determine the interactions of lignin in FUR formation from xylose using formic and sulphuric acid.

A possible alternative, to reduce the reaction time presented in this study, could be to increase the reaction temperature to around 200 °C. As Fig. 4 shows, an area with FUR yields above 60% can be reached at approximately 200 °C in under 6 h. Naturally, the hydrothermal stability of Starbon®450-SO$_3$H and its feasible reuse under similar experimental conditions, merit investigation. An interesting option to avoid further FUR decomposition would be to modify the batch system for a plug-flow reactor with an optimized residence time.

4. Conclusions

Furfural formation from xylose in the presence of Starbon®450-SO$_3$H was studied in a biphasic system using CPME as an organic solvent. When adding Starbon®450-SO$_3$H, the major product of the catalyzed dehydration reaction of xylose was FUR. Minor products detected

in the system were decomposition products, such as humins, but these were not quantified. The maximum mole fraction yield obtained was 70% in 18 h at 175 °C at complete xylose conversion. Whereas the auto-catalyzed system under the same conditions yielded 59% FUR. Starbon®450-SO_3H showed a high selectivity to FUR in both the monophasic and biphasic systems. Under these experimental conditions, it is demonstrated that the reusability potential of the carbon-based mesoporous material is possible without decreasing its catalytic activity.

Acknowledgements

Appendix A. Supplementary data

Supplementary material related to this article can be found, in the online version, at doi:https://doi.org/10.1016/j.apcata.2019.117180.

References

[1] S. Peleteiro, S. Rivas, J.L. Alonso, V. Santos, J.C. Parajó, Bioresour. Technol. 202 (2016) 181–191.
[2] K.J. Zeitsch, K.J. Zeitsch (Ed.), The Chemistry and Technology of Furfural and Its Many by-Products, Elsevier B.V., 2000, pp. 98–103.
[3] G. Gómez Millán, S. Hellsten, J. Llorca, R. Luque, H. Sixta, A.M. Balu, ChemCatChem 11 (2019) 2022–2042.
[4] S.J. Canhaci, R.F. Perez, L.E.P. Borges, M.A. Fraga, Appl. Catal. B 207 (2017) 279–285.
[5] Y. Luo, Z. Li, X. Li, X. Liu, J. Fan, J.H. Clark, C. Hu, Catal. Today 319 (2019) 14–24.
[6] A.S. Mamman, J. Lee, Y. Kim, I.T. Hwang, N. Park, Y.K. Hwang, J. Chang, J. Hwang, Biofuels, Bioprod. Biorefin. 2 (2008) 438–454.
[7] G. Gómez Millán, Z. El Assal, K. Nieminen, S. Hellsten, J. Llorca, H. Sixta, Fuel Process Technol 182 (2018) 56–67.
[8] A.S. Dias, S. Lima, M. Pillinger, A.A. Valente, Catal. Lett. 114 (2007) 151–160.
[9] H. Li, A. Deng, J. Ren, C. Liu, W. Wang, F. Peng, R. Sun, Catal. Today 234 (2014) 251–256.
[10] R. Weingarten, G.A. Tompsett, W.C. Conner Jr, G.W. Huber, J. Catal. 279 (2011) 174–182.
[11] S.J. You, Y.T. Kim, E.D. Park, React. Kinet. Mech. Catal. 111 (2014) 521–534.
[12] C. Moreau, R. Durand, D. Peyron, J. Duhamet, P. Rivalier, Ind. Crops Prod. 7 (1998) 95–99.
[13] R. O'Neill, M.N. Ahmad, L. Vanoye, F. Aiouache, Ind. Eng. Chem. Res. 48 (2009) 4300–4306.
[14] R. Sahu, P.L. Dhepe, ChemSusChem 5 (2012) 751–761.
[15] S. Lima, A. Fernandes, M.M. Antunes, M. Pillinger, F. Ribeiro, A.A. Valente, Catal. Lett. 135 (2010) 41–47.
[16] E.I. Gürbüz, J.M.R. Gallo, D.M. Alonso, S.G. Wettstein, W.Y. Lim, J.A. Dumesic, Angew. Chem. Int. Ed. 52 (2013) 1270–1274.
[17] L.R. Ferreira, S. Lima, P. Neves, M.M. Antunes, S.M. Rocha, M. Pillinger, I. Portugal, A.A. Valente, Chem. Eng. J. 215–216 (2013) 772–783.
[18] A. Yepez, A. Garcia, M.S. Climent, A.A. Romero, R. Luque, Catal. Sci. Technol. 4 (2014) 428–434.
[19] M.J.C. Molina, M.L. Granados, A. Gervasini, P. Carniti, Catal. Today 254 (2015) 90–98.
[20] G.H. Jeong, E.G. Kim, S.B. Kim, E.D. Park, S.W. Kim, Microporous Mesoporous Mater. 144 (2011) 134–139.
[21] I. Agirrezabal-Telleria, J. Requies, M.B. Güemez, P.L. Arias, Appl. Catal. B 115–116 (2012) 169–178.
[22] I. Agirrezabal-Telleria, C. García-Sancho, P. Maireles-Torres, P.L. Arias, Chin. J.
[23] I. Agirrezabal-Telleria, J. Requies, M.B. Güemez, P.L. Arias, Appl. Catal. B 145 (2014) 34–42.
[24] P. Bhaumik, T. Kane, P.L. Dhepe, Catal. Sci. Technol. 4 (2014) 2904–2907.
[25] A.S. Dias, M. Pillinger, A.A. Valente, J. Catal. 229 (2005) 414–423.
[26] S. Kaiprommarat, S. Kongparakul, P. Reubroycharoen, G. Guan, C. Samart, Fuel 174 (2016) 189–196.
[27] E. Lam, J.H. Chong, E. Majid, Y. Liu, S. Hrapovic, A.C.W. Leung, J.H.T. Luong, Carbon 50 (2012) 1033–1043.
[28] A.S. Dias, M. Pillinger, A.A. Valente, Appl. Catal., A 285 (2005) 126–131.
[29] A.S. Dias, M. Pillinger, A.A. Valente, Microporous Mesoporous Mater. 94 (2006) 214–225.
[30] E. Sairanen, K. Vilonen, R. Karinen, J. Lehtonen, Top. Catal. 56 (2013) 512–521.
[31] E. Lam, E. Majid, A.C.W. Leung, J.H. Chong, K.A. Mahmoud, J.H.T. Luong, ChemSusChem 4 (2011) 535–541.
[32] I. Agirrezabal-Telleria, A. Larreategui, J. Requies, M.B. Güemez, P.L. Arias, Bioresour. Technol. 102 (2011) 7478–7485.
[33] C. Sener, A.H. Motagamwala, D.M. Alonso, J.A. Dumesic, ChemSusChem 11 (2018) 2321.
[34] H. Xiong, H.N. Pham, A.K. Datye, Green Chem. 16 (2014) 4627–4643.
[35] C. Termvidchakorn, V. Itthibenchapong, S. Songtawee, B. Chamnankid, S. Namuangruk, K. Faungnawakij, T. Charinpanitkul, R. Khunchit, N. Hansupaluk, N. Sano, H. Hinode, Adv. Nat. Sci. : Nanosci. Nanotechnol. 8 (2017) 035006.
[36] R. Jalili, D. Esrafilzadeh, S.H. Aboutalebi, Y.M. Sabri, A.E. Kandjani, S.K. Bhargava, E. Della Gaspera, T.R. Gengenbach, A. Walker, Y. Chao, C. Wang, H. Alimadadi, D.R.G. Mitchell, D.L. Officer, D.R. MacFarlane, G.G. Wallace, Nat. Commun. 9 (2018) 5070.
[37] V.L. Budarin, J.H. Clark, R. Luque, D.J. Macquarrie, A. Koutinas, C. Webb, Green Chem. 9 (2007) 992–995.
[38] V. Budarin, R. Luque, D.J. Macquarrie, J. Clark, Chem. - Eur. J. 13 (2007) 6914–6919.
[39] V.L. Budarin, J.H. Clark, R. Luque, D.J. Macquarrie, Chem. Commun. (2007) 634–636.
[40] J.H. Clark, V. Budarin, T. Dugmore, R. Luque, D.J. Macquarrie, V. Strelko, Catal. Commun. 9 (2008) 1709–1714.
[41] V. Budarin, J.H. Clark, J.J.E. Hardy, R. Luque, K. Milkowski, S.J. Tavener, A.J. Wilson, Angew. Chem. Int. Ed. 45 (2006) 3782–3786.
[42] K. Watanabe, Molecules 18 (2013) 3183–3194.
[43] G. Gómez Millán, S. Hellsten, A.W.T. King, J. Pokki, J. Llorca, H. Sixta, J. Ind. Eng. Chem. 72 (2019) 354–363.
[44] S. Givry, C. Bliard, F. Duchiron, Carbohydr. Res. 342 (2007) 859–864.
[45] C. Pirola, I. Rossetti, V. Ragaini, La Chimica & L'Industria 2 (2013) 136–145.
[46] R. Leardi, Anal. Chim. Acta 652 (2009) 161–172.
[47] M. Ojeda, A.M. Balu, A.A. Romero, P. Esquinazi, J. Ruokolainen, H. Sixta, R. Luque, ChemCatChem 6 (2014) 2847–2853.
[48] S. Brunauer, P.H. Emmett, E. Teller, J. Am. Chem. Soc. 35 (1938) 309.
[49] E.P. Barrett, L.G. Joyner, P.P. Halenda, J. Am. Chem. Soc. 73 (1951) 373.
[50] A. Pineda, A.M. Balu, J.M. Campelo, R. Luque, A.A. Romero, J.C. Serrano-Ruiz, Catal. Today 187 (2012) 65–69.
[51] A. Aldana-Pérez, L. Lartundo-Rojas, R. Gómez, M.E. Niño-Gómez, Fuel 100 (2012) 128–138.
[52] R. Karinen, K. Vilonen, M. Niemelä, ChemSusChem 4 (2011) 1002–1016.
[53] R. Ranjan, S. Thust, C.E. Gounaris, M. Woo, C.A. Floudas, Mv. Keitz, K.J. Valentas, J. Wei, M. Tsapatsis, Microporous Mesoporous Mater. 122 (2009) 143–148.
[54] V.V. Ordomsky, J. van der Schaaf, J.C. Schouten, T.A. Nijhuis, ChemSusChem 5 (2012) 1812–1819.
[55] V. Choudhary, S.I. Sandler, D.G. Vlachos, ACS Catal. 2 (2012) 2022–2028.
[56] J. Iglesias, J.A. Melero, G. Morales, M. Paniagua, B. Hernández, ChemCatChem 8 (2016) 2089–2099.
[57] M.J. Gracia-Trujillo, M.J. Jurado-Pescuezo, M.D. Gracia-Serrano, J.M. Campelo, D. Luna, J.M. Marinas, A.A. Romero, Stud. Surf. Sci. Catal. 174 (2008) 1331–1334.
[58] M. Baikousi, Y. Georgiou, C. Daikopoulos, A.B. Bourlinos, J. Filip, R. Zbořil, Y. Deligiannakis, M.A. Karakassides, Carbon 93 (2015) 636–647.
[59] C.J. Mena Duran (Ed.), Synthesis and Characterisation of Sulfonated Starbons®, Bio-Based Catalysts, PhD Thesis Ed. University of York, UK, 2014.
[60] A. Thamri, H. Baccar, C. Struzzi, C. Bittencourt, A. Abdelghani, E. Llobet, Sci. Rep. 6 (2016) 35130.
[61] J.C. Yang, M.J. Jablonsky, J.W. Mays, Polymer 43 (2002) 5125–5132.
[62] G. Chen, B. Fang, Bioresour. Technol. 102 (2011) 2635–2640.
[63] E. Damian Risberg, L. Eriksson, J. Mink, L.G.M. Pettersson, M.Y. Skripkin, M. Sandström, Inorg. Chem. 46 (2007) 8332–8348.
[64] H. Yu, Y. Jin, Z. Li, F. Peng, H. Wang, J. Solid State Chem. 181 (2008) 432–438.
[65] A. Amoozadeh, S. Rahmani, M. Bitaraf, F.B. Abadi, E. Tabrizian, New J. Chem. 40 (2016) 770–780.
[66] A. Mittal, S.K. Black, T.B. Vinzant, M. O'Brien, M.P. Tucker, D.K. Johnson, ACS Sustainable Chem. Eng. (2017).
[67] S. Le Guenic, D. Gergela, C. Ceballos, F. Delbecq, C. Len, Molecules 21 (2016) 1102.
[68] J.E. Romo, N.V. Bollar, C.J. Zimmermann, S.G. Wettstein, ChemCatChem 10 (2018) 4805–4816.
[69] A.C. Ferrari, J. Robertson, Phys. Rev. B 61 (2000) 14095–14107.
[70] C.W. Jones, Top. Catal. 53 (2010) 942–952.
[71] Y. Wang, F. Delbecq, W. Kwapinski, C. Len, Mol. Catal. 438 (2017) 167–172.
[72] C.A. Antonyraj, A. Haridas, Catal. Commun. 104 (2018) 101–105.
[73] K. Lamminpää, J. Ahola, J. Tanskanen, Bioresour. Technol. 177 (2015) 94–101.

Catal. 34 (2013) 1402–1406.

Supplementary Information

Furfural production in a biphasic system using a carbonaceous solid acid catalyst

Gerardo Gómez Millán[a,b], Josphat Phiri[a], Mikko Mäkelä[a,c], Thad Maloney[a], Alina M. Balu[d], Antonio Pineda[d], Jordi Llorca[b], Herbert Sixta[a]*

[a]   G. Gómez Millán, J. Phiri, DSc. M. Mäkelä, Prof. Thad Maloney, Prof. H. Sixta
        Department of Bioproducts and Biosystems
        School of Chemical Engineering, Aalto University
        Vuorimiehentie 1, 02150 Espoo (Finland)
        E-mail: herbert.sixta@aalto.fi
[b]   G. Gómez Millán, Prof. J. Llorca
        Department of Chemical Engineering, Institute of Energy Technologies and
        Barcelona Research Center in Multiscale Science and Engineering
        Universitat Politècnica de Catalunya
        Eduard Maristany 10-14, 08019 Barcelona (Spain)
[c]   DSc. M. Mäkelä
        Department of Forest Biomaterials and Technology
        Swedish University of Agricultural Sciences
        Skogsmarksgränd, 90183 Umeå (Sweden)
[d]   Prof. A. M. Balu, Dr. A. Pineda
        Departmento de Química Orgánica
        Universidad de Cordoba
        Campus Rabanales, Edificio Marie Curie (C-3)
        Ctra Nnal IV-A, km 396 Cordoba (Spain)

1. Furfural formation system

In a typical experiment, the samples were prepared by heating 0.75 ml of an aqueous solution of 186 mmol l^{-1} xylose, 2.25 ml of CPME and 21 mg of sulfonated Starbon®450-SO$_3$H using a glass reactor (V = 8 cm^3) with magnetic stirring (600 min^{-1}). The vials were heated up in a silicone oil bath until the desired temperature was reached. Time zero was set when the vials were immersed into the oil bath. Towards the reaction end time, the vials were pulled up from the silicone oil bath and rapidly cooled in an ice bath. The prepared solutions were used for determining FUR yield, selectivity and xylose conversion in different reaction conditions.
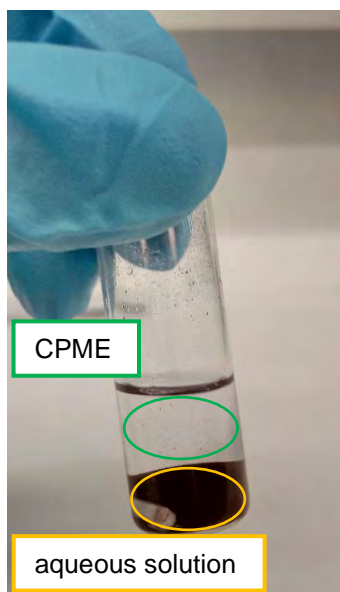
Figure S1. Starbon®450-SO$_3$H in biphasic system (1:3 v/v aqueous to CPME phase ratio).

2. Catalyst characterization

2.1 N_2-Physisorption

The pore width distribution shown in Fig. S2 reveals a narrow pore width of approximately 10 nm.
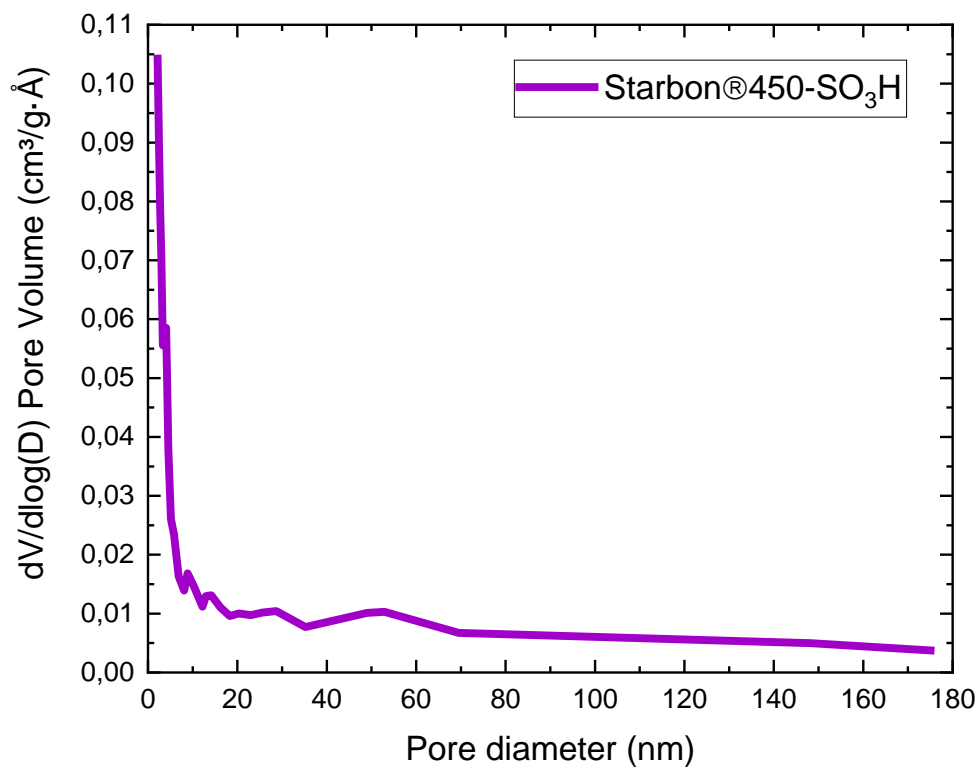
Figure S2. Pore size distribution curve of Starbon®450-SO₃H.

2.2   Infrared Spectroscopy
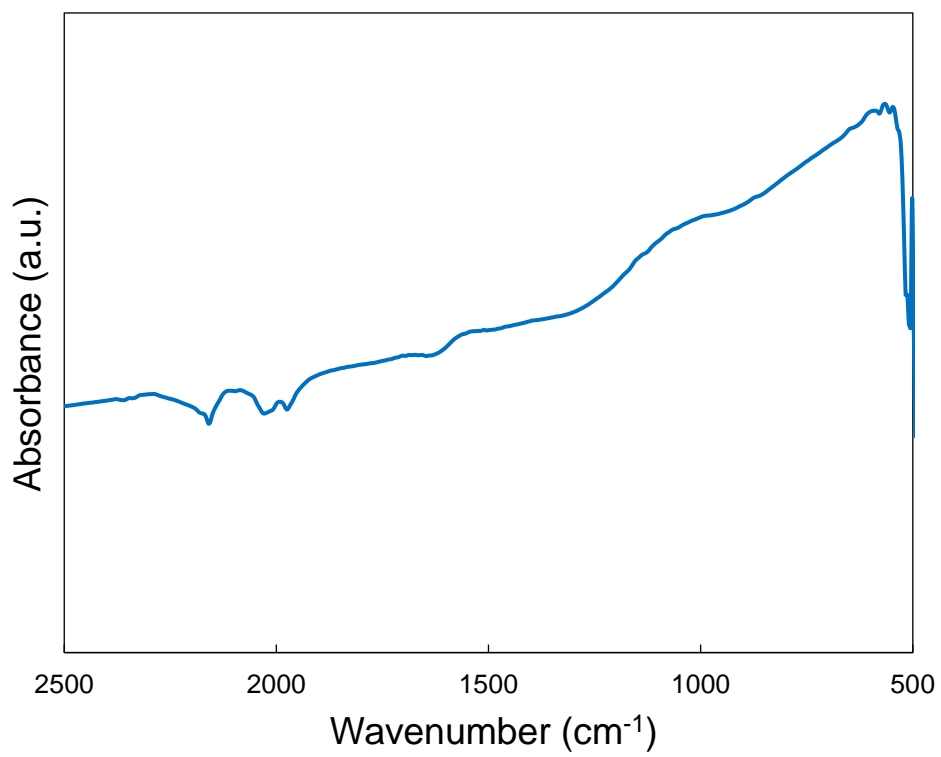
Figure S3. Infrared spectrum of Starbon®450.

2.3   Differential Thermal Analysis (DTA)

The DTA curve for Starbon®450-SO$_3$H exhibits two endothermic peaks at 100 °C and 540 °C due to moisture in the sample and to the combustion of the carbon matrix, respectively [1]. The TGA curve of Starbon®450-SO$_3$H showed a steep weight loss of nearly 70% between 350 °C and 600 °C due to the combustion of carbonaceous material (Fig. S3).
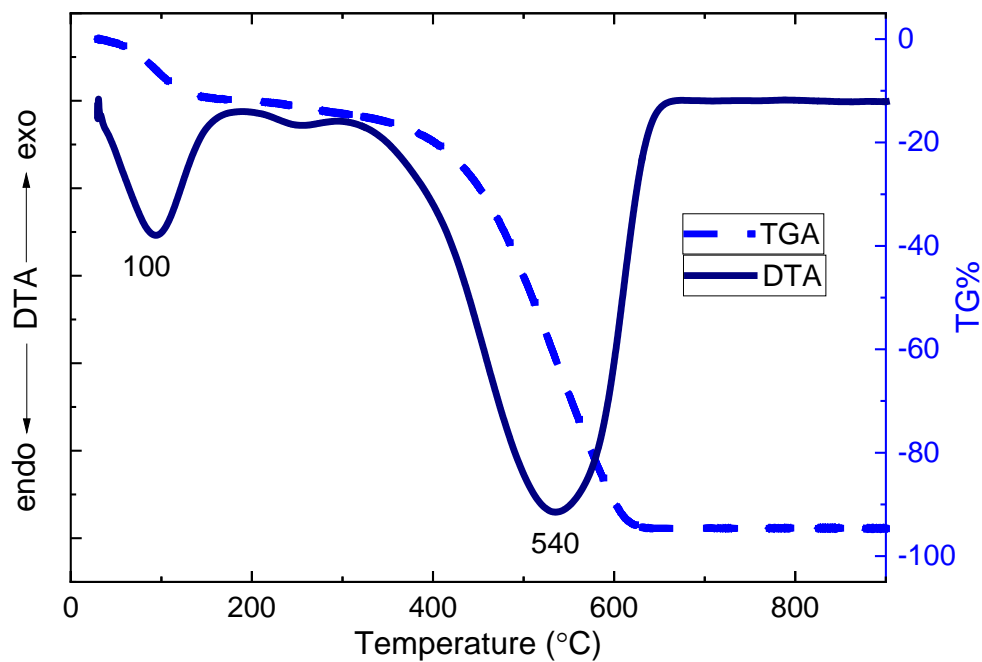
Figure S4. DTA and TGA curves of the initial carbon matrix of Starbon®450-SO$_3$H.

3. Catalytic activity of Starbon®450-SO$_3$H in monophasic (aqueous) system

As Figure S4 displays the auto-catalyzed system of xylose dehydration (3 ml of a 186 mmol l^{-1} xylose solution) at 170 °C in various reaction times (1 – 6 h), the highest FUR yield was 38% at a xylose conversion of 58% after 6 h (Fig. S4a). A selectivity to FUR (74%) was reached after 5 h, which decreased to 66% after 6 h (Fig. S4c). With the addition of Starbon®450-SO$_3$H (50 mg) to the aqueous xylose solution (3 ml of 186 mmol l^{-1}) at 170 °C in various reaction times (1-6 h), the highest FUR yield was 42% at a xylose conversion of 73% (after 6 h, Figure S4b). When adding Starbon®450-SO$_3$H, FUR yield and xylose conversion increase in comparison to the auto-catalyzed system. This is due to the addition of acid sites into the system. Tables S1 and S2 display the numerical values obtained under the present experimental conditions and were used to plot the graph shown (Figure S4).
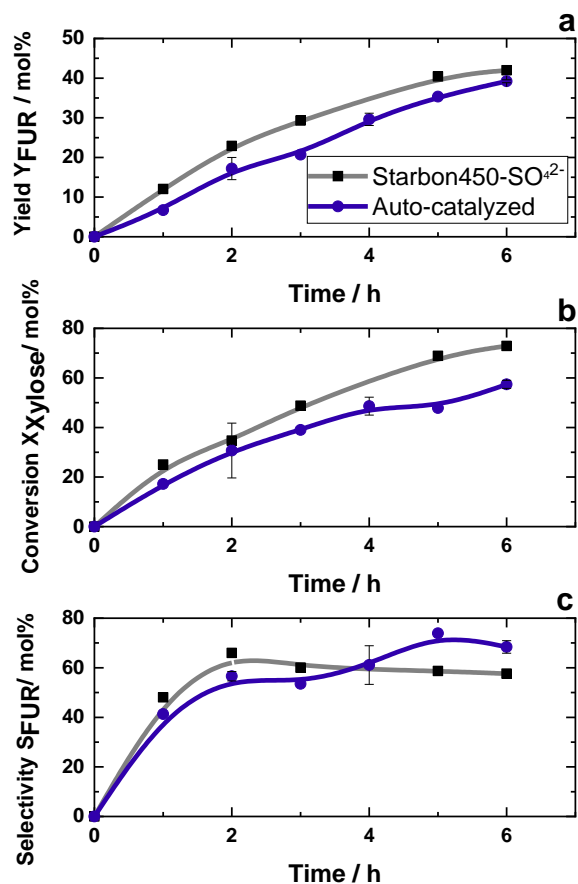
Figure S5. FUR yield (a), xylose conversion (b) and selectivity to FUR (c) at various reaction times during conversion of xylose 186 mmol l^{-1} (black square - using 50 mg of Starbon®450-SO₃H, blue circle – auto-catalyzed system) at 170 °C. Lines are to guide the eye.

Table S1. FUR yield, xylose conversion and selectivity to FUR at various reaction times during conversion of xylose 186 mmol l^{-1} using 50 mg of Starbon®450-SO₃H at 170 °C.

T (°C)	t (h)	Furfural Yield (%)	Xylose Conversion (%)	Selectivity (%)
170	1	12.1	24.7	48.9
170	2	23.0	34.4	66.9
170	3	29.1	49.1	59.2
170	5	40.1	59.1	58.1
170	6	41.7	73.1	57.0

Table S2. FUR yield, xylose conversion and selectivity to FUR at various reaction times during auto-catalyzed conversion of xylose 186 mmol l^{-1} at 170 °C.

T (°C)	t (h)	Furfural Yield (%)	Xylose Conversion (%)	Selectivity (%)
170	1	8.9	23.3	38.2
170	2	14.6	42.8	34.2
170	3	21.9	35.7	61.4
170	5	35.3	47.8	73.9
170	6	39.0	58.5	66.6

4. Partition coefficient for FUR among CPME

A FUR partition coefficient of 3.4 was obtained with an aqueous to CPME fraction ratio of 5:1. This value decreased to 3.3, 3.2, 3.0 and 2.8 as the aqueous-to-CPME fraction ratio increased to 1:2, 1:1, 2:1 and 5:1, respectively. The selection of the aqueous-to-organic phase ratio in a range of 1:5 to 5:1 has a rather low influence on the partition coefficient as highlighted in Fig. S5.
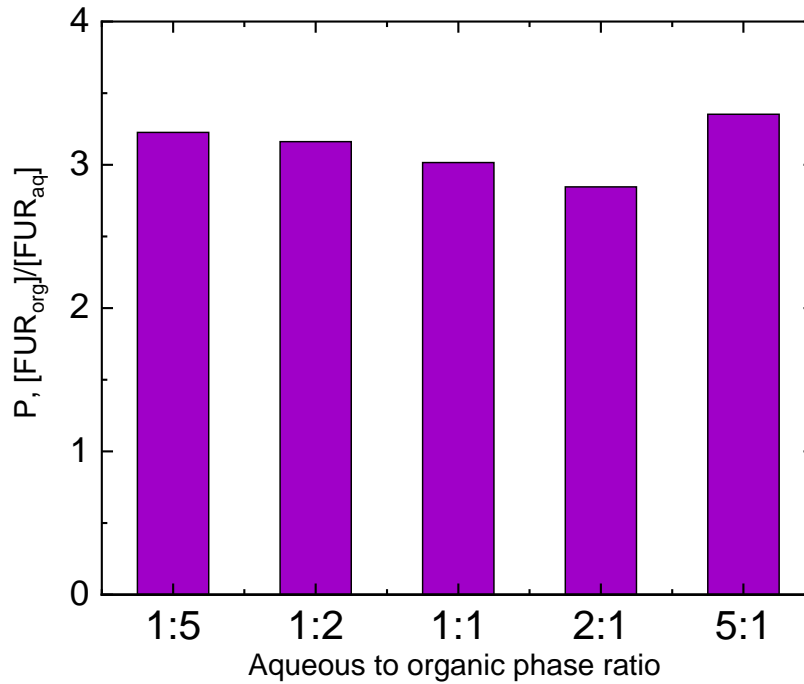
Figure S6. Partition coefficients for FUR among CPME. Partition coefficients were determined for a solution of 5 wt% FUR in water with 25 mg of Starbon®450-SO₃H heated for 60 min at 170 °C (and then cooled down to 4 °C) at five different ratios of aqueous to organic solvent: 1:5, 1:2, 1:1, 2:1 and 5:1 (v/v).

5. Results of analysis of variance

The following model equations were determined for furfural yield (Eq. S.1), xylose conversion (Eq. S.2) and selectivity (Eq. S.3) based on the experimental data:

$$\hat{y}_1 = 61.5 - 2.05x_1 + 20.1x_2 - 23.6x_1x_2 - 6.63x_1^2 - 18.9x_2^2 - 17.9x_1^2x_2 + 12.9x_1x_2^2 \text{ (Eq. S.1)}$$

$$\hat{y}_2 = 95.7 + 22.8x_1 + 25.3x_2 - 18.5x_1x_2 - 27.8x_2^2 \qquad \text{(Eq. S.2)}$$

$$\hat{y}_3 = 62.9 - 7.35x_1 - 7.27x_2 - 16.0x_1x_2 - 7.64x_1^2 \qquad \text{(Eq. S.3)}$$

where $\hat{y}_1$, $\hat{y}_2$ and $\hat{y}_3$ denoted predicted furfural yield, xylose conversion and selectivity, respectively, and x_1 and x_2 the mean-centered and coded experimental conditions temperature and time, respectively. The ANOVA tables for the models are given in Tables S.1-S.3 below.

Table S4. Analysis of variance (ANOVA) table for furfural yield (R^2 = 0.99). The tabulated values have been rounded.

Source	Sum of squares	Degrees of freedom	Mean square	F-value	p-value
Total corrected	4830	10			
Model	4800	7	686	46.1	0.005
Residual	44.6	3	14.9		
Lack of fit	40.7	1	40.7	20.8	0.045
Pure error	3.92	2	1.96		

Table S5. Analysis of variance (ANOVA) table for xylose conversion (R^2 = 0.92). The tabulated values have been rounded.

Source	Sum of squares	Degrees of freedom	Mean square	F-value	p-value
Total corrected	11300	10			
Model	10400	4	2600	18.3	0.002
Residual	853	6	142		
Lack of fit	853	4	213	213	<0.001
Pure error	0	2	0		

Table S6. Analysis of variance (ANOVA) table for selectivity (R^2 = 0.92). The tabulated values have been rounded.

Source	Sum of squares	Degrees of freedom	Mean square	F-value	p-value
Total corrected	1980	10			
Model	1820	4	456	18.1	0.002
Residual	152	6	25.3		
Lack of fit	148	4	36.9	18.8	0.051
Pure error	3.92	2	1.96		

6. X-Ray photoelectron spectroscopy (XPS) studies on reused catalyst

Regarding the binding energy values of the O 1s signals, we exclude the possibility of sample charging because we tested the effect of a flood gun during the analysis and the binding energy values were not affected (Fig. S6).
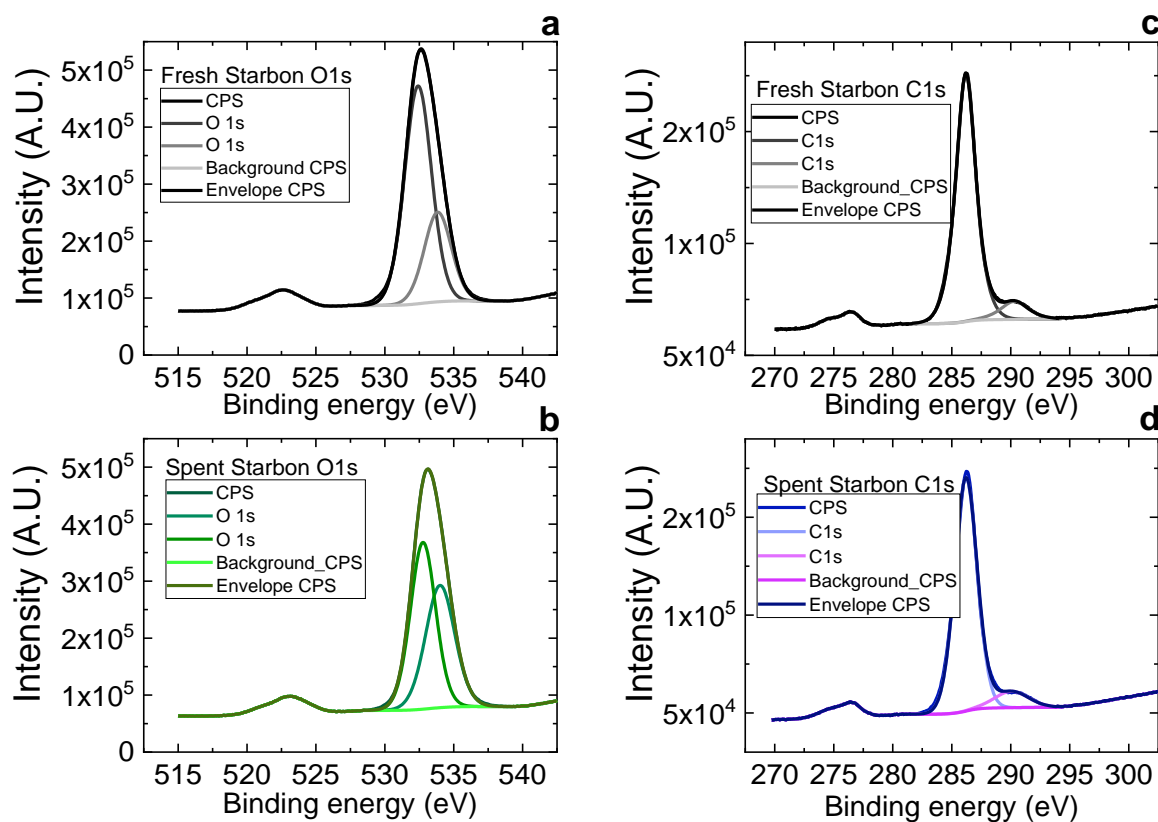
Figure S7. XPS (a,b) O 1s and (c,d) C 1s spectra of Starbon®450-SO$_3$H (a,c) before and (b,d) after hydrothermal reaction at 175 °C in 18 h.

Table S7. XPS data of Starbon®450-SO$_3$H before and after the hydrothermal reaction at 175 °C in 18 h

Sample	Name	Binding Energy (eV)	Atomic conc. (%)
Starbon®450 -SO$_3$H —fresh	O 1s	532.4	59.0
	C 1s	286.2	41.0
Starbon®450 -SO$_3$H —1	O 1s	534	54.1
	C 1s	286.2	45.9

References

[1] V. Budarin, J.H. Clark, J.J.E. Hardy, R. Luque, K. Milkowski, S.J. Tavener and A.J. Wilson, Angew. Chem. Int. Ed. 45 (2006) 3782-3786.

IV

Gómez Millán, G., Bangalore Ashok, R. P., Oinas, P., Llorca, J., Sixta, H. (2019) Furfural production from xylose and birch hydrolysate liquor in a biphasic system and techno-economic analysis. Submitted to *Biomass Conversion and Biorefinery*.

Furfural production from xylose and birch hydrolysate liquor in a biphasic system and techno-economic analysis

Gerardo Gomez Millan,[a,b] Rahul Prasad Bangalore Ashok, [c] Pekka Oinas,[c] Jordi Llorca,[b] Herbert Sixta[a]*

[a]	G. Gómez Millán, Prof. H. Sixta Department of Bioproducts and Biosystems School of Chemical Engineering, Aalto University Vuorimiehentie 1, 02150 Espoo (Finland) E-mail: herbert.sixta@aalto.fi
[b]	G. Gómez Millán, Prof. J. Llorca Department of Chemical Engineering, Institute of Energy Technologies and Barcelona Research Center in Multiscale Science and Engineering Universitat Politècnica de Catalunya Eduard Maristany 10-14, 08019 Barcelona (Spain)
[c]	R.P. Bangalore Ashok, P. Oinas Department of Chemical and Metallurgical Engineering School of Chemical Engineering, Aalto University P.O. Box 16100, 00076 Espoo (Finland)

Abstract

Furfural has been highlighted as one of the top ten most rewarding bio-based building blocks by the United States Department of Energy. In this study, furfural was produced from xylose and birch hydrolysate liquor employing a batch reactor in a biphasic system. The formation of furfural was conducted under auto-catalyzed conditions. 2-sec-butylphenol was used as extractant to promptly extract furfural from the aqueous phase in order to avoid furfural degradation reactions as much as possible. The effect of time, temperature and organic-to-aqueous phase ratio were investigated. The maximum furfural yields from xylose and birch hydrolysate liquor as feedstock under auto-catalyzed conditions when employing SBP were 59% and 54%, respectively. In the monophasic system when using hydrolysate, 46% furfural was yielded. Based on a techno-economic analysis carried out, the total investment cost for a plant integrated with an existing pulp mill or bio-refinery is estimated as 18.36 M€ The project lifetime is assumed as 20 years and the minimum selling price of furfural found to be 1.33 €kg^{-1}. With a furfural selling price of 1.72 €kg^{-1}, the payback period is approximately 5 years and an IRR of 20.7 % is achieved at the end of the project lifetime.

Keywords: furfural, birch hydrolysate liquor, 2-sec-butylphenol, xylose, biorefinery, techno-economic analysis

1. Introduction

Bioeconomy is significantly influencing markets worldwide, therefore new alternative pathways, which shape sustainable development and manage natural resources have to be created in the future. In Finland, bioeconomy models based in forestry processes are noted particularly as the new direction towards a thriving green economy [1,

1

2]. So far, the competitiveness of pulp and paper mills is struggling as a result of digitalization of literature and global increasing capacities especially in equatorial and sub-equatorial countries with larger tree growing quotas and low-cost labor that sets severe economic strain on the producers in temperate latitudes like the Nordics [3]. This ongoing trend can give a new potential to existing forest companies to also develop as significant biobased chemical and biofuel producers, in addition to cellulose-based products. This position urges to transform their mass production of paper-grade pulp en route to other products with smaller production quantity but larger gross margin, such as methane gas from wastewater [4]; bio-oil from lignin [5]; and value-added chemicals like furfural (FUR), hydroxymethylfurfural (HMF) and acetic acid from hydrolysate liquor from dissolving pulp [6]. An attractive sugar contained in high amounts, xylose, has not yet been fully utilized in the paper and pulp industry, which is mixed with lignin-derived compounds and burned to provide process heat [7]. Currently, the Nordic oil company St1 Oy produces FUR, lignin and turpentine as by-products in their Cellulonix® process that aims to form ethanol from saw dust [8].

The current market price of FUR is fluctuating between 800 €/t to 1600 €/t [9]. It is expected that the global FUR market grows from 380 million € to 615 million €[1] by 2026 [10]. Nevertheless, process technologies in industrial scale produce around 50% FUR yield through Quaker Oats technology. Besides, the process is accompanied by environmental concerns including toxic effluents and high energy consumption. China still continues to produce over 70% of the total FUR market volume, followed by Dominican Republic and South Africa. Among the more than 80 chemicals that can be produced directly or indirectly from FUR, furfuryl alcohol is the largest application segment market (accounting approximately 85% of the total FUR market in 2013) with application in the escalating biofuel and food sectors [11]. Other attractive platform molecules obtained from FUR are furan-2,5-dicarboxylic acid and methyltetrahydrofuran.

In order to boost the current FUR yield and tackle current process challenges, recent advances to replace mineral acids (H_2SO_4 and HCl) with solid acids and ionic liquids have been undertaken by academia and industry [6, 12, 13]. Yemiş and Mazza studied the conversion of xylose and xylan into FUR employing three strong mineral acids (hydrochloric acid, sulfuric acid and nitric acid) and three weak acids (phosphoric acid, acetic acid and formic acid) [14]. In the paper, hydrochloric acid and phosphoric acid are the most effective catalysts as strong mineral acid and as weak acid, respectively. Furthermore, organic acids such as formic, oxalic, fumaric and maleic acids have demonstrated being a

---

[1] Original prices reported in USD were converted to EU with a conversion rate of 1 USD = 0.91362 € on September 30th 2019.

good alternative to dehydrate sugars into furanics [15-17]. Especially, oxalic acid has shown good catalytic activity to form FUR from xylose. Hongisiri et al. reported comparable FUR yields when employing oxalic acid and HCl [17].

Various studies have been proposed to avert the production of humins and consequently heighten the FUR yield. An effective approach is to immediately extract FUR from the aqueous phase using an organic solvent. The key considerations to identify a suitable solvent for a biphasic system including FUR extraction are good chemical stability, high boiling point (higher than that of FUR), no azeotrope formation with FUR, mutual solubility of solvent and water should be minimal, and the FUR partition coefficient should be as high as possible [18-20]. Moreover, avoidance of modifiers (salts such as NaCl) is preferred [21]. Salts increase the partition coefficient, but in doing so, corrosion of the reactor and viable deactivation of active sites on solid acid catalysts are created [21, 22]. Ethyl acetate was first used as extracting media by Trimble and Dunlop [23]. Subsequent investigation incorporated studies on diverse organic solvents, e.g. 2-methoxy-4-propylphenol [20], 1-butanol [24], cyclo pentyl methylether (CPME) [25-27], cyclohexanol [28], methyl isobutyl ketone (MIBK) [28, 29], 2-methyltetrahydrofuran (MTHF) [30, 31] and widely-used toluene [28]. A lignin-derived organic solvent, 2-sec-butylphenol [19], offers high partition coefficient for FUR in organic-aqueous systems [20]. Additionally, due to its water-immiscibility nature it does not require phase modifiers and it has a higher boiling point (227 °C) compared to that of FUR (162 °C), which allows for its recovery in higher purity as a top product in a distillation step [20, 30]. The additional separation step adds cost to the process. Therefore the organic layer must be recovered and reused in order for the process to be economically viable [32].

Therefore, we hereby compare the formation of FUR from xylose (used as model compound) and the pentosane fraction present in the birch hydrolysate liquor under auto-catalyzed conditions. We focus on the formation of FUR from xylose and birch hydrolysate liquor using 2-sec-butylphenol as organic solvent. Furthermore, it is necessary to develop an economical and energy efficient process that can produce a concentrated product with a low cost production and a minimum usage of reagents. In the present study, the solvents are recovered for reuse in the process.

2. Experimental

2.1. Materials

2-sec-butylphenol (97.5%) was purchased from Sigma Aldrich and were used in the experiments without further purification. D-Xylose powder (99%), formic acid (98%), levulinic acid (99%), acetic acid (99%), furfural (98%) and

hydroxymethylfurfural (99%) were purchased from Sigma Aldrich and used for the preparation of calibration standards for HPLC analysis. Millipore grade water was used for preparing the solutions.

The birch hydrolysate was supplied by Stora Enso (Stora Enso, Imatra, Finland), which was used for the dehydration reaction experiments. The composition of the hydrolysate can be seen in Table A1 (in the Supplementary Information).

2.2. Methods

2.2.1. Catalytic activity tests

Birch hydrolysate from Stora Enso (Imatra, Finland) was filtered by using a glass filter with porosity 4 (Duran). The composition of the liquor was determined according to the analytical method NREL/TP-510-42623 [33]. The first set of experiments was performed with xylose in the absence of catalyst. These experiments can be considered as auto-catalyzed reaction system where some fragmentation products (namely carboxylic acids) or intermediates, formed during the hydrothermal treatment, may have a catalytic effect [34-36]. The second set of experiments was performed using the birch hydrolysate liquor.

In a typical experiment, a borosilicate glass reactor ($V = 10$ cm^3) was loaded with 3 ml of a xylose solution (186 mol m^{-3}) or the birch hydrolysate liquor. The xylose concentration used is similar to that found in the birch hydrolysate liquor (Table A1 in the Supplementary Information). The hydrothermal reaction includes magnetic stirring (600 min^{-1}) and microwave-assisted heating ($\leq$850 W, Monowave 300, Anton Paar GmbH, Graz, Austria). After the reaction took place, the reactor was rapidly cooled to 60 °C by utilizing compressed air. The highest temperature and the longest reaction time studied at the present work were 210 °C and 180 min, respectively. After the reaction occurred, the solutions were tested for FUR yield, selectivity to FUR and xylose conversion at the reaction temperatures of 170, 190 and 210 °C with different reaction times in the range of 30-180 min.

Due to the slow settling of the aqueous and organic phases, which is related to the relative similar densities (d_4^{20}) of both water and 2-sec-butylphenol (0.982) [18], samples were centrifuged after hydrothermal reaction using a Minispin® centrifuge (Eppendorf AG, Germany) for 6 min with a rotation speed of 8000 rpm.

2.2.2. Determination of FUR and by-products

The liquid samples were analyzed by High Performance Liquid Chromatography (HPLC) operating a Dionex Ultimate 3000 HPLC (Dionex, Sunnyvale, CA, USA) device equipped with refractive index (RI) and ultraviolet (UV) diode

4

array detectors. Product separation was achieved on a Rezex ROA-Organic Acid H$^+$ (8%) LC column (7.8 mm × 300 mm, Phenomenex, USA). Aqueous sulfuric acid (0.0025 mol l^{-1}) was used as eluent with a flow rate of 0.5 ml min^{-1}. The column temperature and the RI-detector temperature were set to 55 °C. The FUR concentration was determined by the UV-detector at a wavelength of 280 nm. The xylose concentration was analyzed simultaneously by the RI-detector and the UV-detector at 210 nm [37]. The samples were filtered through a 0.45 □m syringe filter before the analysis.

FUR from the organic phase was analyzed by gas chromatography with a flame ionization detector (GC-FID) relative to acetone as internal standard (IS). The column used was a DB-WAXetr (30 m, 0.32 mm i.d., 1 µm film thickness) from Agilent Technologies Inc. The injected samples (0.5 µL) were subjected to a splitless ratio of 20:1 in the inlet, which was maintained at 250 °C and pressure of 13 psi. Helium was used as the carrier gas. The oven was initially maintained at 80 °C for 1 min, after which the temperature was increased to 250 °C at 30 °C min^{-1}. The FID was operated at 250 °C with hydrogen, air, and helium delivered at 30 mL min^{-1}, 380 ml min^{-1}, and 29 ml min^{-1}, respectively.

In this study conversion, selectivity to FUR and FUR yield [12, 30, 38] were calculated according to equations 1, 2 and 3, respectively. The following equations have been used for the mathematical evaluation of the obtained results when using xylose solution (186 mol m^{-3}):

$$X_{xyl} = \frac{c_{xyl}^{in} - c_{xyl}^{f}}{c_{xyl}^{in}} \times 100 \ [\%] \qquad\qquad \text{(Eq. 1),}$$

$$Y_{fur} = \frac{c_{fur}}{c_{xyl}^{in}} \times 100 \ [\%] \qquad\qquad \text{(Eq. 2),}$$

$$S_{xyl}^{fur} = \frac{c_{fur}}{c_{xyl}^{in} - c_{xyl}^{f}} \times 100 \ [\%] \qquad\qquad \text{(Eq. 3),}$$

where X, S, Y are the– conversion of xylose, selectivity to FUR and FUR yield, respectively; c is the– concentration in mol m^{-3} (the subscripts xyl, fur, in, f refer to xylose, FUR, initial, final).

When hydrolysate liquor was used; pentose conversion, selectivity to FUR and FUR yield were calculated equations 4, 5 and 6, respectively.

5

Conversion of pentoses (namely arabinose and xylose), selectivity to FUR and FUR yield were determined in accordance with the previous section employing hydrolysate liquor as reactant.

$$X_{Pentoses} = \frac{c^0_{Pentoses} - c^e_{Pentoses}}{c^0_{Pentoses}} \times 100 \ [\%] \qquad \text{(Eq. 4)},$$

$$Y_{fur} = \frac{c^e_{FUR\_ut} - c^0_{FUR\_ut}}{c^0_{Pentoses\_t} - c^0_{FUR\_ut}} \times 100 \ [\%] \qquad \text{(Eq. 5)},$$

$$S^{fur}_{Pentoses} = \frac{c_{fur}}{c^0_{Pentoses} - c^e_{Pentoses}} \times 100 \ [\%] \qquad \text{(Eq. 6)},$$

where X, S, Y are the– conversion of xylose, selectivity to FUR and FUR yield, respectively; c is the– concentration in mmol (the subscripts and superscripts to be read as follows: *pentoses*, *fur*, *ut*, *t*, *0*, *e,* are the– pentoses (arabinose and xylose), FUR, hydrolysate liquor untreated, hydrolysate liquor treated according to the National renewable Energy Laboratory, before and after reaction, respectively).

2.2.3. Techno-economic analysis methodology

The process feasibility is evaluated by carrying out a techno-economic analysis consisting of conceptual process design, mass and energy balance calculations and total investment cost estimations. A discounted cash flow analysis is performed to determine the minimum selling price of FUR, payback period, net present value (NPV) and internal rate of return (IRR).

The equipment mapping, sizing and the purchased equipment cost estimation is performed using Aspen Process Economic Analyzer (Aspen Technologies, Inc., USA) based on 1st quarter 2014 pricing and updated to 2018 prices in euros by considering the chemical engineering plant cost index (CEPCI) and currency conversion. A delivery allowance of 10 % is applied and the delivered equipment cost is calculated using equation 7.

$$Delivered \ equipment \ cost \ (DEC) = 1.1 * purchased \ equipment \ cost \qquad \text{(Eq. 7)}$$

The fixed capital investment is determined using equation 8. The direct and indirect costs are estimated as a fraction of the delivered equipment costs using factors from Peters et al. by considering a solid-fluid processing plant [39]. Direct costs include costs related to purchase of equipment, equipment installation, piping, electrical systems, buildings, yard improvements and service facilities. Indirect costs account for costs arising from engineering and supervision, construction, legal expenses, contractor fees. The contingency cost is calculated as 25 % of the sum of direct and indirect costs. The OSBL (Outside battery limits) cost is estimated as 20% of the total direct cost (TDC)

and the working capital is taken as 10 % of the fixed capital investment. Total investment is calculated following equation 9.

$$Fixed\ capital\ investment\ (FCI) = total\ direct\ cost + total\ indirect\ cost +$$
$$contingency\ cost + OSBL \qquad \text{(Eq. 8)}$$

$$Total\ investment = FCI + working\ \text{capital} \qquad \text{(Eq. 9)}$$

The annual operating cost is calculated as the sum of fixed operating costs, variable operating costs and general expenses. The fixed operating costs account for operating labor, employee benefits, supervision, laboratory, insurance and taxes, maintenance and plant overheads. Variable operating costs include raw material and utility costs and are estimated based on mass and energy balances obtained from process simulation models of Aspen plus®. The operating labor cost is calculated by considering 2.9 operators per shift position [39] and one supervisor. The number of shifts is taken as 5 with monthly wages of 3000 €and 5000 €for the operators and supervisor respectively. General expenses is taken as 10 % of the sum of fixed and variable operating costs and accounts for costs related to administration, distribution and marketing and research and development.

The plant is operated in continuous mode (8000 h/yr) with a FUR production capacity of 5 kt/yr and a project lifetime of 20 years with 100 % equity financing. Capital expenses are incurred in year 1 of the project without any operating costs or revenues. In year 2, the working capital is invested and the plant starts operating at full capacity, thereby generating revenue. Since profit is made by the plant from year 2 onwards, depreciation can be charged and is calculated using straight-line depreciation with a 10-year recovery period. In year 20, the working capital is released and is accounted as positive increment to the cash flow. The parameters used in the techno-economic analysis are summarized in Table 1. The major assumptions for the techno-economic analysis are as follows:

- The process utilizes pre-hydrolysate stream from the bio-refinery or pulp-mill as a raw material and therefore upon integration of the process, it assumed that the pre-hydrolysate cost is negligible and not taken into consideration when estimating the annual operating costs.

- The FUR reactor is energy intensive and therefore, it is assumed that the energy demands for the reactor is met by utilizing the excess energy available in the pulp mill or bio-refinery.

- Furthermore, it is assumed that the lignin removal from the pre-hydrolysate is carried out in the pulp-mill or bio-refinery and costs related to this are not taken into consideration in the techno-economic analysis.

7

Table 1. Parameters of techno-economic analysis.

Techno-economic analysis parameters	
Evaluation year	2018
Production capacity	5 kt/yr.
Project lifetime	20 years
Discount rate	10%
Taxation	20%
Contingency cost	25 % of sum of direct and indirect costs
Working capital	10% of FCI
OSBL	20% of TDC
Employee benefits	25% of operating labor
Supervision	20% of operating labor
Laboratory	20% of operating labor
Insurance and Taxes	3% of FCI
Maintenance	3% of FCI
Plant overhead	65% of sum of operating labor, supervision and maintenance
Operating supplies	1% of FCI
General expenses	10% of sum of fixed and variable costs

3. Results and Discussion

3.1. Partition coefficient of furfural

The partition coefficient of FUR was investigated by conducting hydrothermal reactions wherein a solution of 5 wt% FUR in aqueous phase was heated with SBP for 30 min at 190 °C at seven ratios of aqueous to SBP: 1:5, 1:3, 1:2, 1:1, 2:1, 3:1 and 5:1 (by volume). Fig. A1 (in the Supplementary Information) exhibits the FUR partitioning (P) achieved, where P was calculated using equation 10 [28].

$$P = \frac{[FUR]_{org}}{[FUR]_{aq}} \qquad \text{(Eq. 10)}$$

A FUR partition coefficient of 35 and 36 were obtained with an aqueous to SBP phase ratio of 1:5 and 1:3 (by volume), respectively. This value decreased to 31, 22, 16, 9 and 3 as the aqueous to SBP fraction ratio increased to 1:2, 1:1, 2:1, 3:1 and 5:1 (v/v). Similarly, partition coefficient decreases when the aqueous to organic phase ratio increases has been also observed when using 2-MTHF, CPME and isophorone [30]. It is assumed that at high aqueous to organic phase ratios, the organic solvent is not able to extract FUR from the aqueous phase, thus FUR remains in the aqueous phase where it could undergo degradation reactions.

8

3.2. Effect of aqueous to organic phase ratio

According to the National Center for Biotechnology Information [40], SBP is insoluble in water. However, mutual solubilities of water and SBP have been measured in a recently published paper at various temperatures from 30 to 210 °C [18]. It is observed that solubility of water in SBP used in the present paper is minimal under the given experimental conditions.

The effect of aqueous-to-SBP phase ratio on xylose conversion and FUR formation was examined. Therefore, seven ratios of aqueous to SBP phase (1:5, 1:2, 1:1, 2:1, 5:1 by volume) were proposed employing an aqueous solution containing 186 mmol l^{-1} and SBP in biphasic systems at a temperature of 190 °C for 0.5 h. The FUR yields obtained are presented in Fig. A2 (in the Supplementary Information) and are determined utilizing equation 2. FUR yield builds up as the aqueous to organic ratio increases from 1:5 up to 1:1 (by volume, Fig. A2). At ratios of aqueous to organic volumes of 2:1 to 5:1, we propose that a larger FUR yield is halted by the formation of increased degradation products. The highest FUR yield (13%) is obtained at 190 °C in 0.5 h when using SBP in an aqueous to SBP phase ratio of 1:2 and 1:1 (by volume).

Selectivity to FUR and xylose conversion can be observed in Fig. A3 (in the Supplementary Information). The xylose conversion varied from 30 to 43%. The selectivity to FUR increases as the aqueous to SBP phase ratio raises from 1:5 to 1:1 (by volume), from there on it declines when increasing the aqueous to SBP phase ratio to 5:1. A recent paper using isophorone, 2-MTHF and CPME corroborated similar results [30]. This could occur as a result of the saturation of the SBP to extract FUR, hence FUR remains in the aqueous phase and degradation reactions might take place.

Effect of reaction time and temperature in the biphasic system

The effect of reaction time and temperature on the formation of FUR was investigated by performing reactions from 0.5 to 3 h at 170, 190 and 210 °C in a biphasic system including SBP and a xylose solution of 186 mol m^{-3}. SBP was employed as organic solvent in an aqueous to organic phase ratio of 1:1 (by volume). Fig. 1 presents the effect of reaction time when employing SPB on FUR yield, xylose conversion and selectivity to FUR. As it can be seen in Fig. 1b, FUR yield and xylose conversion are significantly influenced by the reaction temperature, which is in accordance to previous reports on this field [41].

9

As observed in Fig. 1a, after the first 1 h of the hydrothermal reaction the FUR yield exhibited a threefold increase by raising the reaction temperature from 170 to 190 °C. The highest FUR yield (59%) was reached at 190 °C in 3 h. The peak of the selectivity to FUR (Fig. 1c) was 60%, 59% and 47% at temperatures of 170, 190 and 210 °C, respectively. Reaction temperature has also an effect on selectivity to FUR under these laboratory conditions as it has been observed in similar biphasic systems using cyclopentyl methyl ether (CPME), isophorone and 2-methyltetrahydrofuran (MTHF) [30]. It can be observed that selectivity to FUR at the lowest temperature studied (170 °C) displays the highest value in the biphasic system.

An interesting effect, that can be seen in Fig. 1a, is that at times greater than 1.5 h, the FUR yield reached at 190 °C exceeds the FUR yield achieved at 210 °C. At high reaction temperatures (210 °C) it is assumed that SBP no longer extracts FUR as efficiently. Hence FUR is prone to remain in the aqueous phase rather than in SBP, therefore degradation reactions of FUR take place faster. A similar effect can be seen when employing CPME, isophorone and MTHF [30].
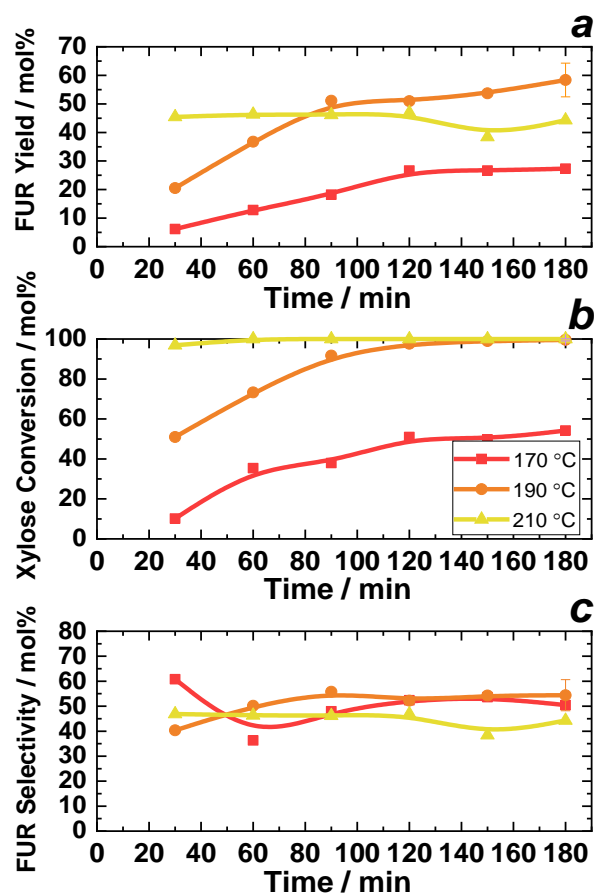
Fig. 1. Effect of reaction temperature and time on (a) FUR yield, (b) xylose conversion, (c) selectivity to FUR in the conversion of 186 mol m^{-3} xylose to FUR with an aqueous to SBP phase ratio of 1:1 (by volume).

3.3. Furfural degradation in the biphasic system

To broaden understanding of the behavior of FUR under the conditions of microwave-assisted reaction in the presence of SBP, it is indispensable to understand its degradation rate. The FUR degradation experiments were determined employing SBP at the reaction temperatures of 170, 190 and 210 °C under auto-catalyzed system. The experimental data exhibiting the residual fractions of FUR encountered in the aqueous and organic phases at different reaction times are displayed in Fig. A4 (in the Supplementary Information). The figure illustrates the effect of the reaction temperature and time when employing 1:1 aqueous to SBP phase ratio on the degradation rate of FUR. The results demonstrate a clear dependency of FUR degradation on the temperature and time, as it can be noticed that when rising the reaction temperature and time, the FUR degradation advances. The highest degree of degradation, 28%, was detected at 210 °C after 3 h. In a similar manner, published papers have presented likewise data in monophasic systems [35, 42, 43]. Similarly, data published recently when employing isophorone as organic solvent in biphasic systems described a similar effect on FUR formation [30]. Contrastingly, when employing 2-methyltetrahydrofuran (2-MTHF) and cyclopentyl methyl ether (CPME) as organic solvents for biphasic reactions, FUR yields reached 71 and 78%, respectively. Besides, a lower FUR degradation degree (12%) was reported under similar conditions when using CPME. This could be due to reactions happening between FUR and unsaturated hydrocarbons via condensation, e.g. SBP and isophorone. Markevich et al. reported the reactivity of double bonds in compounds with functional groups, especially they noted that FUR could be as reactive as acceptor of dimethylcyanomethyl radicals [44].
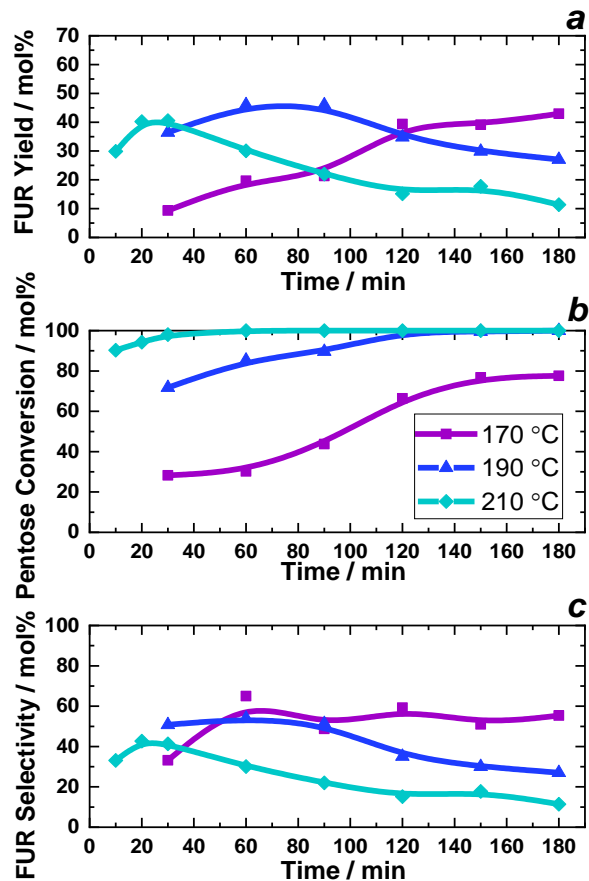
3.4. Auto-catalyzed dehydration of birch hydrolysate

Hydrothermal reactions of birch hydrolysate were assessed. In addition to xylose and arabinose, birch hydrolysate contains unhydrolyzed xylose and arabinose polymers (xylo-oligosaccharides and arabino-oligosaccharides, respectively). Fig. 2 shows the FUR yield, pentose (xylose and arabinose) conversion and selectivity to FUR under various reaction times (between 10 min and 180 min) at temperatures of 170, 190 and 210 °C. As it can be seen in Fig. 2b, FUR yield and pentose conversion are significantly influenced by the reaction time and temperature, which is in accordance to previous reports on this field [12, 16, 17, 41, 45, 46].

11

As observed in Fig. 2a, after the first 0.5 h of the hydrothermal reaction the FUR yield was increased by a factor of four by raising the reaction temperature from 170 to 190 °C. The largest FUR yield (46%) was obtained at 190 °C in 1 h. At temperatures of 170, 190 and 210 °C, the highest selectivity to FUR (Fig. 2c) was 65%, 51% and 43%, respectively. Reaction temperature has also an effect on selectivity to FUR under these conditions. It can be observed that selectivity to FUR at the lowest temperature studied (170 °C) displays the highest value in the present system.

In a work published recently, when using a xylose solution (28 g l^{-1}) under auto-catalyzed conditions FUR yield increased significantly when increasing the reaction temperature from 190 to 210 °C. Contrastingly, when birch hydrolysate liquor is used and dehydrated under auto-catalyzed conditions at 210 °C FUR yield does not surpass the FUR yield obtained at 190 °C. Under high reaction temperatures (210 °C) it is possible that the produced FUR and intermediate mix contained in the hydrolysate liquor takes place faster. Hence FUR is prone to decompose in a shorter reaction time at high temperatures via condensation (reactions between FUR and intermediates, i.e. pentose and hexose isomers) or resinification (reactions between FUR molecules).

When using birch hydrolysate liquor (3 ml) at 190 °C in 60 min, 5.3 mg of humins were formed in the auto-catalyzed system (Fig. A5 in the Supplementary Information). These insoluble polymers can be valorized as recently published literature demonstrates [47, 48]. The formed humins were analyzed using N_2-physisorption, and the sample displays a low surface area of 4 m^2 g^{-1} (Table A2 in the Supplementary Information).

Fig. 2. Effect of temperature and reaction time on (a) FUR yield, (b) xylose conversion, (c) selectivity to FUR during auto-catalyzed conversion of birch hydrolysate liquor.

3.5. Furfural formation from birch hydrolysate in the biphasic system

The formation of FUR from birch hydrolysate was investigate under optimized conditions for the dehydration of pentoses as it was determined in the previous sections (190 °C, 1:1 aqueous to SBP phase ratio (by volume), under microwave irradiation). The initial composition of the birch hydrolysate is given in Table A1 (in the Supplementary Information).

The highest FUR yield (54%) was reached at 190 °C in 3 h using an aqueous to SBP phase ratio of 1:1 (by volume) under complete pentose conversion (Fig. 3a and Fig. 3b). Pentose conversion (Fig. 3b) increased from 80% to 94% when increasing reaction time from 0.5 h to 1 h at 190 °C.

13

Under similar conditions (190 °C in 3 h using an aqueous to CPME phase ratio of 1:1 (by volume)), a recent published article reported a FUR yield of 68% using a birch hydrolysate liquor containing similar xylo-oligosaccharide concentration [30]. This high yield was reached due to the absence of degradation reactions between FUR and CPME.
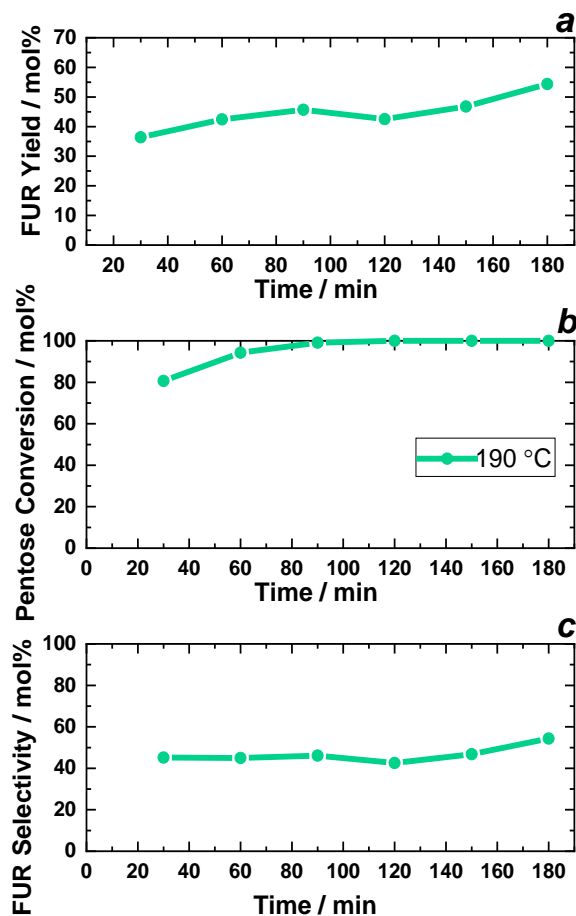

Fig. 3. (a) FUR yield, (b) pentose conversion, (c) selectivity to FUR when employing birch hydrolysate (1.5 ml) and SBP (1.5 ml) at 190 °C under microwave irradiation.

3.6. Process simulation

Process simulation model was developed in Aspen Plus® v8.8 (Aspen Technology, Inc., USA) by using the universal quasi-chemical (UNIQUAC) thermodynamic method and is shown in Fig. 4**.**

The pre-hydrolysate stream (S1) from the bio-refinery after lignin separation consisting mostly of xylose (xylo-oligosaccharides (64%) and monomeric xylose (36%)) and water is introduced into an agitated reactor along with 2-sec-butylphenol (SBP) for extracting FUR into the organic phase. The reactor is operating at a temperature of 190 °C

14

and 12.1 bar pressure with a residence time of 3 hours. The stoichiometric reactor model (RSTOIC) available in Aspen Plus is used to simulate the auto catalyzed reaction of xylose to yield FUR. The outlet stream from the reactor is cooled to 50 °C and sent to a disk centrifuge unit for separation of the organic and aqueous phases. A separator block is utilized to model the phase separation in the disk centrifuge with a block split fraction of 0.972 for FUR in the organic phase. The aqueous phase pre-dominantly consisting of water (99 wt. %) is separated and can be reused in the bio-refinery for pre-hydrolysis.
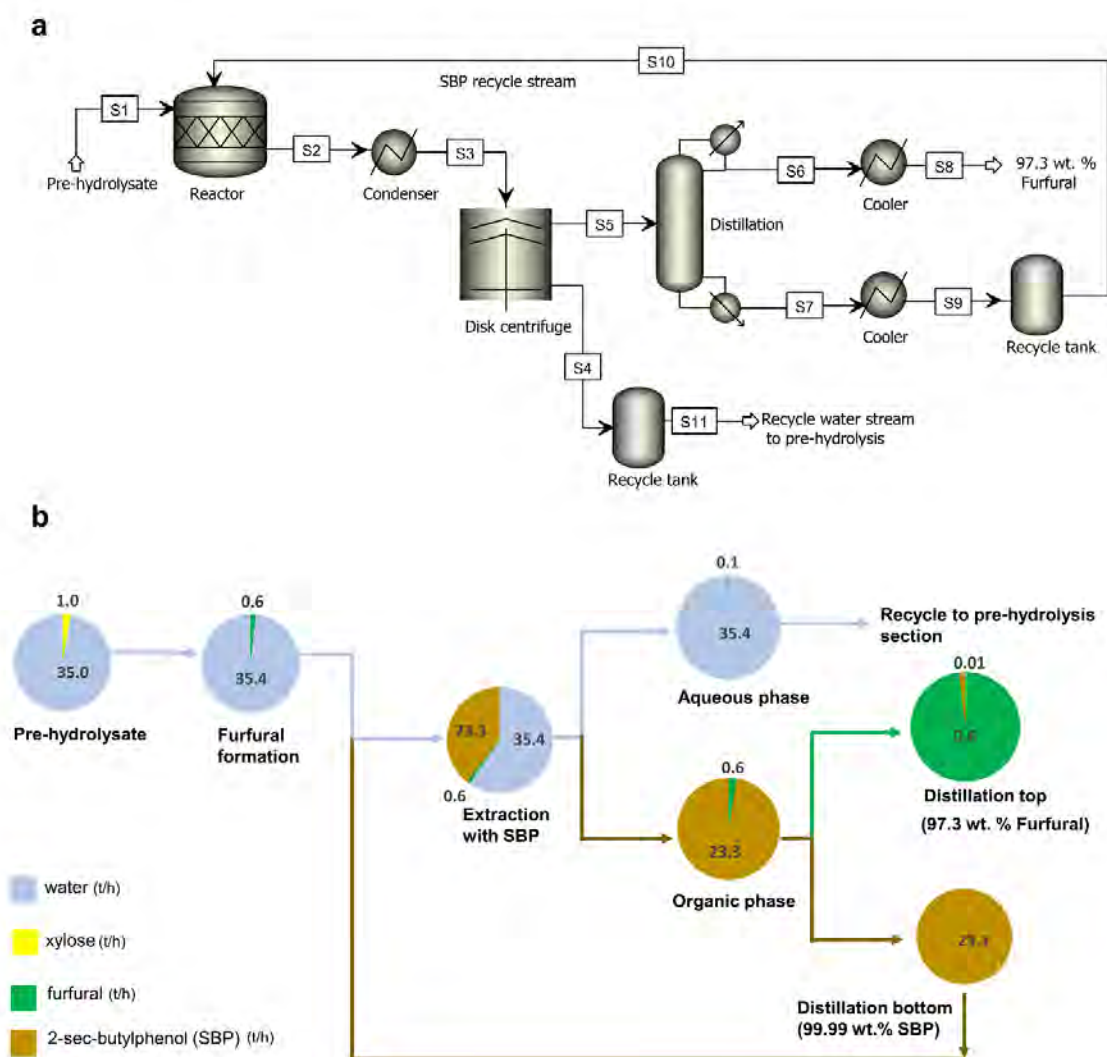
Fig. 4. (a) Process simulation diagram for the production of furfural from birch wood pre-hydrolysate liquor, (b) Mass balance for the production of furfural from birch wood pre-hydrolysate (5 kt per year). The reagents used are given a

unique color and the proportion of reagents is displayed using a pie chart. Flow of streams is indicated with the color of the majority component.

The organic phase consisting of FUR and SBP is introduced into a distillation column operating with 40 ideal stages at atmospheric pressure and a reflux ratio of 1. The RADFRAC rigorous distillation column in Aspen Plus is used to model the distillation process. 97.3 wt% FUR is recovered in the top fraction at 161 °C and the bottom fraction consisting of pure SBP is recycled back for reuse in the extraction step. The mass balance is shown in Fig. 4 and the energy balance with utility requirements is shown in Table 2.

The total heating duty indicates the total energy supplied for the heating of process streams and the total cooling duty indicates the total energy removed by cooling. The process includes the use of utilities such as high-pressure steam for the reboiler, cooling water for heat exchangers and electricity for pumps. It is assumed that the cooling water is recirculated to a cooling tower for re-use in the process.

**Table 2**. Process energy balance and utility requirements.

Energy balance	
Total heating duty (MW)	2.38
Total cooling duty (MW)	26.76
Utility requirements	
Cooling water (t/h)	4203.36
Steam (kg/h)	4990.75
Electricity (kW)	217.93

3.7. Process economics

The total investment cost for a plant with a FUR production capacity of 5kt/yr. is found to be 18.36 M€(Table 3). The contribution of individual process equipment to the total direct cost (TDC) is shown in Fig. 5. The reactor unit is the most expensive and accounts for 35 % of the TDC followed by heat exchangers and distillation column which contribute to 23 % and 21 % of the TDC respectively. The annual operating cost consists of fixed costs, variable costs, general expenses and is calculated as 5.09 M€ The revenue for the process comes mainly from selling FUR and additional revenue from high-pressure steam condensate that is sold as district heat.

Table 3. Estimation of fixed capital and total investment.

Component	M€
Delivered equipment cost	3.04
Total direct cost	9.18
Total indirect cost	2.70
OSBL	1.84
Contingency	2.97
Fixed capital investment	16.69
Working capital	1.67
Total investment	18.36
Fixed costs	2.91
Raw materials and utilities	1.72
General expenses	0.46
Annual operating cost	5.09
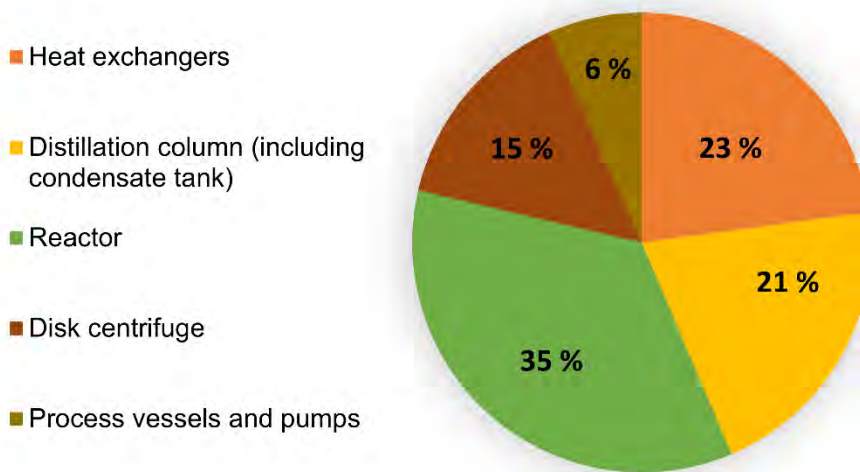
Fig. 5. Contribution of individual equipment to the total direct cost (TDC).

Bbosa and Brown recently completed a techno-economic analysis of a corn stover-ethanol biorefinery concept where they set a maket price of FUR of 933 €/t [49]. Currently, the prices available in Alibaba are in a range from 910 to

17

1630 €/t [50][2]. Dalvand et al. determined the market potential of FUR and its derivatives in a recent study [51]. They identified a set of six FUR derivatives to determine the best combination of FUR derivatives and what proportion of FUR should be converted into each derivative. The authors reported a FUR market price of 1359 €/t. A recent techno-economic evaluation of bioethanol and FUR coproduction, where they reported a price of 2.37 €/gallon and 1540 €/t, respectively [52]. These two chemical compounds were produced from corn stover via biochemical and thermochemical routes. Olcay et al. used aqueous phase processing to produce furfural as one of the products from biomass and reported a FUR MSP of 1.53 €/kg [53]. MSP reported in this paper is quite close to price reported in literature and the existing market price of petrochemical based furfural. The minimum selling price of FUR is calculated at NPV equal to zero with a discount rate of 10 % and is found to be 1.33 €/kg with the payback period being 8.9 years. However, when the FUR selling price is increased to 1.72 €/kg, the payback period is 5 years with an NPV of 12.3 M€ at the end of the project lifetime as shown in Fig. 6. The internal rate of return is determined by adjusting the discount rate until the NPV at the end of year 20 is equal to zero and is calculated as 20.7 %. The equations used for the calculation of NPV and payback period are given in the Supplementary Information.

The effect of production capacity on the MSP of FUR, total investment and annual operating cost is shown in Table 4. When the production capacity is doubled, it is observed that there is an increase in the total investment and operating costs and at the same time, the MSP of FUR drops to 1.12 €/kg. Tables A3 and A4 (in the Supplementary Information) show the raw materials, utility prices and cost factors, respectively.

Table 4. Effect of production capacity on MSP, total investment and operating costs.

Production capacity (t/yr.)	Operating costs (M€/yr.)	Total investment (M€)	MSP (€/kg)
5000	5.09	18.36	1.33
10000	8.08	31.16	1.12

3.8. Sensitivity analysis

A sensitivity analysis is carried out to evaluate the effect of various economic factors on the minimum selling price of FUR as shown in Fig. 6. It was observed that annual operating cost, discount rate and total investment had the biggest

---

[2] Original prices reported in USD were converted to EU with a conversion rate of 1 USD = 0.90612 € on September 10th 2019.

impact on the MSP. For instance, when the operating costs and the total investment increased by 20 %, there was a 13.3 % and 7.2 % increase in the MSP respectively. Similarly, when the discount rate was increased by 50 %, the MSP increased by 11.8 %. Variation in the taxation rate and project lifetime had comparatively smaller influence on the MSP.
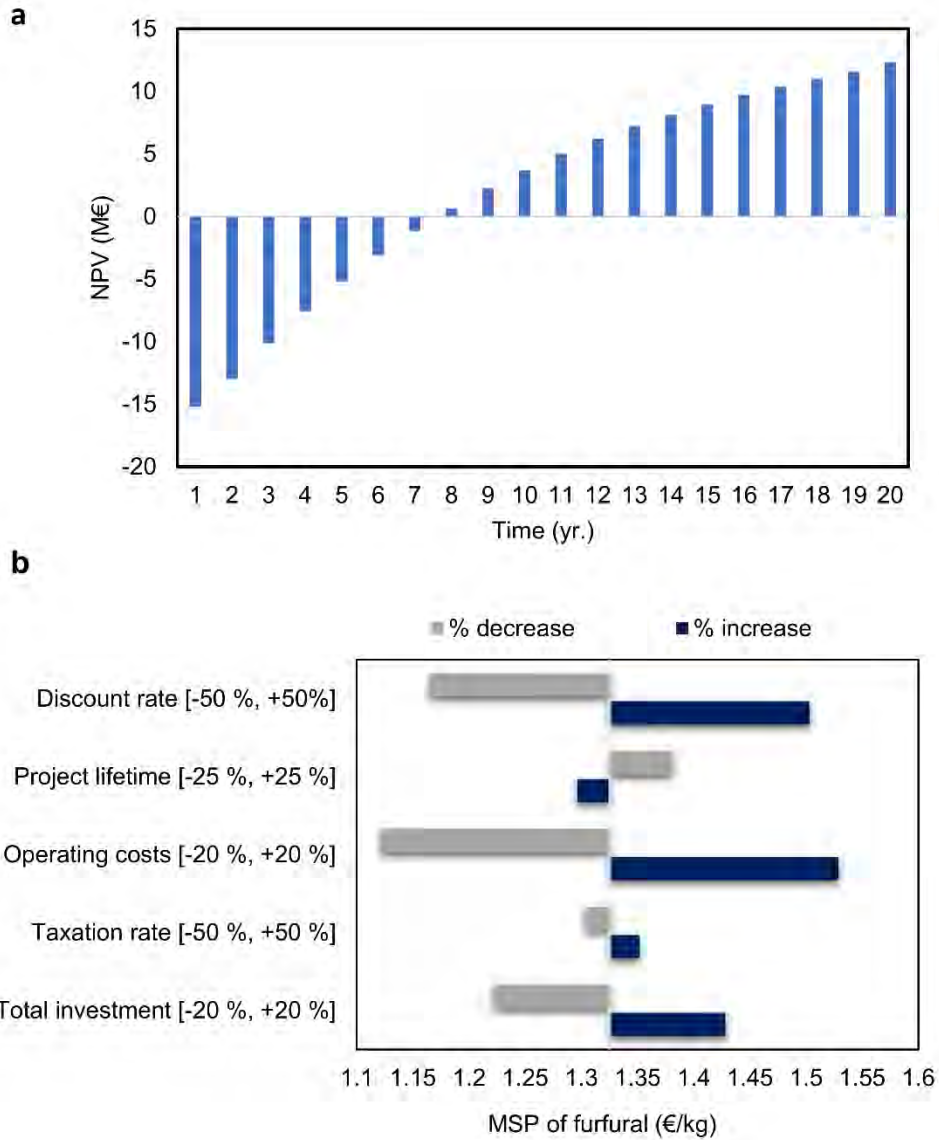
Fig. 6. (a) NPV plotted as a function of the project lifetime, (b) Sensitivity analysis for evaluating influence of various economic factors on the MSP of furfural. The base values of the economic factors: discount rate = 10 %; project lifetime = 20 years; operating costs = 5.09 M€/year; taxation rate = 20 % and total investment = 18.36 M€

4. Conclusions

The conversion of xylose and the resulting FUR yield were studied under well-controlled conditions in a biphasic system with a water-immiscible organic solvent using a model compound, xylose solution, and subsequently birch hydrolysate liquor.

The most favorable aqueous to SBP under auto-catalyzed conditions was 1:1 (by volume) to extract FUR in the conversion of xylose and birch hydrolysate into FUR. The highest FUR yield, when using a xylose solution, is 59% in a two-phase system employing SBP as organic solvent. When using birch hydrolysate liquor in a biphasic system, a FUR yield of 54% is obtained at 190 °C in 3 h under auto-catalyzed conditions.

Based on the techno-economic analysis, the MSP of FUR is found to be 1.33 €/kg for a plant operating with a production capacity of 5 kt/yr. With a FUR selling price of 1.72 €/kg, the payback period is calculated as 5 years resulting in a positive NPV of 12.3 M€ at the end of the project lifetime and an internal rate of return of 20.7%. The sensitivity analysis indicated that the annual operating cost, discount rate and total investment have the largest impact on the MSP of FUR.

5. Acknowledgements

References

[1] Mustalahti I. The responsive bioeconomy: The need for inclusion of citizens and environmental capability in the forest based bioeconomy. Journal of Cleaner Production 2018; 172: 3781-90.

[2] Ministry of Employment and Economy. The Finnish bioeconomy strategy: sustainable growth from bioeconomy 2014.

[3] Lê HQ. Wood biorefinery concept based on γ-valerolactone/water fractionation 2018: pp 61.

[4] Rodriguez-Chiang L, Vanhatalo K, Llorca J, Dahl O. New alternative energy pathway for chemical pulp mills: From traditional fibers to methane production. Bioresource Technology 2017; 235: 265-73.

[5] Hashmi SF, Meriö-Talvio H, Hakonen KJ, Ruuttunen K, Sixta H. Hydrothermolysis of organosolv lignin for the production of bio-oil rich in monoaromatic phenolic compounds. Fuel Processing Technology 2017; 168: 74-83.

[6] Gómez Millán G, Hellsten S, Llorca J, Luque R, Sixta H, Balu AM. Recent Advances in the Catalytic Production of Platform Chemicals from Holocellulosic Biomass. ChemCatChem 2019; 11: 2022-42.

[7] Zeitsch KJ. 1. Introduction. In: Zeitsch KJ, editor. the chemistry and technology of furfural and its many by-products: Elsevier; 2000, p. 1-2.

[8] Talvitie H, Pitkänen P. Cellunolix® ethanol plant to be built in Finland 2014.

[9] CCM. CCM: China's market price of furfural bounces back in April 2016.

[10] Bhisey R. Furfural Market to Reach US$ 672.58 Mn by 2026; Rise in Demand for Furfuryl Alcohol to Drive Market: Transparency Market Research 2019; 2019.

[11] Grand View Research. Furfural Market Analysis By Application (Furfuryl Alcohol, Solvent) And Segment Forecasts To 2020 2015.

[12] Gómez Millán G, El Assal Z, Nieminen K, Hellsten S, Llorca J, Sixta H. Fast furfural formation from xylose using solid acid catalysts assisted by a microwave reactor. Fuel Process Technol 2018; 182: 56-67.

[13] Peleteiro S, Rivas S, Alonso JL, Santos V, Parajó JC. Furfural production using ionic liquids: A review. Bioresour Technol 2016; 202: 181-91.

[14] Yemiş O, Mazza G. Acid-catalyzed conversion of xylose, xylan and straw into furfural by microwave-assisted reaction. Bioresour Technol 2011; 102: 7371-8.

[15] Lamminpää K, Ahola J, Tanskanen J. Acid-catalysed xylose dehydration into furfural in the presence of kraft lignin. Bioresour Technol 2015; 177: 94-101.

[16] Kootstra AMJ, Mosier NS, Scott EL, Beeftink HH, Sanders JPM. Differential effects of mineral and organic acids on the kinetics of arabinose degradation under lignocellulose pretreatment conditions. Biochem Eng J 2009; 43: 92-7.

[17] Hongsiri W, Danon B, de Jong W. The effects of combined catalysis of oxalic acid and seawater on the kinetics of xylose and arabinose dehydration to furfural. Int J Energy Environ Eng 2015; 6: 21-30.

[18] Lin L, Ma S, Li P, Zhu T, Chang H. Mutual Solubilities for the Water-2-sec-Butylphenol System and Partition Coefficients for Furfural and Formic Acid in the Water-2-sec-Butylphenol System. J Chem Eng Data 2015; 60: 1926-33.

[19] Azadi P, Carrasquillo-Flores R, Pagan-Torres Y, Gurbuz EI, Farnood R, Dumesic JA. Catalytic conversion of biomass using solvents derived from lignin. Green Chem 2012; 14: 1573-6.

[20] Gürbüz EI, Wettstein SG, Dumesic JA. Conversion of Hemicellulose to Furfural and Levulinic Acid using Biphasic Reactors with Alkylphenol Solvents. ChemSusChem 2012; 5: 383-7.

[21] Romo JE, Bollar NV, Zimmermann CJ, Wettstein SG. Conversion of Sugars and Biomass to Furans Using Heterogeneous Catalysts in Biphasic Solvent Systems. ChemCatChem 2018; 10: 4805-16.

21

[22] Argyle DM, Bartholomew HC. Heterogeneous Catalyst Deactivation and Regeneration: A Review. Catalysts 2015; 5.

[23] Trimble F, Dunlop AP. Recovery of Furfural from Aqueous Solutions. Ind Eng Chem Anal Ed 1940; 12: 721-2.

[24] Zhang J, Zhuang J, Lin L, Liu S, Zhang Z. Conversion of D-xylose into furfural with mesoporous molecular sieve MCM-41 as catalyst and butanol as the extraction phase. Biomass and Bioenergy 2012; 39: 73-7.

[25] Gómez Millán G, Phiri J, Mäkelä M, Maloney T, Balu AM, Pineda A, et al. Furfural production in a biphasic system using a carbonaceous solid acid catalyst. Appl Catal , A 2019.

[26] Le Guenic S, Gergela D, Ceballos C, Delbecq F, Len C. Furfural Production from d-Xylose and Xylan by Using Stable Nafion NR50 and NaCl in a Microwave-Assisted Biphasic Reaction. Molecules 2016; 21: 1102.

[27] Campos Molina MJ, Mariscal R, Ojeda M, López Granados M. Cyclopentyl methyl ether: A green co-solvent for the selective dehydration of lignocellulosic pentoses to furfural. Bioresour Technol 2012; 126: 321-7.

[28] Mittal A, Black SK, Vinzant TB, O'Brien M, Tucker MP, Johnson DK. Production of Furfural from Process-relevant Biomass-derived Pentoses in a Biphasic Reaction System. ACS Sustainable Chem Eng 2017.

[29] Weingarten R, Cho J, Conner J,Wm.Curtis, Huber GW. Kinetics of furfural production by dehydration of xylose in a biphasic reactor with microwave heating. Green Chem 2010; 12: 1423-9.

[30] Gómez Millán G, Hellsten S, King AWT, Pokki J, Llorca J, Sixta H. A comparative study of water-immiscible organic solvents in the production of furfural from xylose and birch hydrolysate. J Ind Eng Chem 2019; 72: 354-363.

[31] vom Stein T, Grande PM, Kayser H, Sibilla F, Leitner W, Dominguez dM. From biomass to feedstock: one-step fractionation of lignocellulose components by the selective organic acid-catalyzed depolymerization of hemicellulose in a biphasic system. Green Chem 2011; 13: 1772-7.

[32] Sheldon RA. Green and sustainable manufacture of chemicals from biomass: state of the art. Green Chem 2014; 16: 950-63.

[33] Sluiter A, Hames B, Ruiz R, Scarlata C, Sluiter J, Templeton D. Determination of Sugars, Byproducts, and Degradation Products in Liquid Fraction Process Samples. Technical Report NREL/TP-510-42623 2008.

[34] Sairanen E, Vilonen K, Karinen R, Lehtonen J. Functionalized Activated Carbon Catalysts in Xylose Dehydration. Top Catal 2013; 56: 512-21.

[35] Lamminpää K, Ahola J, Tanskanen J. Kinetics of furfural destruction in a formic acid medium. RSC Adv 2014; 4: 60243-8.

[36] Lamminpää K, Ahola J, Tanskanen J. Kinetics of Xylose Dehydration into Furfural in Formic Acid. Ind Eng Chem Res 2012; 51: 6297-303.

[37] Givry S, Bliard C, Duchiron F. Selective ketopentose analysis in concentrate carbohydrate syrups by HPLC. Carbohydr Res 2007; 342: 859-64.

[38] Pirola C, Rossetti I, Ragaini V. Are conversion, selectivity and yield terms unambiguously defined in chemical and chemical engineering technology?. La Chimica & L'Industria 2013; 2: 136-145.

[39] Peters M, K. Timmerhaus RW, editors. Plant Design and Economics for Chemical Engineers. 5th ed: McGraw Hill; 2003.

[40] NCBI homepage U.S. National Library of Medicine National Center for Biotechnology Information. PubChem: 2-Sec-Butylphenol (Compound); 2019.

[41] Danon B, Hongsiri W, van der Aa L, de Jong W. Kinetic study on homogeneously catalyzed xylose dehydration to furfural in the presence of arabinose and glucose. Biomass Bioenergy 2014; 66: 364-70.

[42] Marcotullio G, de Jong W, Tavares Cardoso MA, Verkooijen AHM. Bioenergy II: Furfural Destruction Kinetics during Sulphuric Acid-Catalyzed Production from Biomass. International Journal of Chemical Reactor Engineering 2009; 7(1):A67.

[43] Danon B, van der Aa L, de Jong W. Furfural degradation in a dilute acidic and saline solution in the presence of glucose. Carbohydrate Research 2013; 375: 145-52.

[44] Markevich IN, Borisova GS, Glebova NN, Sharaev OK, Ostrovskaya IY, Gol'berg AI. Relative reactivities of double bonds in compounds with functional groups towards the dimethylcyanomethyl radical. Bulletin of the Academy of Sciences of the USSR, Division of chemical science 1989; 38: 789-92.

[45] Sahu R, Dhepe PL. A One-Pot Method for the Selective Conversion of Hemicellulose from Crop Waste into C5 Sugars and Furfural by Using Solid Acid Catalysts. ChemSusChem 2012; 5: 751-61.

[46] Chen XJ, Liu XQ, Xu FL, Bai XP. Degradation Kinetics of Xylose and Arabinose in Subcritical Water in Unitary and Binary System. Advanced Materials Research 2012; 450-451: 710-4.

[47] van Zandvoort I. Towards the Valorization of Humin By-products: Characterization, Solubilization and Catalysis 2015.

[48] Hoang TMC, Lefferts L, Seshan K. Valorization of Humin-Based Byproducts from Biomass Processing - A Route to Sustainable Hydrogen. ChemSusChem 2013; 6: 1651-8.

[49] Bbosa D, Mba-Wright M, Brown RC. More than ethanol: a techno-economic analysis of a corn stover-ethanol biorefinery integrated with a hydrothermal liquefaction process to convert lignin into biochemicals. Biofuels, Bioprod Bioref 2018; 12: 497-509.

[50] Alibaba. Factory wholesale low price furfural 2019; 2019.

[51] Dalvand K, Rubin J, Gunukula S, Clayton Wheeler M, Hunt G. Economics of biofuels: Market potential of furfural and its derivatives. Biomass and Bioenergy 2018; 115: 56-63.

[52] Hossain MS, Theodoropoulos C, Yousuf A. Techno-economic evaluation of heat integrated second generation bioethanol and furfural coproduction. Biochemical Engineering Journal 2019; 144: 89-103.

[53] Olcay H, Malina R, Upadhye AA, Hileman JI, Huber GW, Barrett SRH. Techno-economic and environmental evaluation of producing chemicals and drop-in aviation biofuels via aqueous phase processing. Energy Environ Sci 2018.

SUPPLEMENTARY INFORMATION

Furfural production from xylose and birch hydrolysate liquor in a biphasic system with techno-economic analysis

Gerardo Gomez Millan,[a,b] Rahul Prasad Bangalore Ashok, [c] Pekka Oinas,[c] Jordi Llorca,[b] Herbert Sixta[a]*

[a]	G. Gómez Millán, Prof. H. Sixta Department of Bioproducts and Biosystems School of Chemical Engineering, Aalto University Vuorimiehentie 1, 02150 Espoo (Finland) E-mail: herbert.sixta@aalto.fi
[b]	G. Gómez Millán, Prof. J. Llorca Department of Chemical Engineering, Institute of Energy Technologies and Barcelona Research Center in Multiscale Science and Engineering Universitat Politècnica de Catalunya Eduard Maristany 10-14, 08019 Barcelona (Spain)
[c]	R.P. Bangalore Ashok, P. Oinas Department of Chemical and Metallurgical Engineering School of Chemical Engineering, Aalto University P.O. Box 16100, 00076 Espoo (Finland)

* Corresponding author.

E-mail address:

herbert.sixta@aalto.fi (Herbert Sixta)

1. Partition coefficient of furfural
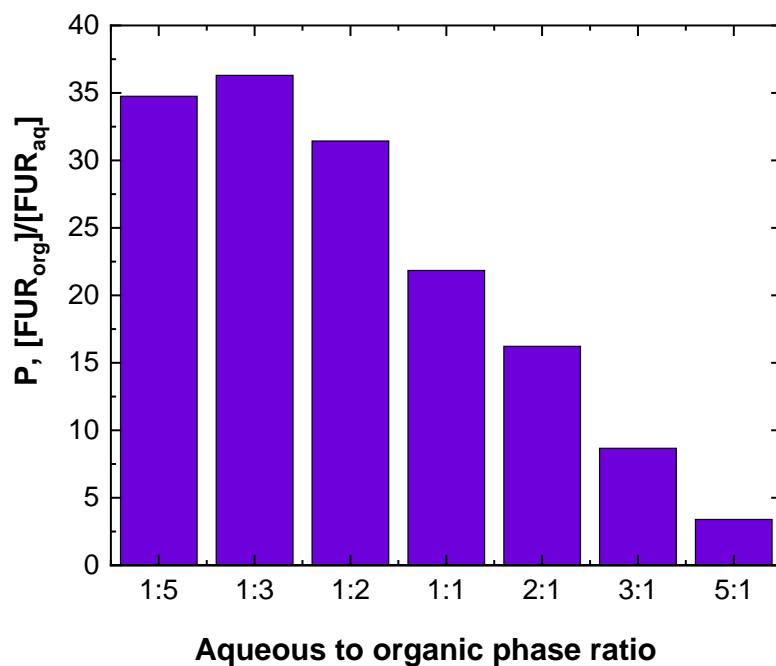
Fig. A1. Partition coefficients for furfural among 2-sec-butylphenol. Partition coefficients were determined for a solution of 5 wt% furfural in water heated to 190 °C for 30 min and then cooled down to 60 °C at seven different aqueous-to-organic phase ratios: 1:5, 1:3, 1:2, 1:1, 2:1, 3:1 and 5:1 (by volume).
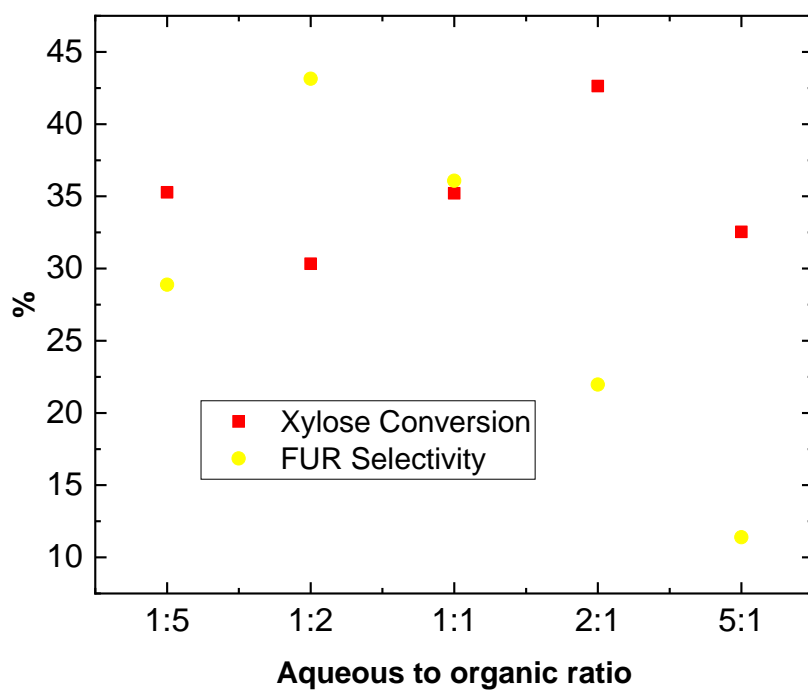
2. Effect of aqueous to organic phase ratio
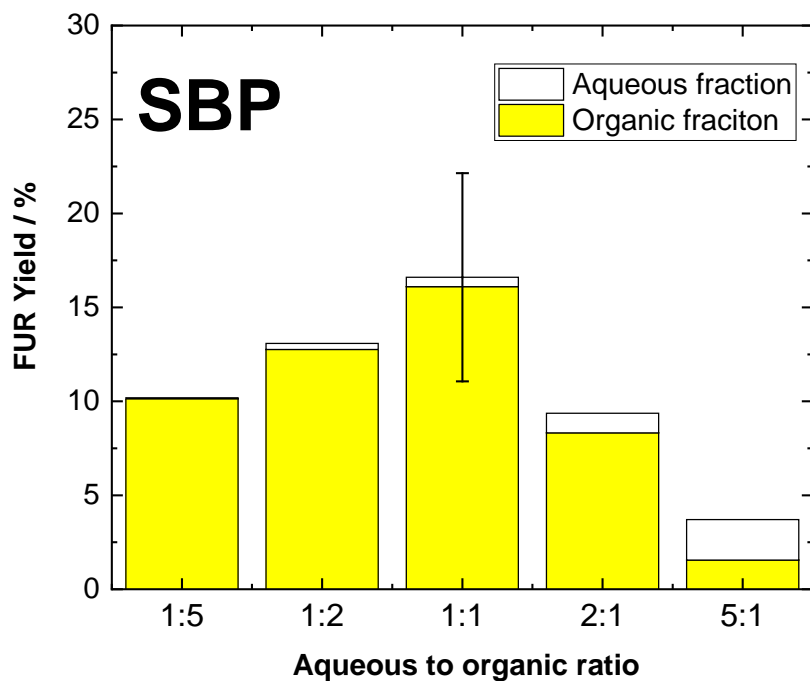
Fig. A2. Effect of aqueous to 2-sec-butylphenol phase ratio on furfural yield. The effect was established for a solution of xylose (186 mol m^{-3}) heated at 190 °C in 0.5 h at seven distinct ratios of aqueous to organic solvent: 1:5, 1:2, 1:1, 2:1, 5:1 (by volume).

3. Furfural formation analysis

Fig. A3. Effect of aqueous to organic ratio on xylose conversion and FUR selectivity when using SBP as organic phase. The effect was determined for a solution of xylose (186 mmol l^{-1}) heated at 190 °C in 30 min at five different ratios of aqueous to organic solvent: 1:5, 1:2, 1:1, 2:1, 5:1 (v/v).

4. Furfural degradation in the biphasic system
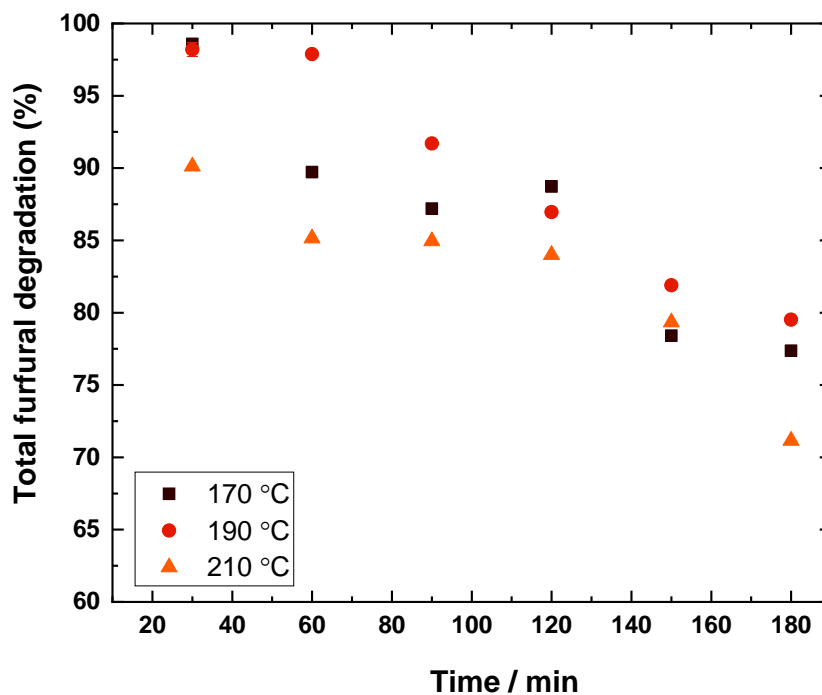
Fig. A4. The remaining FUR at various reaction times when employing an aqueous to SBP phase ratio of 1:1 (by volume) under auto-catalyzed degradation reaction. The degradation of FUR was ran for a solution of 5 wt% furfural (squares – 170 °C, circles – 190 °C, triangle – 210 °C).

5. Birch hydrolysate composition

Table A1. Initial composition of the birch hydrolyate after filtration

	Monomeric form, [g l^{-1}]	Total, [g l^{-1}]
Arabinose	0.61	0.55
Rhamnose	0.54	0.84
Galactose	0.69	1.47
Glucose	0.62	1.76
Xylose	9.15	26.17
Mannose	0.22	1.62
Lignin	-	0.17
HMF	0.22	0.10
Furfural	2.27	3.62

6. Humin formation

The conditions to form humins (insoluble polymers) as a by-product are the optimum conditions at highest FUR yield. 5.3 mg of humins were obtained under auto-catalyzed system at 190 °C in 60 min using 3 mL of birch hydrolysate. After the hydrothermal reaction, the insoluble matter was filtered by using a glass filter with porosity 4 (Duran) and dried overnight at 105 °C.

Fig. A5. Furfural and humin formation under auto-catalyzed conditions at 190 °C in 60 min employing 3 ml of birch hydrolysate.

A Micromeritics Tristar II-Physisorption Analyzer was utilized to record the nitrogen sorption isotherms for fresh and spent catalysts. The sample was dried at 105 °C and exposed to nitrogen gas for 12 h before measurement and the isotherms were taken at 77 K. The specific surface area (A_{BET}) was determined by the Brunauer-Emmett-Teller (BET) model [1] at relative pressures between 5 and 35% where the data points were observed to arrange linearly. The specific pore volume (V_p) was estimated from N_2 uptake at a p/p_0 value of 0.99 while recording approximately 150 equilibrium data points.

The pore width distribution (d_p) was deduced from the desorption branch using the Barrett-Joyner-Halenda (BJH) method [2].

Table A2. Textural properties of humins (i.e., BET (A_{BET}), pore volume (V_p) and pore diameter (d_p).

	A_{BET}/m^2 g^{-1}	V_p/cm^3 g^{-1}	d_p/nm
Humin	3.7	4.0×10^{-3}	3.4

7. Techno-economic analysis

Table A3. Raw material and utility prices.

Component	Price
2-sec-butylphenol (SBP)	450 €/t [3]
Cooling water (CW)	0.24 €/m^3 [4]
High-pressure (HP) steam	40 €/t
Electricity	65.5 €/MWh [5]
District heat	78.64 €/MWh [6]

Table A4. Direct and indirect cost factors [7].

Direct costs	Fraction of DEC
Equipment installation	0.39
Instrumentation and control	0.26
Piping and electrical systems	0.41
Buildings	0.29
Yard improvements	0.12
Service facilities	0.55

Indirect costs	
Engineering and supervision	0.32
Construction	0.34
Legal expenses	0.04
Contractor's fee	0.19

Process economics

The equations used for the calculation of NPV and payback period are as follows:

$Gross\ profit\ = revenue - operating\ cost$ Eq. S1

$Depreciation\ = 0.1 * Fixed\ capital\ investment\ (FCI)$ Eq. S2

$Taxable\ income = Gross\ profit - Depreciation$ Eq. S3

$Taxes\ paid = Taxation\ rate * Taxable\ income$ Eq. S4

$Cash\ flow = Gross\ profit - Taxes\ paid - FCI$ Eq. S5

$Net\ present\ value\ (NPV) = \sum_{n=1}^{n=t} \frac{Cash\ flow_n}{(1+DR)^n}$ Eq. S6

Where,

$Cash\ flow_n$ = cash flow in year n; DR = discount rate

$Payback\ period = \frac{Total\ investment}{Average\ cash\ flow}$ Eq. S7

References

1. S. Brunauer, P.H. Emmett, E. Teller, Adsorption of gases in multimolecular layer, J. Am. Chem. Soc. 35 (1938) 309.

2. E.P. Barrett, L.G. Joyner, P.P. Halenda, The determination of pore volume and area distributions in porous substances. I. Computations from nitrogen isotherms, J. Am. Chem. Soc. 73 (1951) 373.

3. J.Q. Bond, A.A. Upadhye, H. Olcay, G.A. Tompsett, J. Jae, R. Xing, D.M. Alonso, D. Wang, T. Zhang, R. Kumar, A. Foster, S.M. Sen, C.T. Maravelias, R. Malina, S.R.H. Barrett, R. Lobo, C.E. Wyman, J.A. Dumesic, G.W. Huber, Production of renewable jet fuel range alkanes and commodity chemicals from integrated catalytic processing of biomass, Energy Environ. Sci. 7 (2014) 1500-1523.

4. S. Jones, P. Meyer, L. Snowden-Swan, A. Padmaperuma, E. Tan, A. Dutta, J. Jacobson, K. Cafferty, Process Design and Economics for the Conversion of Lignocellulosic Biomass to Hydrocarbon Fuels: Fast Pyrolysis and Hydrotreating Bio-oil Pathway; Sponsor Org.: USDOE Office of Energy Efficiency and Renewable Energy (EERE), Bioenergy Technologies Office (EE-3B) (2013).

5. International Energy Agency, Key world energy statistics 2018 2019 (2018).

6. Statistics Finland, Statistics: Energy prices [e-publication].
Prices of imported fuels rose in the last quarter of 2017 2019 (13 March 2018).

7. M. Peters, R.W. K. Timmerhaus, Plant Design and Economics for Chemical Engineers (2003).